Modifying Commercial RFID Tags using Polydimethylsiloxane based Polymers for Sensing Purposes.

Aaron John Richard Hillier

A thesis submitted to the University of Kent in partial fulfilment of

the requirements for the degree of Doctor of Philosophy.

University of Kent, Canterbury,

Kent,

CT2 7NT

September 2019

Declaration

I declare that this thesis is my own work, and has been written

in my own words. Appropriate care has been taken to

accurately reference the works of others where necessary.

Signed -

Aaron John Richard Hillier

27th September 2019

Abstract

In the last decade, RFID sensing has grown rapidly. Passive RFID tags are attractive due to their low cost, theoretically infinite lifespans, small form factor and the ability to be read without a line of sight required. This has resulted in an enormous increase in research and commercial interest, with RFID sensing growing at an ever expanding rate. Previous RFID sensing has relied upon exploiting the reader side of RFID systems, or incorporating bespoke sensors into RFID systems. Newer classes of sensing tags now allow for useable sensing information to be provided by the tag antenna in the form of a sensor code that relates to a stimuli affecting the tag.

A popular research avenue for RFID has been utilising stimuli responsive materials. Using stimuli responsive polymers and other materials has previously relied upon exploiting the analogue changes that result when the stimuli responsive material is affected by an analyte of interest. The primary advantage of using stimuli responsive materials over bespoke sensing components is that the simpler components can be utilised. Nowadays, commercial sensing tags can be purchased for as little as £2.75, that can provide digital information about environmental conditions. Whilst dedicated sensors for other analytes would be expected to have a higher cost, incorporating polymeric materials into lower cost sensors and repurposing them to sense a range of analytes presents an attractive alternative.

A commercially available RFMicron RFM-2100 AER moisture sensing tag was modified with polydimethylsiloxane (PDMS) to allow for sensing of aqueous electrolytes of variable concentration. Coating the tag with the hydrophobic layer also allowed for the system to return to be reusable. The system also demonstrated the ability measure the relative amount of water (or alcohol) in water/alcohol mixes.

A two part reactive silicone cross-linked polymer was also investigated for the purpose of repurposing the tag to be used as a pH sensor, but was found not to produce enough (if any) changes in response with variable pH. Following this work, a preliminary investigation showed the potential for a

PDMS/PANI (polyaniline) composite was tested as a pH responsive coating for the RFMicron RFM-2100 AER. The system was capable of measuring 5 distinct ranges of pH, but only on the first use of the system, as after this the system became incapable of measuring pH changes aside from those associated with the large change in dielectric properties of extremely low pH solutions.

Publications and presentations arising from this project

Peer reviewed Journal articles:

A Passive UHF RFID Dielectric Sensor for Aqueous Electrolytes, Hillier A, Makarovaite V, Gourlay C, Holder S, Batchelor J, *IEEE Sensors Journal 2019* vol: 19 (14) pp: 5389-5395[128].

Poster Presesntations:

A Passive UHF RFID Dielectric Sensor for Aqueous Electrolytes, Macro group young researchers meeting, Kent, 2019.

A passive UHF RFID pH sensor, LAPC antennas and propogation conference, Loughborough, 2017

Smart polymers for wireless medical sensing devices, Warwick polymer conference, Warwick, 2016.

Acknowledgements

Firstly, I would like to give my sincere thanks to Dr Simon Holder, Professor John Batchelor for giving me the opportunity to do this research. I would like to thank them both for their continued support, vast knowledge, and the time they spent training me and moving my research in the right direction. I'd like to especially thank Simon, who has spent a great deal of time with me, given me an opportunity to stay at the university and has challenged me to better myself continuously over the last 7 years as a supervisor and through my undergraduate studies. It is because of you both that this collaborative work was possible and you have my utmost gratitude.

Secondly, I'd like to thank Dr Campbell Gourlay and Viktorija Makarovaite. Campbell has offered insight and provided numerous good suggestions during the span of the whole project and Viktorija has provided help and collaborated throughout my time here, and without them the project wouldn't have continued to move in the right direction.

Thanks goes to the incredible labmates I have had for the past few years. Notably Alex, who provided so much help teaching me so many core techniques at the start of my project and has always been (most likely against his will) a great sounding board for ideas. Thanks must next go to my labmate and housemate Matt, who has constantly been of help during my time here and is always the first to go out of his way to help myself and others in the lab. Thanks must also go to Yarry and Jed, my former labmates and housemates who have been immensely helpful and helped me grow as a researcher during my time here. Thanks also goes to Giada, Athin-aaa, Anna & Toby, who have all made my final year in the lab brighter and I have no doubt will go on to do incredible things here. I also give thanks to my other friends in the department past and present, Nanami, Ian, Oni, Oliver & Stella.

Huge thanks must also go to all my friends from my undergraduate degree, most notably my study buddy India and my best friend Nathanial. India has motivated me and believed in me even when I didn't, through undergraduate degree and even more so during my postgraduate degree, giving me the encouragement i've needed, even when I've doubted myself. To Nathanial, I am eternally grateful

thank for, as my dad quoted "getting him through for the last few years". We may always quip and relentlessly mock one another, but without a doubt you've been like a brother to me over the last 7 years and you have my eternal thanks for all you've done to help me.

I would finally like to thank my whole family for believing in me and supporting me as wholeheartedly as they have, especially my mum and dad, without whom none of this would have been possible. Without you I wouldn't be the man I am today. You've constantly been there for me for the last 27 years, believing in me, encouraging me and supporting me wherever you could, whenever you could. Words can never thank you enough.

List of abbreviations

AAS	Atomic absorption spectroscopy
CAB	Cellulose acetate butyrate
CL	Chemiluminescent
DAK	Dielectric assessment kit
DF	Dual frequency
DMSO	Dimethyl sulfoxide
EAS	Electronic article systems
FT-IR	Fourier transform infrared
GHz	Gigahertz
HF	High frequency
Hz	Hertz
IDC	Interdigitated capacitor
IFF	Identify friend or foe
ISM	Industrial, scientific and medical radio band
LCE	liquid crystal elastomer
LiCl	Lithium chloride
LED	light emitting diode
LiCl	Lithium chloride
LF	Low frequency
NaCl	Sodium chloride
NFC	Near field communication
NMP	N-methyl-2-pyrrolidone
NMR	Nuclear magnetic resonance
MAS	Magic angle spinning

MHz	Megahertz
MWCNT's	Multi-wall carbon nanotubes
PANI	Polyaniline
PANI-DNNSA	Polyaniline-dinonylnaphthalene sulfonic acid
PANI-PSS	Polyaniline-polystyrene sulfonate
PBMA	Poly(n-butyl methacrylate)
PDMS	Polydimethylsiloxane
PEDD	Paired emitter diode device
PEDOT:PSS	Poly(3,4-ethylenedioxythiophene)
PEUT	Polyetherurathane
PHEMA	Poly(2-hydroxy ethyl methacrylate)
PTFE	Polytetrafluoroethylene
SWCNT's	Single walled carbon nanotubes
UHF	Ultra high frequency
RbCl	Rubidium chloride
RFID	Radio frequency identification
RTV	Room temperature vulcanisation
TEOS	Tetraethylorthosilicate
T_g	Glass transition temperature
T_{gel}	Gel point
TSH	Thyroid stimulating hormone
VNA	Vector network analyser
WCS	Wireless chemical sensor

Contents

Chapter 1: Introduction

1.1. Introduction to Radio Frequency Identification (RFID)

Radio frequency identification is defined as a means of utilising electromagnetic fields for the purposes of identifying objects using a tag[1]. For a general RFID setup, 4 components are required; an RFID reader, a PC, a transmit antenna and a reader antenna, & an RFID tag. The basic flow of operation for an RFID system is as follows; a tag will be placed on a desired object, then a command will be sent from the PC to operate the RFID reader, which will then use the transmitter antenna to interrogate the RFID tag. The RFID tag is then powered by the wireless signal from the reader antenna, sending back identifying information to the reader, which is processed by the PC, shown in Figure 1.1:
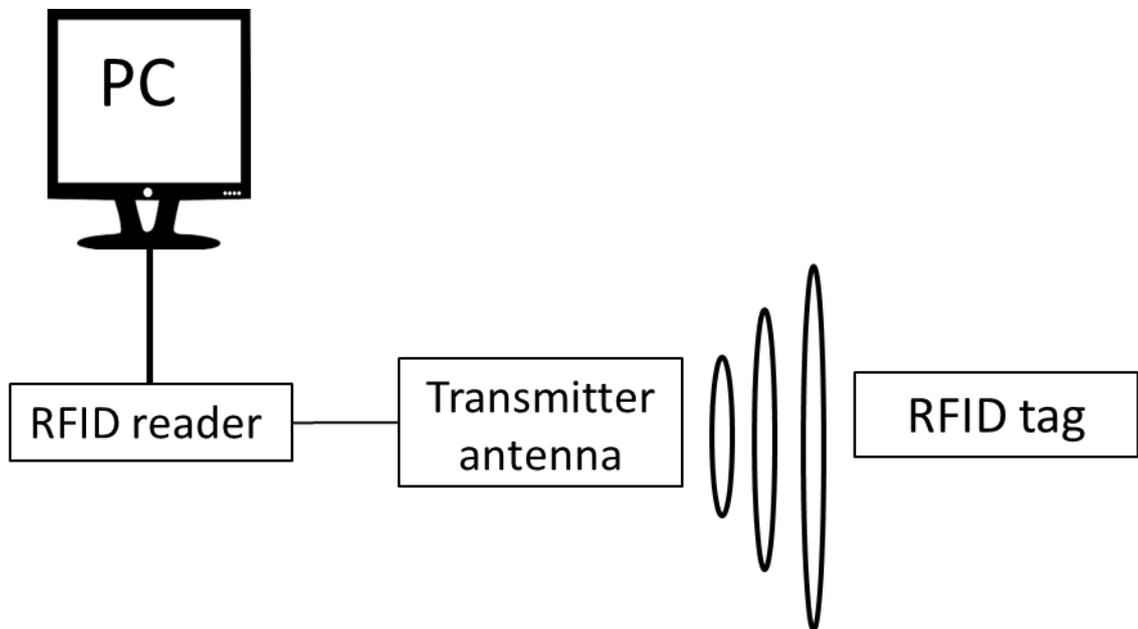
Figure 1.1 - Block diagram of a general RFID system.

RFID systems are frequently employed in inventory[2] as they allow for convenient and automatic identification. By simply attaching the tag to the item, it can be identified (so long as the reader is within the working distance of the tag) without needing a line of sight to the tag being interrogated. Depending on the desired function, several different types of RFID system can be employed, and the type of system employed will also be influenced by the necessary power requirements for the tag, the most suitable operating frequency to use (or also the required frequency if regulatory restrictions apply), or the required functions for the system to be able to utilise (such as sensing data, or being able to be used in a multiplexed reader array).

1.2. History of RFID

Radio waves were first employed as a means of detection in the Second World War[3]. The most commonly known of these systems was the development of RADAR, developed by Watson-Watt. RADAR was used as a rudimentary (although revolutionary at the time) method of detecting inbound aircraft. Whilst being able to determine inbound aircraft through radio waves was a useful tool in war time, the system was only capable of determining the existence of an unknown object, meaning that the system could not discriminate between friendly or hostile aircraft. In order to overcome this issue, the British later developed the Identity friend or foe (IFF) system, which allowed the allied aircraft to be discriminated via identifying signals generated by transponders that were placed. This is widely considered to be the first true example of RFID.

The necessity for this technology through wartime was later culminated in Harry Stockman's paper[4] published in 1948, entitled *"communication by means of reflected power".* The 50's and 60's saw continued and steady growth in the field, predominantly at a research level. Contributions over the course of this time (notably works from R.F Harrington[5,6]) slowly developed to the field to the point where the tail-end of the 60's would finally utilize RFID in a commercial setting, in the form of electronic article surveillance (EAS) systems[6]. These were employed as anti-theft systems, with the basic premise that tag activation occurred when they were in close proximity to a reader located at a door of a store. The presence of the tag being detected would sound an alert. These are known as 1-bit tags, as only the presence or absence of the tags can be observed. This was ideal for an anti-theft application, as the tags used are relatively inexpensive, can be removed after purchase. Such was the success of this system in the 60's, that it is still used today as an effective anti-theft countermeasure. The success of this system in an industrial setting paved the way for further development of RFID systems in the 1970's; Several contributors from a wide-array of sectors, including government bodies, industry, independent inventors and academia, respectively. Many had contributed to the development of RFID systems at this point, but the first patent was awarded to Charles Walton[6],

considered by many as one of the "fathers of RFID"[7]. Two patents were awarded to Walton in quick succession. At the same time, a string of companies and institutes were developing a plethora of systems with wide scale applications in mind. RCA were developing their *"Electronic identification system"* in 1975[8], and followed accordingly in 1977 with the *"electronic license plate for motor vehicles"*[9]. Momentum had gathered rapidly, but these systems were still in their infancy and not ready to implement practically. Nonetheless, the development of RFID in general during the 70's meant that the number of people researching the field had grown considerably. This allowed for the 80's to become the decade in which RFID would begin to be successfully implemented for practical applications. The most prevalent of these was the successful implementation of electronic toll systems, which were adopted in Spain, France, Italy, Portugal and Norway, as well as several parts of the United States. As the necessity for these systems grew, so did the development of RFID systems as a whole. The applications of RFID were also diversifying, and regulations followed pertaining to both power and frequency restrictions. Nonetheless, RFID has continued to grow at an ever accelerating rate.

1.3. Modern uses of RFID

Since the turn of the 21st century, RFID has now become increasingly commonplace in everyday life. Contactless payment, electronic door locks and passports from many countries are all prevalent examples of everyday items that rely upon RFID technology. Exploring farther than the consumer level, RFID is now commonplace in an industrial setting. Inventory systems, livestock monitoring, and location monitoring of hospital patients are just a few examples of settings where RFID has been adopted.

With the ever expanding growth of RFID, the number of applications that it now used for has become remarkably wide reaching. Its use in the security sector has already been mentioned, and at the time of writing the number of countries that have adopted biometric passports that utilise RFID since it was first employed by Malaysia (in 1998) is now 120[10]. Since mid-2017, the number of passports in circulation that are biometric now exceeds the number of non-biometric passports (57 %), totalling over 1 billion e-passports now in usage. The reaches of RFID within

airports do not only extend to passports, however. Several airlines have adopted electronic tagging systems in an effort to improve baggage location monitoring, as well as adopting permanent tagging systems to streamline the check in process, for instance, quantas[11] offers purchasable tags that allow people to bag drop luggage more easily. Airport security utilises RFID for access control. RFID is now favoured over the formerly used magnetic strips, which were effective but would wear away over time due to having to be directly swiped against a magnetic strip reader. Using RFID for airport security allows individual users to be given access to certain locations, as well as also being able to track where and when a user gains access.

Other sectors in transport and logistics also utilise RFID. As previously mentioned, electronic toll roads are used by fitting RFID systems to vehicles as a means of automatic payment, allowing for congestion to be reduced on roads as there is no requirement to slow down in order to pay a toll operator. However, this is not the only implementation of RFID to user transport. In New York, the same toll collection tags are monitored using readers placed at intersections that allow live traffic monitoring to be performed. This information is then utilised by a traffic management centre to alter flow of traffic using traffic lights, alleviating congestion[12]. Vehicle theft is also being made more difficult thanks to intelligent license tags, known as *"iltag's"* [13]. Similar systems are now being utilised in California[14], with the general premise of the system being a tamper proof tag that ceases to operate if removed, preventing transfer of the smart label.

RFID labelling has also been used for quality control in manufacturing processes. The Ford motor company facility in Mexico has migrated away from paper based systems in favour of RFID[15]. The paper based system was ineffective, mostly due to how easily paper based documentation can be lost. This would often result in production errors. In this instance RFID facilitated a more streamlined manufacturing process that also allowed a chain of supply and a chain of manufacturing to be established. This idea of using RFID for record keeping is not only used by the motoring trade. In the same way that individual serial number could be written onto tags for any given vehicle, this has also been applied to evidence logging in forensic evidence management. In this field where a chain of custody is vital, being able to log the handling of a

piece of evidence through a paperless logging system is not only faster, but reduces the likelihood of handling errors. The system is currently used by the Dutch forensic institute[16]. In a recent NIST Report[17], it was concluded after a cost-benefit analysis that using RFID would "enhance the management of forensic evidence and, to a certain extent, improve the administration of justice".

1.4. RFID operating principles and components

An RFID tag is comprised generally of a substrate, an antenna and an integrated chip[18] (there are other components which can be integrated into an RFID system which will be discussed in relevant sections later in this chapter). The primary purpose of an RFID tag is information transmission to a reader within operational range. The substrate is the support layer for the other components that can also offer a protective layer. Different substrates are chosen depending on the type of tags being used, but also depending on the environmental conditions the tag is to be used in[19]. The integrated chip serves to store and process data as well as modulate incoming signals, whilst the antenna serves to harvest the aforementioned incoming signals transmitted from a reader and to transmit the reverse signal.

Depending on the required application, the tag may have additional components to meet a requirement, such as an integrated battery or an incorporated sensor. Depending on all of these requirements, and functionalities, RFID tags have a series of sub-categories with which they can be placed. Whilst there are several criteria that can determine the category of a tag, the predominant one is the power source[20].

1.4.2. Active and passive RFID systems

The two primary sub-categories of RFID systems are active and passive systems. Each type of system is typically favoured due to the application they are needed for. Active systems incorporate a battery into the tag[21]. The benefits of this are two-fold. The read distance of the active based system increases (up to 100 m), and the amount of system memory increases to 128 kilobytes (compared to as much as 64 kilobytes in a passive system). Due to the internal battery in active systems, they have a limited lifespan, so they are only typically chosen when a

large read distance or a high internal memory is absolutely necessary. Furthermore, the addition of an internal battery massively increases the price of each unit, being the most expensive component in the system. Passive systems do not require a battery and are not limited in their lifetime by battery charge. The system receives its power by harvesting energy from the transmitting antenna. Because there is no requirement for a battery, the systems are very cheap and can be miniaturised. The method by which these systems transmit data is either through inductive coupling or through modulated backscatter. **Figure 1.2** shows some commercially available examples of the three main categories of RFID systems available:
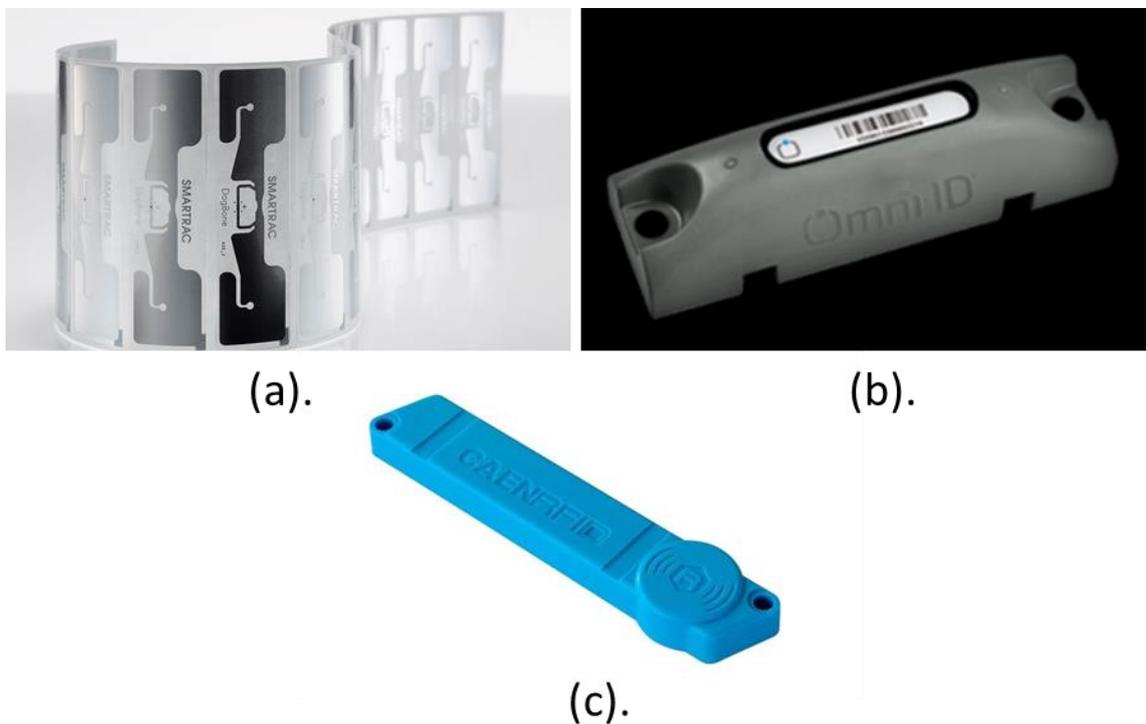
Figure 1.2 - (a) Smartrac's commercially available passive RFID sensing tag[22]. (b) OmniID's commercially available Power100 long-range active RFID tracking system[23]. (c) CAEN's commercially available semi-passive temperature monitoring RFID tag[24]

A third category of tags, known most commonly as semi-passive tags (but also semi-active) are also used as a type of bridge device. In these devices, the tag relies upon the reader to supply power used for broadcasting, with other components like micro-controller's[25] being powered by a battery. Because the battery is not being used to power the entire system, the longevity of semi-passive tags tends to be longer than a fully active tag. Moreover, the read distances are

generally increased compared to their passive counterparts as the tag battery improves the transponder sensitivity and improves the depth of modulation in the backscattered signal as passive tags to a reader. The flexibility of semi-passive tags arises from the option to use backscatter or inductive coupling to communicate rather than the two possible methods that active systems use, which are beacon (where the tag periodically emits a signal) or transmitter (where the tag only emits a signal upon receiving an interrogating signal from a reader).

1.4.3. RFID operating frequencies

As the abbreviation suggests, RFID systems work using radio waves. There are three main frequency bands which RFID systems operate within; low frequency (LF), high frequency (HF) and ultra- high frequency (UHF) (dual frequency (DF) does exist but is typically covered under the umbrella of high frequency[26]). **Error! Reference source not found.** shows the frequency bands and some properties of the different bands mentioned:

- Less affected by moisture and metals
  - Shorter read range
  - Slower speed
  - Lower data transfer rates
- More affected by moisture and metals
  - Longer read range
  - Higher speed
  - Higher data transfer rates

125-131 kHz | 6.8 MHz | 13.56 MHz | 433 MHz | 860-960 MHz | 2.4-5GHz

Low frequency (LF) | Dual frequency (DF) | High frequency (HF) | Ultra High frequency (UHF) | Bluetooth/WIFI
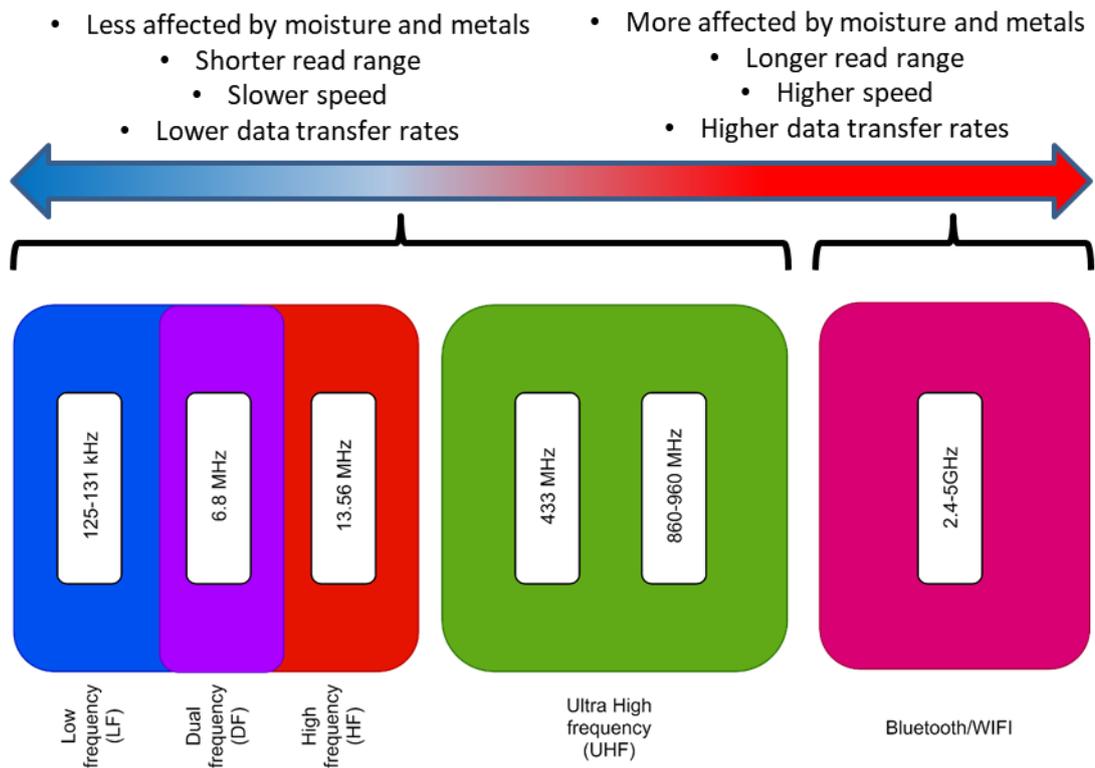
Figure 1.3 – RFID frequency bands (compared to other popular wireless communication methods).

Within these three bands, there are narrow allocations given to nations globally to avoid interference issues. LF systems use frequencies anywhere between 30-300 KHz (although more commonly a narrow band of 125-134.2 KHz is used)[26], HF systems operate with a range of 3-30 MHz, but the most common operating frequency employed is 13.56 MHz[27]. UHF systems can operate between a very wide range (between 300 MHz – 3GHz) but most commonly operate between 865-928 MHz, with some UHF active tags operating at 433 MHz[28]. As active tags usually have higher memory, they only operate at UHF, primarily at the aforementioned 433 MHz. The primary advantage of using LF frequencies is that they are fairly unaffected by adverse environmental conditions as they have longer wavelengths, to the point where radio waves are capable of penetrating metals and water[29]. However, the amount of data that can be transferred is lower than in higher frequency systems. Moreover, the read range of LF tags is considerably lower than HF or UHF. UHF tags are heavily affected by environmental conditions. The short wavelengths used in them mean that metals contacting with radio waves will cause reflection, and water in the surrounding environment will result in absorption of radio waves. However, UHF has the highest read range of the three distinct operating frequencies[30]. HF frequencies are not as adversely affected by their surrounding environment. Metals will still cause reflection of radio waves, but water does not have the same adverse effects on HF tags as in UHF systems. The read range for HF frequencies is lower than that of UHF systems, but higher than in LF systems. As the only RFID systems used in this thesis are passive systems, they will be the focal point of this introduction, so will comprise the bulk of the literature examined where possible.

1.4.4. Passive tag operating principles

1.4.4.1. Backscattering

Backscattering systems utilise incoming radio waves from a reader antenna in order to transmit data via reflecting said radio waves. The incoming radio waves will deliver power to the tag. This in turn powers the integrated chip. The chip will then switch its input impedance between two states[31], facilitating transfer of data. Because the degree to which the tag can reflect the radio waves differs so greatly in either impedance state, switching states is essentially modulating the

degree of backscatter[32], hence why this transmission method is known as modulated backscatter[33].

1.4.4.2. Inductive coupling

Inductive coupling is the other communication system employed in passive systems. Inductive coupling makes use of a phenomenon known as mutual inductance. If two (or possibly more) wire coils are magnetically linked[27], a change in the current of one coil will invoke a change in the voltage of the other coil. As such, tags that utilise inductive coupling require a wire coil in their design to act as the antenna. The reader antenna also has a coil in this communication method. The magnetic field generated by the reader coil induces a change in the tag coil voltage. This in turn powers the integrated chip[30]. Unlike in modulated backscatter, where the integrated chip switches input impedance in order to facilitate data transfer, the integrated chip switches a connected resistor on and off. Current changes in the tag coil fluctuate as a result of the resistor being switched. These currents then affect the magnetic field, which in turn will vary the voltage in the coil within the reader antenna. These variations in voltage are detected by the reader antenna. This is known as load modulation[34]. Inductive coupling only works in near field regions[35] is predominately used in LF and HF systems[36], and are almost always passive systems.

1.5. RFID standards

Whilst the physical and operational differences between different RFID systems have been discussed, the standards that are used to classify them have not been discussed. Global standards are provided by several bodies (including EPCglobal and the international standards organisation). There are three main groupings for classification; memory[37], operating frequency[38,39] and generation[40]. These are listed in Table 1.1, Table 1.2 & Table 1.3:

Table 1.1 - Table showing types of RFID tag based on electronic product code classification.

Electronic product code (EPC) type	Tag type
Class 0	Read only, passive, manufacturer programmed, cannot be written to by user.
Class 1	Single writeable, read only. Can be written to once and cannot be reprogrammed.
Class 2	Rewriteable passive, reprogrammable
Class 3	Semi-passive, reprogrammable
Class 4	Active, reprogrammable
Class 5	Reader, reprogrammable

Table 1.2 - Table showing classes of RFID tag based on generation.

	1st Generation	2nd Generation
Frequency operational range	860-930 MHz	860-960 MHz
Memory capacity	64, 96 bits	96-256 bits
Reprogrammable	Class 0- read only Class 1- single-write, read only	none
Additional features	none	Faster read time, improved reliability.

Table 1.3 - Table showing classes of RFID tag based on operating frequency.

Frequency band	Operational frequency	Wavelength	Application
LF	125-134.2 KHz	2.4 Km	Wildlife monitoring
HF	13.56 MHz	22 meters	Contactless card payment, key card access
UHF	865.5-867.6 MHz (Eur) 915 MHz (U.S.) 950-956 MHz (Japan)	32.8 cm	Inventory, Sensing tags,
Industrial, scientific and medical reserved band (ISM)	2.4 GHz	12.5 cm	Inventory

1.6. Tag substrates

Tag substrates are a highly important consideration when designing an antenna depending on the required purpose. Whilst it is common for substrates to act purely as a protective layers for the tag, bespoke substrates have been employed for niche applications. Rumens[41] et al used a PDMS based substrate; furthermore, substrates can be designed to be flexible so that they allow the attached antenna to conform to a surface. Alternatively, to reduce costs deliberately inexpensive substrates can be used such as paper[42]. This can allow for lower cost fabrication techniques to be utilised such as inkjet printing. Novel substrates have been fabric[43] based substrates that allow for strain to be measured as a function of power loss. Commercially available tags have also employed substrates to enhance sensing capabilities by using water permeable substrates with humidity sensors[44]. 3D printed substrates[45] have also been used recently, allowing for UHF RFID tags to be embroidered as the fabrication of 3D printed substrates uses layer by layer deposition.

1.7. Wireless sensing platforms

RFID tags with sensing capabilities have been developed at an ever expanding rate in the last few years. Although deployment of RFID systems has normally been for inventory management, sensing via RFID is an increasingly attractive application due to the low maintenance, relatively low cost and positional tracking capabilities.
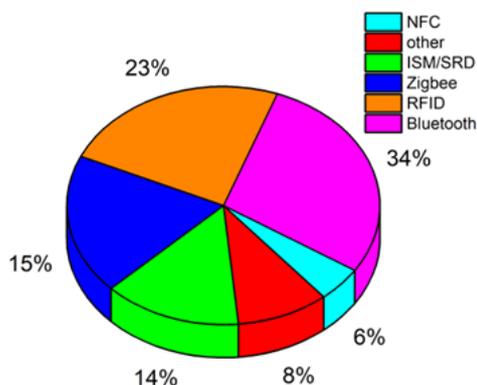
Figure 1.4 - Plots of survey data taken from[46] showing the usage of different communication methods in wireless chemical sensors.

A recent survey of wireless chemical sensors publications[46] found that RFID systems make up nearly a quarter of all systems utilised RFID (shown in Figure 1.4), despite the fact that 95% of all RFID sensing publications were only submitted in the final 3 years of the survey span, showing that RFID is the one of the fastest growing platforms with regards to wireless chemical sensing. Particularly with positional tracking, being able to log information regarding an environment locally via a tag is highly advantageous. Sensing tags are now available commercially, with several different variables that can be monitored. Such is the volume of available tags, only a few will be discussed for each variable of interest.

1.7.2. Temperature sensing RFID tags

Temperature monitoring is an application that is highly desirable for several applications such as food quality control[47]. Pharmaceutical monitoring applications are also highly advantageous, for example blood bag monitoring[48], where knowing storage temperature (as blood must be kept within a $2 - 6$ °C temperature window[49]) and being able to inventory are both vital to

ensuring safe usage for transfusions. Other biological systems such as vaccines also benefit from means of high throughput cold-chain management systems[50].

There is a plethora of commercial offerings for temperature monitoring systems, and temperature monitoring systems are also widely researched. Farsens offer class 1 gen 2 semi-passive UHF tags that can measure ambient temperature and surface temperature[51]. The predominant use case for it is asset tracking where temperature monitoring is also required, such as monitoring temperatures of perishable goods. For monitoring temperature without the necessity for longer read distances or higher memory, there are a plethora of passive tags that utilise RFMicron's Magnus® S3 chip[52] which allows for temperature sensing. The chip utilises a diode that has a change in voltage as a function of temperature. This is then interpreted via software based on a 12-bit sensor code that is relayed to the reader. Both of these systems monitor temperature changes between $40 - 85$ °C.

1.7.3. Chemical sensing RFID tags

In premise, a chemical sensor requires a receptor that is capable of recognising an analyte of interest in some capacity, and a means of transduction that allows this recognition to be interpreted into a useful analytical signal[53]. When considering wireless chemical sensors (WCS's) they have an additional element that facilitates the transmission of this information through wireless communication.

The receptor element of a chemical sensor can have several mechanisms that allow for recognition[54]. Chemical receptors undergo some form of chemical reaction (with the involvement of the analyte). This then gives rise to an analytical signal[54]. Physical sensors do not undergo a chemical reaction, but instead exposure to the analyte results in a change in a property that can be quantified as an analytical signal. Some examples of known physical variables that change in chemical sensors are absorbance[55], refractive index[56], conductivity[57] or a change in mass[58]. In the aforementioned instances, the physical transduction mechanism is also the chemical receptor mechanism. With regards to WCS's, a general schematic can be used

to define the specific components required, shown in a block diagram (elaborated from[53,54,59,])

in Figure 1.5:
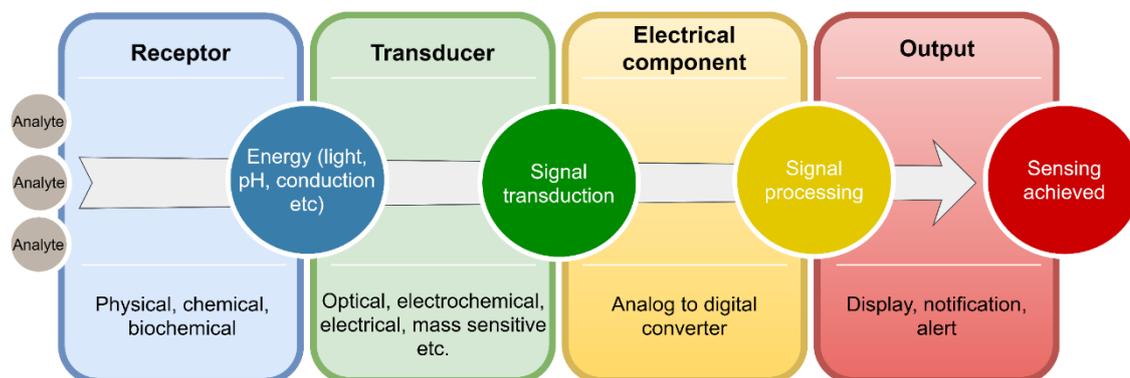
Figure 1.5 - Block diagram showing the main components that comprise a wireless chemical sensor.

There are several transduction mechanisms that can be employed in wireless chemical sensors. According to the IUPAC definition[54], there are seven different classifications for chemical sensors, with several sub-categories within each class. The most commonly used transduction mechanisms employed are optical (most of which are considered physical receptors), electrochemical devices such as potentiometers[60], electrical (commonly metal oxide based[61]), and mass sensitive devices such as piezoelectrics[62]. Aside from these are magnetic[63], thermometric systems which typically exploit a thermal by-product of a known reaction (and then measure the resultant heat produced using a thermistor[64] & a class for all other physical properties (the most common among which being radiation[65]).

Whilst wireless chemical sensing as a field extends far beyond solely using RFID to achieve sensing, there have been several systems that have utilised RFID for chemical sensing. Some of the most common analytes to monitor wirelessly are Glucose, lactate, and uric acid, as well as volatile organic compounds. Kassal[66] et al developed a smart bandage that could monitor uric acid concentration. The bandage incorporated a potentiostat that had electrodes which were highly responsive to changes in hydrogen peroxide concentration. To make the sensor uric acid selective, the sensor incorporated urate oxidase, an enzyme that forms hydrogen peroxide via

oxidation of uric acid. Steinberg[67] et al demonstrated an RFID based potentiostat that could detect glucose concentration by connecting the system to commercially available glucose test strips, allowing the system to detect glucose concentration between 1-10 mM. Steinberg[68] et al have also demonstrated that methanol vapour can be sensed through a conductometric sensor that incorporates poly(3,4-ethylenedioxythiophene) PEDOT:PSS as a sensing polymer. The PEDOT:PSS film changes is resistance with increased methanol exposure, which can be detected and subsequently relayed wirelessly. Inorganic gasses have also been monitored using an RFID based platform. Clement[69] et al utilised Multi-wall carbon nanotubes (MWCNT's) with a conventional passive RFID tag. The MWCNT's were deposited via airbrushing onto a sensor substrate incorporated into the tag. The MWCNT's were oxygen functionalised to increase NO_2 sensitivity, allowing a sensing range of 10-100 ppm. Potyrailo et al[70] developed a passive RFID gas sensor that incorporated a polyetherurethane (PEUT) sensing layer. The novelty of this work was not in the sensing material used, which has been used in several works previously[71,72,73]. The novelty in the work was based upon the approach used to combat the known temperature dependence of polymer loaded gas sensors[74]. Instead of using an uncoated sensor that acts as a reference system to compensate for temperature fluctuations, a dedicated temperature sensor is incorporated into the tag that allowed sensing of water vapour with an environmental temperature change 25-40 °C.

A passive RFID chemiluminescence based monitoring tool was developed by Yazawa[75] for the purpose of point of care monitoring. The system utilised a sandwich immunoassay in a flow channel reactor, which captures target antigens and then exploits a chemiluminescent (CL) substrate. The signal from the CL substrate then corresponds to the amount of the amount of a given analyte, in this instance thyroid stimulating hormone (TSH). The system had a remarkably high sensitivity (0.08 ng/ml), and coupled the CL sensor to a temperature sensor. The purpose of this was two-fold. Environmental temperature could be monitored, and was also used as a calibration means for the CL sensor, that has a temperature dependent response.

1.7.4. pH sensing platforms

pH is the most commonly studied analyte with regards to wireless sensors[46]. The introduction will focus more generally on wireless pH sensing platforms as Chapter 4 identifies passive RFID systems utilised for pH sensing. The most common method of sensing pH is with an ion selective potentiometer; however, this transduction mechanism is elaborated upon in Section 1.7.6.

Aside from potentiometric devices, colormetric wireless sensing systems have been employed frequently to sense pH[76]. The basic operating principle involves capitalising on the colormetric change in pH indicator dyes. The resultant change in the absorption or fluorescence of the dye is then measured by an optical measuring system (commonly a spectrophotometer, fluorimeter[77] or a diode). Indicator dyes have an associated change in colour due to changes in electronic structure as a result of being protonated or deprotonated. The most commonly used indicator dyes for optical pH sensors are the bromocresol series, which almost all wireless pH sensors have utilised, with a few exceptions that will be described.

Whilst the type of indicator dye used is largely the same in optical wireless pH sensors, the design of the system based on its required application and the communication method employed has varied. Czugala[78] et al used a bromocresol purple indicator dye and incorporated it into a paired emitter diode device (PEDD). The PEDD measures changes in reflectance, and allowed for pH between 5-9 with good agreement to a reference pH probe, and was demonstrated to accurately measure the pH of a series of solutions obtained from different parts of a river (again in good agreement with a pH probe). The device was fitted with a Bluetooth transmitter that allowed data to be transmitted to a laptop in real time.

Whilst the previous example focused on water monitoring applications, other approaches have had a heavy focus on wearable pH sensors. Morris[79] et al developed textile based patch that housed an optical detection system that used bromocresol purple as the indicator dye. Whereas the previous example developed a robust casing to house their sensing platform (given the harsher environmental conditions involved in its use), this work intended to make a wearable for sweat monitoring. The design of the sensor was similar to a bandage. The sensor was

incorporated into the bandage. The bandage was made of a superabsorbent material (absortex®) that acted as a wick. Sweat was absorbed by the wick, which was designed so that a channel of the absorbent material would be in close proximity to the pH sensitive dye (essentially acting as a microfluidic channel). The dye would then change colour when sweat of variable pH was exposed to it, detected by the light emitting diode (LED) housed within the sensor. a schematic diagram from the paper is shown in Figure 1.6. Although the schematic is specific to the wearable sensor made in the publication, it serves as a good exemplar of wireless optical pH sensors with regards to requiring a light sensing element (transducer) near the pH sensitive dye (receptor):
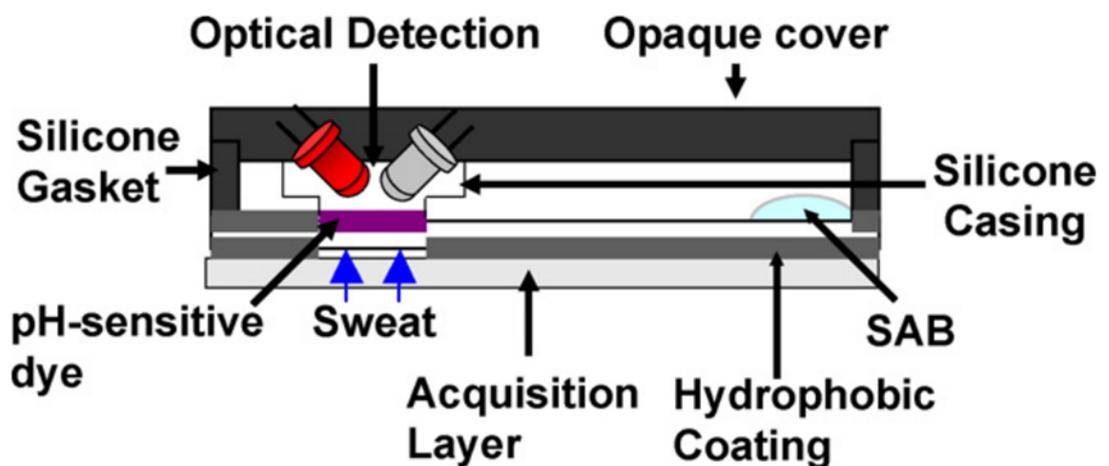
Figure 1.6 – Schematic diagram taken from[79]**, used as an exemplar of an optical pH sensor.**

Works by Curto[80] et al have also used similar designs to the sensor used by Morris et al, with the primary difference being the employed communication method. Morris used the industrial, scientific and medical radio band (ISM) whereas Curto used their wearable with bluetooth. Both sensor platforms could sense pH change in sweat from 5-9.

Whilst Bromocresol dyes are by far the most common dyes used in wireless optical pH sensors, other works have utilised other dyes to achieve pH sensing. Caldara[81] et al used 7-hydroxyphenoxazone (the primary constituent of litmus paper) as a pH sensitive dye that could accurately predict pH between 4-10. The system was designed as a wearable belt, and could

communicate live readouts of sweat pH levels. The system was more obtrusive than the aforementioned patch designed, but did allow for sensing in a wider range.

With regards to potentiometric devices aside from RFID sensors, Bembnowicz[82] et al designed a versatile sensor that could sense several variables, including sodium and lactate content, as well as pH. The system comprised of an ion selective potentiometer connected to a Bluetooth transmitter that was housed in a bespoke 3-D printed assembly. The system allowed for sensing of pH reliably between 2-9. Bluetooth is a popular transmission mode for pH sensing systems. Cheng[83] et al developed a Bluetooth based sensor designed for use as a blood electrolyte monitoring system. The system could sense pH between 2-12 using a bespoke potentiometric sensor that used a tin oxide/indium tin oxide substrate. Exposure to variable pH resulted in a change in the read voltage of the potentiometer, which could then be sent via Bluetooth to a nearby PC for post-processing to determine blood pH, in good agreement with a reference system.

1.7.5. Fringing field "co-planar" capacitive sensors

Capacitive sensing systems are extremely desirable sensing systems that allow for invasive sensing of the dielectric properties of materials within proximity of the sensing tag. These systems have been deployed primarily for humidity monitoring, both commercially (such as the RFMicron RFM2100-AER which is the commercial tag that is modified throughout this work). Fringing field capacitors exploit a phenomenon known as the "fringe effect", also referred to as the edge effect[84]. In a classic capacitor, two parallel plates made of a thin conductive material will pass an electrical charge between the plates, typically with a material in between the slabs. The amount of charge stored in a capacitor is defined as:

$$C = \frac{\varepsilon A}{d} = \frac{k \varepsilon_0 A}{d}$$

Equation 1.1 – Equation for calculating capacitance in a parrallel plate capacitor.

Where C is capacitance, ε is the relative permittivity, A is the area of the metal plates and d is the separation distance between the two plates. In the second equation, k is the permittivity of

a material in between the plates, and ε_0 is the permittivity of free space. Materials with a higher permittivity result in an increased charge between the plates, thereby increasing the capacitance between the plates. Because of this, it is possible to use capacitors as relative permittivity sensors.

Whilst the equation above describes a parallel plate capacitor well as a model, it does not perfectly account for every variable that has an overall effect on capacitance. Whilst the electric fields mostly either store of charge between the plates or travel from one plate to the other, some of the electric fields propagate and fringe out either side of the plates. In an infinitely long parallel plate this would not occur, however in an actual capacitor, electric fields can extend out from the plates. These fields can interact with materials outside of the plate separation area, increasing the cumulative capacitance of the system. Whilst this is normally considered undesirable, the effect can be exploited for sensing purposes. If the plates on a parallel plate capacitor were to be flattened out, then the electric fields that would normally travel (mostly) linearly would instead predominantly fringe out from one plate to the other.
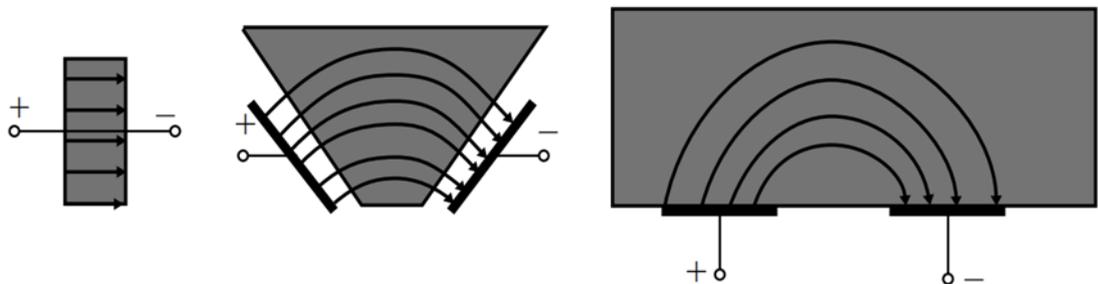
Figure 1.7 - Image taken from[85] demonstrating the "Fringe effect" in coplanar capacitors.

This means that the fringing fields can travel through a material in close proximity to the side that the electrodes face. This principle has been exploited to allow for invasive sensing. Wobscholl[86] et al developed a fringing field capacitor that was built into an active RFID system to measure the relative permittivity of soil/water mixes. The system would detune its normalised frequency as soil moisture content increased due to the fact that water is very high dielectric material. This means the system could accurately predict moisture content from a read distance of 30-100 Meters, and could be calibrated to operate correctly with different soils.

Capacitive sensing has also been exploited in passive RFID systems Quintero[87] et al demonstrated that a polyaniline/carbon nanocomposite could be used for capacitive sensing of ammonia concentration (via conductometric sensing) and relative humidity capacitively in tandem using two different sensing electrodes incorporated into one tag. The humidity sensor element of this system was successfully fabricated through layer by layer inkjet printing cellulose acetate butyrate (CAB) onto one of the interdigitated electrodes. Addition of the CAB to the interdigitated electrodes facilitated the sensing of relative humidity between 20 - 60 % at a range of temperatures.

Oikonomou[88] et al developed a multivariable capacitive sensor that allowed for the sensing of three distinct analytes; ethanol, ethyl acetate and water. This was achieved by coating the interdigitated sensors (IDC's) in three different polymeric coatings, polydimethylsiloxane (PDMS), poly(2-hydroxy ethyl methacrylate) (PHEMA) and poly(n-butyl methacrylate) (PBMA). Each polymer has vastly different swelling ratio to each of the analytes (PDMS has a high affinity for ethyl acetate, PHEMA a high affinity to water and PBMA a high affinity to ethanol). Exploiting this, the system could sense the three different variables within the singular unit.

Shafiq[89] et al developed a reusable capacitive sensor that allowed for sensing of temperature in cold chain supply management. The system used a liquid crystal elastomer (LCE) as an actuator. LCE's undergo a phase transition at variable temperature that causes contraction of expansion of the LCE. This was exploited here to facilitate temperature sensing by loading the LCE in between the antenna and a ground plane. As temperature changes, the LCE expands or contracts, pushing the antenna away from the ground plane (shown in Figure 1.8):
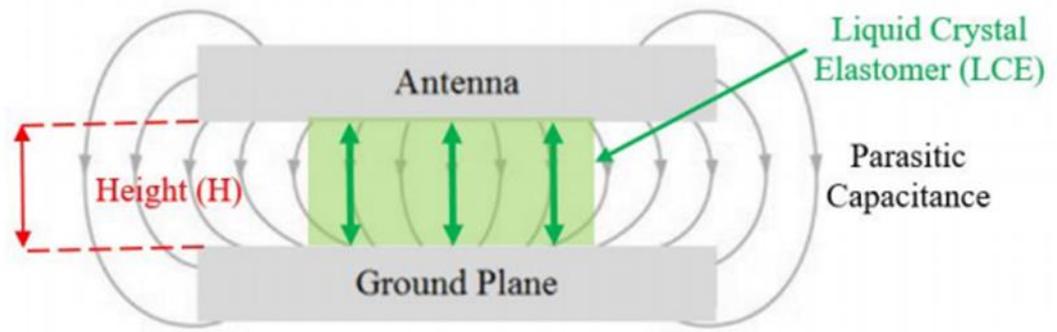
Figure 1.8 – Schematic diagram showing the LCE loaded tag used in[89]**.**

The actuation changes the resonant frequency of the antenna between 902-928 MHz as the antenna is moved towards (or away from) the ground plane, altering the degree of parasitic capacitance from the ground plane. As the temperature at which LCE's undergo phase transition can be modified, the design can be tuned for different temperatures.

1.7.6. Ionic content sensing tags

The majority of ionic content monitoring has been performed on Bluetooth platforms rather than RFID, with publications such as the "SWEATCH"[90], a wearable that allows that allows for real time monitoring of sodium content using a potentiometer housed within the wearable. The information can also be shared with a paired smartphone for ease of use. In this vain, sports monitoring systems are very well researched making up 22 % of wireless chemical sensors and is the predominant application of ionic content monitoring systems. Ionic monitoring systems almost exclusively utilise an Ion selective electrode[91](this is also true of wireless pH sensors), of which an exemplar is shown in Figure 1.9:
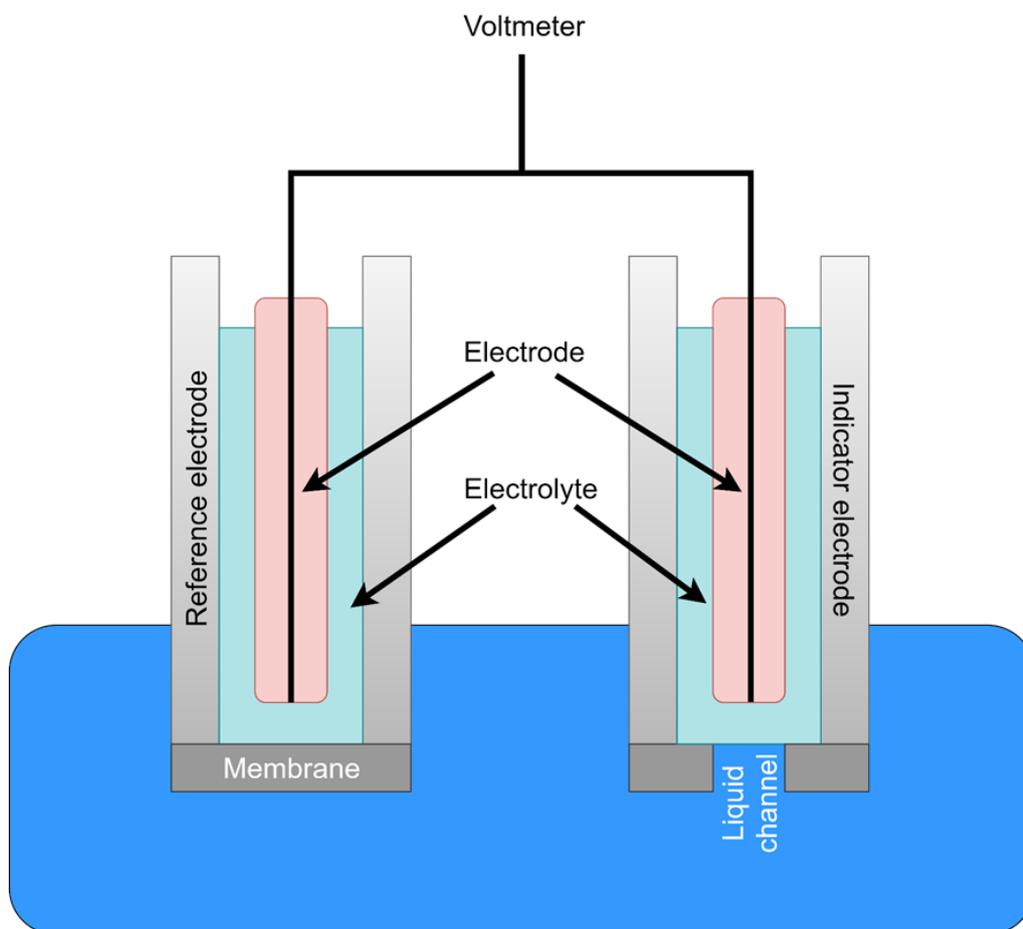
Figure 1.9 – Generic schematic diagram of an ion selective electrode, recreated from[92]**.**

With wireless sensors, although an ion selective electrode will not typically be in the generic

form factor shown in Figure 1.9, they require a reference and an indicator electrode. The

electrolyte housed within the glass (typically a strongly concentrated aqueous electrolyte[77]). The

reference electrode is used to provide a stable potential, whilst the indicator electrode will have

a variable potential. The indicator electrode contains a glass membrane comprised of metal salts

and silica. Ions in solution can interact with the membrane, resulting in a potential change. This

potential change is then measured, determining analyte concentration. Several publications

have exploited ion selective potentiometers for Ionic content sensing in a variety of different

approaches. In a similar vain to the "SWEATCH", Matzeu[93] et al developed an unobtrusive patch

designed to monitor Na$^+$ content in sweat. The ZigBee based system coupled an Ion selective

electrode with a sensing layer of PEDOT based films that dramatically increased the sensitivity

of the system. The sensor was incorporated into a chip with a microfluidic channel, and was

optimised after laboratory based trials to work for the monitoring of Na$^+$ content of sweat produced during cycling sessions, and was capable of monitoring Na$^+$ concentration 10^{-5} & 10^{-1} M. Kaisti[94] et al developed a hand-held Bluetooth sensor and demonstrated the systems capability to monitor K$^+$ concentration from 0.1-100 mM. Furthermore, the sensor included a polyaniline-dinonylnaphthalene sulfonic acid (PANI-DNNSA) as a transducing layer that reduced "drift" in the system. Bandodkhar[95] et al coupled a Ag/AgCl electrode with a polyvinyl butyral membrane that could be screen printed onto a paper substrate. The system could not only be used for in-situ monitoring, but was also reusable.

Examples of a passive RFID system is a wearable developed by Rose et al[96]. A wearable sensor patch was developed that incorporated a potentiometer in its design, allowing for sensing of Na$^+$ content at 50mM, with a 96 % degree of accuracy. The 13.56 MHz tag could also be read using an android smartphone, allowing for in situ monitoring. The "lab on a chip" concept has also extended out to passive RFID systems for ionic content monitoring. Novell et al[97] developed a 13.56 MHz passive RFID system that could be used to monitor ionic content in the range of 0 – 35 mg/ml. The accuracy of the device was compared against a highly sophisticated atomic absorption spectrometer (AAS) with very similar discretion capability with regards to Magnesium content in water samples. The device was also successfully tested practically in a glass vessel. Steinberg et al[98] developed a passive RFID system that incorporated an ion selective optode for use as a potassium ion monitoring system. The system was the one capable of monitoring K$^+$ concentration and was found to produce sensing results comparable to an analytical spectrophotometer. The system worked by exploiting changes in absorption of a photochromic dye that was coupled with a low power photometer. Furthermore, the system could be used with a smartphone and powered via NFC to allow for K$^+$ content sensing between 10^{-3} and 10^{-5} M.

1.7.7. Dielectric properties of materials

The absolute permittivity of a material, typically denoted as ε, is a measure of the amount of capacitance in a particular medium/material in the presence of an applied electric field[99]. A given

amount of charge required to yield one unit of electric flux in a particular medium is the specific definition of permittivity. A material that has a higher permittivity will have a lower amount of electric flux in a material that has a high permittivity, and vice versa for a low permittivity material.

1.7.7.1. Relative permittivity and polarisation

Relative permittivity of a material (commonly known as dielectric constant[100]) Is an expression of the permittivity of a material comparative to vacuum permittivity (8.8541878128(13) × 10^{-12} F·m^{-1})[101]. This is denoted formulaically as:

$$\varepsilon_r(\omega) = \frac{\varepsilon(\omega)}{\varepsilon_0}$$

Equation 1.2 – Equation for calculating relative permittivity.

A dielectric material is considered an electrical insulator. The application of an electric field to a dielectric material will result in a realignment of electrical charges throughout the material, at the atomic level and throughout the bulk of the material. These different methods of alignment are known as polarisation processes, and there are several different mechanisms of polarisation, all of which can contribute to a materials permittivity[102]. The types of polarisation mechanisms are as follows; Ionic, dipolar, atomic and electronic polarisation. These mechanisms are all frequency dependant[103]. In all mechanisms, when the applied electric field changes direction, polarisation will also change direction accordingly. The time it takes for the orientation to change (either by rotation in dipole polarisation or changing the direction of charge in others) is known as the relaxation time[104]. The frequency dependence of each polarisation process is as a result of the relaxation time. When the relaxation time is slower than the frequency of the applied electric field, that polarisation process no longer contributes to the polarisation of the material as it cannot keep up with the electric field. Figure 1.10 shows how each polarisation mechanism is affected by frequency:
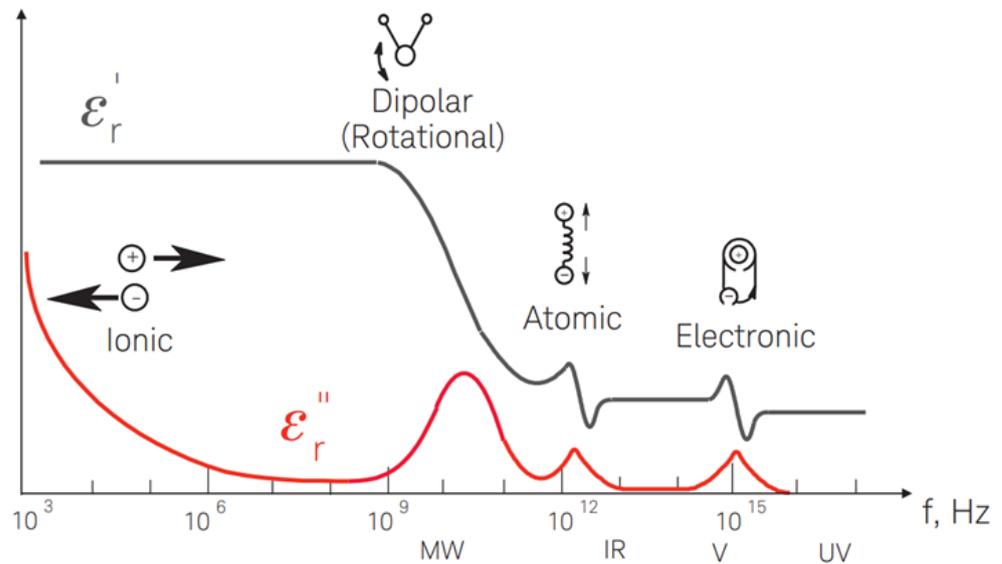
Figure 1.10 - Frequency dependence of dielectric polarisation mechanisms, taken from[104].

Both the real (ε') and imaginary (ε") part of permittivity change with each given polarisation mechanism. Ionic polarisation has the slowest relaxation time, and occurs at lower frequencies, followed by dipolar, atomic and then electronic polarisation (which can occur even at optical frequencies). These mechanisms can also be temperature dependant; Ionic polarisation mechanisms have an increased relative permittivity with increasing temperature due to diffusion of ions facilitated by the increased temperature. Contrastingly, dipole polarisation decreases with increased temperature. This is due to an increase in random motion. At higher temperature, the kinetic energy of a system is elevated, elevating motion. The application of an electric field results in the realignment of molecules, however random motion means that not all dipoles will be aligned in the same instant. As temperature increases, the elevated motion means there is an increased deviation from being aligned with the electric field, lowering the relative polarisation of the material. The higher the degree of polarisation of a material in the presence of an applied electric field, the higher the relative permittivity of the material, and the more electrical energy can be stored in the material.

1.7.7.2. Relative permittivity of aqueous electrolytes

The addition of aqueous electrolytes to a liquid media significantly changes the conductivity of the medium. However, they can also alter the dielectric properties of the material, predominantly in two ways. The ions can associate, forming an ion pair with a larger dipole moment and contributing to polarisation. The ions can also cause a realignment of molecules as a result of solvation[105]. For the example of an aqueous electrolyte in water, the hydration of the ion in water results in water molecules rearranging about the ion, as shown in Figure 1.11. Having the ion situated prevents water molecules from effectively aligning when an electric field is applied. This is the predominant reason that permittivity of water decreases with the addition of salts[106].
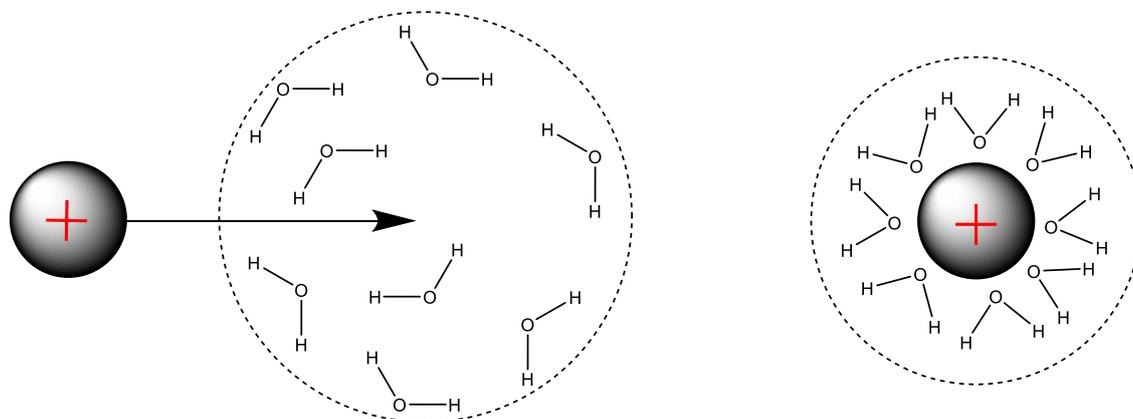
Figure 1.11 - Hydration of a solute solvent mixture.

1.7.7.3. Dielectric loss

Dielectric loss is defined as a materials ability to dissipate electromagnetic energy from an applied electric field, typically in the form of heat[107]. Loss is caused by the dissipation of energy when an electromagnetic field alternates. Reconsidering Figure 1.10, it should be noted that dielectric losses (ε") are notably higher around at the resonant frequencies for each polarisation mechanism. At resonant frequency for the given polarisation mechanism, as polarisation starts to lag relative to the applied field, dissipation increases massively (it is this phenomena that is exploited in microwaves to heat water). Losses tend to be higher in high permittivity

materials[108]. Dielectric loss is typically expressed as a ratio of the real and imaginary permittivity, known as tan δ[109], denoted as:

$$tan\,\delta = \frac{\varepsilon^{''}}{\varepsilon'}$$

Equation 1.3 – Equation for calculating tan δ.

1.8. Polymers

1.8.2. Copolymers and crosslinking

1.8.2.1. Co-polymers

Co-polymers are defined as polymers as that consists of more than one type of monomer in the polymer chain[110]. Within this, there are additional categories used to subdivide types of copolymer based upon the sequence in which the monomers are ordered in the chain. The main types are block copolymers, random copolymers[111], alternating copolymers and gradient copolymers. Block copolymers have long sequences of the same monomer, followed by another extended unit of a different monomer. If two monomers are considered as A and B, for a 10 unit exemplar chain this can be described as (AAAAA-BBBBB). In a random copolymer, the monomers have no specific order and can react together independent of the preceding monomer unit. With alternating copolymers, the monomers in the reaction will have the order (A-B-A-B-A-B-A-B-A-B)[112]. The monomers used in this instance usually have a significantly preferred reactivity to the other monomer in the system, giving rise to the alternating nature of the copolymer. Finally, gradient copolymers[113] will form when there the reactivity of a monomer to an identical monomer unit is preferential to that of a different type of monomer in the system. This means that the majority of the chain will consist of a distribution of chains that will have a high concentration of a repeating unit with one monomer. Eventually, as the preferred monomer concentration decreases the likelihood of the less preferential monomer reacting increases. Finally, when the first monomer is fully used in the polymerisation, the other monomer will react, resulting in a chain with asymmetric concentrations of each monomer at either end of the chain, with a normal distribution of each monomer in the centre of the chain.

1.8.2.2. Cross-linking

Cross-linking is the formation of networks via the joining of multiple polymer chains[114]. The predominant cross-linking mechanisms of interest in this thesis are with regard to polysiloxanes, so cross-linking will only be briefly discussed as a standalone subject here.
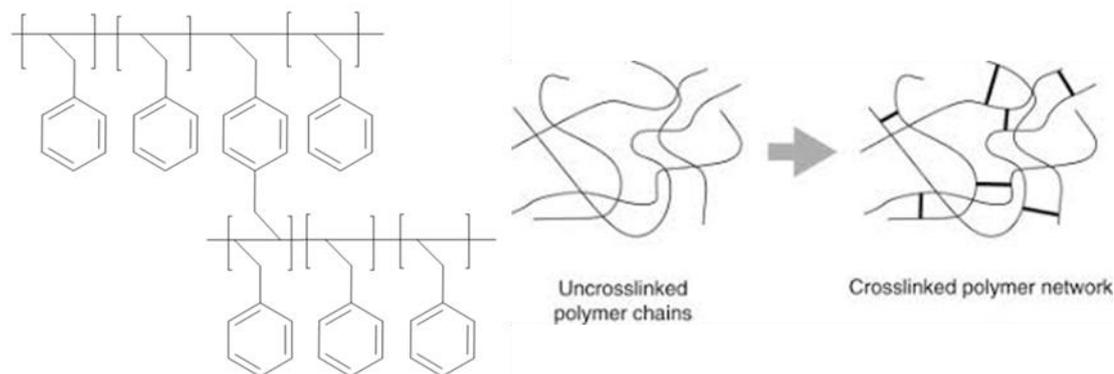
Figure 1.12 - Exemplar of styrene and divinylbenzene cross-linking, and a visual representation of cross-linked polymer network formation taken from[114]**.**

Cross-linking is a mechanism that can be employed in most polymer systems. The most common method of cross-linking is through utilising a monomer that has two different sites that can be polymerised from (known as a bifunctional monomer). Common bifunctional monomers are compounds such as divinylbenzene and bisphenol A-glycidyl methacrylate. The former is used in organic chemistry often, and is co-polymerised with styrene to make a cross-linked polymer that is used as an ion exchange resin[115], with the latter being used as a dental adhesive[116], usually with various other acrylates to form a cross-linked polymer networks. Thermosetting polymers undergo cross-linking reactions when heated, resulting in the formation of rigid polymers that once set do not melt even after cooling. The most famous example of a thermosetting polymer is vulcanised rubber[117], invented by Charles Goodyear, which involves the treatment of natural rubber using sulphur, forming a cross-linked network[118].

Polymer cross-linking results in drastic changes to the properties of the system. Cross-linked polymers have increased mechanical strength and massively increased glass transition temperature (T_g)[119]. Furthermore, cross-linked polymers become insoluble, have increased

brittleness and unlike polymer counterparts no longer have a true melting point (although high enough temperatures will result in degradation).

1.9. Polysiloxanes and silicone elastomers

Polysiloxanes are inorganic polymers that are widely used commercially and in research. There is a considerable amount of interest in this class of compounds due to a wide array of useful properties, primarily (but not limited to) thermal stability, low glass transition temperatures and flexibility. Several polysiloxanes have been of great interest in both industry and research, but none more so than polydimethylsiloxane (shown in Figure 1.13) (PDMS), which is also the most utilised polymer system in this work. Part of the attractiveness of this series of polysiloxanes is the number of useful properties that they possess, being chemically inert, hydrophobic, non-toxic, non-flammable and (usually) optically transparent, as well as their ease of processability means that they are used for an enormous array of applications, including (but not limited to) surfactants[120], microfluidic devices[121], sensing applications[122], lubricants[123] and coatings[124].
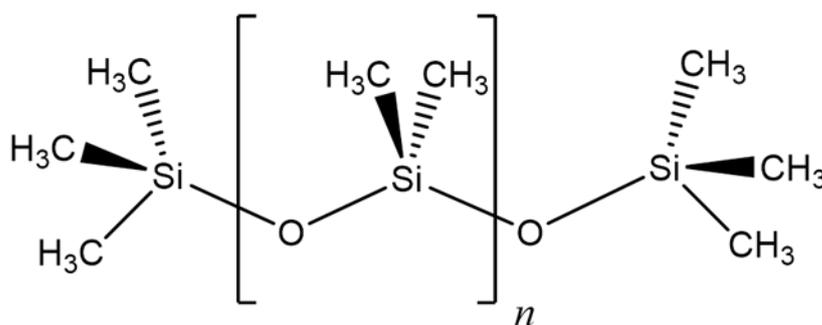
Figure 1.13 - General structure of polydimethylsiloxane (PDMS).

One of the most defining properties of PDMS is its flexibility, which is attributed to characteristics associated with the $Si - O$ bond that comprises the backbone of the molecule. The Si - O bond has a length of 1.64 Å[125] and a bond angle between $Si - O - Si$ of 142.5°. The relatively long bond length coupled with the already obtuse bond angle means that the energy required to open the bond to 180° is very low. These factors attribute to the very low glass transition temperature and melting point, whilst the bond strength of the $Si - O$ bond (and the $Si - C$ bond with regards to the side chains) gives rise to the thermal stability of polysiloxanes. This flexibility in geometry can also be readily modified by alteration of the side chains or

addition of less flexible groups to the polymer backbone, most of which will increase T_g of PDMS as the methyl side are amongst the lowest T_g substituent groups. The methyl chains also play an important role in the hydrophobicity of PDMS, as the side chains that come off of the siloxane backbone directly affect the surface properties. As a result of the flexibility of the backbone, siloxanes can reorder side chain groups with relative ease. Despite the fact that silicates have a very high surface energy, the alkyl substituents in PDMS have a very low surface energy. In PDMS, these two factors mean that the methyl groups can be easily reordered to the surface, resulting in hydrophobic groups being presented at the interface. These two factors give rise to the hydrophobic nature of PDMS.

1.9.2. Synthesis of polysiloxanes

Polysiloxanes are synthesised through polymerisation of functional silanes. These used to be most commonly synthesised via Grignard reaction. One of the most common polysiloxane precursors formed by this reaction is dichlorodimethylsilane using tetrachlorosilane. The process was invented by Frederic Stanley Kipping[126] at the turn of the twentieth century following the invention of the Grignard reaction by Victor Grignard and Paul Sabatier[127]. The reaction scheme for a Grignard reaction of tetrachlorosilane is shown in Figure 1.14:

Whilst this is an effective method for synthesis of the precursor, industrial synthesis of

$$SiCl_4 + 2MeMgX \longrightarrow Me_2SiCl_2 + 2MgClX$$

Figure 1.14 - General reaction scheme for the synthesis of dichlorodimethylsilane via Grignard reaction.

polysiloxanes was not feasible until the 1940's as the Grignard reaction is not a suitable method of dichlorodimethylsilane synthesis in a bulk scale for industrial purposes, however. Industrially, PDMS is now made via the reduction of sand. Sand (SiO_2) is reduced, typically in an electric furnace, breaking down into silicon and diatomic oxygen. Following this, silicon is exposed to methyl chloride in the presence of a copper catalyst, forming a series of methylchlorosilanes, one of which being dichlorodimethylsilane[128]. Dichlorodimethylsilane is then treated with water,

resulting in a hydrolytic polycondensation that yields both linear and cyclic polysiloxanes[129]. Either product is then used to make longer chain polysiloxanes.

1.9.3. Crosslinking of polysiloxanes

There are three main types of crosslinking mechanism used with polysiloxanes are addition, peroxide and condensation curing mechanisms, all of which will be discussed in more detail.

1.9.3.1. Condensation cure crosslinking

Condensation cure crosslinking is the predominant crosslinking mechanism used in this thesis. Condensation curing systems are room temperature crosslinking reactions[130], that are categorised by two main types; room temperature vulcanisation 1 (RTV-1) and RTV-2. RTV-1 systems are one component systems whereas RTV-2 is a two component system[131]. The primary difference between RTV-1 and RTV-2 systems is that RTV-1 systems require ambient moisture in order to cure. Because of this, curing is initiated at the air-component interface and then permeates inwards through diffusion. Whilst RTV-2 systems do not require ambient moisture in order to cure, the presence of moisture will progress the speed of curing dramatically. Both RTV-1 and RTV-2 mechanisms use organometallic tin catalysts to facilitate crosslinking[132]. One of the most common RTV-2 reactions used in this thesis is one of the most common RTV-2 curing systems used generally, the curing of Silanol terminated PDMS. In this system, PDMS with Silanol (Si – OH) terminated groups is cross-linked with an alkoxysilane with multiple crosslinking moieties (most commonly tetraethylorthosilicate, TEOS) in the presence of an organotin salt. The formation of a polymer network happens as each of the end chains of the PDMS reacts with

one of the four units on the TEOS, shown schematically in Figure 1.15:
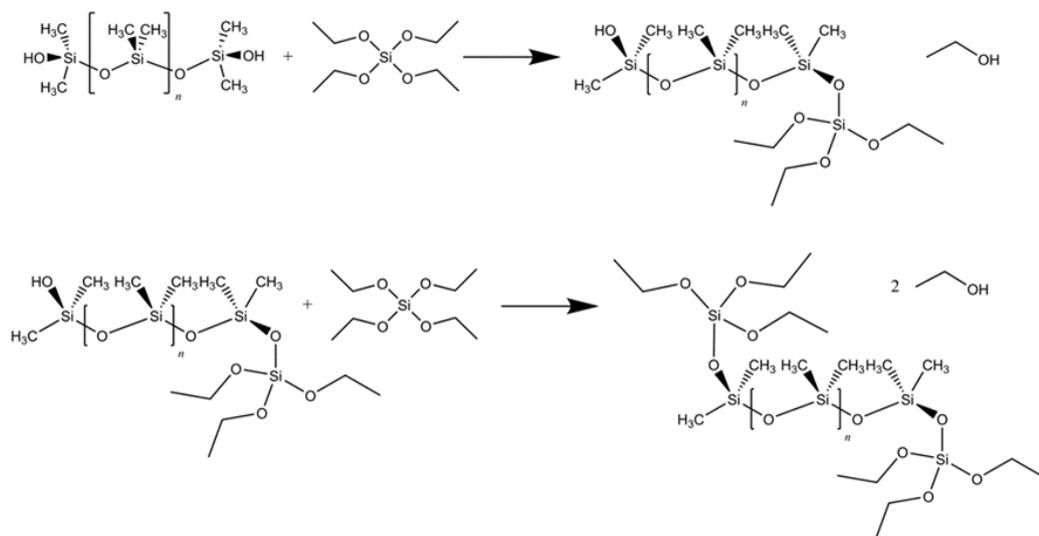
Figure 1.15 - Crosslinking mechanism of Silanol terminated PDMS with tetraethylorthosilicate (TEOS).

1.9.3.2. Peroxide cure crosslinking

Peroxide curing systems are high temperature vulcanisation systems. In these crosslinking systems, free radicals are formed in a peroxide based cross-linker suspended in the system via thermal decomposition[133]. After decomposition, one of the produced peroxide radicals reacts with a methyl side group on the siloxane backbone via hydrogen atom abstraction[134]. This results in the formation of a radical methylene species. Two methylene radicals (one from each siloxane chain involved in the cross-linking) will then dimerise[135], forming the cross-link shown in Figure
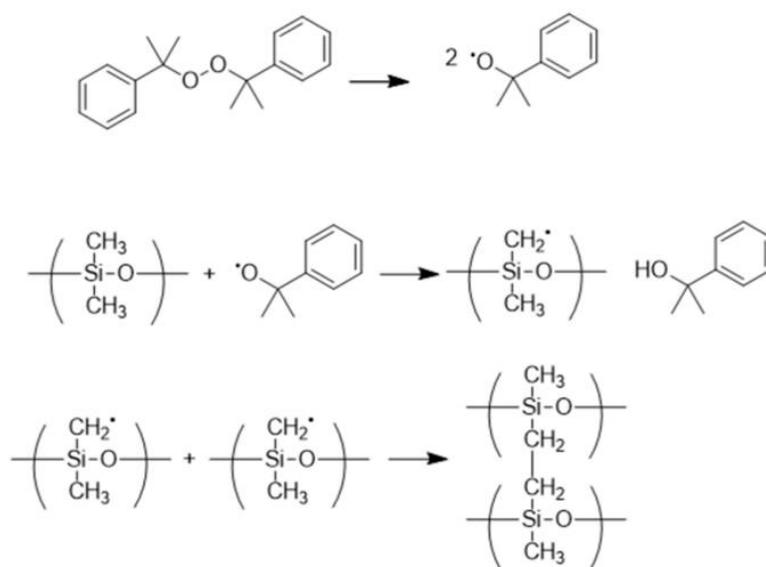
Figure 1.16 - Exemplar peroxide curing reaction of dicumyl peroxide and polydimethylsiloxane.

1.16:

1.9.3.3. Addition cure crosslinking

Addition cure systems, known more frequently as hydrosilylation reactions, occur through reaction of an olefin group with an Si-H group, with either group being on either the siloxane chain or the cross-linker[136]. This is a catalytic reaction that typically uses a platinum or rhodium complex, mostly due to the fact that the first reported hydrosilylation reactions were performed using diacetyl peroxide[137], but was later replaced with metal based catalysts due to the sensitivity of peroxide catalysts. One of these metal catalysts was chloroplatanic acid, but the industry standard platinum catalyst for this reaction is Kartsted's catalyst (more stable and less

air sensitive) .The reaction does not have any side products, but does mean that as the cross-linking proceeds that the metal complex will be trapped in the cross-linked matrix over time. In the Chalk-Harrod mechanism, the first step in hydrosilylation is the oxidative addition of the Si – H bond to the metal centre. Following this, the alkene co-ordinates with the metal complex and undergoes insertion to the metal hydride.
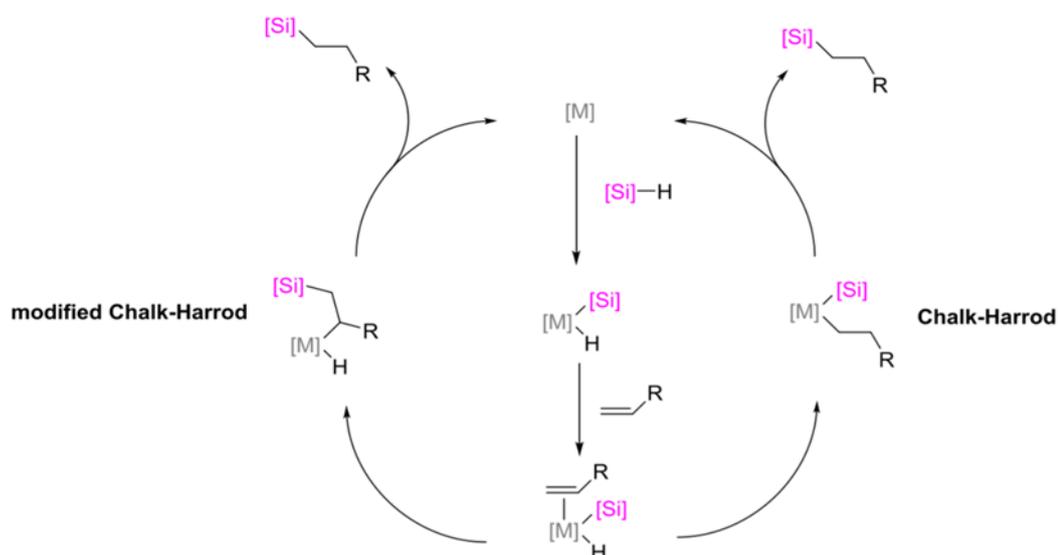

Figure 1.17 - Chalk-Harrod and the modified Chalk-Harrod mechanism taken from[136]**.**

This is followed by reductive elimination of the Si-C, completing the addition. In the modified Chalk-Harrod mechanism[136], the reaction instead proceeds via insertion of the ethylene group into the metal silyl bond. Following this, the reductive elimination of the C – H bond gives the vinylsilane product[138]. In the exemplar reaction shown in, the multiple vinyl groups on the tetravinylsilane allow for one Si – H bond on the terminated PDMS species to be adjoined, and with 4 binding sites a network polymer forms as the reaction proceeds. Hydrosilylation is not solely used as a crosslinking mechanism, and is used to functionalise Si –H groups with allyl species, such as reactive silicones as demonstrated by pinteala[139].

1.10. Aims of the thesis

The primary aim of this thesis was to incorporate polymeric materials into commercially available RFID tags, with intent to alter functionality as a result of incorporating the polymeric material. The tag used in this thesis was the RFMicron RFM2100-AER, a dogbone type antenna

used as a capacitive moisture sensor. The main desire for using commercially available tags over a bespoke counterpart was two-fold. Firstly, performance differences between tags from variables such as fabrication defects would be minimised, allowing any observed changes between incorporating different polymeric materials to be observed with less variation between tags. Secondly, being able to modify and repurpose an existing tag without the requirement for the addition of bespoke sensing components would allow for minimised cost change on a single unit.

Chapter 2 of this thesis demonstrates the effects of modification of the RFMicron tag by way of coating it with an inert polymeric species, cross-linked Silanol terminated PDMS elastomers. The tag is designed to detune when exposed to water. By addition of a hydrophobic boundary layer, the reduction of the effect of bulk water detuning the tag was compared as film thicknesses were sequentially increased. Following this, the tag was then exposed to aqueous electrolyte solutions between 0-2 M using a PDMS layer of 500 μm. The system was found to be able to effectively discriminate aqueous electrolyte concentrations between 0-2 M with a step of 0.1 M. Results found in this chapter have been published in Hillier A, Makarovaite V, Gourlay C, Holder S, Batchelor J, *IEEE Sensors Journal 2019* vol: 19 (14) pp: 5389-5395[140].

Chapter 3 follows on from chapter two of this thesis. Whereas in the first chapter, the inert PDMS layer was used to evaluate the effect of high conductivity aqueous electrolyte solutions on tag performance, chapter 3 focuses on solutions with negligible conductivity relative to aqueous electrolytes. Water/organic solvent mixes were used to demonstrate the effect of sequentially lowering solution permittivity on the coated tag, by way of increasing the content of organic solvent (low permittivity) relative to water (high permittivity).

Chapters 4 and 5 both aim to incorporate a pH responsive boundary layer to the RFMicron, by two different methods. In chapter 4, a reactive silicone two part mix of chloromethylphenethyl terminated PDMS/aminopropyl PDMS was cross-linked together so as to leave unreacted amine side chains in the cross-linked network. In chapter 5, PDMS/PANI (polyaniline) composites were used, with variable PANI loading and preparation methods of the elastomer mix employed to

improve the processability of the PANI composite. The overall aim of this chapter was to capitalise on the desirable high conductivity change of PANI, whilst also benefitting from the desirable mechanical properties of PDMS to make a composite layer that allowed for the sensing of pH changes when coupled with the highly sensitive capacitive sensing tag.

Chapter 6 of this thesis summates the overall conclusions of the research conducted, as well as a discussion of future work that could be undertaken based on the conclusions drawn from this research.

1.11. References:

1   *Comput. Secur.*, 2006, **25**, 18–26.
2   A. Sarac, N. Absi and S. Dauzère-Pérès, *Int. J. Prod. Econ.*, 2010, **128**, 77–95.
3   L. Brown, *A radar history of World War II : technical and military imperatives*, Institute of Physics Pub, 1999.
4   H. Stockman, *Proc. IRE*, 1948, **36**, 1196–1204.
5   R. F. Harrington, *IEEE Trans. Microw. Theory Tech.*, 1963, **11**, 454–455.
6   R. F. Harrington, *Proc. Inst. Electr. Eng.*, 1964, **111**, 617.
7   *Charles Walton, father of RFID technology, dies at 89, https://www.engadget.com/2011/11/29/charles-walton-father-of-rfid-technology-dies-at-89/*, .
8   E. C. . C. JONES, *RFID IN LOGISTICS : a practical introduction.*, CRC PRESS, 2019.
9   RCA, *Electronic license plate for motor vehicles*, 1974.
10   *The electronic passport 2018-2020: trends and best practices, https://www.gemalto.com/govt/travel/electronic-passport-trends*, .
11   *Permanent bag tags | Qantas GB*, .
12   *ITS International - New York's award-winning traffic control system, https://www.itsinternational.com/sections/nafta/features/new-yorks-award-winning-traffic-control-system/*, .
13   *Smart License May Cut Car Theft - 2002-10-11 - Page 1 - RFID Journal, https://www.rfidjournal.com/articles/view?89*, .
14   *California Digital License Rplate Pro - Galpin Motors, https://www.galpin.com/rplatepro/*, .
15   *RFID tags improve tracking, quality on Ford line in Mexico - Control Engineering, https://www.controleng.com/articles/rfid-tags-improve-tracking-quality-on-ford-line-in-mexico*, .
16   *Dutch Forensic Institute Uses RFID to Control Crime Evidence - 2008-10-22 - Page 1 - RFID Journal, https://www.rfidjournal.com/articles/view?4410*, .
17   and A. M. Shannan Williams, Melissa Taylor, Jeffrey Irland, *RFID Technology in Forensic Evidence Management An Assessment of Barriers, Benefits, and Costs*, 2014.
18   F. Bibi, C. Guillaume, N. Gontard and B. Sorli, *Trends Food Sci. Technol.*, 2017, 62, 91–103.
19   K. V. S. Rao, P. V. Nikitin and S. F. Lam, *IEEE Trans. Antennas Propag.*, 2005, 53, 3870–3876.
20   H. K. Patil and T. M. Chen, *Comput. Inf. Secur. Handb.*, 2017, 317–337.
21   S. Ahson and M. Ilyas, *RFID handbook : applications, technology, security, and privacy*, CRC Press, 2008.
22   K. E. Belsey, A. V. S. Parry, C. V Rumens, M. A. Ziai, S. G. Yeates, J. C. Batchelor and S. J. Holder, *J. Mater. Chem. C*, 2017, **5**, 3167–3175.

23 *www.omni-id.com, https://www.omni-id.com/active-rfid-tags/*, 2016.

24 *Temperature   Logger   UHF   Semi-Passive   Tag   -   CAEN   RFID, https://www.caenrfid.com/en/products/a927z/*, .

25 V. Chawla and D. Ha, *IEEE Commun. Mag.*, 2007, **45**, 11–17.

26 N. Park, in *Lecture Notes in Computer Science (including subseries Lecture Notes in Artificial Intelligence and Lecture Notes in Bioinformatics)*, Springer, Berlin, Heidelberg, 2011, vol. 6922 LNAI, pp. 488–496.

27 *The RF in RFID: UHF RFID in Practice - Daniel M. Dobkin*, .

28 J. M. Laheurte, C. Ripoll, D. Paret and C. Loussert, *UHF RFID Technologies for Identification and Traceability*, Wiley Blackwell, Chichester, UK, 2014, vol. 9781848215924.

29 G. Benelli and A. Pozzebo, in *Radio Frequency Identification from System to Applications*, InTech, 2013.

30 K. Finkenzeller, *RFID Handbook: Fundamentals and Applications in Contactless Smart Cards, Radio Frequency Identification and Near-Field Communication, Third Edition*, .

31 *Antenna theory and design : Warren L. Stutzman, Gary A. Thiele - Details - Trove*, .

32 T. Ohira, *Handb. Smart Antennas RFID Syst.*, 2010.

33 S. M. Roy and N. C. Karmakar, in *Handbook of Smart Antennas for RFID Systems*, John Wiley and Sons, 2010, pp. 13–56.

34 V. Chawla and D. S. Ha, *IEEE Commun. Mag.*, 2007, **45**, 11–17.

35 *RFID+ Study Guide and Practice Exams*, Elsevier, 2007.

36 *RFID: A Guide to Radio Frequency Identification - V. Daniel Hunt, Albert Puglia, Mike Puglia*, .

37 S. A. Weis and S. A. Weis, *RFID (Radio Frequency Identification): Principles and Applications*, .

38 D. Sen, P. Sen and A. M. Das, *RFID for energy & utility industries*, PennWell, 2009.

39 *ISO - ISO/IEC 18000-6:2010 - Information technology — Radio frequency identification for item management — Part 6: Parameters for air interface communications at 860 MHz to 960 MHz, https://www.iso.org/standard/46149.html*, .

40 *ISO - ISO/IEC 18000-63:2013 - Information technology — Radio frequency identification for item management — Part 63: Parameters for air interface communications at 860 MHz to 960 MHz Type C, https://www.iso.org/standard/59643.html*, .

41 C. V. Rumens, M. A. Ziai, K. E. Belsey, J. C. Batchelor and S. J. Holder, *J. Mater. Chem. C*, 2015, **3**, 10091–10098.

42 V. Lakafosis, A. Rida, R. Vyas, L. Yang, S. Nikolaou and M. M. Tentzeris, *Proc. IEEE*, 2010, **98**, 1601–1609.

43 J. Zhang, G. Y. Tian, A. M. J. Marindra, A. I. Sunny and A. B. Zhao, *Sensors*, **17**, 265–298.

44 *RFM2100 wireless flexible moisture sensor - RFMicron, http://rfmicron.com/rfm2100-wireless-flexible-moisture-sensor/*, .

45 M. Rizwan, M. Guibert, A. Massicart, J. Torres, L. Sydanheimo, L. Ukkonen, T. Bjorninen and J. Virkki, in *2017 Progress in Electromagnetics Research Symposium - Fall (PIERS - FALL)*, IEEE, 2017, pp. 818–822.

46 P. Kassal, M. D. Steinberg and I. M. Steinberg, *Sensors Actuators B Chem.*, 2018, **266**, 228–245.

47 T. Athauda and N. C. Karmakar, *Wirel. Power Transf.*, 2019, 1–14.

48 D. S. Kim, S. K. Yoo, H. O. Kim, B. C. Chang, H. S. Bae and S. J. Kim, in *Proceedings of the IEEE/EMBS Region 8 International Conference on Information Technology Applications in Biomedicine, ITAB*, 2008, pp. 320–322.

49 J. Hardwick, *ISBT Sci. Ser.*, 2008, **3**, 177–196.

50 F. O. O. Gomes, L. De Paula, J. C. S. Santos, L. Courcelle, D. Piovani, F. Viera, F. Henes and M. Lubaszewski, in *Proceedings - IEEE International Symposium on Circuits and Systems*, Institute of Electrical and Electronics Engineers Inc., 2015, vol. 2015-July, pp. 2113–2116.

51 *BAP   -   Temperature   -   Farsens   Wireless   Sensors, http://www.farsens.com/en/products/battery-assisted-passive-sensors/temperature/*, .

52   *RFM3300-E   Magnus®-S3   M3E   Passive   Sensor   IC   -   Axzon   website,*
      https://axzon.com/rfm3300-e-magnus-s3-m3e-passive-sensor-ic/, .

53   S. Coyle, V. F. Curto, F. Benito-Lopez, L. Florea and D. Diamond, in *Wearable Sensors:*
      Fundamentals, Implementation and Applications, Elsevier Inc., 2014, pp. 65–83.

54   A. Hulanicki, S. Glab and F. Ingman, *Pure Appl. Chem.*, 1991, **63**, 1247–1250.

55   L. W. Burgess, *Sensors Actuators B. Chem.*, 1995, **29**, 10–15.

56   X.-D. Wang and O. S. Wolfbeis, *Fiber-Optic Chemical Sensors and Biosensors (2013–2015)*,
      2015.

57   A. Somov, A. Baranov, A. Savkin, D. Spirjakin, A. Spirjakin and R. Passerone, *Sensors*
      Actuators, A Phys., 2011, **171**, 398–405.

58   F. L. Dickert, O. Hayden and M. E. Zenkel, *Anal. Chem.*, 1999, **71**, 1338–1341.

59   N. Bhalla, P. Jolly, N. Formisano and P. Estrela, *Essays Biochem.*, 2016, **60**, 1–8.

60   Y. Mendelson, in *Introduction to Biomedical Engineering*, Elsevier, 2012, pp. 609–666.

61   A. Dey, *Mater. Sci. Eng. B Solid-State Mater. Adv. Technol.*, 2018, 229, 206–217.

62   *Novel   piezoelectric   transducers   for   high   voltage   measurements,*
      https://www.researchgate.net/publication/277095786_Novel_piezoelectric_transducer
      s_for_high_voltage_measurements, .

63   A. Lenk, R. G. Ballas, R. Werthschützky and G. Pfeifer, 2011, pp. 247–311.

64   J. Janata, *Principles of Chemical Sensors*, Springer US, 2009.

65   J. Lancaster, *Med. Phys.*, 1986, **13**, 546–546.

66   P. Kassal, M. Zubak, G. Scheipl, G. J. Mohr, M. D. Steinberg and I. Murković Steinberg,
      Sensors Actuators B Chem., 2017, **246**, 455–460.

67   M. D. Steinberg, P. Kassal, I. Kereković and I. M. Steinberg, *Talanta*, 2015, **143**, 178–183.

68   M. D. Steinberg, I. Žura and I. Murkovic Steinberg, *Sensors Actuators B Chem.*, 2014, **196**,
      208–214.

69   A. Ramos, P. Clement, A. Lazaro, E. Llobet and D. Girbau, *IEEE Antennas Wirel. Propag.*
      Lett., 2015, **14**, 1145–1148.

70   R. A. Potyrailo and C. Surman, *A Passive Radio-Frequency Identification (RFID) Gas Sensor*
      With Self-Correction Against Fluctuations of Ambient Temperature, 2013.

71   F. Josse, R. Lukas, R. Zhou, S. Schneider and D. Everhart, *AC-impedance-based chemical*
      sensors for organic solvent vapors, 1996, vol. 35.

72   F. Razan, C. Zimmermann, D. Rebière, C. Déjous, J. Pistré, M. Destarac and B. Pavageau,
      in *Sensors and Actuators, B: Chemical*, 2005, vol. 108, pp. 917–924.

73   D. Then, A. Vidic and C. Ziegler, *Sensors Actuators, B Chem.*, 2006, **117**, 1–9.

74   S. J. and and R. B. Brown*, *Chemical Sensors with Integrated Electronics*, American
      Chemical Society, 2008.

75   Y. Yazawa, T. Oonishi, K. Watanabe, A. Shiratori, S. Funaoka and M. Fukushima, *J. Biosci.*
      Bioeng., 2014, **118**, 344–349.

76   D. Wencel, T. Abel and C. McDonagh, *Anal. Chem.*, 2014, 86, 15–29.

77   M. Aller and J. Pennell, *The Measurement, Instrumentation and Sensors Handbook*, 1999.

78   M. Czugala, R. Gorkin, T. Phelan, J. Gaughran, V. F. Curto, J. Ducrée, D. Diamond and F.
      Benito-Lopez, , DOI:10.1039/c2lc40781g.

79   D. Morris, S. Coyle, Y. Wu, K. T. Lau, G. Wallace and D. Diamond, *Sensors Actuators, B*
      Chem., 2009, **139**, 231–236.

80   V. F. Curto, S. Coyle, R. Byrne, N. Angelov, D. Diamond and F. Benito-Lopez, *Sensors*
      Actuators, B Chem., 2012, **175**, 263–270.

81   V. F. Curto, S. Coyle, R. Byrne, N. Angelov, D. Diamond and F. Benito-Lopez, *Sensors*
      Actuators, B Chem., , DOI:10.1016/j.snb.2012.02.010.

82   P. Bembnowicz, G. Z. Yang, S. Anastasova, A. M. Spehar-Délèze and P. Vadgama, in *2013*
      IEEE International Conference on Body Sensor Networks, BSN 2013, 2013.

83   J. F. Cheng, J. C. Chou, T. P. Sun, S. K. Hsiung and H. L. Kao, *IEEE Sens. J.*, 2012, **12**, 967–
      977.

84   W. M. Saslow, *Electricity, magnetism, and light*, Academic Press, 2002.

85   X. Hu and W. Yang, , DOI:10.1108/02602281011010772.

86   D. Wobschall and D. Lakshmanan, in *IEEE Sensors, 2005.*, IEEE, pp. 8–11.

87   A. Vásquez Quintero, F. Molina-Lopez, E. C. P. Smits, E. Danesh, J. Van Den Brand, K. Persaud, A. Oprea, N. Barsan, U. Weimar, N. F. De Rooij and D. Briand, *Flex. Print. Electron.*, , DOI:10.1088/2058-8585/1/2/025003.

88   P. Oikonomou, A. Botsialas, A. Olziersky, I. Kazas, I. Stratakos, S. Katsikas, D. Dimas, K. Mermikli, G. Sotiropoulos, D. Goustouridis, I. Raptis and M. Sanopoulou, *Sensors Actuators, B Chem.*, 2016, **224**, 266–274.

89   Y. Shafiq, J. Gibson, H. Kim, C. P. Ambulo, T. H. Ware and S. V. Georgakopoulos, *IEEE Trans. Antennas Propag.*, , DOI:10.1109/TAP.2019.2921150.

90   T. Glennon, C. O'Quigley, M. McCaul, G. Matzeu, S. Beirne, G. G. Wallace, F. Stroiescu, N. O'Mahoney, P. White and D. Diamond, *Electroanalysis*, 2016, **28**, 1283–1289.

91   S. Głąb, M. Maj-Żurawska and A. Hulanicki, in *Reference Module in Chemistry, Molecular Sciences and Chemical Engineering*, Elsevier, 2013.

92   *1.7: Ion Selective Electrode Analysis - Chemistry LibreTexts*, .

93   G. Matzeu, C. O'Quigley, E. McNamara, C. Zuliani, C. Fay, T. Glennon and D. Diamond, *Anal. Methods*, 2016, **8**, 64–71.

94   M. Kaisti, Z. Boeva, J. Koskinen, S. Nieminen, J. Bobacka and K. Levon, , DOI:10.1021/acssensors.6b00520.

95   A. J. Bandodkar, D. Molinnus, O. Mirza, T. Guinovart, J. R. Windmiller, G. Valdés-Ramírez, F. J. Andrade, M. J. Schöning and J. Wang, *Biosens. Bioelectron.*, 2014, **54**, 603–609.

96   D. P. Rose, M. E. Ratterman, D. K. Griffin, L. Hou, N. Kelley-Loughnane, R. R. Naik, J. A. Hagen, I. Papautsky and J. C. Heikenfeld, *IEEE Trans. Biomed. Eng.*, 2015, **62**, 1457–1465.

97   M. Novell, M. Steinberg, M. Steinberg, F. X. Rius and F. J. Andrade, , DOI:10.1039/c3an00727h.

98   M. D. Steinberg, P. Kassal, B. Tkalčec and I. Murković Steinberg, *Talanta*, 2014, **118**, 375–381.

99   J. P. Dunsmore, *Handbook of Microwave Component Measurements*, John Wiley & Sons, Ltd, Chichester, UK, 2012.

100   *IEEE Std 211-1997*, 1998.

101   CODATA Value: vacuum electric permittivity, https://physics.nist.gov/cgi-bin/cuu/Value?ep0, (accessed).

102   R. A. Potyrailo, N. Nagraj, Z. Tang, F. J. Mondello, C. Surman and W. Morris, , DOI:10.1021/jf302416y.

103   Sam-Shajing Sun, Larry R. Dalton, Sam-Shajing Sun and Larry R. Dalton, Introduction to Organic Electronic and Optoelectronic Materials and Devices (Optical Science and Engineering Series), https://dl.acm.org/citation.cfm?id=1386924, (accessed).

104   E. Capacitor, *Dielectric Properties of Materials Industry Applications/Products*, .

105   N. E. Hill, *Dielectric properties and molecular behaviour*, Van Nostrand Reinhold, London,;New York, 1969.

106   G. Theses and S. Bhat, *Salinity (conductivity) sensor based on parallel plate capacitors Scholar Commons Citation*, 2005.

107   *Microwave/RF Applicators and Probes*, Elsevier, 2015.

108   B. K. P. (Brendan K. P. Scaife, *Principles of dielectrics*, Clarendon Press, 1989.

109   L. F. (Lin F. Chen, *Microwave electronics : measurement and materials characterization*, Wiley, 2004.

110   N. Hadjichristidis, S. Pispas and G. Floudas, *Block Copolymers*, John Wiley & Sons, Inc., Hoboken, USA, 2002.

111   A. Rudin and P. Choi, *The Elements of Polymer Science and Engineering*, Elsevier Inc., 2013.

112   J. M. G. (John M. G. Cowie, *Alternating copolymers*, Plenum Press, 1985.

113   L. Billon and O. Borisov, *Macromolecular self-assembly*, wiley, 2016.

114   Indole-3-carbinol - an overview | ScienceDirect Topics,

https://www.sciencedirect.com/topics/engineering/chemical-crosslinking, (accessed).

115   D. H. James and W. M. Castor, in *Ullmann's Encyclopedia of Industrial Chemistry*, Wiley-VCH Verlag GmbH & Co. KGaA, Weinheim, Germany, 2011.

116   Silux | C29H36O8 - PubChem, https://pubchem.ncbi.nlm.nih.gov/compound/Bis-gma#section=Uses, (accessed).

117   J. E. Mark, B. Erman and M. Roland, *The science and technology of rubber*, .

118   M. Akiba and A. S. Hashim, *Prog. Polym. Sci.*, 1997, **22**, 475–521.

119   Glass Transition Temperature - an overview | ScienceDirect Topics, https://www.sciencedirect.com/topics/biochemistry-genetics-and-molecular-biology/glass-transition-temperature, (accessed).

120   M. Bohnet, *Ullmann's encyclopedia of industrial chemistry*, .

121   J. C. McDonald, D. C. Duffy, J. R. Anderson, D. T. Chiu, H. Wu, O. J. A. Schueller and G. M. Whitesides, *Electrophoresis*, 2000, **21**, 27–40.

122   J. C. Lötters, W. Olthuis, P. H. Veltink and P. Bergveld, *J. Micromechanics Microengineering*, 1997, **7**, 145–147.

123   L. S. Tottey, S. A. Coulson, G. E. Wevers, L. Fabian, H. McClelland and M. Dustin, *J. Forensic Sci.*, 2019, **64**, 207–217.

124   U. Eduok, O. Faye and J. Szpunar, , DOI:10.1016/j.porgcoat.2017.05.012.

125   H. Sten~i~kt$, B. Post and I. Fankuchen, *The Crystal Structure of Octamethyl Cyclotetrasiloxane**, 1955, vol. 8.

126   K. L. Mittal and A. (Antonio) Pizzi, *Handbook of sealant technology*, CRC Press, 2009.

127   The Nobel Prize in Chemistry 1912 - NobelPrize.org, https://www.nobelprize.org/prizes/chemistry/1912/summary/, (accessed).

128   E. G. Rochow and W. S. Tatlock, John Wiley & Sons, Ltd, 2007, pp. 56–58.

129   A. Mitra and D. A. Atwood, in *Encyclopedia of Inorganic Chemistry*, John Wiley & Sons, Ltd, Chichester, UK, 2006.

130   Chemistry and Properties of Crosslinked Polymers | ScienceDirect, https://www.sciencedirect.com/book/9780124322509/chemistry-and-properties-of-crosslinked-polymers, (accessed).

131   J. Kouyoumdjian, V. A. Chalian and B. K. Moore, *J. Prosthet. Dent.*, 1985, **53**, 388–391.

132   E. Yousif, *Arch. Org. Inorg. Chem. Sci.*, , DOI:10.32474/aoics.2018.03.000161.

133   The Rubber Formulary | ScienceDirect, https://www.sciencedirect.com/book/9780815514343/the-rubber-formulary, (accessed).

134   Handbook of Thermal Analysis and Calorimetry | ScienceDirect.com, https://www.sciencedirect.com/handbook/handbook-of-thermal-analysis-and-calorimetry, (accessed).

135   M. Kutz, *Applied Plastics Engineering Handbook*, Elsevier Inc., 2011.

136   R. Hofmann, M. Vlatković, F. Wiesbrock, R. J. Hofmann, M. Vlatković and F. Wiesbrock, *Polymers (Basel).*, 2017, **9**, 534.

137   *Hydrosilylation*, Springer Netherlands, 2009.

138   S. Sakaki, N. Mizoe and M. Sugimoto, *Theoretical Study of Platinum(0)-Catalyzed Hydrosilylation of Ethylene. Chalk-Harrod Mechanism or Modified Chalk-Harrod Mechanism*, 1998.

139   M. Pinteală, V. Harabagiu, C. Cotzur and B. C. Simionescu, *Eur. Polym. J.*, 1994, **30**, 309–312.

140   A. J. R. Hillier, V. Makarovaite, C. W. Gourlay, S. J. Holder and J. C. Batchelor, *IEEE Sens. J.*, 2019, **19**, 5389–5395.

Chapter 2: A Passive UHF RFID Dielectric Sensor for Aqueous Electrolytes.

2.1. Introduction

The second most commonly researched analyte with regards to wireless chemical sensors (commonly referred to as WCS's)[2] are aqueous electrolytes. The predominant bulk of research within the study of aqueous electrolytes has been sweat monitoring, with less of an emphasis on bulk aqueous electrolyte monitoring. One such example of sweat monitoring is the "SWEATCH"[3], a Bluetooth based wearable that can monitor sodium ion concentration in sweat and relay information to a connected smartphone. Another approach has utilized RFID systems[4] with adhesive backings that can be applied as a wearable, and can relay potentiometric information about sodium content in sweat to a smartphone via NFC. The common sensing method in all of the above examples is an ion selective potentiometer. Cheaper disposable alternatives have also been proposed for usage in the pharmaceutical industry[5].

A less common but effective means of sensing of a multitude of variables has been to repurpose pre-existing RFID tags with chemically sensitive materials. Some variables that have been monitored through this approach have been ammonia concentration[6], gas sensing[7] and solvent vapour monitioring[8]. These systems are often designed with the purpose of monitoring a specific variable. solvent vapour monitoring has also been achieved within our group using polydimethylsiloxane (PDMS) substrates coupled with a prototype RFID sensor[9]. Various solvent vapours were used to displace a feed loop adhered to the top of the substrate, resulting in an increased transmitted power required upon displacement.

Until recently, sensing has been only been achievable by using the above method described in the PDMS swelling sensor, whereby a drop-off in a performance variable is exploited. The extent to which a tag is adversely affected is post processed and this determines the degree of sensing. This method is considered a "one-way" method of sensing, where the sensing is performed on the reader side[10]. Newer tags are now available that can perform impedance matching when exposed to a detuning condition, and are primarily used for low water content moisture sensing.[11,12] In the case of [12],this allows sensing data to be procured from the tag side in the form of a 5-bit sensor code, meaning that the requirement for post processing is reduced.

Furthermore, tags are more impervious to performance drop-offs. However in the case of [12], the water permeable substrate limits the tag to being single-use. This system utilizes a fringing field capacitor. Traditional parallel plate capacitors, which have been used for the measurement of aqueous electrolyte solutions[13], have taken advantage of the "conductivity effect" that increases the capacitive loading to determine the salinity of aqueous analytes. A fringing field capacitor resembles a parallel plate capacitor in that it measures capacitance; however the method by which it does is predominantly through fringing fields, fully exploiting a phenomenon known as the "fringe effect"[14]. As the fields extend out away from the plates, the material under test doesn't need to be loaded in between the plates. Instead, the fields can permeate the material away from the plates, and capacitance of the material can be measured invasively.

Here, we repurpose the commercially available RFMicron RFM 2100-AER using a PDMS layer, with the intention of being able to tune the degree of bulk water (or analyte) that the tag can be exposed to, whilst also making the single-use tag reusable. Furthermore, we aim to utilize the coated tag for sensing of bulk quantities of aqueous electrolytes.

2.2. Experimental

2.3. Materials and apparatus

Silanol-terminated polydimethylsiloxane (PDMS) (cSt 1000, M_W 26,000) was obtained from fluorochem Ltd and used as received. Tetraethylorthosilicate (TEOS) (99%), tin (II) ethyl hexanoate (95%), rubidium chloride (RbCl) and lithium chloride (LiCl) were purchased from Sigma Aldrich. TEOS was used as received, whereas tin (II) ethyl hexanoate was prepared as a 1 M solution in toluene before use and RbCl and LiCl were dissolved in water and used as stock solutions between 0-2 M. Sodium chloride (NaCl) potassium chloride (KCL) and toluene (lab grade) were purchased from Fisher Scientific. KCl solutions were dissolved in water and used as stock solutions between 0-2 M and NaCl stock solutions were made between 0-5 M. Homogenous mixing of the elastomer components was achieved using a DAC 150FV2-K speedmixer[15] and elastomers were then doctor bladed onto an RFMicron RFM-2100 AER using an automatic precision film applicator MTCX4, purchased from MTV-Messtechnik (blade width

=70 mm, thickness adjustability 0-3000 μm)[16]. RFID measurements were performed on Voyantic® Tagformance equipment[17]. Relative permittivity measurements were performed using a Speag DAK 3.5 dielectric measurement probe attached to a Rohde & Schwarz ZXX vector network analyser. FT-IR measurements were performed using a Shimadzu IRAffinity spectrometer with a Specac Golden Gate™ ATR sampling accessory, and each sample was subjected to 64 scans, at a resolution of 4 cm^{-1} (between 500-4500 cm^{-1}).

2.3.1. Tag design
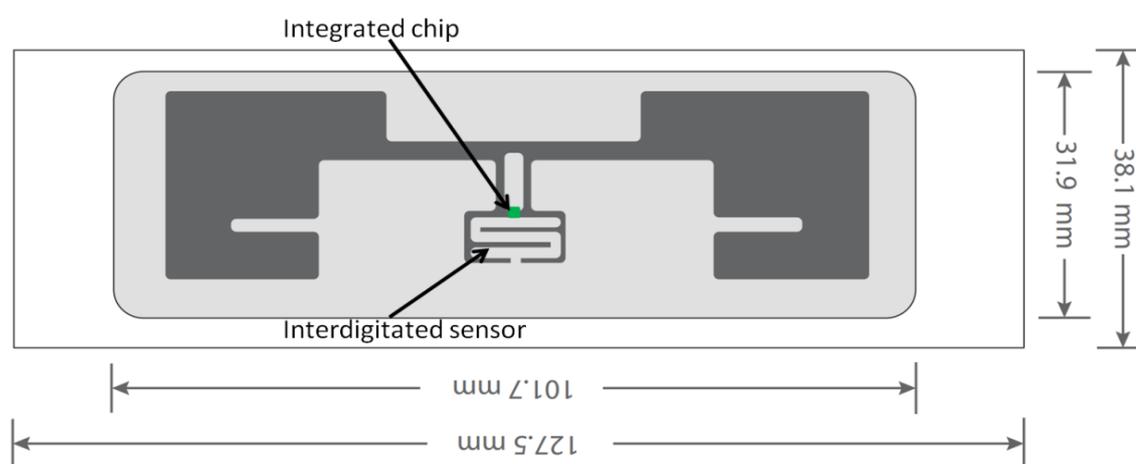
Figure 2.1 - Schematic diagram of the RFMicron RFM-2100 AER, with the interdigitated electrode and the integrated chip indicated. The dimensions of the acetate backing are also included.

The tag used for film application studies was the RFMicron RFM-2100 AER, shown in Figure 2.1. The previous application of this tag was as a passive moisture sensor. The AER version is designed for use in the European bandwidth (865.6-867.6 MHz)[18]. The tag houses an interdigitated capacitive (IDC) sensing electrode, as well as an auto-tuning chip. The chip is designed to auto-tune, switching its internal capacitance between 1.9-2.9 pF dependent on how mismatched the circuit is from external stimuli. The resulting tuning state from external stimuli is then transmitted as a "sensor code" value to the reader. The tag is fabricated on a PET substrate. The tag antenna conductor is made from aluminium. As these tags are designed to be

stuck onto substrates for passive monitoring, the topside of the tag is coated in an adhesive. This is then covered in an acetate backing[12].

2.3.2. Synthesis of PDMS elastomers

Silanol-terminated PDMS (16.00 g, 6.16 x10-4 mol), cross-linking agent TEOS (0.26 g, 12.48 x 10-4 mol, stoichiometric ratio of 1:4 as TEOS has 4 available binding sites), and tin(II) ethyl hexanoate (0.72 cm3, 0.6 M solution in toluene) were mixed at 3500 rpm for 120 seconds in total (this system was modified from the same system used in [9]). Initially the PDMS and the TEOS are mixed together for 60 seconds, and then the tin catalyst is
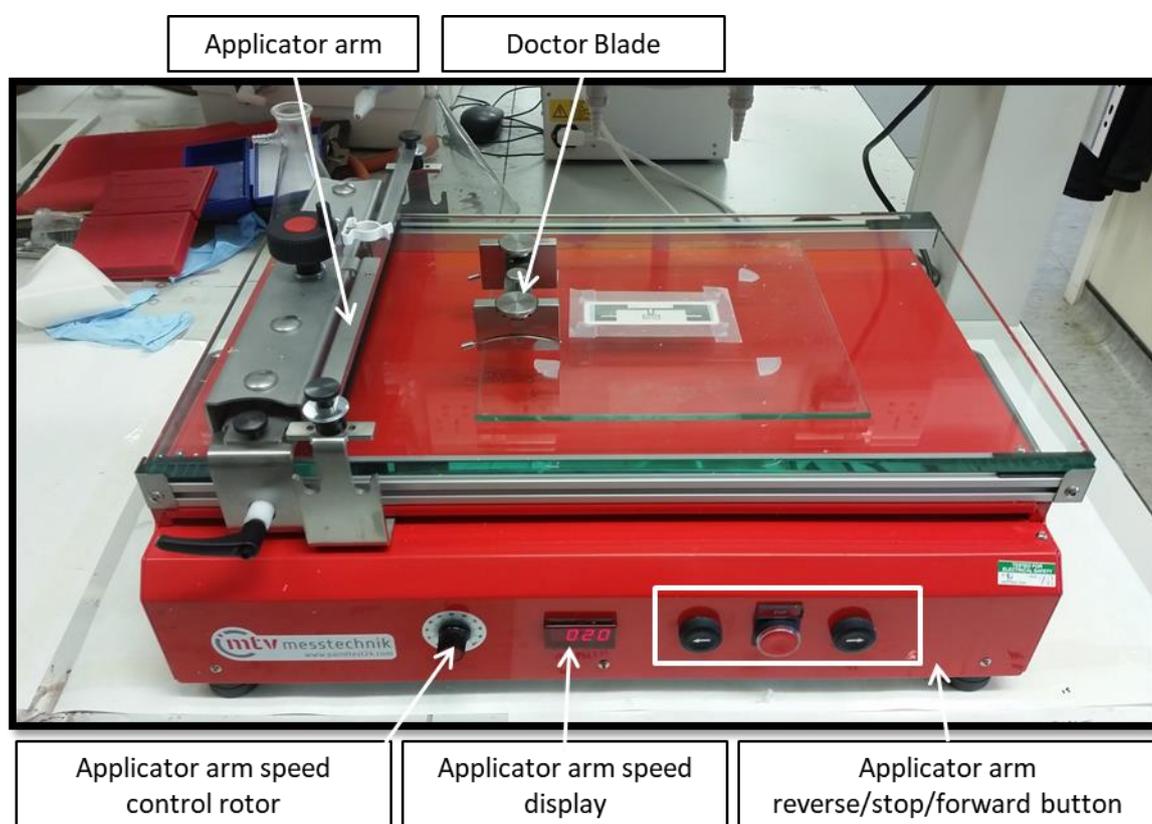
Figure 2.2 – Picture showing the MTV-Messtechnik doctor blade with an adhered RFID tag on a glass substrate.

added and the mix is spun for a further 60 seconds at 3500 rpm. This was due to the fact that without first homogenising the cross-linking agent with the PDMS, adding the catalyst would result in areas with higher degrees of cross-linking. The mixture was then poured onto the top of the RFMicron RFM-2100 AER and then the doctor blade is set to a required thickness and

moved along by a speed adjustable arm (labelled in Figure 2.2). The amount of TEOS used in the system is an excess of TEOS (relative to the groups of Si-OH that the Si-OEt groups in the TEOS can crosslink with). Whilst by Carothers theory, this should still result in crosslinking, the excess TEOS can result in TEOS-TEOS condensation via moisture cure.

2.3.3. Film application procedure

The reaction mix was spread across the substrate from left to right using the doctor blade (as shown in Figure 2.3 (a) & Figure 2.3 (b). Following this, the applicated film was allowed to cure at room temperature for 1-2 hours, and then was moved to a 65° C oven overnight.
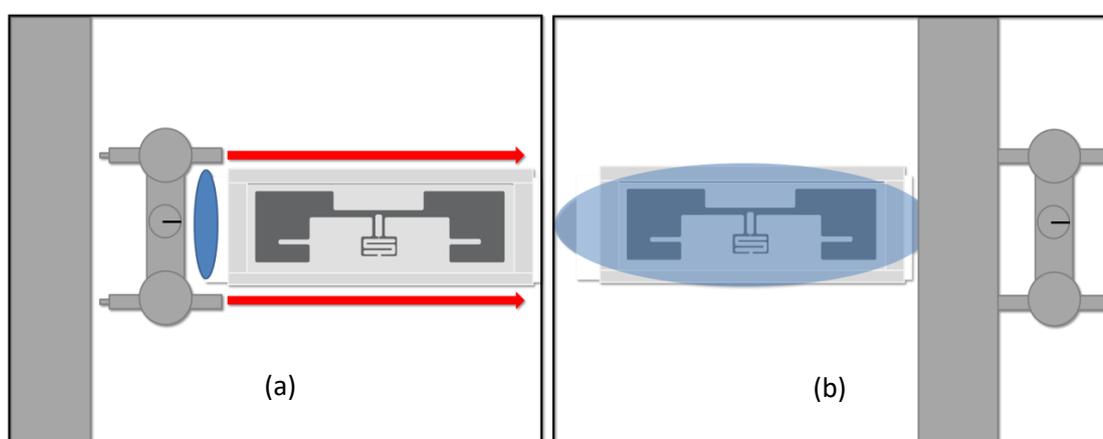
Figure 2.3 - (a) & (b) - Schematic diagram showing the PDMS thin film doctor blading process. In (a), the curing PDMS elastomer (coloured in blue) is poured in a space between the tag and the doctor blade, within the boundary of the doctor blades runners. (b) Shows the PDMS elastomer after the applicator arm has pushed the doctor blade across the width of the tag.

2.3.4. Relative permittivity measurements

Relative permittivity measurements were performed on a DAK 3.5 dielectric assessment kit. All NaCl solutions measured using the DAK 3.5 were performed within a temperature controlled room (22 °C) (so as to minimize relative permittivity changes from a fluctuation in temperature). Solution temperature was monitored using a laser thermometer prior to each measurement. The solutions were also weighed by mass before being measured (so that 200ml of solution was measured for each concentration).

The measurement set up for the DAK can be seen in Figure 2.4:
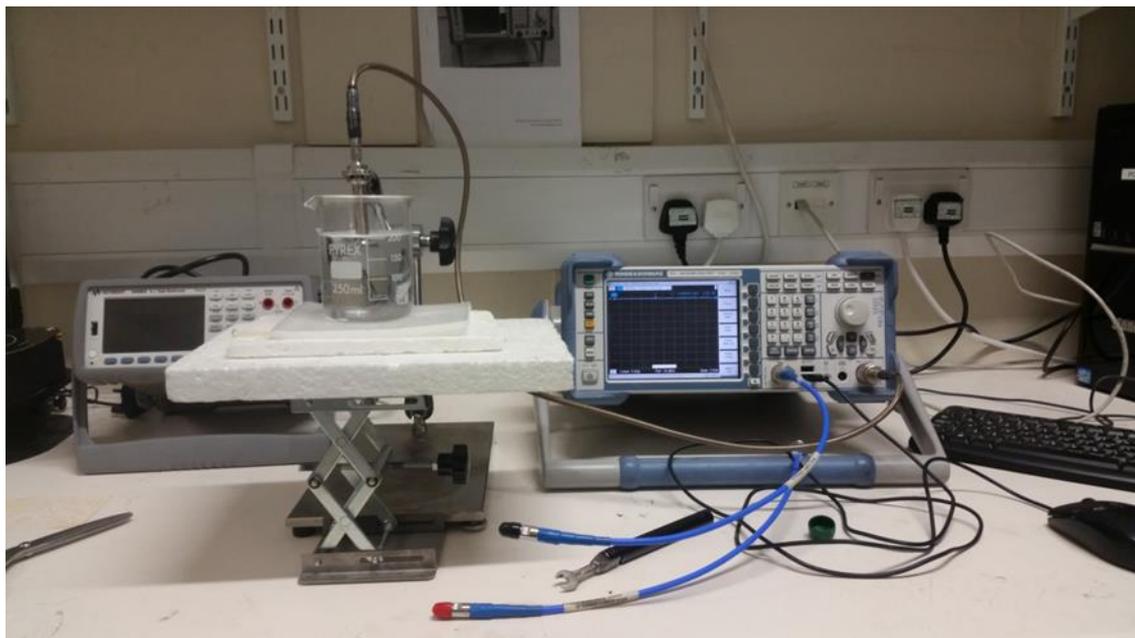
Figure 2.4 - Picture showing the DAK 3.5 dielectric assessment kit, and an exemplar set-up for aqueous electrolyte measurements.

As the probe requires a large volume of liquid (approx. 200 ml) only NaCl was tested, between 0-2 M. The remaining relative permittivity's for other salts tested used in this chapter quoted were taken from literature.

2.3.5. RFID studies on PDMS coated RFMicron RFM-2100 AER

All RFID measurements were performed on Voyantic Tagformance Equipment[19]. The measurements for the variable thickness studies and the aqueous electrolyte measurements were performed over a frequency range of 800-860 MHz and a fixed transmitted power of 9 dBm. The exceptions to this are the sensor optimization study where the frequency range used was 845-865 MHz. The film thickness used for all measurements was 500 µm (with the exception of the variable film thickness studies).

The distance between the reader and the tag for all measurements was calibrated to 30 cm. The reader was positioned underneath the tag so that the underside of the tag faced the reader. Liquids deposited onto tags were deposited from an auto-pipette (0.8 ml in total).

In order to ensure that the deposited liquid remained in a fixed area for deposition studies, a 3D printed hollow well was adhered atop the sensor area (as can be seen in Figure 2.5 (a) and (b)
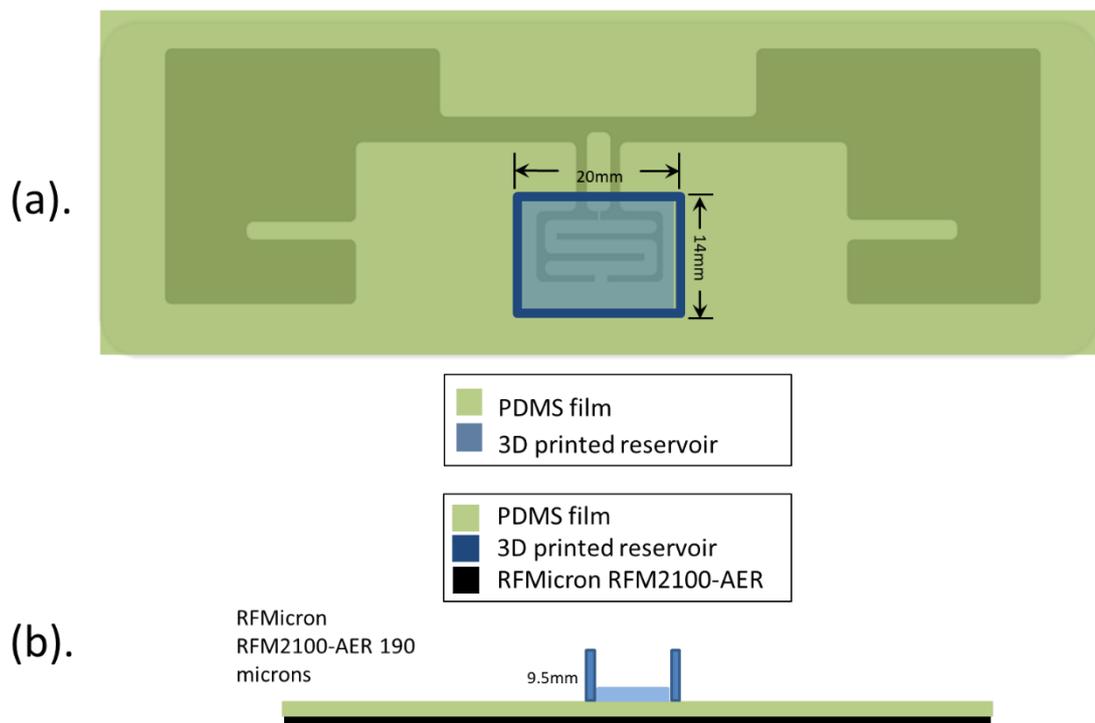

Figure 2.5 – (a) - Schematic diagram of the PDMS coated RFMicron RFM-2100 AER, showing the area the 3D printed well was adhered to, and (b) - Schematic diagram showing the side-on view of the PDMS coated RFMicron RFM-2100 AER and the 3D printed well.

After each measurement, the surface of the tag was dried with tissue paper, rinsed with deionized water, and then dried again. When the averaged sensor value of the tag matched the averaged sensor value for the tags original dry value, the next measurement was performed. Aqueous salt solution measurements were taken in triplicate. The measurement setup is shown in Figure 2.6:
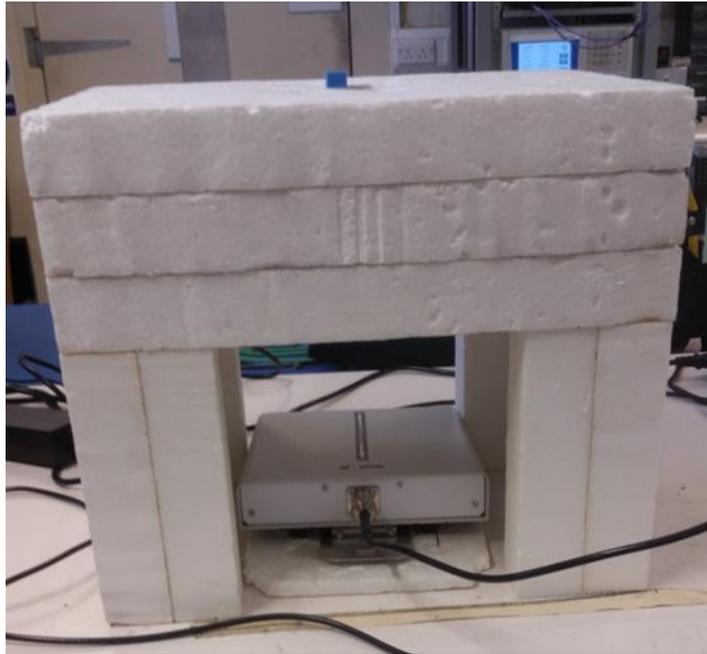
Figure 2.6 - Photograph of the Tagformance reader and the RFMicron RFM 2100-AER atop the Styrofoam block.

2.3.6. FT-IR spectroscopy of PDMS/TEOS elastomers

FT-IR measurements were performed using a Shimadzu IRAffinity spectrometer with a Specac Golden Gate™ ATR sampling accessory, and each sample was subjected to 64 scans, at a resolution of 4 cm-1 (between 500-4500 cm-1).

FT-IR values for tetraethylorthosilicate:

C-H stretch (CH3), asym. (2981). C-H stretch (CH2), asym. (2929). C-H stretch, asym. (2890). C-H bend (CH3), asym. (1443). C-H bend (CH3), sym. (1391). C-H twist (1294). C-H (CH3) (1164), (995). C-O stretch (ether), asym. (1072) C-C-O (525).

FT-IR values for polydimethylsiloxane (cSt 1,000):

C-H stretch (CH3),(2966). Si-CH3 stretch, asym (1438). Si-CH3 stretch, sym (1261). Si-O-Si stretch (1103), (1120). Si-C stretch (786).

2.3.7. Results and discussion

2.3.7.1. Characterization of PDMS elastomers

The elastomer films produced were transparent at all thicknesses. The FT-IR spectra for both materials and the cross-linked PDMS elastomer. The significant vibrational peaks values of PDMS and TEOS agreed with those reported in the literature[20], shown in Figure 2.7:
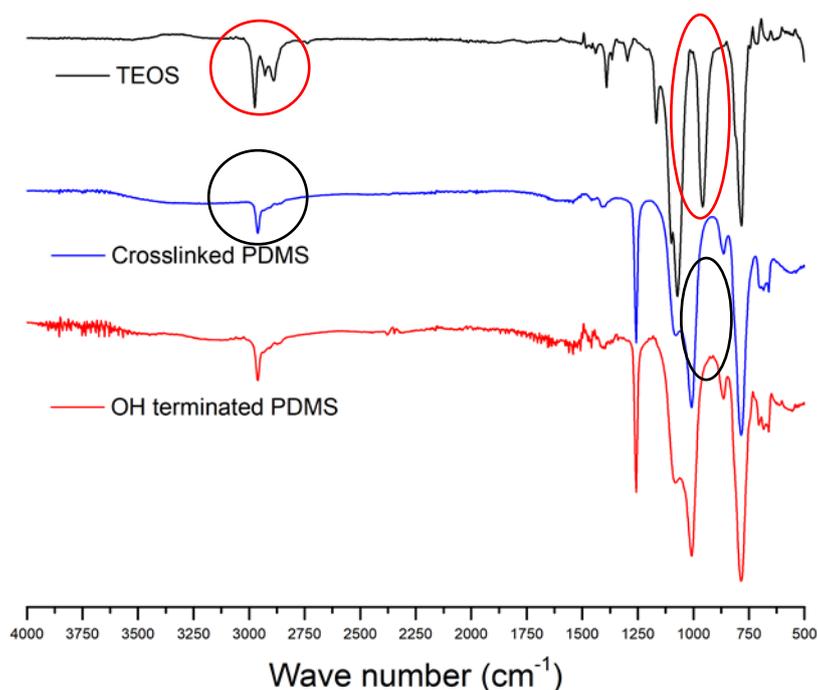
Figure 2.7 - FT-IR spectra of tetraethylorthosilicate (TEOS), Silanol terminated polydimethylsiloxane (PDMS) (cSt 1000), and the cross-linked product of TEOS/PDMS.

The noteworthy change in the cross-linked PDMS is the disappearance of the $C - H$ stretch (CH_2) present in the TEOS IR spectrum (2929 cm^{-1})[21] and the $C - O$ stretch (995 cm^{-1})[22] circled in red on the TEOS IR spectrum (the areas where the peaks aren't present on the cross-linked PDMS spectrum was also circled).

2.3.8. PDMS/TEOS elastomer film application thickness studies

PDMS is a low permittivity material (approx. 2.8) that should not impede the performance of the tag to a large extent. However, if a high dielectric solution is placed atop the sensor area of the coated tag, the addition of the boundary layer means that the fringing fields produced by the sensor electrodes will travel a certain distance in a low permittivity medium before

51

encountering the high permittivity material. By gradually increasing the thickness of the PDMS/TEOS elastomer, a point should eventually be reached where the sensor value when under high permittivity load will be the same as the sensor value when no high permittivity material is deposited on the sensor. A schematic is shown in Figure 2.8 to show how increasing the PDMS (low permittivity) layer should result in Fringing fields being less effected as thickness increases:
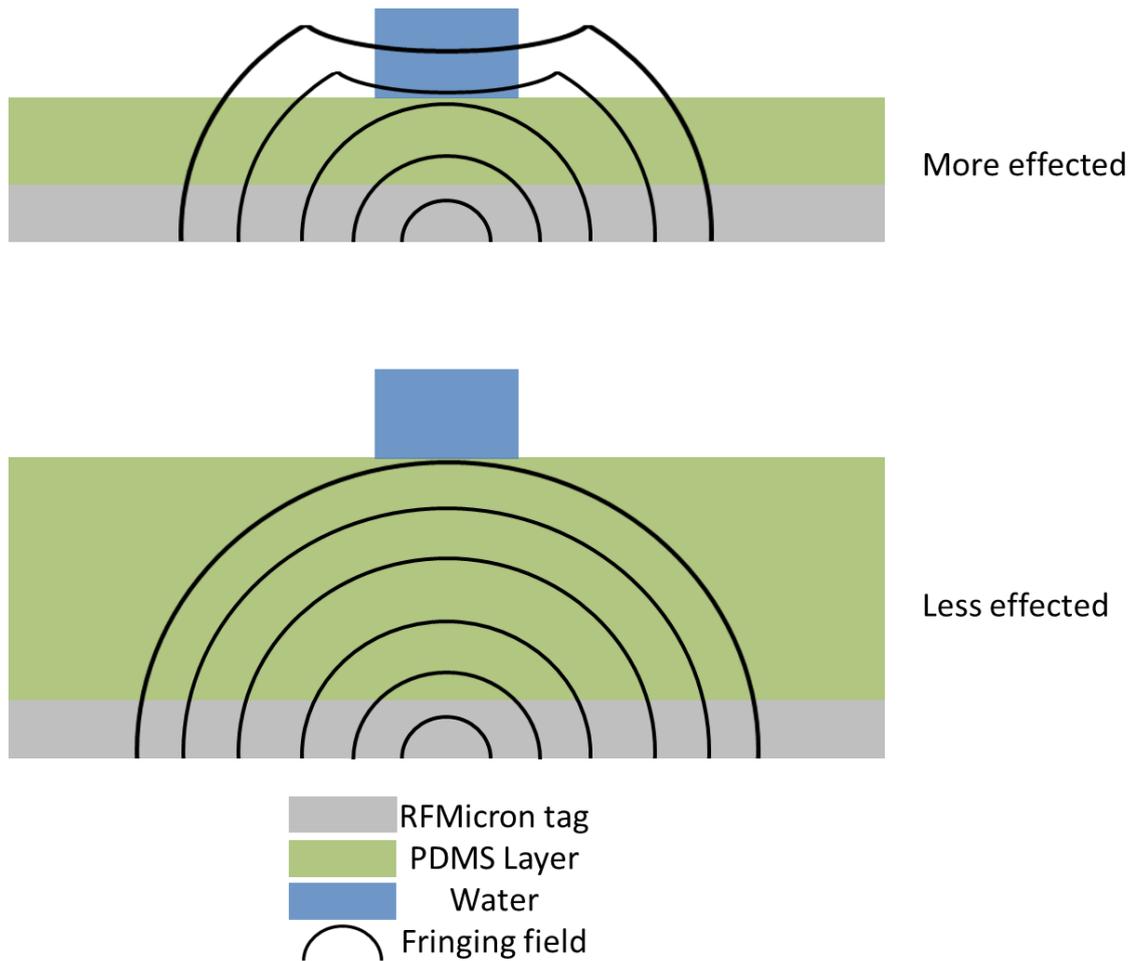

Figure 2.8 – Schematic diagram showing how increasing PDMS layer thickness reduces high permittivity load on the tag.

As the elastomer mix undergoes curing, it transitions from fluid mix to a solid rubber like material. Whilst this makes it suitable for usage with a doctor blade, the mix will still undergo this transition after being doctor bladed. As the material still possesses fluidic properties, it will disperse until it solidifies. This dispersal means that the height at which the material is applied and the height at which the material is when it sets differ. Doctor blading was performed with the doctor blade set to deposit at a set height. Then PDMS films were deposited over the glass substrate and had the derived thickness (measured by Vernier callipers), shown in Figure 2.9:
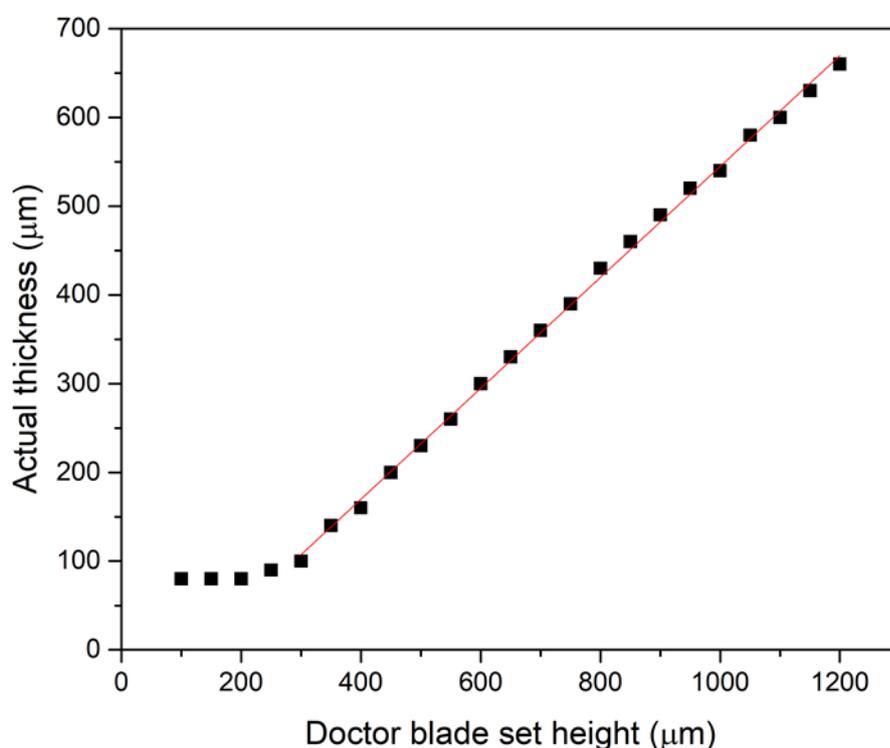
Figure 2.9 – Plot of measured thickness (determined using Vernier callipers) of PDMS/TEOS elastomers compared to the applicated height set on the doctor blade.

The linear fitting equation for the line fit performed in Figure 2.9 is shown in

$$y = 0.58x - 42.54$$

Equation 2.1 – Equation of the linear fit in Equation 2.9 derived from the PDMS film height study.

Figure 2.9 shows a linear relationship between the set doctor blade height and the actual derived thickness. The linear fit here excludes the doctor blade set heights of 100-250 µm. This is due to the fact that an observed thickness of 80 µm persisted for all 4 sample sets. The derived fitting allows for film thicknesses via doctor blading to be calculated for the system (up to 700 µm).

2.3.9. Permittivity measurements of aqueous salt solutions

The relative permittivity of a material (formerly known as dielectric constant[23]) is a measure of how a material responds when an electric field is applied. Relative permittivity is the ratio of the permittivity of the material under test to vacuum permittivity. This is defined as:

$$\varepsilon_r = \frac{\varepsilon}{\varepsilon_0}$$

Equation 2.2

Where ε_r is the relative permittivity, ε is the absolute permittivity (the permittivity of the material) and ε_0 is the permittivity of a vacuum 8.85×10^{-12} F/m[24]. The method chosen to measure the permittivity of solutions was a dielectric assessment kit (DAK). The DAK is an open ended coaxial probe which operates at 200 MHz- 20 GHz. Fringing fields are produced that can permeate through the material in contact with the probe at the interface of the two, with higher dielectric materials causing a greater reflectance. This can be related to the relative permittivity of the material under test. The sensitivity of the instrument is such that when in use it is imperative to reduce positional movements that will affect measurements. The system is calibrated by using three different load materials; copper, air, and a solution with a known permittivity. The copper is used to short the probe, and the known liquid was water. Reverse osmosis water was used to improve the purity of the calibration liquid. The result of the calibration is that the resultant reflection coefficients of any measurement are normalized, which means changes in reflection coefficient seen after the calibration are real changes that are then measured by the Vector network analyser (VNA) attached to the DAK. As such, any measured reflection coefficient is due to a change in permittivity of the material under test.

2.3.10. Auto-tuning RFID tags sensing principle

As previously mentioned, the RFMicron RFM-2100 AER houses an integrated chip (called the Magnus S2) that can alter its internal capacitance between 1.9-2.9 pF dependent on the external stimulus (or load material) applied to the interdigitated sensor. Conventional microchips that don't modulate their impedance (known as static impedance microchips) will have a degraded read range as a consequence of a change in the immediate environment.
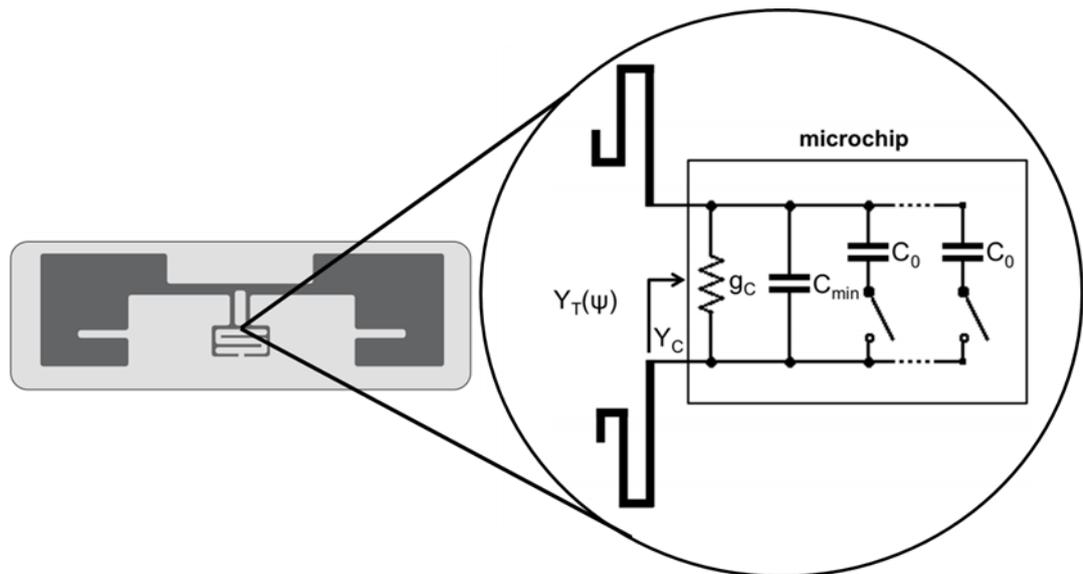

Figure 2.10 - Schematic diagram of the RFMicron RFM-2100 AER, and a circuit diagram of an equivalent circuit diagram of a self-tuning chip from[4].

(stimuli such as metals or high dielectric liquids). The loss of read range is due to the adverse change in the gain of the antenna. As such, sensing architectures that utilize static impedance chips do so in an analogue fashion (in that the degree to which the antenna performance degrades is the transduction mechanism).

The integrated chip relies upon a series of capacitors (as can be seen Figure 2.10). C_{min} is a capacitor responsible for the baseline capacitance of the chip (1.9 pF). The additional capacitors are all denoted as C_0. The overall capacitance for this self-tuning network has previously defined this[25,26] as:

$$C_T(n) = C_{min} + nC_0$$

Equation 2.3

Where $C_T(n)$ represents the total capacitance of the self-tuning network, C_{min} represents the minimum capacitance of the network, n represents an integer value that represents the extent to which the network has had to retune, and C_0 represents the remaining cumulative capacitance for all capacitors that aren't C_{min}. As suggested by the name, the self-tuning network automatically modulates so that the maximum amount of power that can be delivered to the chip from the antenna is delivered. In order to appreciate the effect of the effect of an environmental condition of the on the self-tuning network, the susceptance (the inverse of reactance, or how susceptible a circuit is to conducting a changing current) can be used. As the susceptance of the microchip will be equivalent to the capacitance of the microchip (denoted as $B_C(n) = C_T(n)$), the compensation of the microchips susceptance (when the admittance of the tag deviates due to an environmental stimuli) in order to perform a matching can be written as:

$$B_C(n) + B_T(\Psi) = 0$$

Equation 2.4

Where B_T is the tag susceptance, and Ψ is the environmental stimuli. Whilst this shows that a retuning effort can be made by the chip, the amount it can compensate is finite.

The antenna susceptance that can be compensated must fall within the following range:

$$C_{min} - NC_0 \leq B_T \leq -C_{min}$$

Equation 2.5

Where N is a saturated (or maximum) sensor code value. As the sensor code value changes when there is a poor matching between the antenna and the chip, and the change in admittance is affected by an external stimulus, the sensor code can be used as a means of measuring

56

environmental changes digitally. It therefore follows that whilst the dependant variable is the

sensor value, the transduction mechanism is actually the antenna susceptance.

2.3.11. Sensor code of PDMS coated RFMicron RFM-2100 AER

2.3.11.1. 290 μm PDMS layer water deposition study

In the first test, the RFM-2100 AER had its sensor response measured in air and when exposed to water. This was then compared to a tag that had a 290 μm PDMS coating, which was also tested in air and when exposed to water. Sensor responses are shown in Figure 2.11:
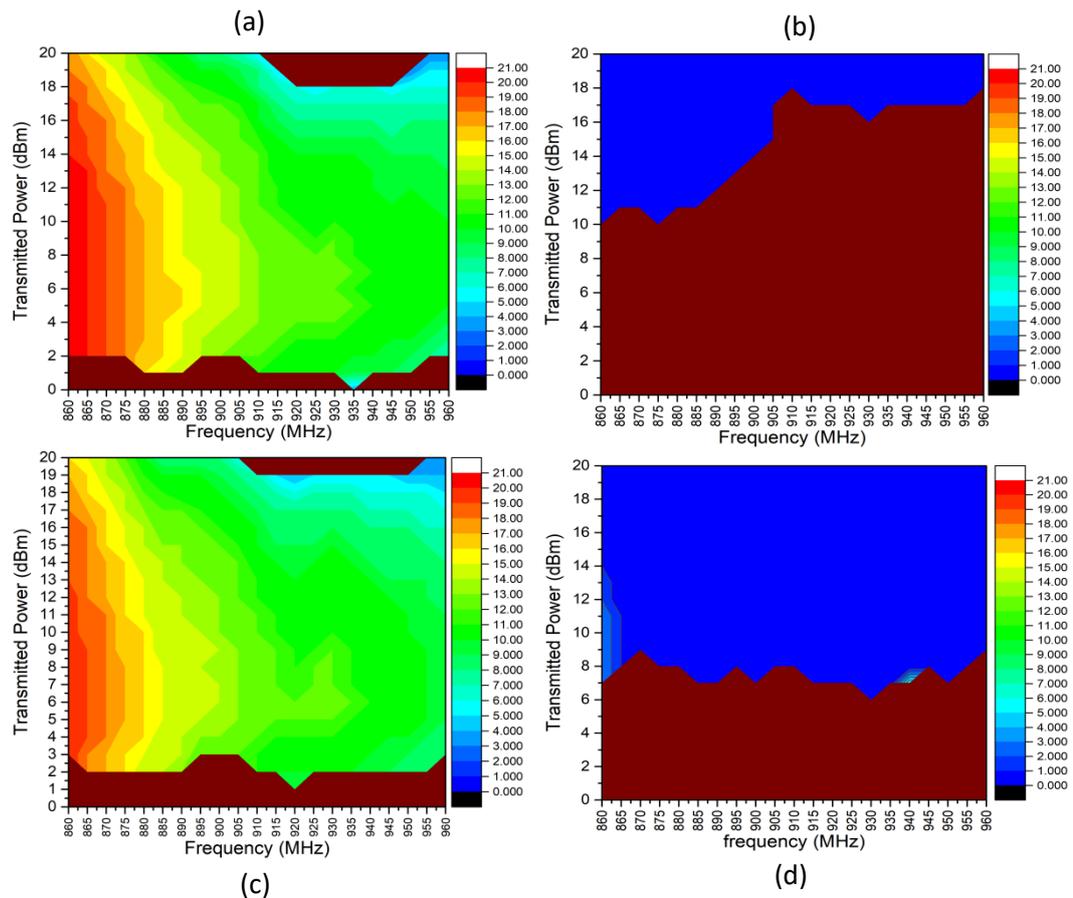
Figure 2.11 - (a) Sensor response of the unmodified RFMicron RFM-2100 AER with reading performed in air. (b) RFMicron RFM-2100 AER with reading performed when exposed to 0.8 ml of water. (c) RFMicron RFM-2100 AER with a 290 μm thick PDMS film with reading performed in air. (d) RFMicron RFM-2100 AER with a 290 μm thick PDMS film with reading performed when exposed to 0.8 ml of water.

Figure 2.11 (a) shows that whilst the sensor code value varies significantly with frequency; the variation with sensor code value with transmitted power value is far less changeable in comparison. The addition of a low dielectric PDMS layer of 290 μm doesn't have a visibly large effect on the sensor intensity measurements performed in air (Figure 2.11 (a) and (c)). When the sensor intensity values of Figure 2.11 (b) and (d) are compared, the addition of a 290 μm layer of PDMS has reduced the minimum threshold of N/A values (represented by the brown colour) across the entire frequency range observed. Moreover, Figure 2.11 (b) shows only one integer across the entire frequency and power range (other than the N/A value) of 0. Compare this with Figure 2.11 (d), which has a small gradation of integer values (between 0-2). The addition of a 290 μm PDMS reduces the degree of detuning, however not to the extent where the tag becomes useful for bulk water sensing. Therefore, a thicker film needed to be used to be able to sense bulk water effectively.

Adding bulk water directly to the electrodes of an unmodified tag with no PDMS film introduces a reactance so large that the chip is unable to tune out the impedance change. The unmodified tag is driven past its tuning capability. However, the hydrophobicity of the deposited thin PDMS film means that water does not permeate, but capacitive electric fields are able to fringe through the film between the electrodes and to the liquid. The separation of the liquid from the electrodes reduces the capacitive effect and brings the tag within its tuning range. Considering this as the two materials having a combinative effective permittivity, by increasing the thickness of the dielectric layer closest to the point of field generation (commonly referred to as ε_1[27]), the effect of the high dielectric layer (commonly referred to as ε_2) is minimised. When the high dielectric layer is a lower dielectric than the PDMS film (in this instance air), the effective permittivity of the two layers increases, resulting in the gradual increase in permittivity observed for the air readings as the PDMS layer thickness increases.

2.3.11.2. 400 µm PDMS layer water deposition study

A thicker 400 µm film was used and sensor values were measured (air values were measured and found to be largely unchanged for the 400 µm coated tag, see appendix) against water and compared, shown in Figure 2.12:
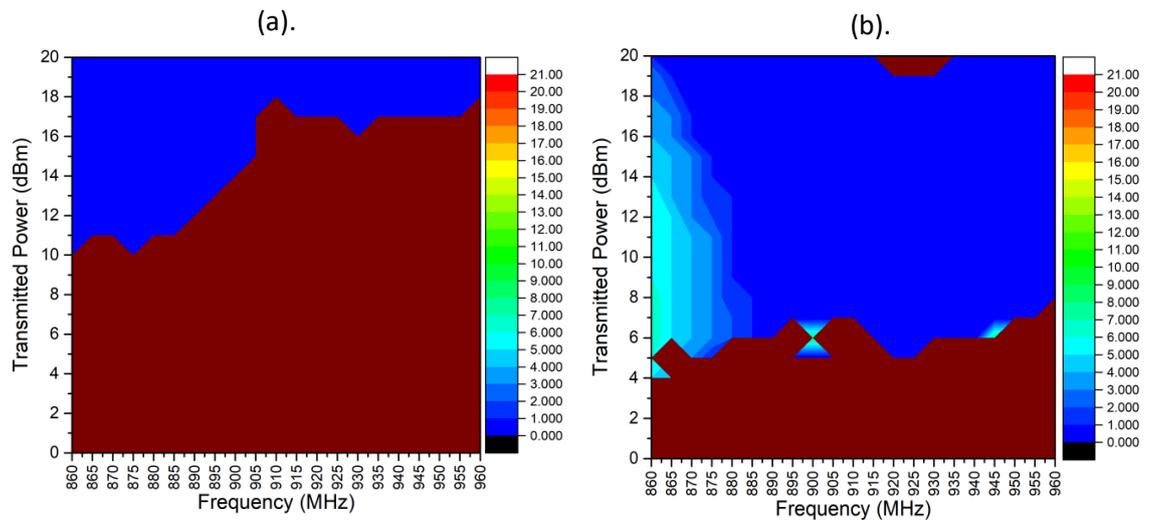

Figure 2.12 – Plots of sensor response of (a) the RFMicron RFM-2100 AER when exposed to water & (d) the RFMicron RFM-2100 AER when exposed to water with a 400 µm thick PDMS film.

Whilst the 400 µm coated tag shows less detuning than the uncoated tag and the 290 µm coated tag, the addition of bulk water still causes a significant detuning of the tag. Nonetheless, the addition of the film does result in sensor value higher than 0 being measured, meaning that increasing the thickness and moving the bulk water away from the interdigitated sensor is reducing the extent of detuning. Further increasing the thickness of the low dielectric layer should mean that when the high dielectric layer is occupied by water, Sensor values increase.

2.3.11.3. 980 μm PDMS layer water deposition study

A 980 μm film was used and sensor values were measured against air and water and compared,

shown in Figure 2.13:
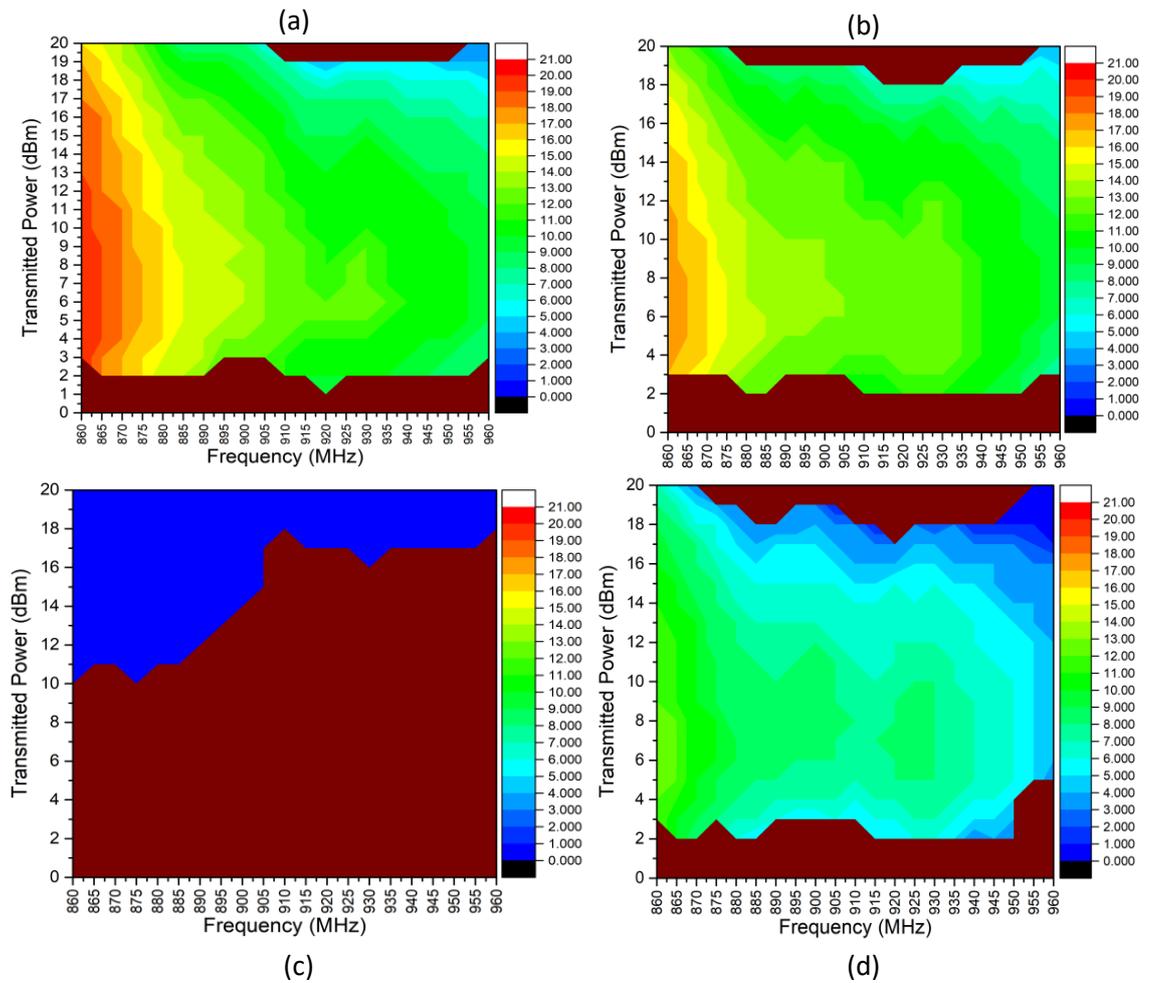
Figure 2.13 – Plots of (a) Sensor response of the unmodified RFMicron RFM-2100 AER with reading performed in air (b). RFMicron RFM-2100 AER with a 980 μm thick PDMS film with reading performed in air (c). unmodified RFMicron RFM-2100 AER with reading performed when exposed to 0.8 ml of water (d). RFMicron RFM-2100 AER with a 980 μm thick PDMS film with reading performed when exposed to 0.8 ml of water.

Further increasing the coating thickness to 980 µm increases sensor values across the entire frequency range. By increasing the low dielectric PDMS layer thickness, when water occupies the high dielectric area the effect on the tag is further decreased.

2.3.11.4. Water deposition studies of RFMicron RFM-2100 AER with PDMS films of variable thickness

In order to determine what thicknesses would be sufficient to cause the sensor values observed between dry and wet readings to converge, a wider thickness range was investigated, both with dry and wet readings, shown in Figure 2.14:
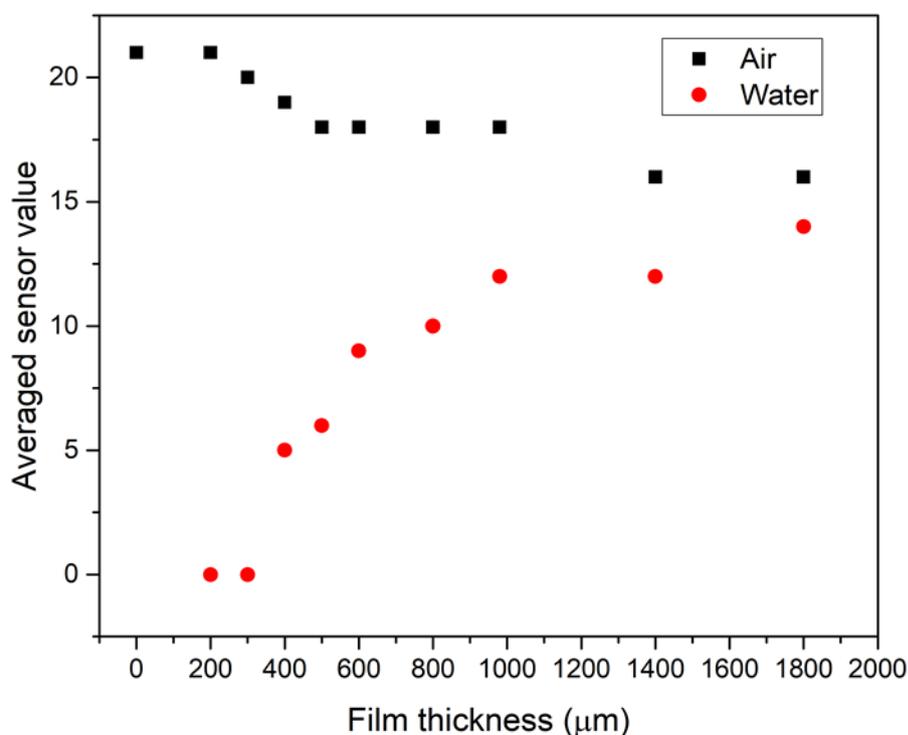
Figure 2.14 – Plots showing the difference in averaged intensity between an RFMicron RFM-2100 AER when dry and when 0.8 ml is deposited on the sensor area.

Figure 2.14 shows averaged sensor values for tags with PDMS films applied with thicknesses ranging between 0 and 1800 µm. The tags were measured dry and with 0.8 mL of deionized water applied to the sensor area. It can be seen that for all tested film thicknesses, it was possible to discriminate between the dry and wetted tags, making bulk water sensing possible.

Also, until a film with a thickness of 400 μm is used there is no change in sensor code value when water is deposited. At 1800 μm, the dry reading and the bulk water sensor code readings converge to the point where the detection limit is almost reached.

The tag can therefore have its sensitivity tuned simply by modifying the thickness of the electrode coating film depending on the required application. Water is a very high permittivity material (ε_r = 80), but a thickness as small as 400 μm was thick enough to reduce the reactance load on the chip. The result of this was a sensor code value higher than zero across the averaged frequency band, meaning that $B_T(\Psi)$ was reduced to the extent that the chip could compensate within its effective tuning range.

2.3.12. Relative permittivity measurements of sodium chloride (NaCl) solutions

A thickness of 500 μm was chosen for the aqueous electrolyte measurements as the relative permittivity of aqueous salt solutions decreases with increased concentration. Furthermore, the thickness of 500 μm is the start of a steep decline in tag sensitivity. If the aqueous electrolyte studies resulted in responses outside of the effective tuning range of the tag, then a thicker film could be used if required (but 500 μm was first tested to reduce the material usage).

Relative permittivity measurements were taken for NaCl solutions of various concentrations between 0-2 M. These were also compared to literature permittivity's obtained from Debye and Cole[28] as seen in Figure 2.15:
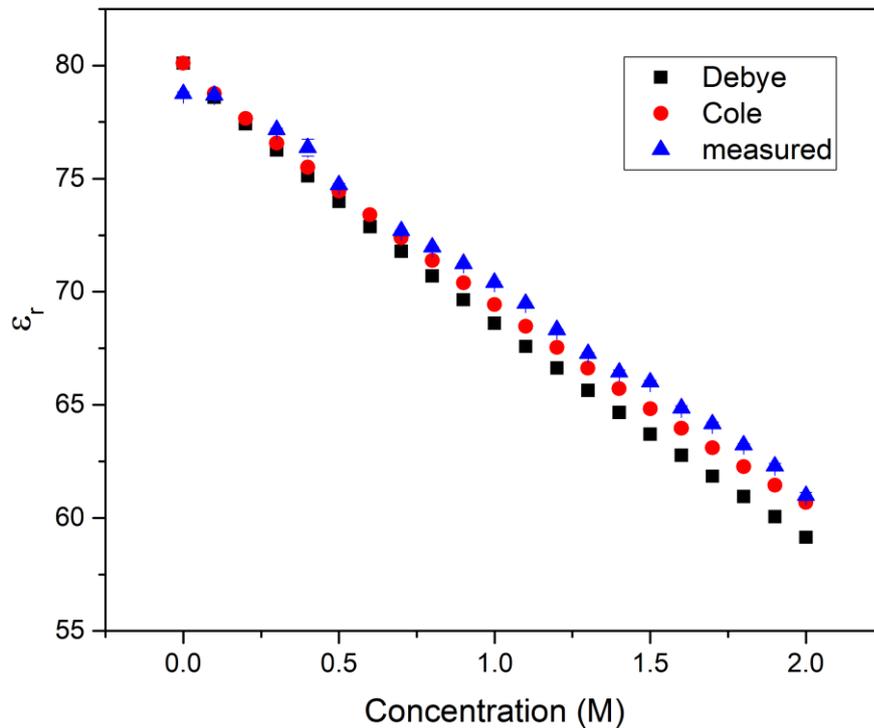
Figure 2.15 - Plot comparing the relative permittivity of NaCl aqueous solutions of the Cole and Debye models and measured permittivities (averaged permittivity between 800 – 860 MHz, with a step of 1 MHz).

The measured values showed a good agreement with the models. All three permittivity values will be compared against the sensor responses obtained for all corresponding salts.

2.3.13. Aqueous electrolyte measurements on modified RFMicron RFM-2100 AER

The averaged values that were used for the aqueous salt measurements used a frequency sweep instead of a power sweep because of this. Furthermore, the addition of water onto the sensor causes a complete mismatching between the antenna and the chip, falling outside of the chips effective tuning range, and resulting in value zero (or N/A values). The highest observed intensity values were found to be in the region of 800-860 MHz, and as a result that region was used for averaged results instead of the 860-960 MHz region shown in Figure 2.11.

Firstly, a 500 µm PDMS coated tag was exposed to a series of salt solutions between the ranges of 0-5 M. Sensor code measurements were obtained for the frequency band used for this was

800-860 MHz (with a step of 5 MHz). The initial sweep was performed with a power sweep of 8-20 dBm. This was then plotted against both concentration and dielectric constant of the solutions, shown in Figure 2.16:
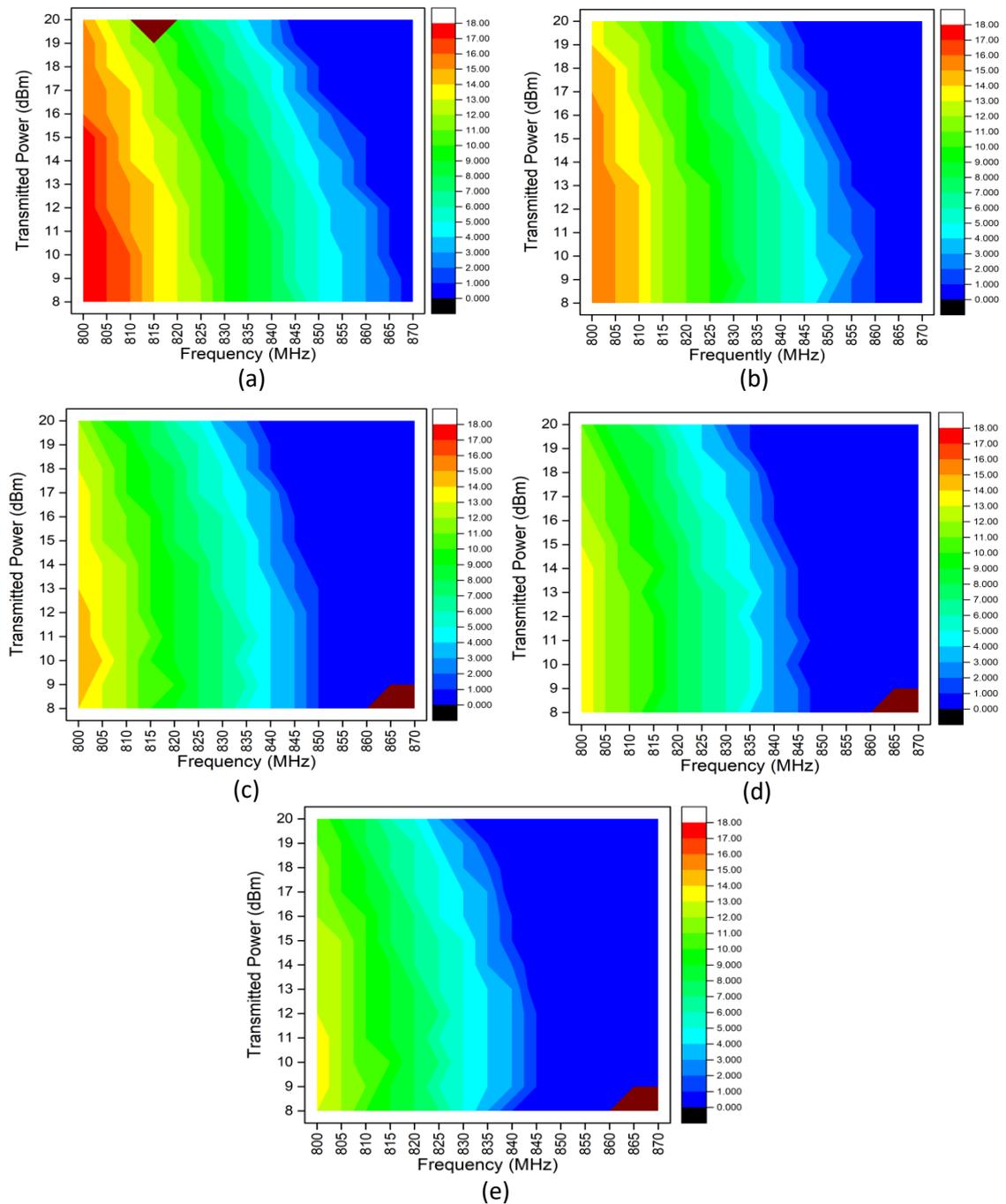
Figure 2.16 - Sensor intensity of Deionised water (b) 0.5 M sensor intensity of NaCl (c) sensor intensity of 1.0M NaCl (d) sensor intensity of 1.5 M NaCl and (e) sensor intensity of 2.0 M NaCl on a PDMS coated RFMicron RFM-2100 AER.

Figure 2.16 shows a gradual decrease in sensor responses from 0-2 M NaCl concentration. At 0 M (Figure 2.16 (a)), response values of 18 can be observed at lower Transmitted powers. In Figure 15 (b), values of 16 are observed at the same frequency. This gradual decrease proceeds as the concentration of NaCl is increased. Furthermore, the initial frequency (from left to right) at which zero values are observed decreases as the NaCl concentration increases. At 0 M, this is at 870 MHz (in the lower power range), whereas for 0.5 M and 1.0 M the initial Zero value readings are seen at 860 MHz and 850 MHz, respectively. 1.5 M and 2.0 M NaCl solutions (Figure 2.16 (c) and (d)) also had a decreased observed zero value (845 MHz), and also had decreased highest observed values within the entire range (of 13-14). In order to observe the changes in the sensing tag with aqueous electrolyte concentration, an average of the values obtained between 800-860 MHz (using a fixed power of 9 dBm) was used. This was mostly because an averaged value uses a larger range of data, and reduces the likelihood of a single outlier value grossly affecting results.

2.3.14. Multiple aqueous electrolyte measurements on modified RFMicron RFM-2100 AER

After performing test measurements with NaCl solutions, a series of aqueous electrolytes were used with variable concentrations, and tested with the PDMS modified RFMicron RFM-2100 AER (500 μm). The concentration range used for LiCl, KCl RbCl was 0-2 M (with a 0.5 M step). NaCl was also tested from 0-5 M (with a 0.5 M step). The resultant sensor responses are shown in Figure 2.17:
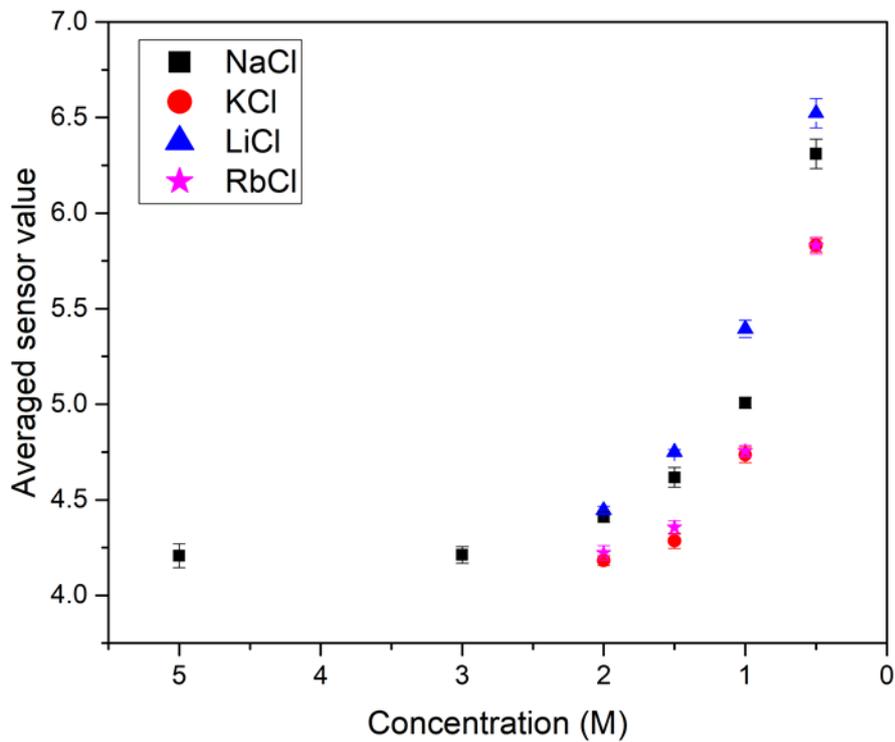
Figure 2.17 - Plot showing the effect of various concentrations of various aqueous salt solutions on the averaged PDMS coated tag sensor values.

Figure 2.17 shows that as the concentration range between 0.5-2 M has the largest associated change in sensor value. Whilst all salts were tested at 0.5-2 M, NaCl was also tested at 3 & 5 M. Multiple salts were used in the lower concentration range (0.5-2 M) to ensure that the sensor values obtained were due to an effect that wasn't a chemo-selective interaction between a specific aqueous salt and the PDMS/TEOS elastomer. A large decrease in the sensor values for the PDMS coated tag between 0.5-2 M was observed with increased aqueous electrolyte concentration. This trend is observed for all salt solutions tested, although the sensor values for each salt differ when the concentration is the same.

Although plotting concentration against sensor values shows a general trend for the effect of increased aqueous electrolyte concentration on sensor values, it doesn't explain what causes the decrease. A comparison of the dielectric properties of aqueous electrolytes against the

sensor code measurements was required. Dielectric values for the salts were plotted against literature values according to literature values obtained from[29,30,31], and is shown in Figure 2.18:
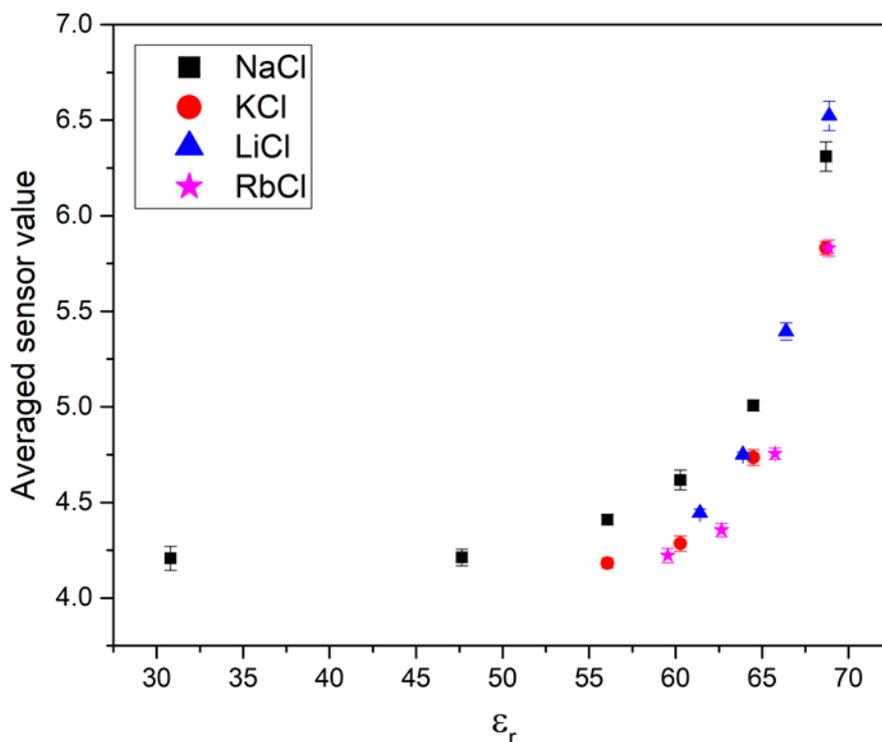
Figure 2.18 - Plot showing relative permittivity plotted against sensor values of various aqueous salt solutions on the averaged PDMS coated tag.

The sensitive concentration range seen in Figure 2.17 is 0.5-2 M. When plotted against relative permittivity (like in Figure 2.18), this relates to a relative permittivity between approx. 70-55. A significant decrease in sensor values can be seen in this area for all salts. All measurements were performed in triplicate, with a narrow error between measurements. However, there is still a sensor code difference between different salts, despite having extremely similar relative permittivity at the same concentration. Nonetheless, the purpose of using multiple salts was to prove that the observed changes in sensor values was not due a specific interaction between any one salt and the PDMS coated tag. The measurements of NaCl at 3 & 5 M do not follow the same decrease in measured sensor code value that is observed with aqueous salts between 0.5-2 M. This lack of change in the sensor data means the tag cannot be used for monitoring of ultra-

high concentration aqueous electrolytes. Further investigation of the area between 0-2 M was required.

2.3.15. NaCl Salt Concentration Measurements

NaCl was scrutinised with a smaller incremental step of 0.1 M between the range of 0-2 M. NaCl was chosen instead of the other 3 salts due to availability and cost-effectiveness. Sensor values were plotted against concentration of the aqueous electrolyte solutions, as well as the dielectric constants for those aqueous electrolyte solutions, as shown in Figure 2.19:
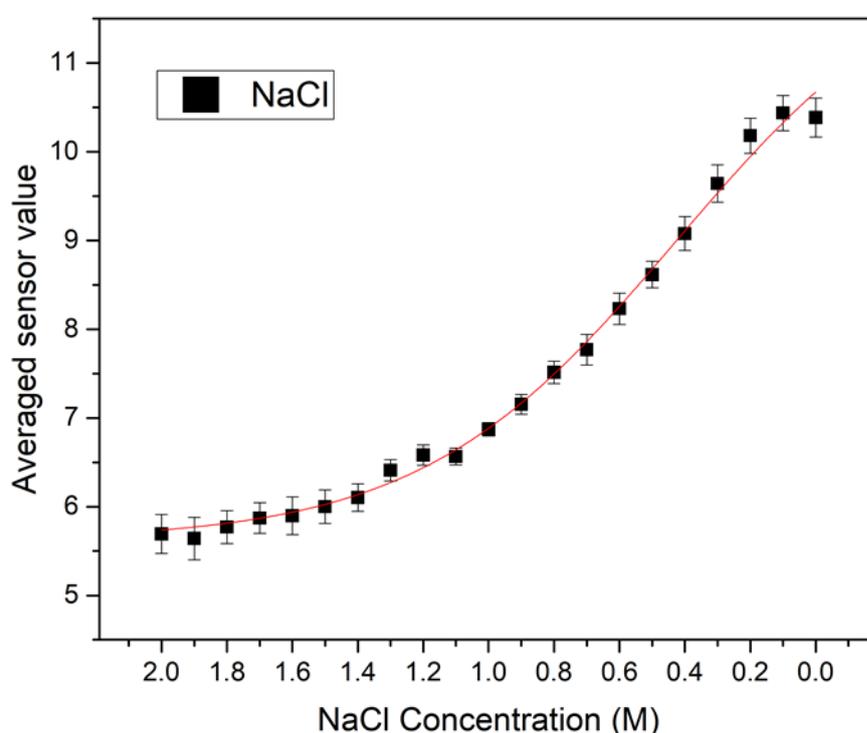

Figure 2.19 - Plot showing the effect of NaCl salt solutions between 0-2 M on the PDMS coated tags averaged sensor code value.

Figure 2.19, it can be seen that as the concentration of the NaCl solution increases, the sensor value for the tag decreases. This is true from a concentration of 0.1 M and higher; all measurements were performed in triplicate and had a minimal associated error. The sigmoidal curve fit and resulting equation were derived according to a Boltzmann distribution using the Levenberg Marquadt algorithm[32]. The derived curve was is shown in Equation 2.6 (R^2 = 0.992):

$$y = 5.23623 \pm 0.22182 + (11.57852 \pm 0.5151 - 5.23623 \pm 0.22182)/(1$$

$$+ e^{\left(\frac{x - 6.40555 \pm 0.48023}{3.55825 \pm 0.49012}\right)}$$

Equation 2.6 – Fitting curve for the curve derived from Figure 2.19.

Instead of using this fitting curve to corroborate a hypothesis (as is the norm when using a fitting curve), the fitting curve in this instance was used as a convenient means of predicting aqueous electrolyte content for a given sensor value measured.

Figure 2.20 shows the same data, plotted against relative permittivity. 3 different permittivity values were used. Models taken from Debye and Cole were both plotted against measured data from the DAK:
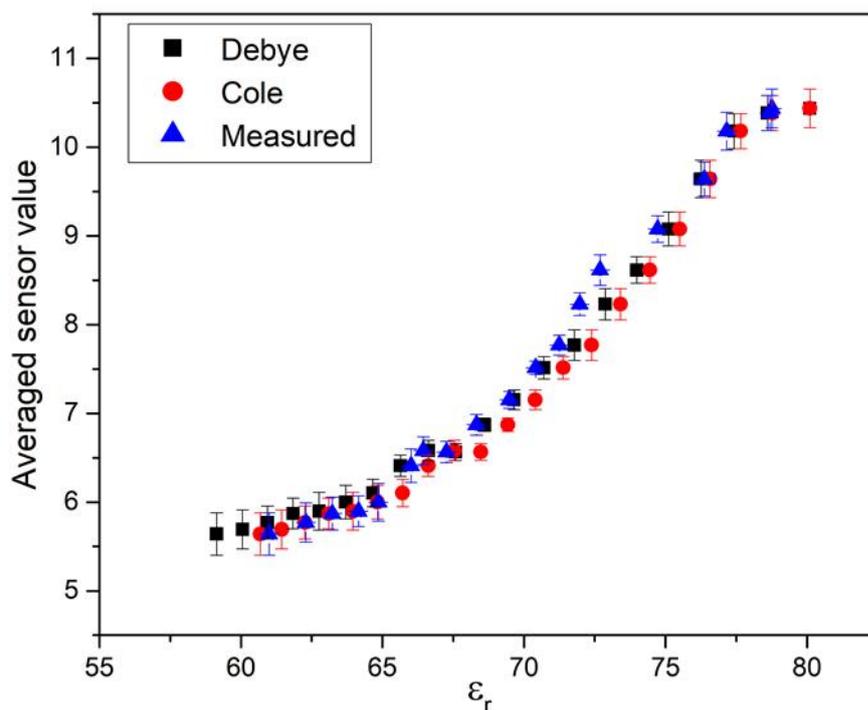
Figure 2.20 - Plots showing the sensor values of aqueous NaCl solutions between 0-2M plotted against relative permittivity's obtained from Debye, Cole and relative permittivity measurements from the DAK.

The effective range of the tag is a permittivity of 60-80 (for NaCl salts), with the range of 65-77.5 being the area with the most sensitive area (between 0.3-1.6 M). However, a reduction in

permittivity of the solution should result in a decrease in capacitive load of the material under test. This in turn should then result in a net decrease in capacitance, however the opposite is observed.

2.3.16. Conductivity effect & fringing field capacitors

As previously discussed, there is a "conductivity effect" associated with capacitors. Permittivity is not the only variable that can have an effect on capacitance in a fringing field capacitor[14]. Conductivity (denoted σ) can also have an effect that increases the measured capacitance[33]. Although typically this is discussed in relation to parallel plate capacitors, the principles transfer to fringing field capacitors. If the capacitive component of the aqueous electrolyte solution is considered as a capacitor and the conductive component of the electrolyte solution is considered as a capacitor in parallel to a secondary capacitor (the sensor). This has been illustrated in Figure 2.21:
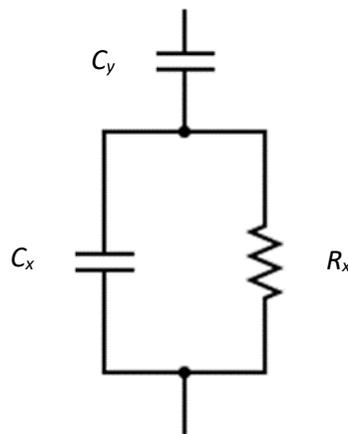
Figure 2.21 – Schematic diagram illustrating the cumulative capacitance of conductivity and relative permittivity in a fringing field sensor.

In Figure 2.21, C_x is the capacitance of the liquid atop the sensor, R_x is the resistive (or conductive) component of the liquid atop the sensor and C_y is a non-invasive capacitive sensor itself. Measured capacitance in this instance is dependent on both C_x and R_x respectively.

2.3.17. Conductivity comparison of variable concentration NaCl

The NaCl sensor code measurements showed that there was a clear decrease in the sensor code values as the concentration of aqueous electrolyte increased. However, this is contrary to what should be observed if only relative permittivity is considered. the previous section described how a conductive element effects a fringing field capacitive sensor, so the conductivity of the NaCl solutions also needed to be known. The DAK measurements show a linear, but large increase in the conductivity of NaCl solutions as concentration increases, as seen in Figure 2.22:
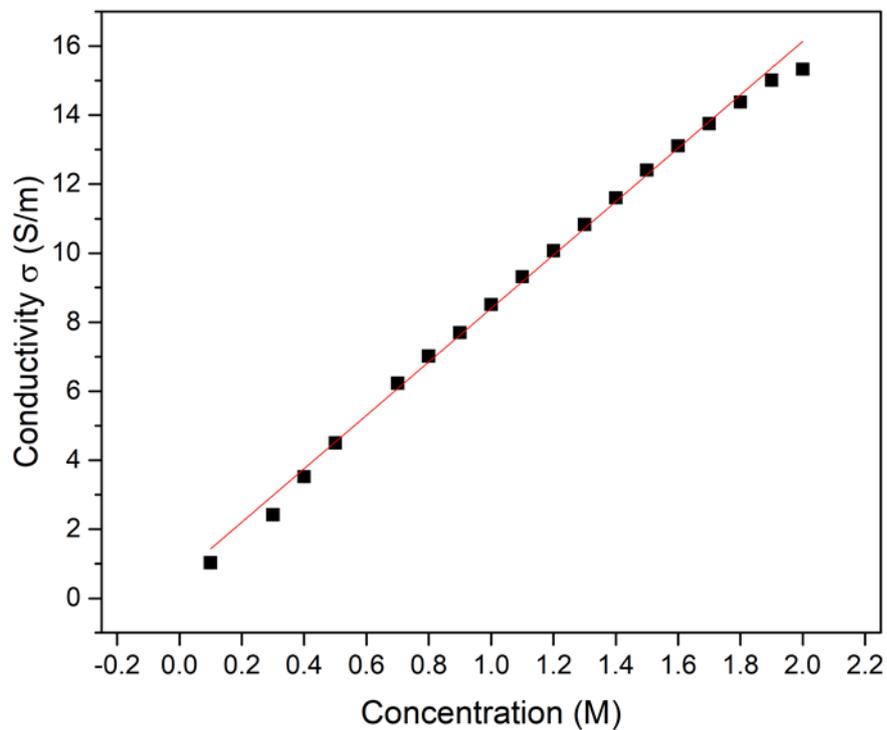
There is a linear increase in conductivity as aqueous electrolyte concentration increases. moreover, the increase in the conductivity of the solution is large enough that it results in the capacitive load on the sensor increasing, despite the fact that the relative permittivity of the solution decreases as the concentration of aqueous NaCl increases. Conductivity was plotted against sensor value, shown in Figure 2.23:
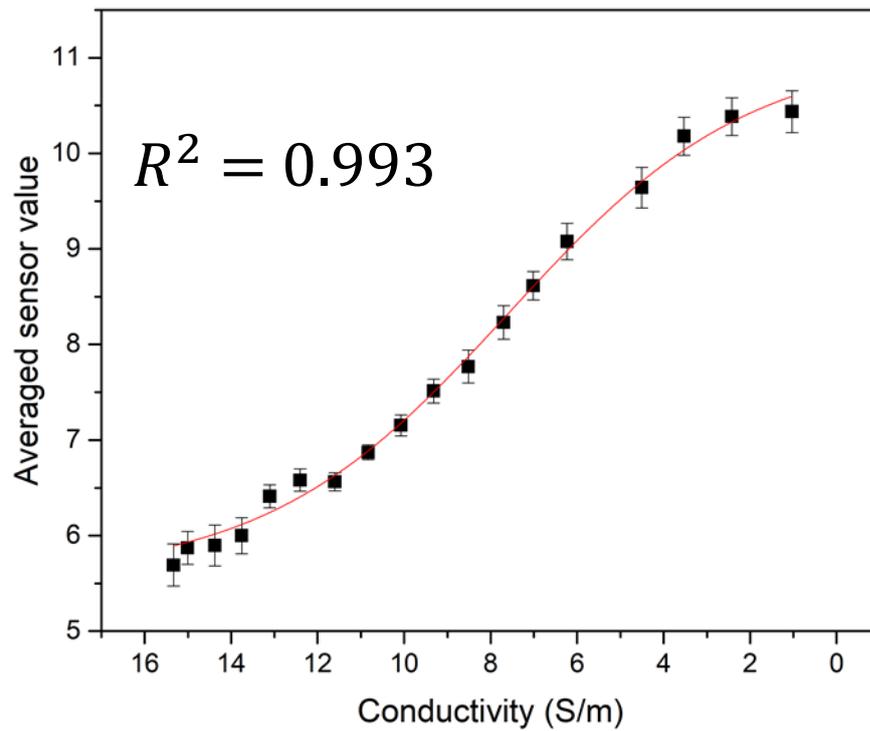
Figure 2.23 - Plot of sensor code of aqueous NaCl plotted against measured conductivity of aqueous NaCl.

Conductivity shows a good fit when compared to sensor value for the PDMS coated tag, but as previously discussed the sensor in this instance is also effected by permittivity. A means of comparison that accounts for both variables is required.

2.3.18. Using tan δ of solutions as a means of accounting for both permittivity and conductivity

A ratio known as the tan δ is a complex expression of both the conductivity and the permittivity of a material, shown in Equation 2.7:

$$\tan \delta = \frac{\varepsilon^{''}}{\varepsilon'}$$

Equation 2.7 – Equation for calculating tan δ.

Where $\varepsilon^{''}$ is the imaginary part of relative permittivity, which relates directly to materials conductivity, and $\varepsilon^{'}$ is the real part of relative permittivity. An increase in a given materials conductivity (when permittivity is unchanged) will result in an increase in the $\tan \delta$. Figure 2.24 shows the change in $\tan \delta$ for aqueous NaCl:

$$R^2 = 0.999$$
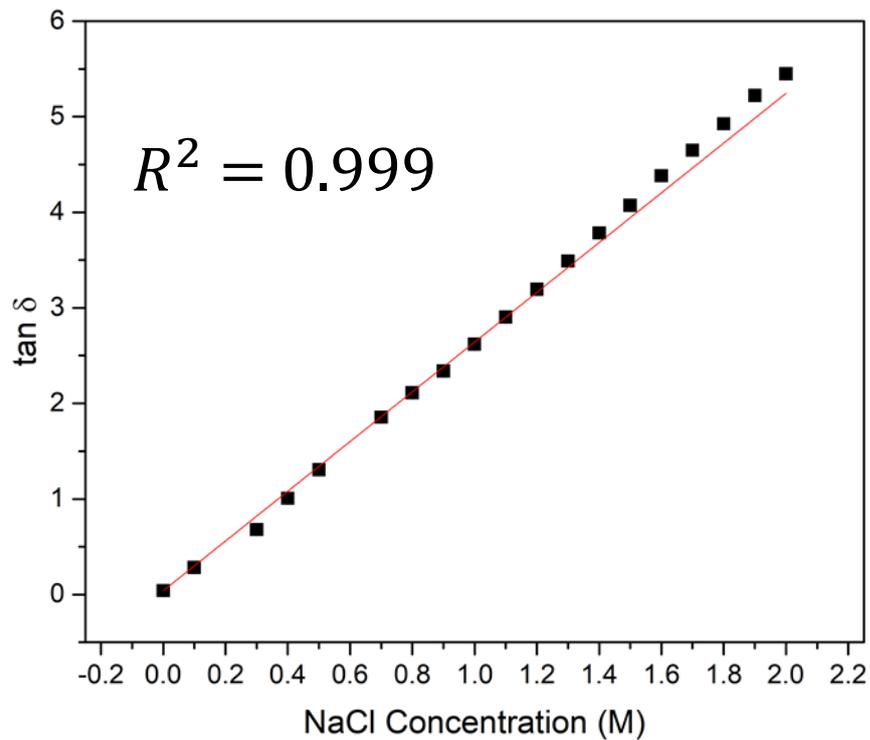
Figure 2.24 – Plot showing the change in the tan δ of Aqueous NaCl solutions from 0-2M from DAK measurements.

Tan δ increases linearly with increased aqueous electrolyte concentration. The derived linear fit is shown in Equation 2.8:

$$y = 2.6\,x \,\pm\, 0.03$$

Equation 2.8 – Equation for the line fit derived in Figure 2.24.

Next tan δ was plotted against sensor values, shown in Figure 2.25:

$$R^2 = 0.996$$
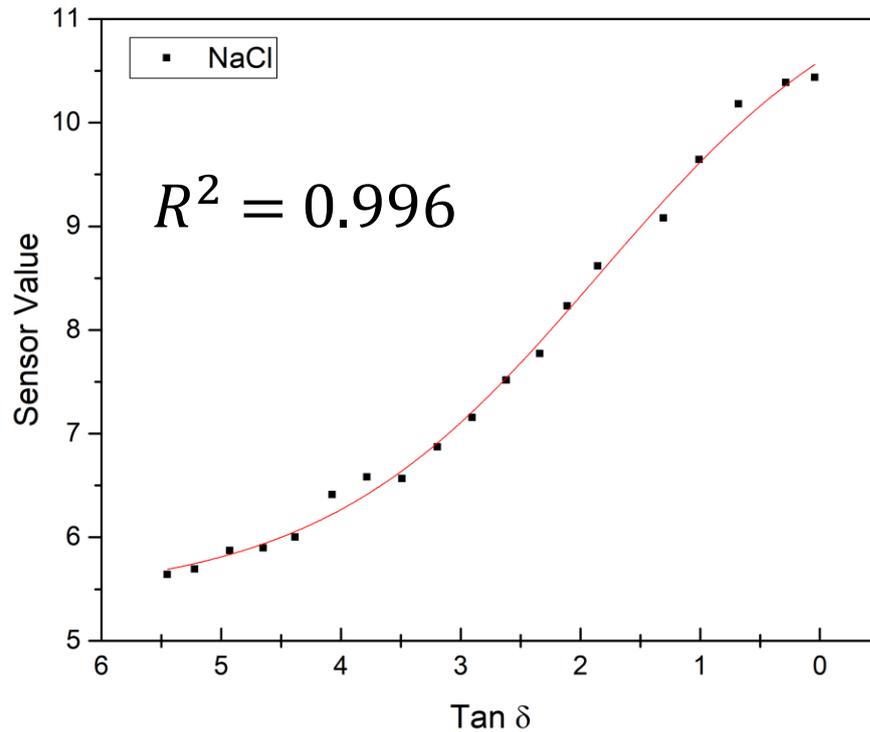
Figure 2.25 – Plots showing sensor code of aqueous NaCl plotted against measured Tan δ of aqueous NaCl on a PDMS coated RFMicron RFM-2100 AER.

Figure 2.25 shows that as the tan δ increases, the sensor code decreases for NaCl solutions. Even when the relative permittivity decrease is accounted for, the large increase in conductivity of NaCl solutions with an increasing concentration results in an increase in the tan δ, and as a result the net capacitive load increases on the PDMS coated RFMicron sensor tag, causing the reactance change in the tag that is compensated for accordingly by adjusting the impedance of the self-tuning chip. As tan δ is expressed using both of the key dielectric properties that have a real effect on capacitance for a fringing field capacitor, it is also the variable that derives the best Boltzmann fit of the sensor data compared to the other two variables.

2.3.19. Sensor optimisation

Detecting a change in aqueous electrolyte concentration between 800-860 MHz with a fixed power averages the sensor values across 12 data points (one per 5 MHz), at a fixed power of 9 dBm. It was investigated whether or not a shortened frequency range (845-865 MHz) could be used to achieve the same sensing capability. Not only would data gathering be faster, but also 845-865 MHz is closer to the European RFID band (868 MHz).
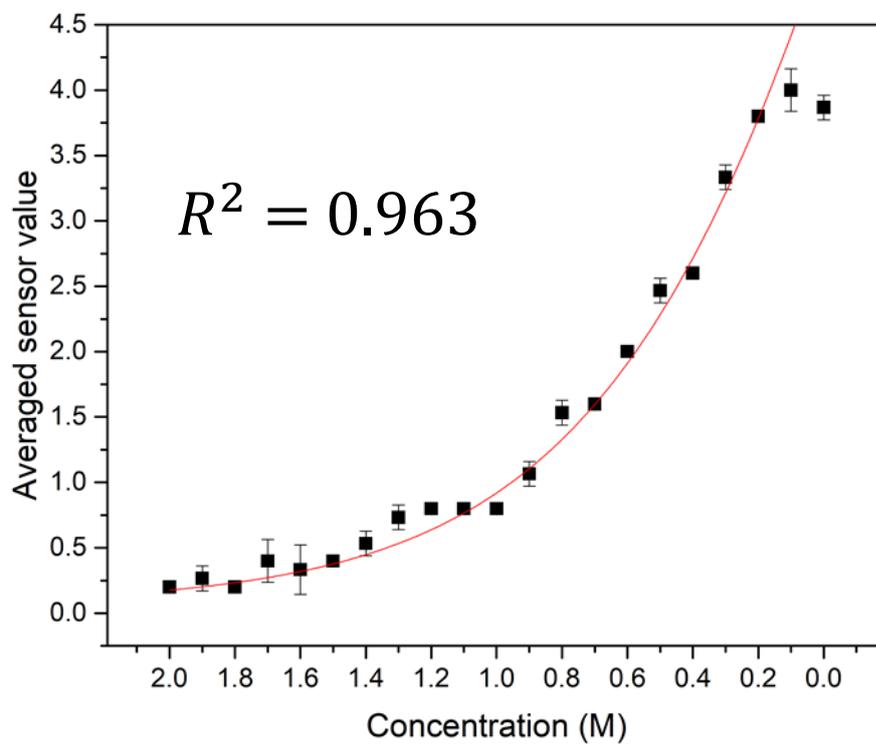

Figure 2.26 - The effect of NaCl salt solutions on the tag averaged sensor code at 845-865 MHz.

Whilst the data for Figure 2.26 compares well with the data from Figure 2.19, the R^2 value is lower in comparison. The fitting equation is shown in Figure 2.26:

$$y = 0.06 + \frac{(16.56 \pm 26.93 - 0.07)}{1 + e^{(\frac{x + 0.39}{0.48})}}$$

Equation 2.9 – Fitting equation of the curve derived from Figure 2.26.

The reduced sensor code range is nonetheless capable of discerning changes in concentration, albeit less capable than the increased frequency range. The reduced sensor range produced repeatable data with a narrow error range; however, the error range was nonetheless larger than the wider frequency ranged data used previously.

2.3.20. Single point sensor optimisation

Following the sensor optimisation study, a study using a single integer value for each
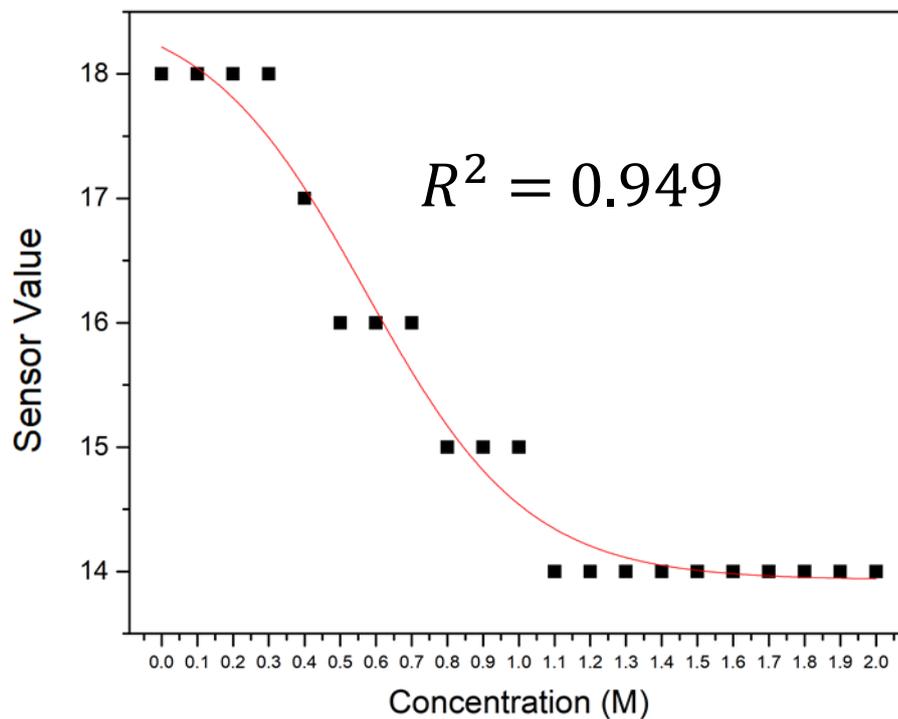
Figure 2.27 – Plots showing the highest integer value for NaCl aqueous solutions between 0-2 M across the 800 – 860 MHz frequency range and across the 8-20 dBm transmitted power range.

concentration was investigated to determine whether further truncating the sweep settings for aqueous salt measurements was practical. There were two approaches that were used for single value sensor measurements. Firstly, the lowest frequency for a given concentration at which a Zero is encountered, and secondly the highest integer value for any given concentration under test. Both of these are shown in Figure 2.27 and Figure 2.28:
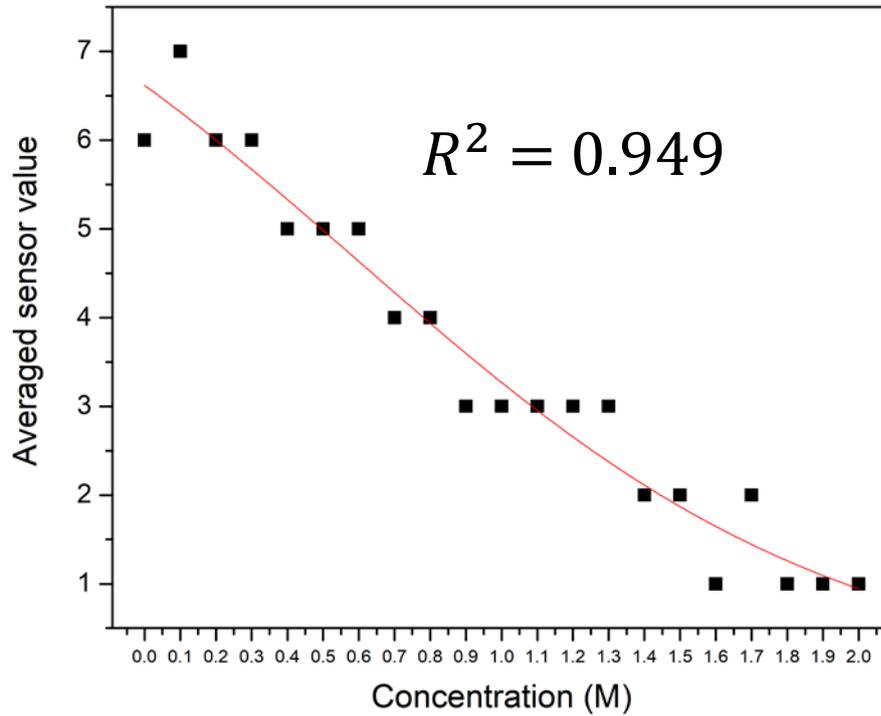
Figure 2.28 - Plot showing the sensor data for NaCl aqueous solutions between 0 - 2 M with a fixed frequency of 845 MHz and a fixed power of 9 dBm.

The fitting equation for Figure 2.27 & Figure 2.28 is shown in EQ A,B respectively:

$$y = -0.14 \pm 1.60 + \frac{(9.44 \pm 4.33 + 0.14 \pm 1.6)}{1 + e^{\left(x - 0.59 \pm \frac{0.47}{0.68 \pm 0.45}\right)}}$$

Equation 2.10 – Fitting equation derived from Figure 2.27.

$$y = -0.14 \pm 1.60$$

Equation 2.11 - Fitting equation derived from Figure 2.28.

The R^2 value for both Figure 2.27 and Figure 2.28 are lower than the R^2 observed for measurements that utilised a larger number of data points. Whilst Figure 2.27. shows a routine decrease in the sensor value as the concentration of NaCl increases, and this data is based upon a single value, it's a less convenient measure of concentration compared with Figure 2.28 as it still requires a large sweep area to ensure that the highest value across the sweep range is included. In Figure 2.28, the general trend of a decrease in sensor value can be observed as concentration increases; however, there are some values (between 1.6-1.7 M) that have

irregular values. Nonetheless, Figure 2.28 shows the capability of the system to give approximate concentration values that sit within a range set. This function could be used as a spot check to determine whether a solution is within a certain tolerable range, and then if required a larger sweep range (such as the sweep ranges used in Figure 2.20 and Figure 2.26) can be used for a higher degree of precision if required.

2.4. Conclusions and future work

The aim of this chapter was to modify an existing commercial UHF RFID tag with a polymer film to alter its functionality. An auto-tuning moisture sensing tag was used. Initially, a PDMS layer was added to increase the hydrophobicity of the tag substrate. The effect of this reduced the moisture sensitivity of the RFMicron RFM-2100 AER modified by this process. This was initially tested with a 200 μm PDMS film, and then a series of PDMS films of differing thicknesses to observe the degree to which the tag could have its moisture sensitivity altered. A notable advantage of the addition of this hydrophobic boundary layer is that the tag (which would previously absorb water and be rendered inoperable after the addition of 0.2 ml of water to the sensor area)[12] is now reusable. The variable film thickness studies showed that as the Thickness of the PDMS layer applied reaches approx. 1.8 mm, the observed sensor value of the tag when no water is applied to the substrate and when water is applied to the substrate converge, nearing a detection limit of sorts. Following this, a 500 μm thick PDMS layer was used with the RFMicron RFM-2100 AER to test whether the system could be used to distinguish aqueous electrolyte solutions of variable concentration. The system could be used to distinguish several aqueous electrolyte solutions by concentration (with a 0.5 M step). This was further scrutinised with NaCl using a 0.1 M step. The system was found to be capable of distinguishing between 0.2-2 M NaCl solutions with a wide sensor sweep (800-860 MHz). Although relative permittivity decreases with regards to aqueous sodium chloride (and the other aqueous electrolyte's tested), as the concentration increases, the capacitive load increases, which corresponds to a decrease in sensor values. With regards to a non-invasive capacitor, both conductivity and relative permittivity have an effect on measured capacitance. The increase in conductivity is very large

in aqueous sodium chloride, to the extent where the measured capacitance increases with concentration. This phenomenon was utilised to be able to observe different sensor output values at varying concentrations of sodium chloride between 0-2 M.

Narrower sweep settings were also used to determine if a sweep range closer to the European RFID bandwidth could provide useable sensing data. It was found with a sweep of 845-865 MHz that solutions between 0.2-2 M could also be discerned, albeit with a larger associated error. Finally, two methodologies that utilise a single data point were used in order to determine if a single point spot-check method could be used to determine aqueous salt concentration. It was found that although using the highest integer value observed could be used to determine a discrete series of concentration ranges, the requirement to sweep a larger power and frequency range in order to derive the largest integer value limits the feasibility of this sensing methodology.

Finally, a single point sensor response at 845 MHz (with a fixed power of 9 dBm) was used. It was found that this methodology could be used to discriminate between a series of concentration ranges, albeit with a lower discrimination capability when compared to the larger sweep settings. This setting could be used as a faster interrogation method, where knowing a more precise salt concentration is less critical. The wider sweep setting could then be utilised if the initial spot check reveals that salt concentration has deviated from an expected range to determine a precise salt concentration.

Future work should focus on increasing the sensitivity of the system whilst retaining the ability to reduce the detuning extent the high permittivity load has on the tag. One suggestion would be to incorporate microfluidic channels in the area above the IDC. This would allow a controlled volume of solution to be drawn into the PDMS layer, increasing sensitivity whilst being able to control the relative volume of solution being allowed into the low permittivity layer, reducing the likelihood of the tag detuning grossly.

2.5. References

1   A. J. R. Hillier, V. Makarovaite, C. W. Gourlay, S. J. Holder and J. C. Batchelor, *IEEE Sens.*

J., 2019, **19**, 5389–5395.

2   P. Kassal, M. D. Steinberg and I. M. Steinberg, *Sensors Actuators B Chem.*, 2018, **266**, 228–245.

3   T. Glennon, C. O'Quigley, M. McCaul, G. Matzeu, S. Beirne, G. G. Wallace, F. Stroiescu, N. O'Mahoney, P. White and D. Diamond, *Electroanalysis*, 2016, **28**, 1283–1289.

4   D. P. Rose, M. E. Ratterman, D. K. Griffin, L. Hou, N. Kelley-Loughnane, R. R. Naik, J. A. Hagen, I. Papautsky and J. C. Heikenfeld, *IEEE Trans. Biomed. Eng.*, 2015, **62**, 1457–1465.

5   R. A. Potyrailo, C. Surman, D. Monk, W. G. Morris, T. Wortley, M. Vincent, R. Diana, V. Pizzi, J. Carter, G. Gach, S. Klensmeden and H. Ehring, *Meas. Sci. Technol.*, 2011, 22, 82001–17.

6   R. A. Potyrailo, N. Nagraj, Z. Tang, F. J. Mondello, C. Surman and W. Morris, *J. Agric. Food Chem.*, 2012, **60**, 8535–8543.

7   R. A. Potyrailo, C. Surman, N. Nagraj and A. Burns, *Chem. Rev.*, 2011, **111**, 7315–7354.

8   S. Manzari, A. Catini, G. Pomarico, D. Natale and G. Marrocco, *IEEE Sens. J.*, , DOI:10.1109/JSEN.2014.2329268.

9   C. V. Rumens, M. A. Ziai, K. E. Belsey, J. C. Batchelor and S. J. Holder, *J. Mater. Chem. C*, 2015, **3**, 10091–10098.

10 J. Siden, X. Zeng, T. Unander, A. Koptyug and H.-E. Nilsson, in *2007 IEEE Sensors*, IEEE, pp. 308–311.

11 S. Kim, T. Le, M. M. Tentzeris, A. Harrabi, A. Collado and A. Georgiadis, in *Proceedings of IEEE Sensors*, 2014, vol. 2014-Decem, pp. 1507–1510.

12 RFM2100 wireless flexible moisture sensor - RFMicron, http://rfmicron.com/rfm2100-wireless-flexible-moisture-sensor/, (accessed 5 December 2017).

13 G. Theses and S. Bhat, *Scholar Commons Salinity (conductivity) sensor based on parallel plate capacitors Scholar Commons Citation*, 2005.

14 X. Hu and W. Yang, , DOI:10.1108/02602281011010772.

15 SpeedMixer™ - DAC 150.1 FVZ-K, https://www.speedmixer.co.uk/dac150.1fvzk.php,

(accessed 22 September 2019).

16   Automatic precision film applicator CX4 - mtv messtechnik oHG webshop, http://mtv-webshop.sucaba.de/MTCX4, (accessed 22 September 2019).

17   Tagformance Pro | Voyantic, https://voyantic.com/products/tagformance-pro, (accessed 22 September 2019).

18   *Regulatory status for using RFID in the EPC Gen2 (860 to 960 MHz) band of the UHF spectrum*, 2019.

19   Voyantic Ltd. » Tagformance lite, http://www.voyantic.com.

20   E. Llez, J. Rubio, F. Rubio, E. Morales and J. L. Oteo, *Synthesis of inorganic-organic hybrid materials from TEOS, TBT and PDMS*, .

21   V. Landry, P. Blanchet and G. Boivin, *J. Nanoparticles*, 2013, **2013**, 1–8.

22   J. A. O'Neill, M. L. Passow and T. J. Cotler, *J. Vac. Sci. Technol. A Vacuum, Surfaces, Film.*, 1994, **12**, 839–845.

23   S. E. Braslavsky, *Pure Appl. Chem.*, 2007, **79**, 293–465.

24   and U. The NIST Reference on Constants, Units, CODATA Value: vacuum electric permittivity, https://physics.nist.gov/cgi-bin/cuu/Value?ep0, (accessed 1 September 2019).

25   M. C. Caccami and G. Marrocco, *IEEE Trans. Antennas Propag.*, 2018, 1–1.

26   M. C. Caccami and G. Marrocco, *2016 IEEE Antennas Propag. Soc. Int. Symp. APSURSI 2016 - Proc.*, 2016, 1273–1274.

27   A. A. Nassr and W. W. El-Dakhakhni, , DOI:10.1088/0957-0233/19/7/075702.

28   K. No, J. Hilland and U. Kaatze, *Dielectric Properties of Aqueous NaCl Solutions at Microwave Frequencies*, 1997.

29   R. Buchner, G. T. Hefter and P. M. May, *Phys. Chem. A*, , DOI:10.1021/jp982977k.

30   T. Chen, G. Hefter and R. Buchner, *J. Phys. Chem*, 2003, **107**, 4025–4031.

31   S. Liu, G.-Z. Jia, & Feng, H. Liu and F.-H. Liu, , DOI:10.1080/00319104.2015.1074044.

32   K. Levenberg, *Q. Appl. Math.*, 1944, **2**, 164–168.

33   P. Azimi and M. Heidari, *Res. J. Appl. Sci. Eng. Technol.*, 2011, **3**, 53–60.

Chapter 3: Passive UHF RFID Dielectric Sensor for Water/Alcohol mixes.

3.1. Introduction

Water impurities in organic solutions pose an issue industrially, specifically for alcohol distillation processes and quality control in organic solvents[1]. The standard method for determining the degree of water impurity in these systems is to use a Karl-fisher titration[2], and more recently automated Karl fisher titration systems[3]. Other handheld systems deployed for less precise determination of water impurities include alcohol hydrometers, available commercially[4] that can determine water content with an accuracy of 0.1% v/v. Whilst these systems are highly accurate, they are very expensive (the hygrometer mentioned costs £2652.72 at the time of writing). Whilst automated Karl-fisher titrations require no manual operation after insertion of the sample, they cannot be used in-situ. Hygrometers can be used in-situ, but require manual operation and opening of containers to read solutions. A means of wireless determination of water/alcohol mixes could provide a low maintenance, high throughput means of quality control assessment. Furthermore, the inventory capabilities of wireless systems present an ideal low cost, and most importantly dual-purpose solution.

Determining water/alcohol mixes have been sparsely investigated through means of wireless sensing, but there has been a large increase in interest in the characterisation of polar organic solutions using wireless systems in the last decade[5]. Although a large focus of this research has been centred upon using spectroscopic techniques to gain an understanding of the interactions between molecules based upon their dielectric properties[6,7], there has been a growth in application based deployment of dielectric spectroscopic systems[8], particularly in the pharmaceutical and biomedical sectors. The most common method of materials characterisation in this field has been through reflectance methods[9], with coaxial probes being the most popular method of materials charecterisation[10]. Such is the popularity of coaxial probes that they are frequently used for in-situ monitoring in industrial processes[11,12]. Coaxial probes can provide very accurate data regarding dielectric properties of materials, but have to be physically connected to a variable network analyser (VNA) in order to be used.

Several works have been published in recent years with an aim to design low-cost systems that facilitate materials characterisation whilst also maintaining an unobtrusive form factor that allows for in-situ monitoring. Lobato-morales[13,14] et al developed two platforms for materials sensing; a substrate integrated waveguide (SIW) and an epsilon near zero tunnel (ENZ) architecture that were initially characterised in the presence of small volumes of organic solvents, and then were implemented into a measurement system. Cole[15] et al developed a chipless system that could distinguish high and low permittivity (as well as high loss) samples. The system utilised a thin film slotted cylindrical cavity. This was wrapped in a polytetrafluoroethylene (PTFE) pipe. Liquid samples loaded into the pipe could be determined, with methanol, ethanol, butanol and water all being characterised. Such was the sensitivity of the system that a second configuration was also demonstrated that allowed for the volume of water within the piping to be determined based on the degree of detuning of the antenna, with an accuracy of 0.1 ml. Zafiri[16] et al have also developed a chipless sensor for liquid sensing, which consisted of an LC resonator that could monitor the effective permittivity of a series of solutions placed into a cuvette (containing 3ml of liquid) placed atop the tag at 120 MHz. Costa[17] et al also developed a frequency selective chipless system that could be applied to a material of interest and then read to interrogate. The system consisted of two 45° tilted dipoles printed onto a Rogers 4333 substrate that had an associated change in resonant frequency when in in contact with variable permittivity materials. Chipless monitoring systems are an attractive option due to their low cost and simplicity, but can only be deployed at higher frequencies (above 1GHz), and requiring a relatively large frequency range to differentiate solutions.

More recent works have focused on the UHF region to overcome the above mentioned issue. Makarovaite[18] et al developed a passive UHF meandering dipole antenna capable of determining several solutions, including methanol, acetone, water, xylene and butan-1-ol. The system shows distinct and measureable differences in resonant frequency for the aforementioned solutions when in close proximity to the label. A practical application was also demonstrated, with the system being capable of determining solution composition when adhered to a petri dish or a

200 ml borosilicate glass bottle. The system could also be read up to 7 metres away. The only disadvantage to the system was the requirement of a 200 MHz band to determine solution composition. Despite the fact this is an enormous improvement to previous examples (especially when considering that the system operates at a lower frequency) a system that can determine changes in dielectric properties of materials within a narrower frequency band would be immensely useful.

In this Chapter, the same PDMS coated RFMicron RFM2100-AER used in chapter 2 was tested for viability as a means of sensing a series of water/organic solvent mixes, ranging from 100% water content to 100% organic solvent content (with a step of 10 % relative wt.% for each system tested). Normally, it is desirable to use different measurement techniques to determine the dielectric properties of high and low loss liquids[19]. Here, we demonstrate that in a low loss environment the PDMS coated tag is capable of discriminating between water/organic systems of varying relative compositions (by using sensing values taken between 800 – 860 MHz).

3.2. Experimental

3.2.2. Materials and methods

The alcohol sensor incorporates the RFMicron RFM 2100-AER, with a PDMS layer over the tag, applied as described in chapter 2. The preparation of the cross-linked PDMS layer is as described in chapter 2 also. As a 500 µm layer proved to be an effective thickness for studies in chapter 2, it was also used for the studies in this chapter. Ethanol (99%+ absolute), methanol (99.5%, extra pure), propanol (99 %), acetone (99.6 %, ACS reagent), and acetonitrile (99.5 %, extra pure) were purchased from FisherSci. A series of commercial alcohols were purchased from a commercial retailer. Chambord (16.5 % alcohol), Sainsbury's Conegliano Prosecco (12 % alcohol), Southern Comfort (35 % alcohol), Disaronno (28 % alcohol) and Marylebone Gin (50 % alcohol) were bought and tested. Unlike the previous chapter, sensor value measurements were performed on Voyantic® Tagformance Pro equipment rather than Tagformance Lite equipment. Although the measurement apparatus used changed, the Tagformance pro is still capable of sensor code

measurements. However, whilst the previous Sweep settings could use a series of fixed transmitted powers to attain a series of sensor code values for a single frequency, the Tagformance Pro shows the sensor value for the turn-on power of the tag at the designated frequency. This means that although the results generated for the materials tested in this chapter also use a single value for each frequency used in a frequency sweep, the power value will vary. As the Tagformance pro has a native capability to read the sensor code, there was no need to use a third-party program to obtain sensor data from the tag. Normally, the Tagformance is set to a mode known as "query mode". In query mode, the transmitter antenna will send a query command that will result in a "reply command" from the tag. The reply command simply means that the tag is recognising interrogation from the reader. When in query mode, the tag will not send any useable sensor code information. To use the tag for sensing purposes, the Tagformance pro must be set to "read mode". In this mode, the tag will be able to send a read command that will allow the 5-bit sensor code to be read. This will translate on the Tagformance software suite as a single integer value (between 0-31) for a measured frequency. Figure 3.1 shows the Tagformance measurement suite software, set up for usage with the RFMicron RFM-2100 AER and for a UHF tag to have its sensor data read:
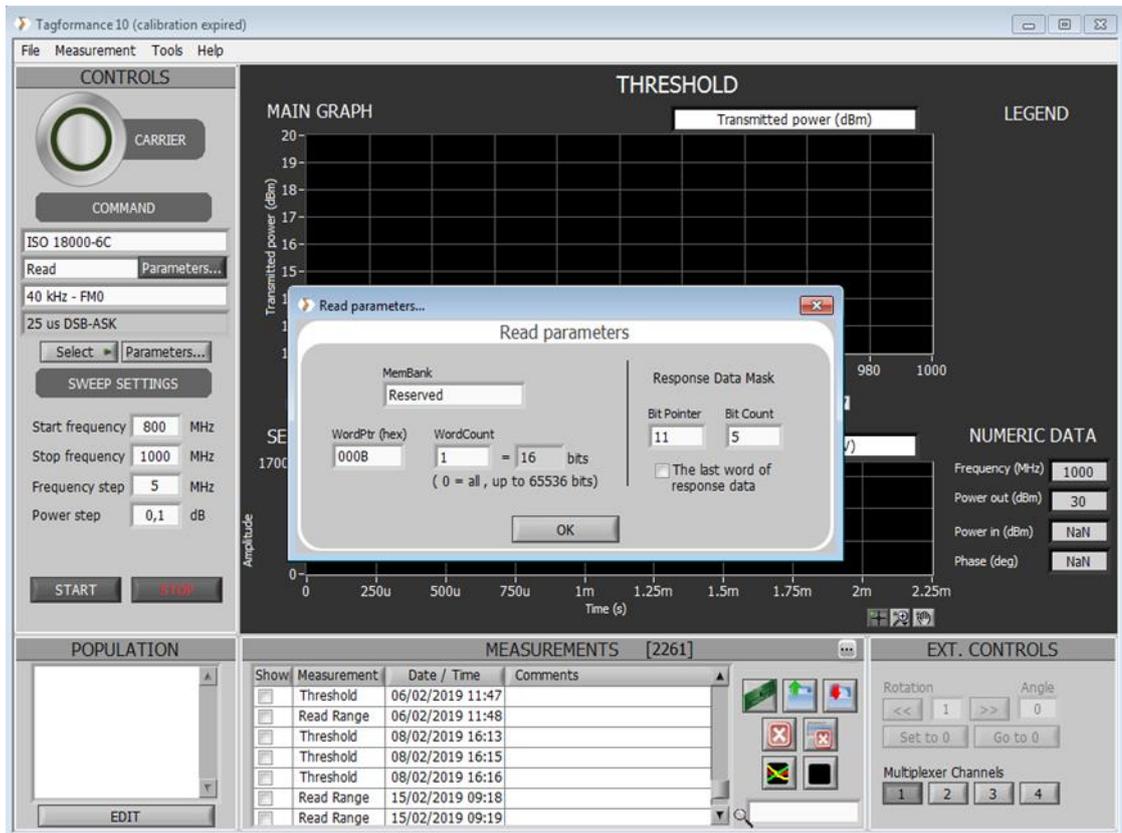
Figure 3.1 - The Tagformance 10 measurement suite, with the read parameter settings to be able to read sensor response data.

The software is very similar to the Tagformance Lite measurement suite[20]; however, the added parameter option means that as well as being able to read standard tag parameters such as read range and transmitted power, sensor response can be obtained once the correct read parameters are input. These sensor responses can also be read in tandem with the aforementioned tag parameters. This is a crucial difference to the sensor bench suite used in the Tagformance Lite software in chapter 2. In the previous reader setup, taking sensor measurements required a separate program. Moreover, running sensor measurements meant that other parameters associated with the tag could not be observed.

Table 3.1 shows the hardware specifications of the Tagformance Pro:

Table 3.1 - Table showing the specifications of the Tagformance Pro.

Parameter	Value	Unit
Frequency range (standard)	800-1000	MHz
Frequency range (wideband)	700-1200	MHz
Frequency resolution	100	kHz
Output power	0-36	dBm
Power resolution	+/- 0.1	dB
Power accuracy	+/- 0.5	dB
Output impedance	50	σ
Sensitivity	-75	dBm
Sensor code measurements	0-31	N/A

3.2.3. Preparation of organic solvent/water samples

3.2.3.1. Relative permittivity measurements

200 ml solutions of 5 different organic liquids Table 3.2 in water were prepared at weight percentages of 0, 10 etc. to 100% (organic liquid as percentage of total weight):

Table 3.2 - Table showing all compounds used in DAK measurements of alcohols

Compound name	Chemical structure	Density
Methanol	H_3C-OH	792 kg/m³
Ethanol	$H_3C-\overset{H_2}{C}-OH$	789 kg/m³
Propan-2-ol	$H_3C-\underset{H}{\overset{OH}{C}}-CH_3$	803 kg/m³
Acetone		784 kg/m³
Acetonitrile	$N{\equiv}C-CH_3$	786 kg/m³
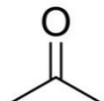
The density of each organic solvent was accounted for when making up the 200ml sample. The volume of solution remained fixed for relative permittivity measurements with the Speag probe. A laser thermometer was used to measure all solution temperatures and all measurements were performed at 22 °C. The permittivity, conductivity and tan δ of each solution of each solution were measured (from 700 – 5995 MHz) 10 times and then averaged from 800 – 860 MHz.

3.2.4. RFID Measurements

Organic solvent/water mixes were prepared for each of the 5, with the same weight percentages as in the relative permittivity studies. 5 g worth of organic solvent/water were mixed together with different relative quantities of water/organic solvent. Samples were prepared in glass vials with seals to reduce evaporation of organic solvents Following this, all samples were allowed to reach 295 K before being used for RFID sensing. Water/alcohol mix depositions were performed as described for aqueous electrolyte depositions in chapter 2. The frequency sweep used for sensor code measurements were 800-860 MHz again, with a step of 5 MHz. As the Tagformance pro can utilize a lower frequency step between measurements for sensor code measurements, a lower step size was used than in the aqueous electrolyte studies performed in Chapter 2.

3.2.5. PDMS swelling studies

For swelling studies, 75 PDMS squares (2 cm x 2 cm x 0.2 cm) were prepared. Silanol terminated PDMS was cross-linked using the same stoichiometric ratios described in chapter 2 relative to both TVS and tin (II) ethyl hexanoate[21]. The PDMS elastomer mix was also homogenised using the same method described in chapter 2. After the speed mixing process, the curing PDMS elastomer mix was poured into a Teflon mould tile. Each mould square had dimensions of 20 x 20 x 2 mm (length x width x depth). PDMS was poured into the mould channel and then visually inspected to ensure that the elastomer was level to the top of the mould. After pouring, the Teflon mould tiles were left to cure for 2 hours before being transferred to a 65oC oven to cure for 18 hours. The tiles were left for 2 hours so as not to disturb the curing elastomer mix, which can result in a lopsided curing. Following the curing process, the cured PDMS squares were removed from the Teflon mould by first running a scalpel down the length and the width of the square mould. Following this, a micro chattaway scalpel was carefully used to pry the PDMS square away from the underside of the mould. Both these measures had to be taken to reduce the likelihood of the square mould tearing during removal. Once removed, the square was cut in half and then each half was weighed on a 100 g x 0.0001 g balance. Following this, each portion

was added to a vial with an excess of water/organic solvent mixture. The squares were left to swell in the solvent mix for 24 hours. Following this, the PDMS squares were removed from the vial using tweezers, and weighed on the same balance used for the dry samples. The degree of swelling by mass was then calculated using Equation 3.1[22]:

$$Q = \frac{(mass\ of\ swollen\ polymer - mass\ of\ dry\ polymer)}{mass\ of\ dry\ polymer}$$

Equation 3.1 – Equation showing how swelling ratio Q was calculated.

Once the swelling factor Q was established, volume of trapped solvent was then calculated within the PDMS network, using the following equation:

$$Qv = Q\frac{1}{\rho}$$

Equation 3.2 – equation showing how swelling ratio by volume Qv was calculated.

Where ρ is the density of the solvent (or water/solvent mix as an average).

3.2.6. Correlation and multiple regression statistical analysis models

Correlation and linear regression were performed in Microsoft Excel. The correlation function used the Pearson product moment coefficient[23], and regression was performed using the regression output tool in Microsoft Excel, described in[24].

3.3. Results and Discussion

3.3.2. Sensor code measurements of water/organic solvent mixes

Sensor code values were obtained for all water/organic solvent mixes, and are shown as values averaged from 800 – 860 MHz with a step of 5 MHz. Unlike in Chapter 2, the Tagformance Pro equipment used for Chapter 3 only provides sensor values at the turn-on power, so one value per frequency step is used to derive an averaged value (so in this case, 12 values averaged from

800 – 860 MHz gives the average value shown for each water/organic solvent mix). Figure 3.2 is

shown below:

(a).

(b)

(c).

(d)

(e)
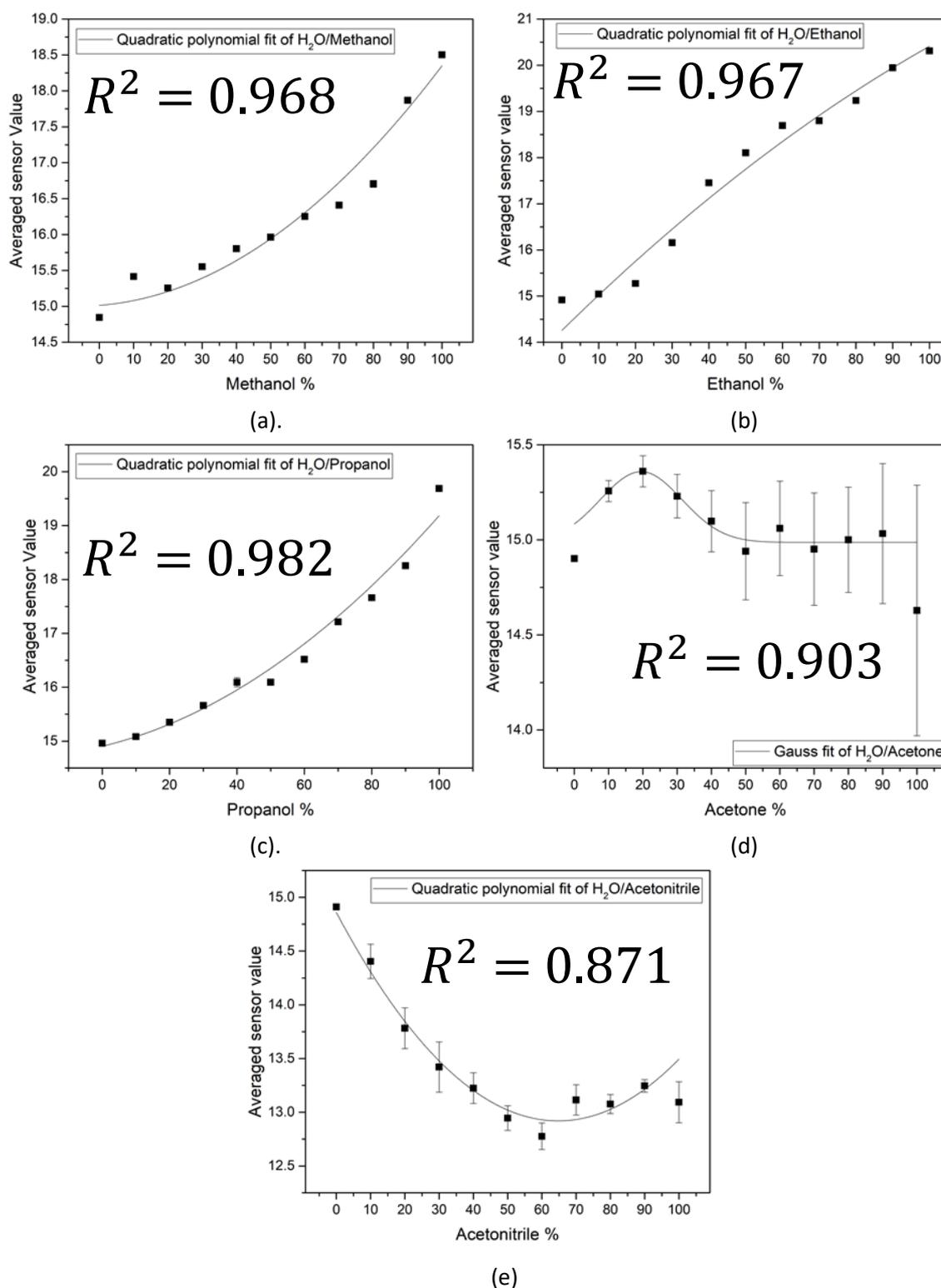
Figure 3.2 - Plot of sensor values for water/organic solvent mixes of (a) methanol (b) ethanol

(c) propanol (d) acetone and (e) acetonitrile.

The water/alcohol mixes showed a relatively consistent trend, with incremental increases in sensor value as the percentage of alcohol increased. Notably, very high percentages of methanol showed a very large increase in sensor value. All water/alcohol mixes also showed very small associated errors when performed in triplicate. The water/acetonitrile mixes showed larger errors between measurements. However, water/acetone mixes showed the largest errors between measurements. Moreover, whist all the water/alcohol mixes have increased sensor values as the relative mass of alcohol to water increases, the sensor values of acetonitrile decrease as its relative mass to water increases, and the fitting curve for acetone/water shows no trend. For all of the alcohols, the fitting curve derived from the data has no point where the curve bottoms out and then increases again. This is useful for sensing purposes, as any overlapping sensor values for differing compositions it means that a given value can have two possible compositions. Fitting equations for the 5 systems are shown in Equation 3.3 - Equation 3.7:

$$y = -0.004x + 2.96e^{-4}x^2 + 15.01$$

Equation 3.3 – Methanol/water sensor value fitting equation.

$$y = 0.008x - 1.66e^{-4}x^2 + 14.26$$

Equation 3.4 – Ethanol/water sensor value fitting equation.

$$y = 0.004\,x - 0.002x^2 + 15.08$$

Equation 3.5 – Propanol/water sensor value fitting equation.

$$y = 0.011 + \left(\frac{14.32}{99.84 \times \sqrt{\frac{\pi}{2}}}\right) \times e^{(-2(\frac{x-55.10}{99.84})^2}$$

Equation 3.6 – Acetone/water sensor value fitting equation.

$$y = 0.004x - 2.96e^{-4}x^2 + 15.01$$

Equation 3.7 – Acetonitrile/water sensor value fitting equation

3.3.3. Dielectric properties of water/organic solvent solutions

3.3.3.1. Relative permittivity of water/organic solvent solutions

It was expected that when the solution conductivity of a system above the PDMS layer of the sensor is low (and as a result the degree of loss), relative permittivity of the system was the predominant factor that affects capacitance. To confirm, dielectric properties of all water/organic solvent mixes were acquired, and relative permittivity is shown inFigure 3.3, and fitting equations were derived for all water/organic solvent systems, shown below in Equation 3.8 - Equation 3.12:

$$y = -0.56x + 9.46e^{-4}x^2 + 77.17$$

Equation 3.8 – Methanol/water relative permittivity fitting equation.

$$y = -0.66\,x + 3.16e^{-4}x^2 + 79.72$$

Equation 3.9 – Ethanol/water relative permittivity fitting equation.

$$y = -1.28x + 0.005x^2 + 79.74$$

Equation 3.10 – Propanol/water relative permittivity fitting equation.

$$y = -0.76x + 0.001x^2 + 77.73$$

Equation 3.11 – Acetone/water relative permittivity fitting equation.

$$y = -0.45x + 78.64$$

Equation 3.12 – Acetonitrile/water relative permittivity fitting equation.
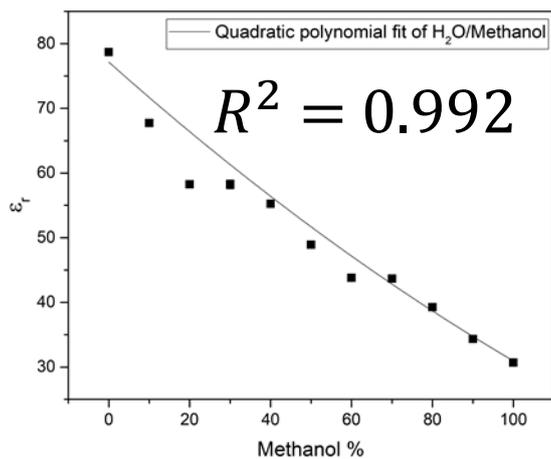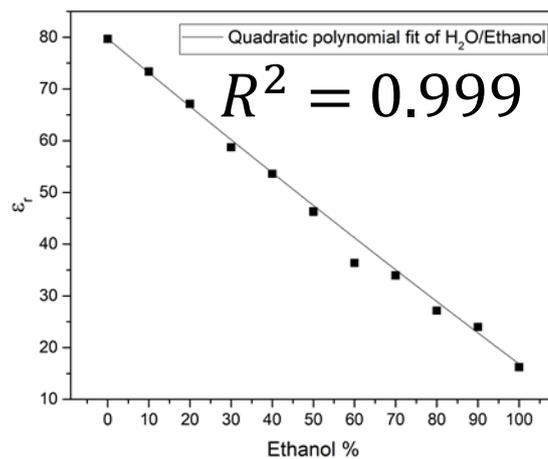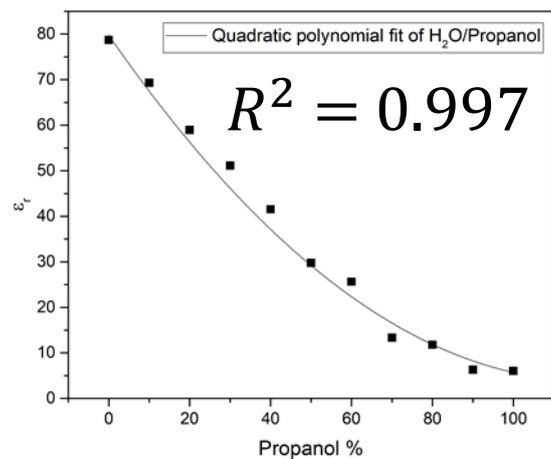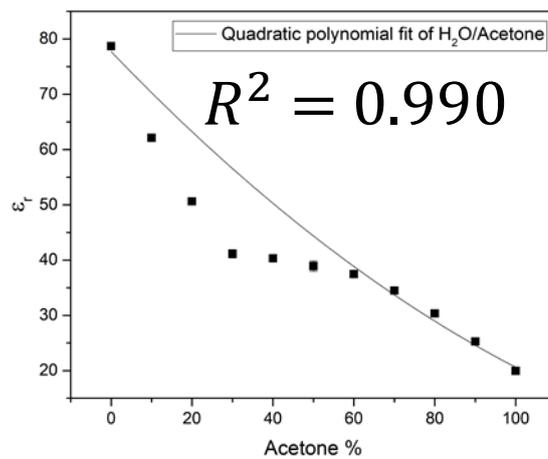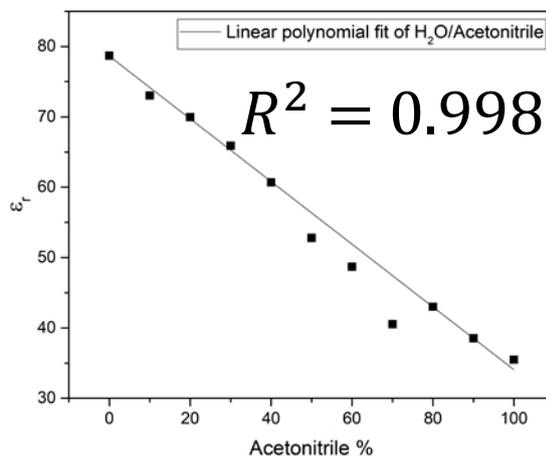
Figure 3.3 - Plots of relative permittivity at 800-860 MHz of water mixes with (a) methanol (b) ethanol (c) propanol (d) acetone & (e) acetonitrile.

Figure 3.3 shows that for every solvent, as the amount of water decreases and the amount of organic solvent increases, the relative permittivity of the system decreases. For the alcohol solutions, there is a decrease in the relative permittivity of all three systems as the relative weight of alcohol increases. This is also true for acetonitrile. Acetone shows a sharp decrease in relative permittivity from 0 - 30% weight volume, followed by a second phase between 30-100% that shows a less steep decrease in permittivity. The respective permittivities of the methanol, ethanol and propanol were 30, 15, & 6. The curves derived for all the alcohols and acetonitrile showed a very good fitting with a high R^2 value. The fitting curve derived from acetone does not show the same goodness of fit as the other solvents.

3.3.3.2. Conductivity of water/organic solvent solutions

Conductivity of water/organic solvent solutions was measured and plotted. Equations for the derived fitting curves are shown in Equation 3.13-Equation 3.17 and plots are shown in Figure 3.4:

$$y = 0.006x - 3.86e^{-5}x^2 + 0.10$$

Equation 3.13 - Methanol/water conductivity fitting equation.

$$y = -0.66x + 3.16e^{-4}x^2 + 79.22$$

Equation 3.14 - Ethanol/water conductivity fitting equation.

$$y = 1.28x - 0.005x^2 + 79.74$$

Equation 3.15 - Propanol/water conductivity fitting equation.

$$y = 6.84e^{-4}x - 2.24e^{-5}x^2 + 0.24$$

Equation 3.16 - Acetone/water conductivity fitting equation.

$$y = -0.003 + (0.205 + 0.003)/(1 + e^{(\frac{x-58.19}{28.88})})$$

Equation 3.17 - Acetonitrile/water conductivity fitting equation.
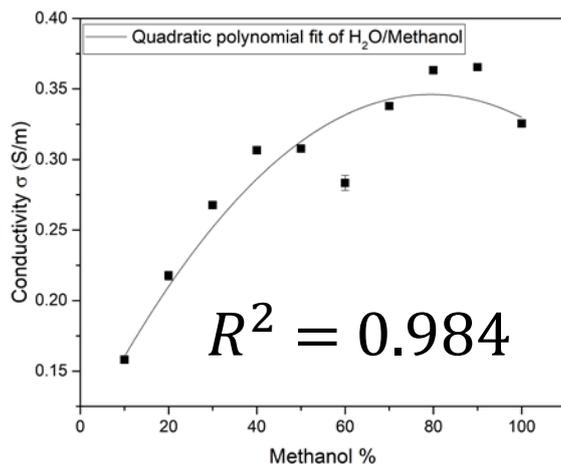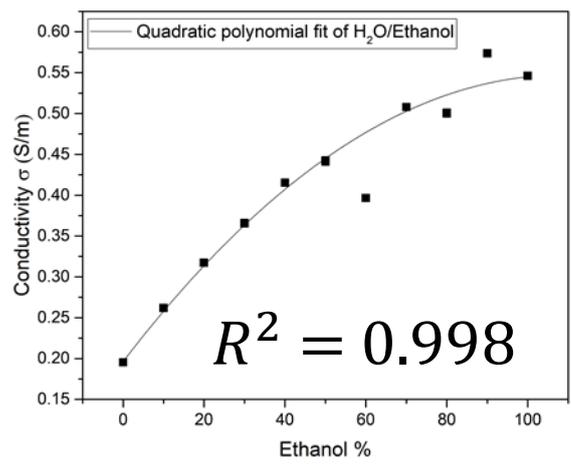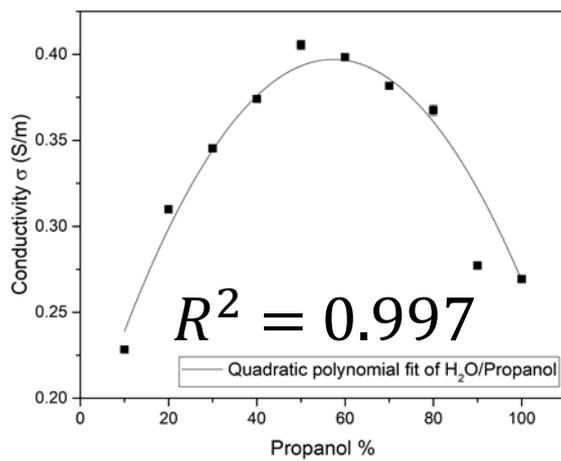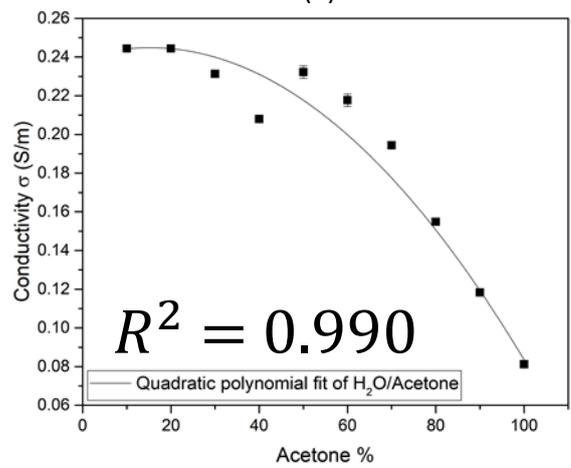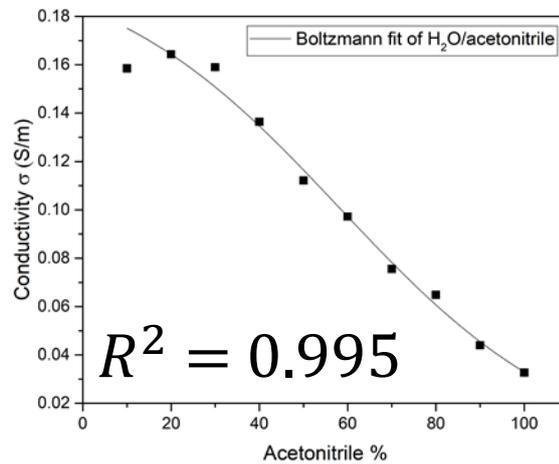
Figure 3.4 - Plots showing the conductivity at 800-860 MHz of water mixes with (a) methanol (b) ethanol (c) propanol (d) acetone & (e) acetonitrile.

Figure 3.4 shows irregular conductivity changes with increased organic solvent concentration. This is most prominent with propanol, however it should be noted that the observed conductivities were very small. All solution mixes conductivities were plotted against NaCl aqueous electrolytes from Chapter 2 to illustrate how small the conductivities of each solvent system are relatively, shown in Figure 3.5:
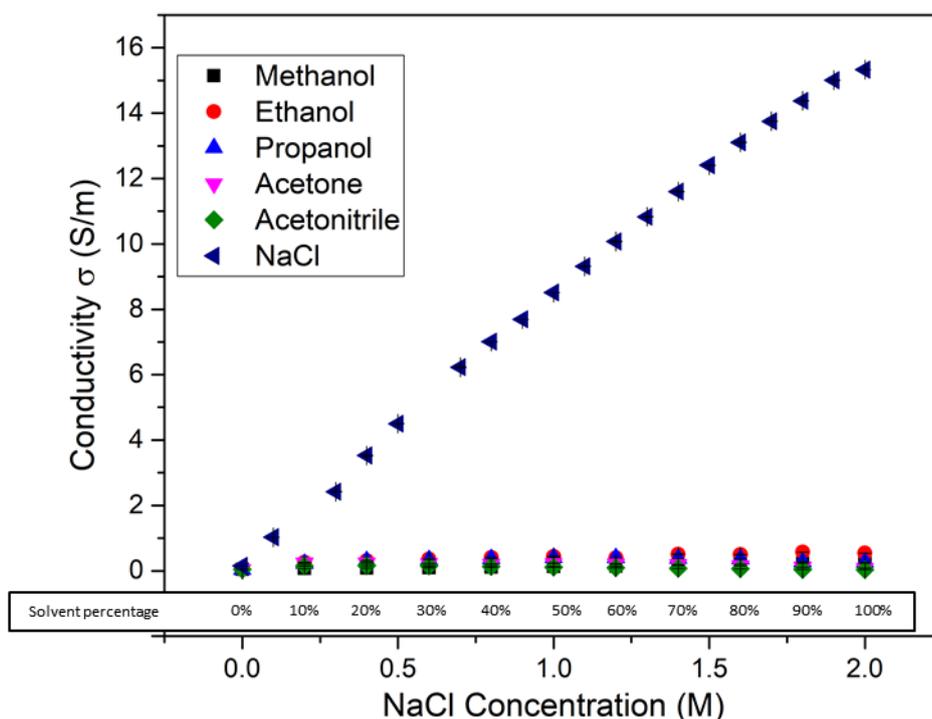
Figure 3.5 – Plot of conductivity for all water/organic solvent compositions against aqueous NaCl (from 0 - 2 M).

These fluctuations in conductivity are negligible when considered to the changes in conductivity observed in NaCl aqueous electrolytes at variable concentrations. As tan δ is the complex ratio of conductivity to permittivity, this should translate to a negligible tan δ when compared to NaCl, as increased conductivity increases tan δ. When conductivity is negligible, the importance of relative permittivity as a predictor for the measured capacitance increases. If conductivity does not strongly contribute to the observed capacitance (and correspondingly sensor code values), the fitting of the measured conductivity against the observed sensor values for the water/alcohol mixes will produce a lower accuracy fitting curve as a result.

3.3.3.3. Tan δ of water/organic solvent solutions

Tan δ of all solutions was plotted against the composition of all water/organic solvent solutions, shown in Figure 3.6:

(a).

(b).

(c).

(d).

(e).
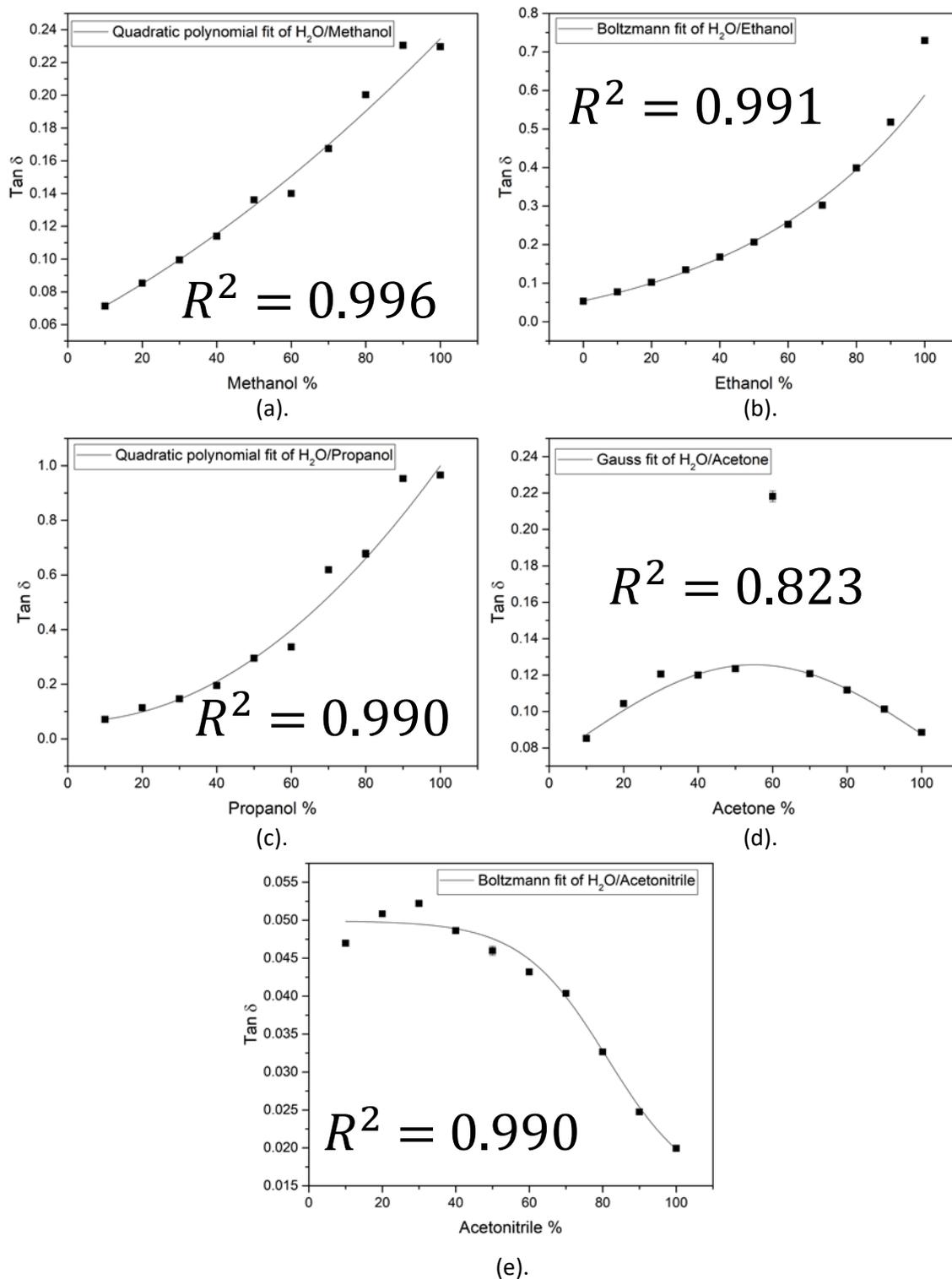
Figure 3.6 - Plot of tan δ at 800 − 860 MHz of water/organic solvent mixes with (a). methanol (b). ethanol (c). propanol (d). acetone and (e). acetonitrile.

3.3.4. Comparison of sensor code against dielectric properties

All sensor code values for water/organic solvent systems were plotted against their measured dielectric properties, in order to determine the predominant variable responsible for sensor code value changes.

3.3.4.1. Comparison of sensor code against relative permittivity

Sensor code values shown in Section 3.3.2 were plotted against relative permittivity data shown in Section 3.3.3.1. Fitting equations are shown Equation 3.18 - Equation 3.22 and plots are shown in Figure 3.7:

$$y = -0.27x + 0.002x^2 = 24.88$$

Equation 3.18 – Methanol/water sensor value vs relative permittivity fitting equation.

$$y = -0.08x - 2.04e^{-4}x^2 = 21.70$$

Equation 3.19 – Ethanol/water sensor value vs relative permittivity fitting equation.

$$y = -0.09x + 5.05e^{-4}x^2 + 18.86$$

Equation 3.20 – Propanol/water sensor value vs relative permittivity fitting equation.

$$y = 14.89 + \left(\frac{14.21}{22.98 \times \sqrt{\frac{\pi}{2}}} \right) \times e^{(-2(\frac{x-53.40}{22.98})^2}$$

Equation 3.21 – Acetone/water sensor value vs relative permittivity fitting equation.

$$y = -0.24x + 0.002x^2 + 18.75$$

Equation 3.22 – Acetonitrile/water sensor value vs relative permittivity fitting equation.

$R^2 = 0.967$

$R^2 = 0.973$

(a).

(b).

$R^2 = 0.982$

$R^2 = 0.787$

(c).

(d).

$R^2 = 0.938$

(e).
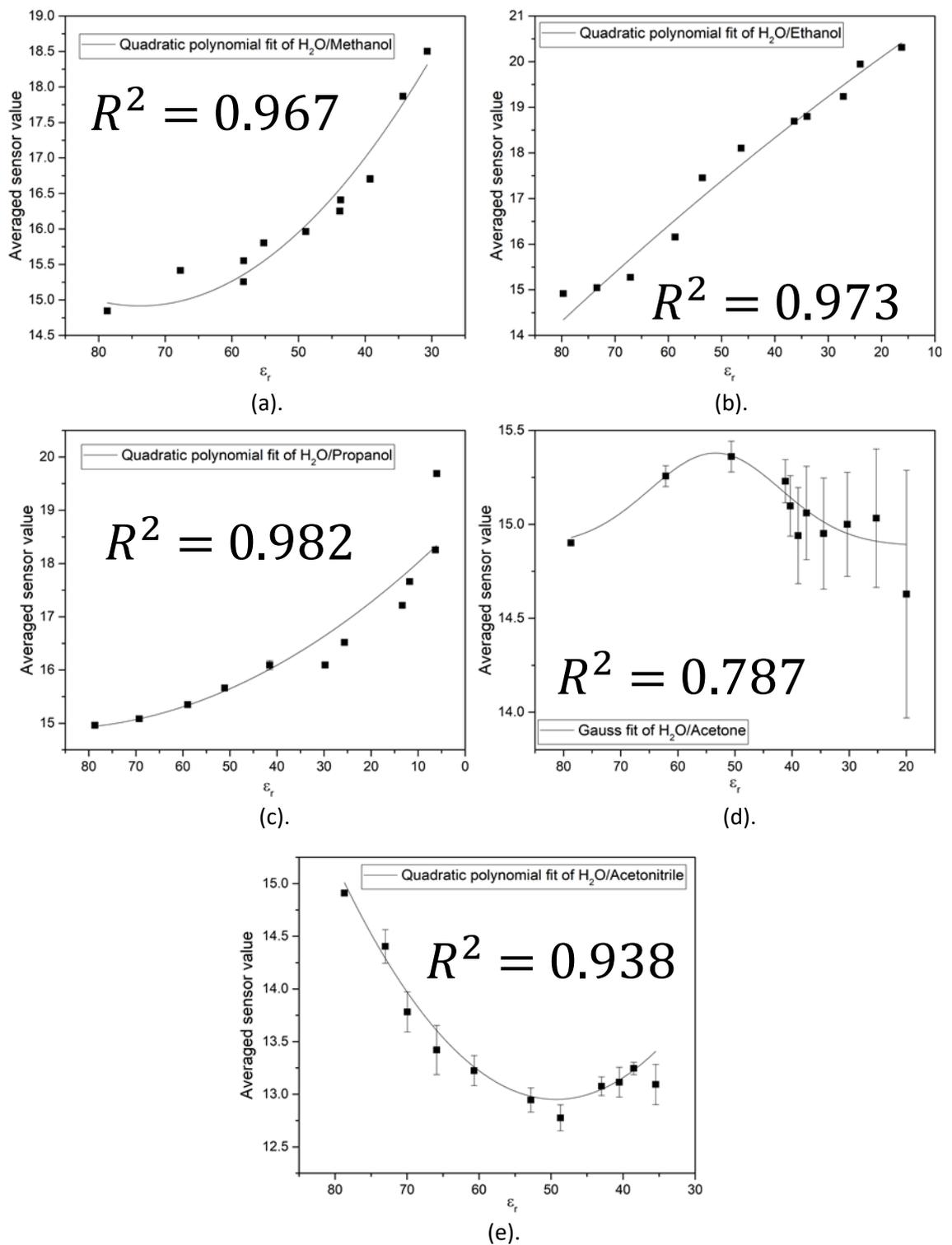
Figure 3.7 - Plots of sensor code against relative permittivity for (a) methanol (b) ethanol (c) propanol (d) acetone and (e) acetonitrile.

The alcohols show a general trend of increasing sensor value as the relative alcohol content increases. However, acetone shows an irregular sensor value across the range, and acetonitrile has a decreasing sensor value as dielectric constant decreases. This is the opposing trend when

compared to what was observed in chapter 2 with the aqueous electrolytes. The decrease in sensor values observed in chapter 2 when aqueous electrolyte concentration was increased was a result of high solution conductivity. Conductivity measurements on the water/organic solvent mixes needed to be performed.

3.3.4.2. Comparison of sensor code measurements against conductivity

Sensor code values shown in Section 3.3.2 were plotted against relative conductivity shown in Section 3.3.3.2. Fitting equations are shown from Equation 3.23 - Equation 3.27 and plots are shown in Figure 3.8:

$$y = -37.64x + 92.92x^2 + 19.03$$

Equation 3.23 - Methanol/water sensor value vs conductivity fitting equation.

$$y = -0.37x + 0.005x^2 + 79.74$$

Equation 3.24 - Ethanol/water sensor value vs conductivity fitting equation.

$$y = -0.24x + 10.81x^2 + 14.46$$

Equation 3.25 - Propanol/water sensor value vs conductivity fitting equation.

$$y = -6.86x + 27.21x^2 + 15.53$$

Equation 3.26 - Acetone/water sensor value vs conductivity fitting equation.

$$y = -31.49x + 181.46x^2 + 14.27$$

**Equation 3.27 - Acetonitrile/water sensor value vs conductivity fitting equation.**
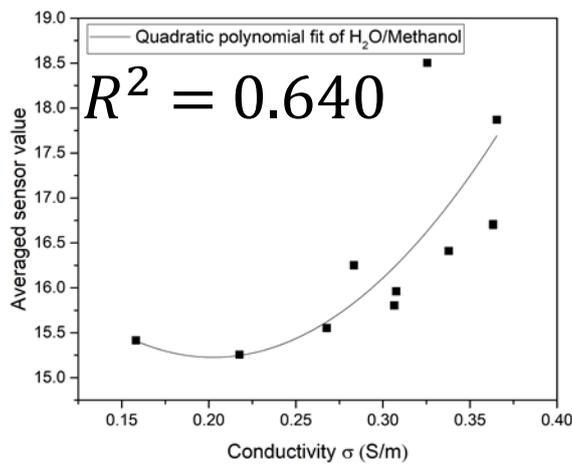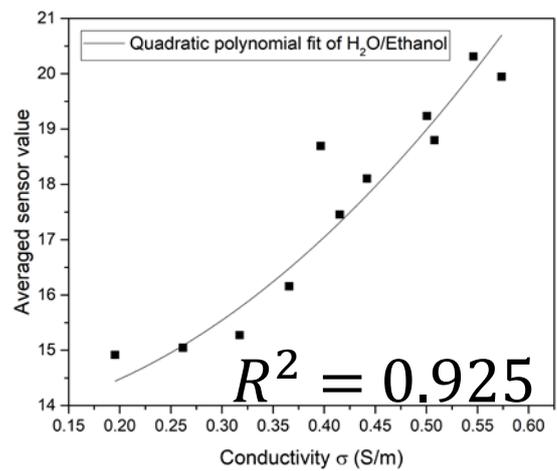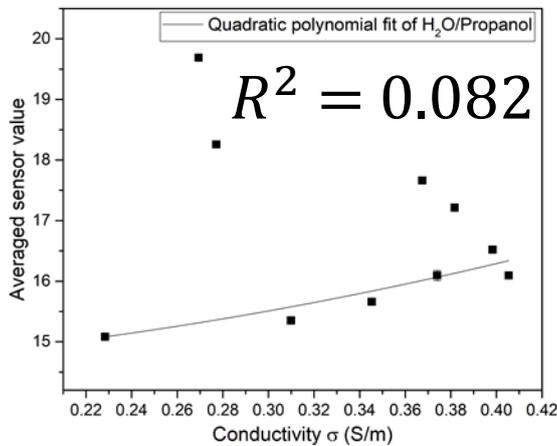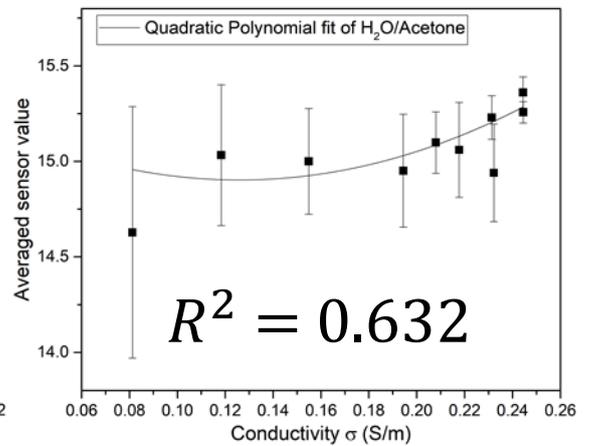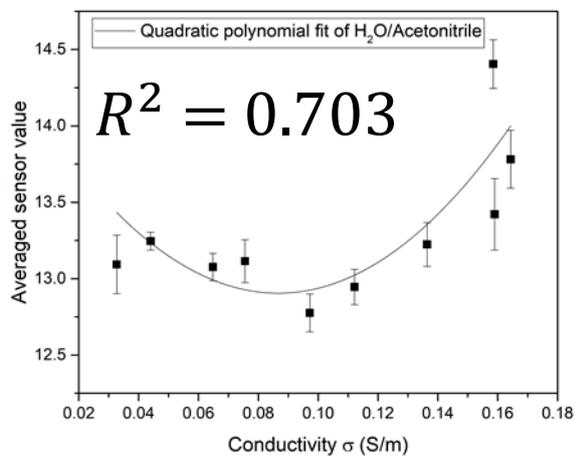
Figure 3.8 - Plots of sensor code vs conductivity for (a) methanol (b) ethanol (c) propanol (d) acetone and (e) acetonitrile.

In all instances, the derived fitting curves comparing sensor values against conductivity gave an R^2 value lower than the fitting curves derived from the comparison of sensor values against relative permittivity. The best fitting seen was for ethanol, albeit lower than the equivalent

fitting compared to relative permittivity. The conductivity of all samples is very small, and the large changes in dielectric properties are changes in relative permittivity. In the case of ethanol, it shows the strongest trend relative to conductivity, and shows the highest conductivity across the system as the ethanol content increases. In the absence of high conductivity, relative permittivity should be the variable that best describes the capacitance change for the sensing tag[25].

3.3.4.3. Comparison of sensor code against tan δ

In Chapter 2, tan δ was found to be the predominant variable that best described the change in sensor values with increasing concentrations of aqueous electrolytes. In a low conductivity system, lowered tan δ should result in relative permittivity change being a more accurate descriptor of sensor value changes. To confirm, sensor values were plotted against tan δ. The derived fitting equations are shown in equation Equation 3.28 - Equation 3.32 and plots are shown in Figure 3.9:

$$y = -7.93x + 82.02x^2 + 15.50$$

Equation 3.28 - Methanol/water sensor value vs tan δ fitting equation.

$$y = 20.003 + (-12.06 + 20.003)/(1 + e^{\left(\frac{x - 0.123}{0.09}\right)})$$

Equation 3.29 - Ethanol/water sensor value vs tan δ fitting equation.

$$y = 6.55x - 2.28x^2 + 14.62$$

Equation 3.30 - Propanol/water sensor value vs tan δ fitting equation.

$$y = 15.05 + \left(\frac{0.01}{0.02 \times \sqrt{\frac{\pi}{2}}}\right) \times e^{\left(-2\left(\frac{x - 0.10}{0.03}\right)^2\right)}$$

Equation 3.31 - Acetone/water sensor value vs tan δ fitting equation.

$$y = 0.004x - 2.96e^{-4}x^2 + 15.01$$

Equation 3.32 - Acetonitrile/water sensor value vs tan δ fitting equation.


(a).

(b).

(c).

(d).

(e).
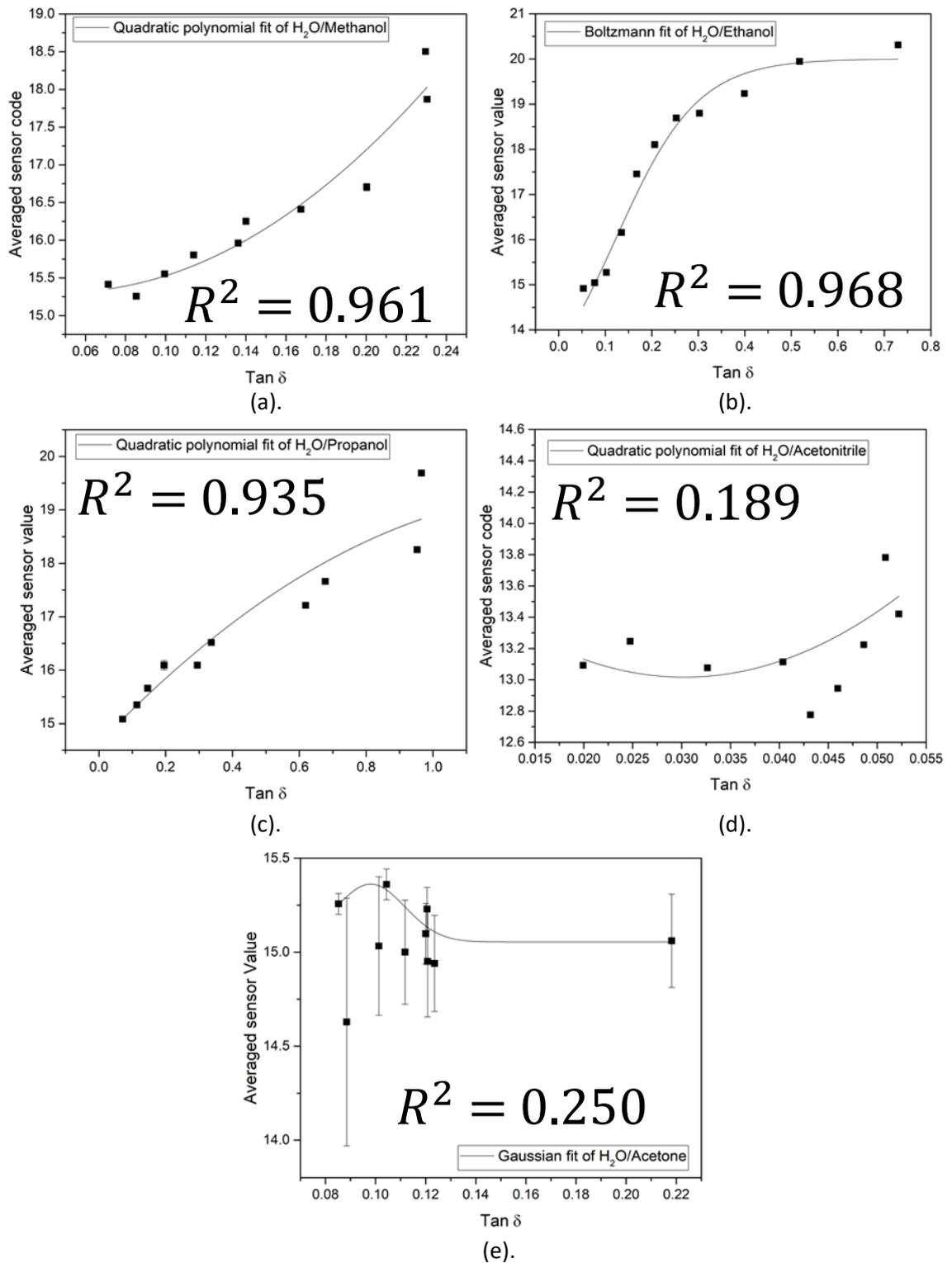
Figure 3.9 – Plots of sensor code vs tan δ for (a) methanol (b) ethanol (c) propanol (d) acetone and (e) acetonitrile.

For the alcohol solutions, the very low conductivities resulted in relative permittivity becoming the predominant variable that determines sensor output. In all instances, the fits for the derived curves were lower for tan δ than it was for relative permittivity, so much so that the fits for acetone and acetonitrile are meaningless. Tan δ is derived from both permittivity and conductivity.

3.3.5. Comparison of dielectric properties against measured sensor code values

As seen in Figure 3.4 and Figure 3.5, the conductivity and tan δ of water/alcohol mixes differs significantly from that of aqueous NaCl solutions. To see what the predominant variable was concerning the water/alcohol solutions, the sensor code was subjected to a correlation analysis. All 5 water/organic solvent mixes against relative permittivity & conductivity. Tan δ was not included as it is a variable that is dependent on the other two variables being used for the correlation and regression. The correlation function compares two datasets (one x variable and one y variable), and determines the relationship between the two datasets. The equation used to do this is as follows:

$$Correl(X,Y) = \frac{\sum(x-\overline{x})(y-\overline{y})}{\sqrt{\sum(x-\overline{x})^2\sum(y-\overline{y})^2}}$$

Equation 3.33 – Correlation analysis equation.

Where $\overline{x}$ and $\overline{y}$ are the means of each respective variable. Table 3.3 lists the calculated correlation coefficients for each respective water/solvent mix against both dielectric properties:

Table 3.3 - Correlation coefficients of all solvents sensor codes plotted against dielectric properties.

Solvent	Conductivity correl.	ε correl.
Methanol	0.743	-0.903
Ethanol	-0.987	-0.946
Propanol	0.110	-0.897
Acetone	0.749	0.369
Acetonitrile	0.725	-0.725

For all alcohols the relative permittivity of all alcohol solutions show a strong negative correlation with the measured sensor code data. This is also true of the conductivity of ethanol, but is significantly lower considering methanol, and conductivity does not correlate with the sensor code measurements obtained for propanol.

Regarding acetone and acetonitrile, no variable very strongly correlates with the obtained sensor code data. Conductivity is the variable that most strongly correlates for both variables; however, this is still a weak correlation comparative to the alcohol mixes. This suggests that there is a quaternary variable affecting sensor values obtained with the PDMS coated tags sensor code for the acetone and the acetonitrile mixes. This could also explain the increase in the range between averages for water/acetone mixes. It was expected that for both acetonitrile and acetone, increasing the relative amount of organic solvent would cause a gradual increase in sensor values as the relative permittivity of the bulk material decrease, this was not observed.

3.3.6. Comparison of predicted against measured sensor values relative to dielectric properties

In order to determine the importance of each dielectric parameter in determining sensor values, the fitting curves obtained for each graph that plotted sensor value against a dielectric parameter was used to determine the sensor value that the curve would predict for the known dielectric parameters for each of the water/solvent compositions. Multiple regression was performed in excel on both relative permittivity and conductivity. Regression studies describe how an independent variable is numerically related to a dependant variable. This form of statistical analysis considers both variables against the sensor values in tandem, and produces a fitting curve, as well as predicted sensor values from the fitting model produced. The regression model produced for multiple regression will produce a line that can be defined as:

$$\mu_y = \beta_0 + \beta_1 x_1 + \beta_2 x_2 \dots$$

Equation 3.34 – Equation for the multiple regression model.

Where μ_y is the predicted or expected value of the dependant variable, β_0 is the value of y when all the independent variables (the x variables) are equal to zero, β_1 and β_2 are the estimated regression coefficients for each of the predictor variables being used (specifically, β_1 relates to the coefficient of the relative permittivity component of the solution, and β_2 relates to the coefficient of the conductivity of the solution), and x_1 and x_2 are the distinct independent variables under test. The number of β and x components involved in the line produced will depend entirely on the number or parameters used for the multiple regression, so in this instance, the above equation will be the full equation. Furthermore, it will provide a significance value (denoted as a Significance-F value) that describes how statistically significant and reliable the results produced from the analysis are. This was then plotted against the observed sensor values for all compositions. The three scenarios under test are as follows; linear regression of permittivity alone, linear regression of conductivity alone, and multiple regression of both

permittivity and conductivity (this differs from tan δ as it allows for both variables to be individually considered against the sensor value).

3.3.6.1. Comparison of predicted against measured sensor values of the methanol/water system relative to dielectric properties

Predicted sensor values derived from the regression model were plotted against averaged values shown in Section 3.3.2. The derived fitting equations are shown in Equation 3.35 - Equation 3.37 and plots are shown in Figure 3.10 - Figure 3.12:

$$y = 0.99x + 0.076$$

Equation 3.35 - Methanol/water averaged sensor value vs predicted sensor value (relative permittivity only) fitting equation.

$$y = 0.58x + 0.58$$

Equation 3.36 - Methanol/water averaged sensor value vs predicted sensor value (conductivity only) fitting equation.

$$y = 0.84x + 2.52$$

Equation 3.37 - Methanol/water averaged sensor value vs predicted sensor value (relative permittivity & conductivity) fitting equation.
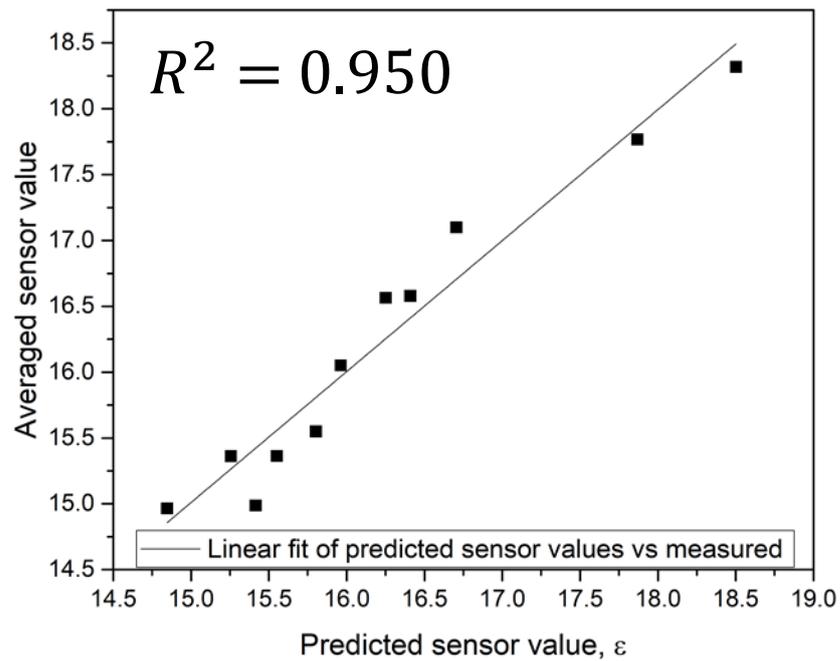
Figure 3.10 – Plot showing methanol/water averaged sensor value vs predicted sensor value (relative permittivity only).
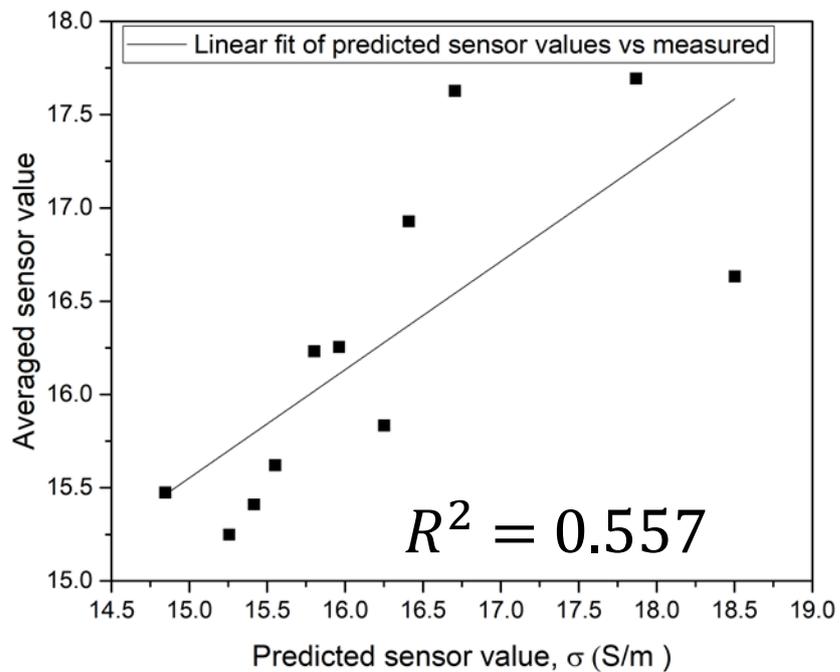

Figure 3.11 - Plot showing methanol/water averaged sensor value vs predicted sensor value (conductivity only).
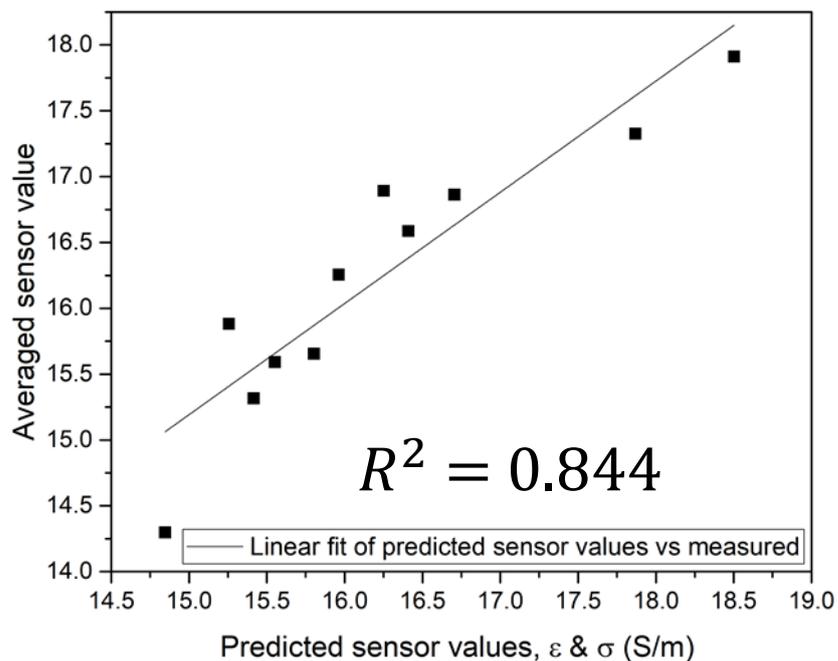
Figure 3.12 - Plot showing methanol/water averaged sensor value vs predicted sensor value (relative permittivity &conductivity).

If the curves derived from the measured sensor values (from the dielectric parameter the curve was fitted from) could perfectly predict the sensor value of the water/solvent mix then the x variable would be equivalent to the y variable for the predicted values vs the measured values. A linear fitting of the predicted against the measured values for a fitting curve that perfectly predicts the sensor values would therefore have a line slope of 1. The greater that the line fit deviates from 1, the lower the accuracy of the parameter under test. The R^2 value obtained from the line fit also needs to be considered as well, as you can have a slope that is derived from values that are not representative of the line that is being fitted from them. Considering both of these components, the most suitable predictor of sensor values considering methanol is relative permittivity. The slope of the line fit is 0.99, incredibly close to a perfect line fit.

3.3.6.2. Comparison of predicted against measured sensor values of the ethanol/water system relative to dielectric properties

Predicted sensor values derived from the regression model were plotted against averaged values shown in Section 3.3.2. The derived fitting equations are shown in Equation 3.38 - Equation 3.40 and plots are shown in Figure 3.13 - Figure 3.15:

$$y = 1.009x - 0.19$$

Equation 3.38 - Ethanol/water averaged sensor value vs predicted sensor value (relative permittivity only) fitting equation.

$$y = 0.92x + 1.36$$

Equation 3.39 - Ethanol/water averaged sensor value vs predicted sensor value (conductivity only) fitting equation.

$$y = 0.98x + 0.44$$

Equation 3.40 - Ethanol/water averaged sensor value vs predicted sensor value (relative permittivity and conductivity) fitting equation.
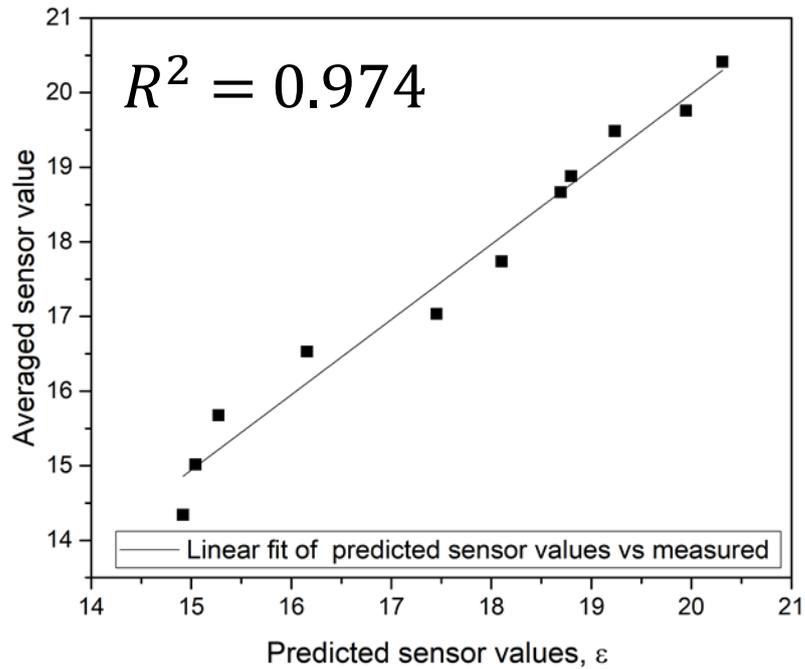
Figure 3.13 - Plot showing ethanol/water averaged sensor value vs predicted sensor value (relative permittivity only).
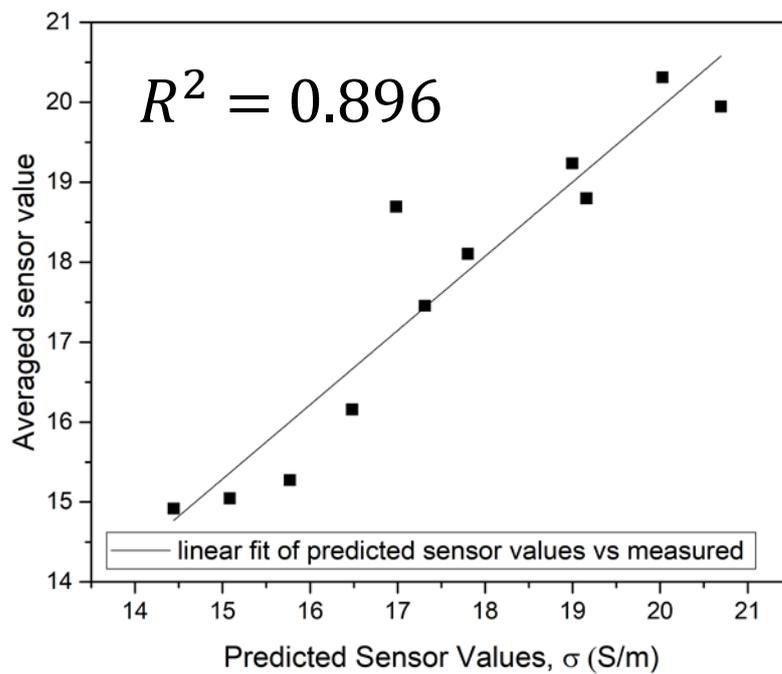

Figure 3.14 - Plot showing methanol/water averaged sensor value vs predicted sensor value (conductivity only).
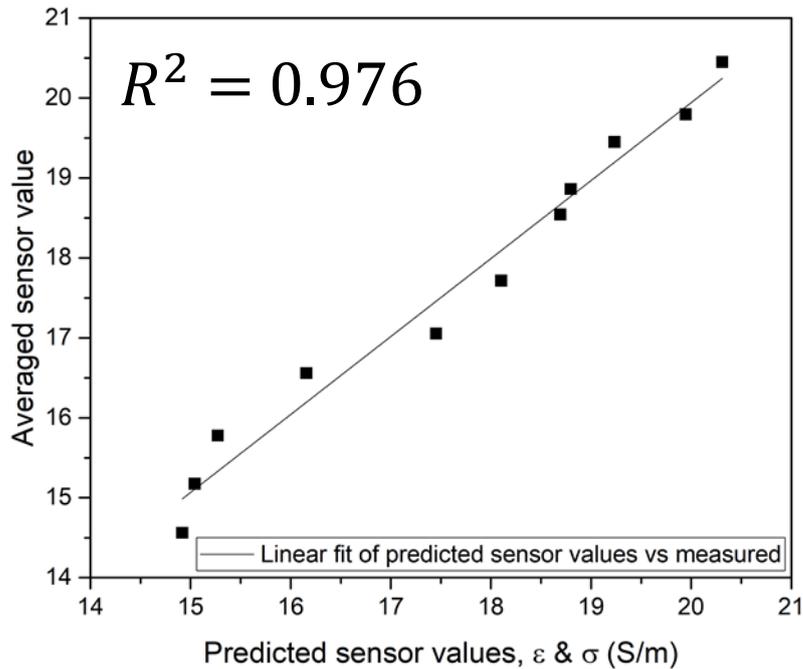
Figure 3.15 - Plot showing ethanol/water averaged sensor value vs predicted sensor value (relative permittivity &conductivity).

With regards to ethanol, permittivity and the derived model considering both variables are both effective predictors of sensor values. Whilst the derived line fit is slightly more reflective of the plotted data with regards to both variables, the slope of the line for relative permittivity is remarkably close to 1. Whilst both models show very good likeness to the observed sensor values, the slope observed in the relative permittivity comparison means that the best predictor of the sensor values in this instance is again the single variable of relative permittivity.

3.3.6.3. Comparison of predicted against measured sensor values of the propanol/water system relative to dielectric properties

Predicted sensor values derived from the regression model were plotted against averaged values shown in Section 3.3.2. The derived fitting equations are shown in Equation 3.41 - Equation 3.43 and plots are shown in Figure 3.16 - Figure 3.18:

$$y = 0.83x + 2.82$$

Equation 3.41 - Propanol/water averaged sensor value vs predicted sensor value (relative permittivity only) fitting equation.

$$y = 0.02x + 15.32$$

Equation 3.42 - Propanol/water averaged sensor value vs predicted sensor value (conductivity only) fitting equation.

$$y = 0.94x + 0.95$$

Equation 3.43 - Propanol/water averaged sensor value vs predicted sensor value (relative permittivity and conductivity) fitting equation.
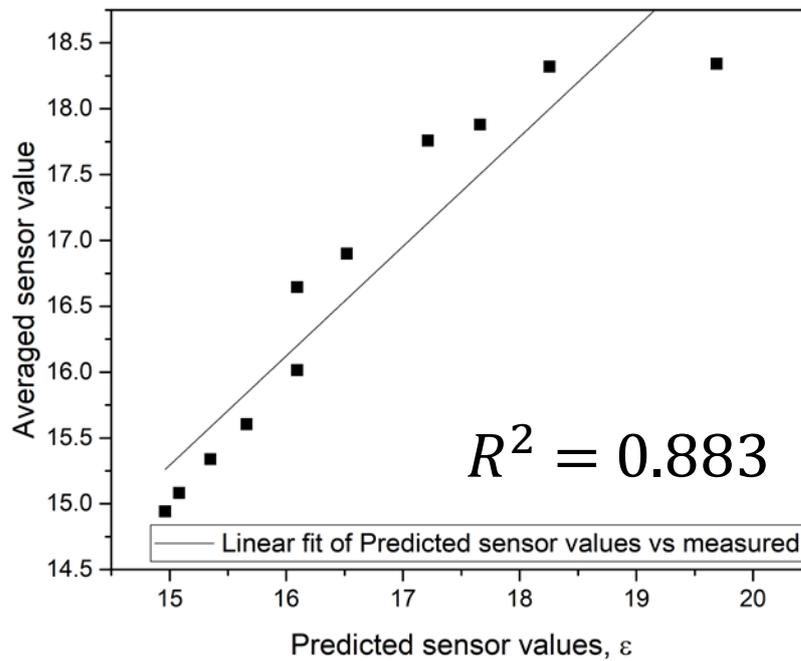
Figure 3.16 - Plot showing propanol/water averaged sensor value vs predicted sensor value (relative permittivity only).
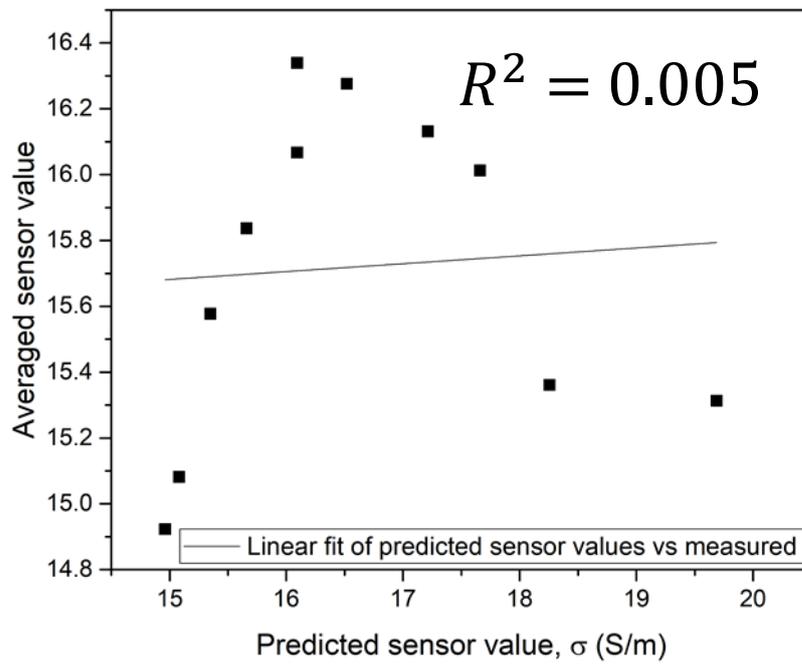
Figure 3.17 - Plot showing propanol/water averaged sensor value vs predicted sensor value (conductivity only).
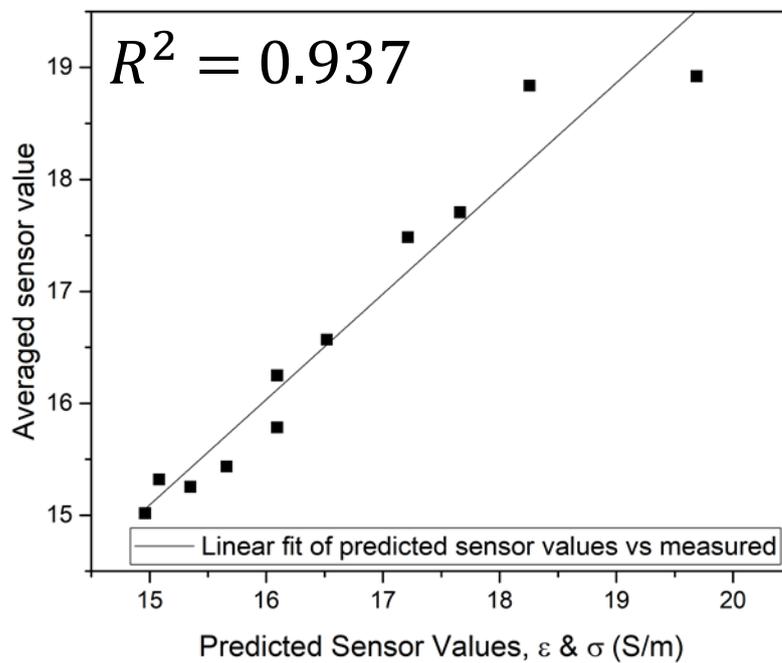
Figure 3.18 - Plot showing propanol/water averaged sensor value vs predicted sensor value (relative permittivity and conductivity).

With regards to propanol, the most accurate predictor of sensor values was found to be the model that considers both variables. The line slope derived from the comparison deviates more so than the slopes that were the best predictors in the other alcohols, and the goodness of the line fit also deviates to greater degree than the other two alcohols. It was unexpected that the model that considers both dielectric parameters would be the most accurate predictor of sensor values with regards to propanol, as the model showed that relative permittivity was the best predictor in the previously modelled alcohols, especially considering that there is not a linear change in system conductivity as the amount of propanol in the system increases.

3.3.6.4. Comparison of predicted against measured sensor values of the acetone/water system relative to dielectric properties

Predicted sensor values derived from the regression model were plotted against averaged values shown in Section 3.3.2. The derived fitting equations are shown in Equation 3.44 - Equation 3.46 and plots are shown in Figure 3.19 - Figure 3.21:

$$y = 0.68x + 4.91$$

Equation 3.44 - Acetone/water averaged sensor value vs predicted sensor value (relative permittivity only) fitting equation.

$$y = 0.47x + 7.89$$

Equation 3.45 - Acetone/water averaged sensor value vs predicted sensor value (relative conductivity only) fitting equation.

$$y = 0.57x + 0.076$$

Equation 3.46 - Acetone/water averaged sensor value vs predicted sensor value (relative permittivity & conductivity) fitting equation.
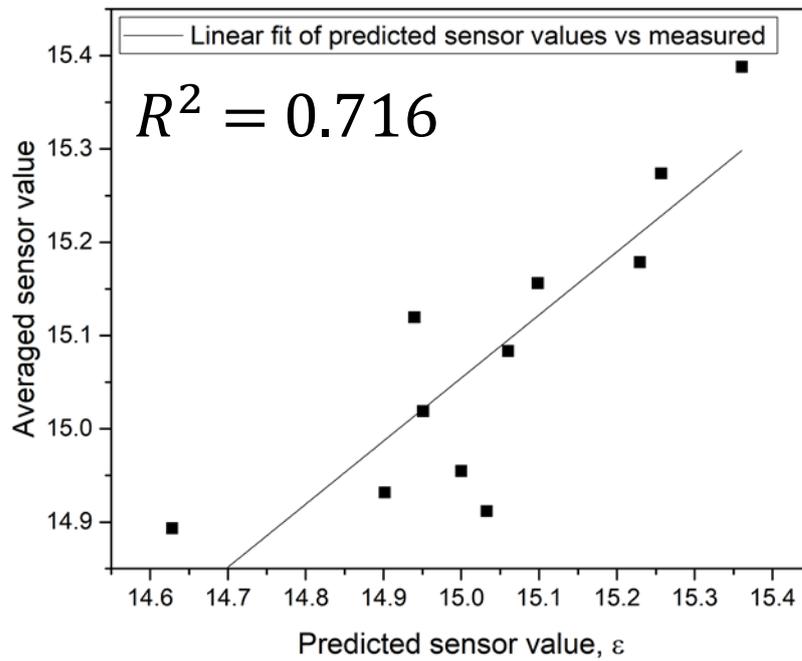
Figure 3.19 - Plot showing acetone/water averaged sensor value vs predicted sensor value (relative permittivity and conductivity).
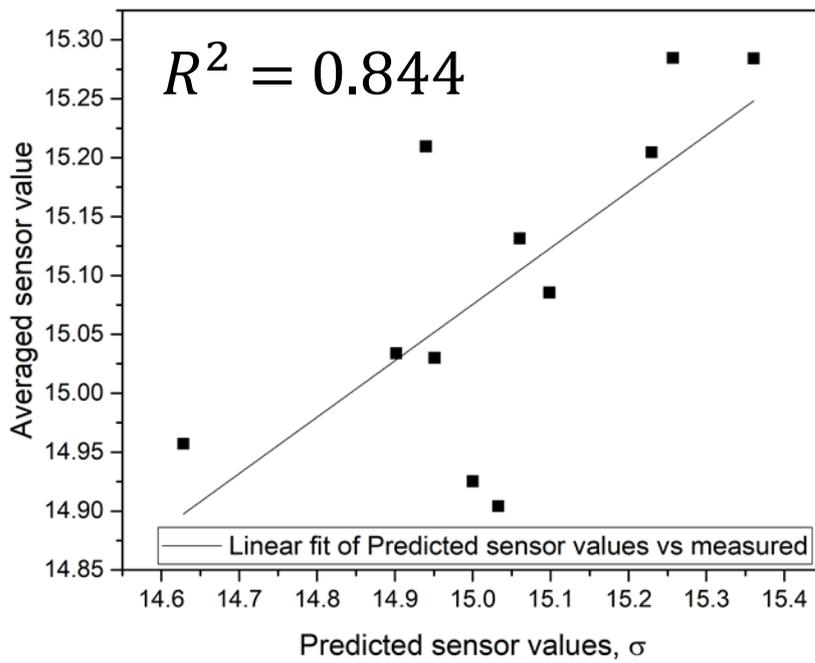

Figure 3.20 - Plot showing acetone/water averaged sensor value vs predicted sensor value (relative permittivity and conductivity).
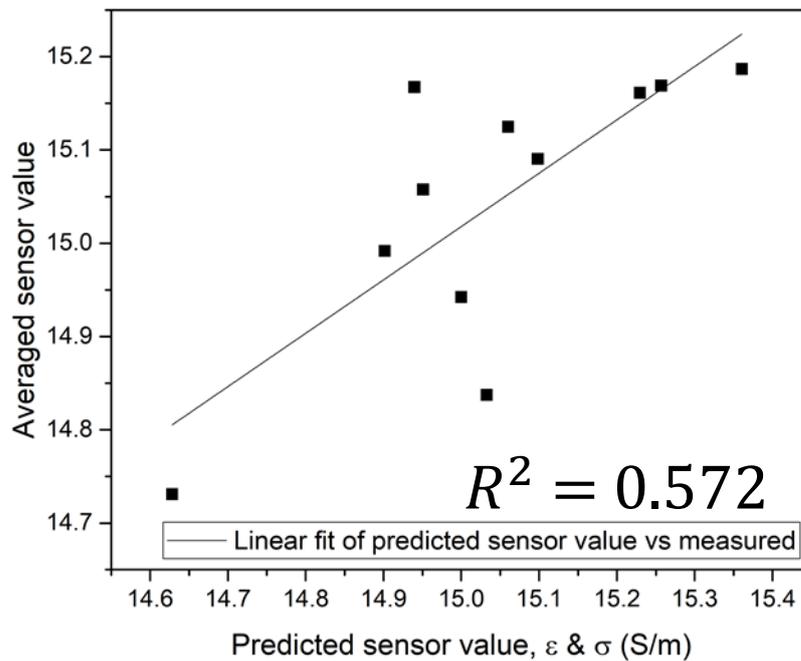
Figure 3.21 - Plot showing acetone/water averaged sensor value vs predicted sensor value (relative permittivity and conductivity).

With regards to acetone, none of the models are good predictors of sensor values. In all instances, the slopes of the line fits produced show a strong deviation from the ideal slope of 1. Furthermore, the R^2 values of said line fits are very low. Certainly, the dielectric parameters alone do not fully describe what effect increasing acetone content has on the sensing tag. There is at the least a quaternary variable (aside from permittivity, conductivity and tan δ) that is affecting the observed sensor values.

3.3.6.5. Comparison of predicted against measured sensor values of the acetonitrile/water system relative to dielectric properties

Predicted sensor values derived from the regression model were plotted against averaged values shown in Section 3.3.2. The derived fitting equations are shown in Equation 3.47 - Equation 3.49 and plots are shown in Figure 3.22 - Figure 3.24:

$$y = 0.96x + 0.66$$

Equation 3.47 - Acetonitrile/water averaged sensor value vs predicted sensor value (relative permittivity only) fitting equation.

$$y = 0.89x + 1.50$$

Equation 3.48 - Acetonitrile/water averaged sensor value vs predicted sensor value (conductivity only) fitting equation.

$$y = 0.99x + 0.076$$

Equation 3.49 - Acetonitrile/water averaged sensor value vs predicted sensor value (relative permittivity & conductivity) fitting equation.

$$R^2 = 0.964$$
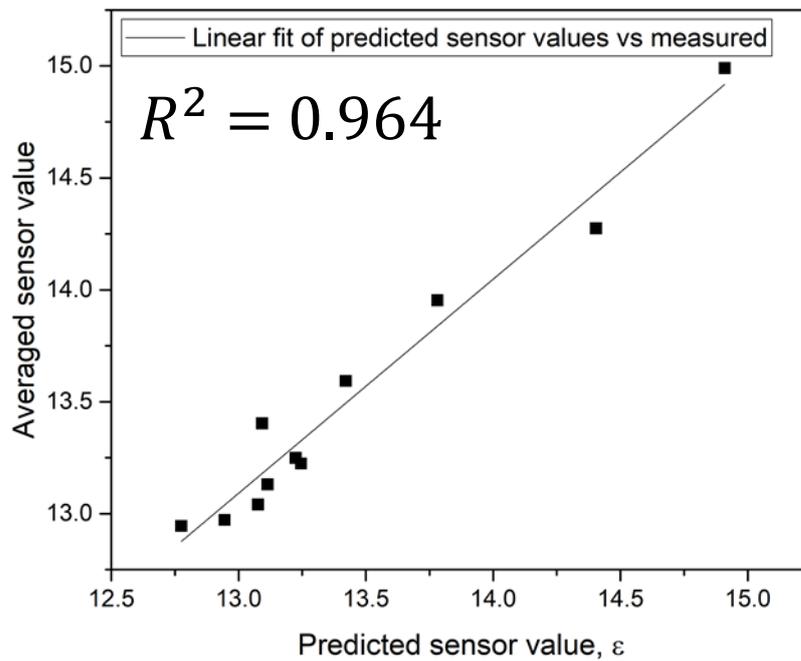
Figure 3.22 - Plot showing acetonitrile/water averaged sensor value vs predicted sensor value (relative permittivity only).


$$R^2 = 0.816$$
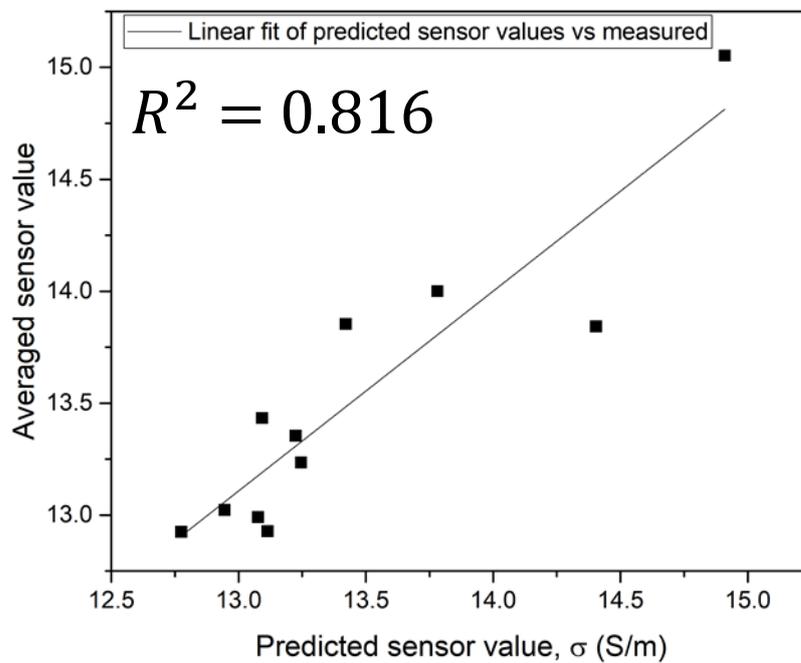
Figure 3.23 - Plot showing acetonitrile/water averaged sensor value vs predicted sensor value (conductivity only).
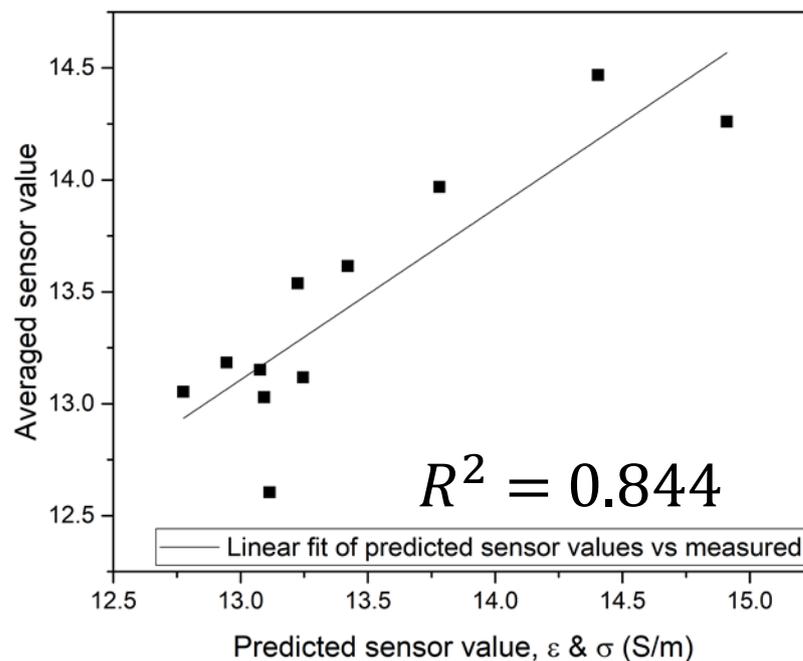
Figure 3.24 - Plot showing acetonitrile/water averaged sensor value vs predicted sensor value (relative permittivity & conductivity only).

With regards to acetonitrile, the prediction that utilises both variables produces a near perfect line slope. However, the line fit derived from the prediction based off relative permittivity was more reflective of the data, with a better likeness of fit. Furthermore, the slope of the derived line fit was very close to the ideal line fit slope of 1 (albeit lower than the predictive model that considers both variables).

3.3.7. PDMS swelling study

In order to understand why the associated errors for the non-alcoholic organic solvents was significantly greater than the alcohols, a swelling study was performed on PDMS squares to see if the water/organic solvent mixes induced swelling in the PDMS. If any mix had a very high swelling value, this either could attribute to an abnormal sensor value or could explain large ranges in error. The rationale for this was that swelling of the PDMS by a low dielectric would result in a change in the bulk permittivity of the bottom layer (denoted as ε_1 in Figure 3.25) upon
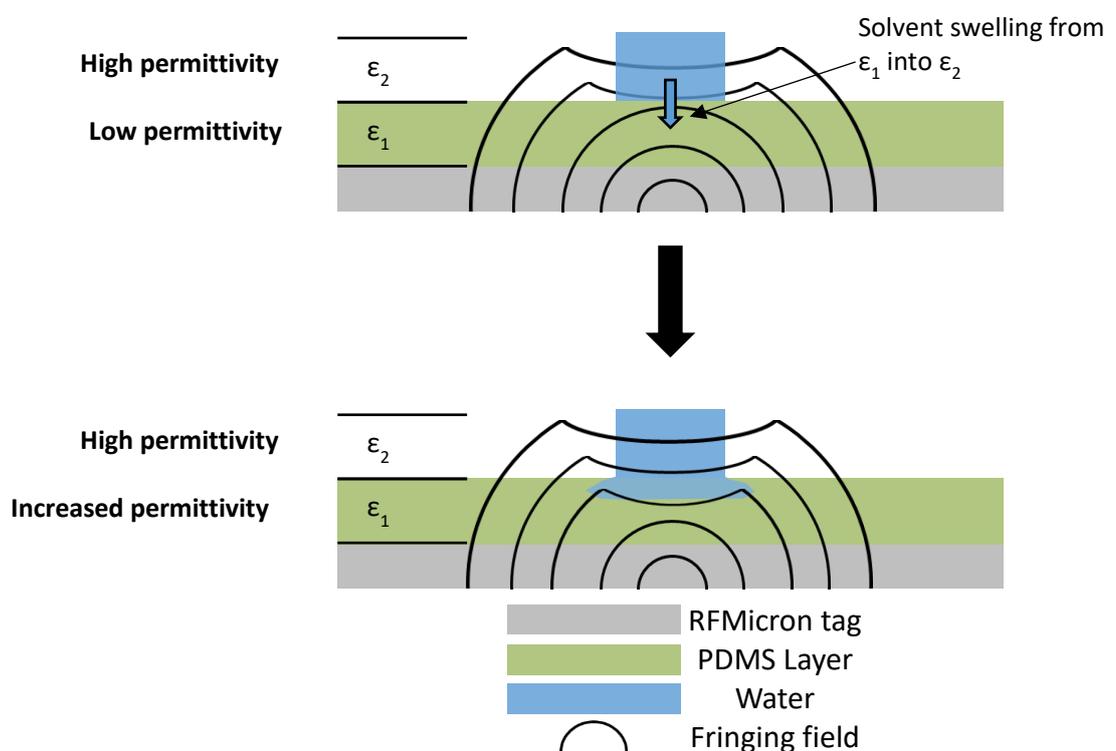

Figure 3.25 – Schematic diagram showing a proposed swelling effect in the PDMS coated RFMicron tag.

swelling. The changes on sensor value should be two-fold. Firstly, swelling a solvent into the PDMS layer will result in an increased bulk permittivity for ε_1. Furthermore, based on the film thickness studies from Chapter 2, the closer a high permittivity material is to the tag, the more of an effect it has on the tag. This means that if any solvent moves from ε_2 into ε_1, the effect it will have on the tag should be increased. The final effect that swelling a solvent into the network could have is that ε_2 could be pushed further away from the sensor as a result of a volume change

from swelling, meaning the effect of ε_2 would be reduced as the volume of ε_1 increased. Whilst the literature shows the swelling of all 6 of the solvents used for the study, there was no literature on the swelling of water/organic solvent mixes into cross-linked PDMS networks. All of the solvent mixes that were used had a PDMS sample swollen in an excess of the solvent mix, and then had both the Q value and the Qv value plotted (which was an average of the density of both water and the organic solvent dependant on the percentage of each in the mix), as follows:
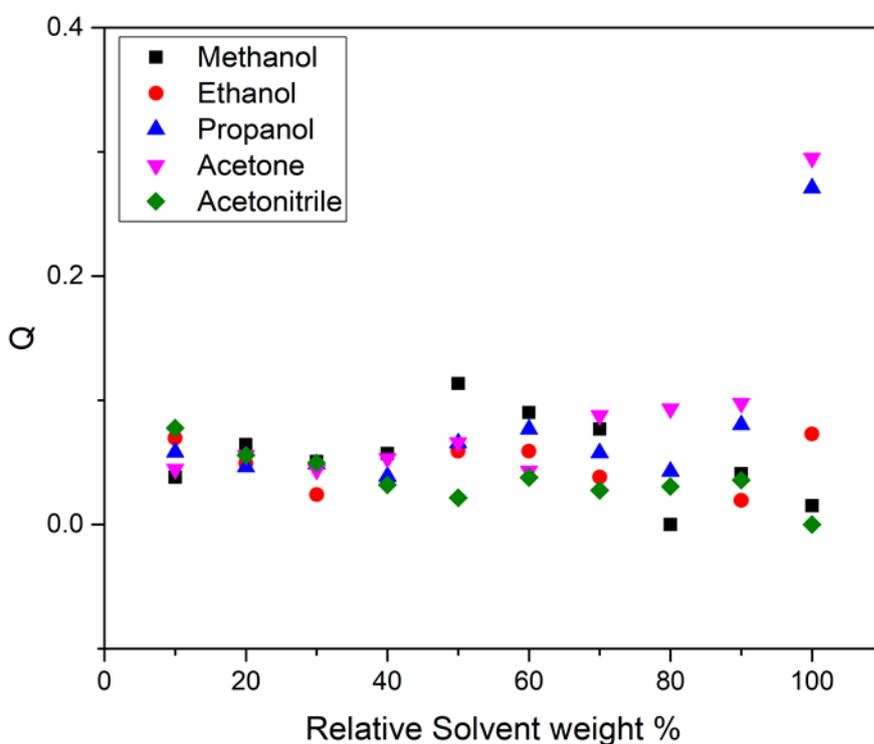

**Figure 3.26 – Plot of swelling factor (Q) of each water/solvent mix.**
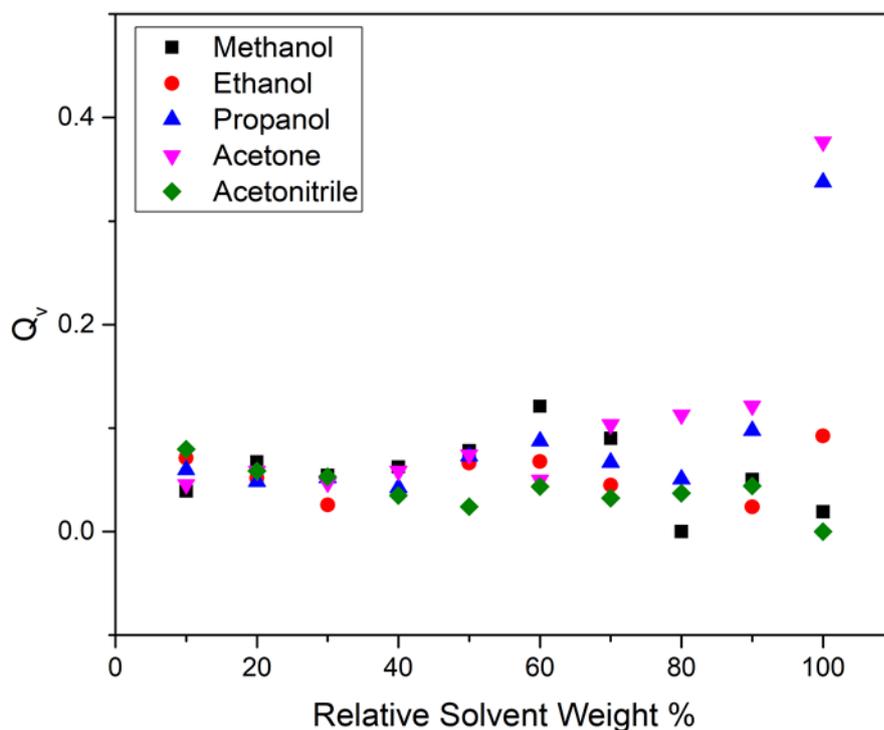
Figure 3.27 – Plot of swelling factor by relative volume (Qv) of each water solvent mix.

Swelling factors were all below 0.5 across all systems, and only acetone and propanol showed high degrees of swelling. Any quantity of water in the system massively reduced swelling factor for both systems, but the swelling values of the 100% organic solvent systems showed good agreement with literature[26]. Acetonitrile shows minimal swelling throughout the entire system relative to the other solvents. Nonetheless, both systems had swelling factor added to the regression model's to determine if inclusion of swelling factor improved the predictive models. Whilst swelling values are in the order of Q = 0.05, which is normally quite a minimal volume, this could have changes in sensor values, for at least two predominant reasons. The first reason would be that any introduction of a solvent system to the PDMS network would cause an increase in the bulk permittivity of the layer, potentially lowering sensor values. However, the swelling may also cause an increase in the layer thickness. This would mean that any further deposited solvent would be measured from a distance farther away than the previous sample, which could result in a lower measured sensor when deposited.

Propanol was also included due to the comparable swelling factor to acetone. Methanol and ethanol are included in the appendix. Fitting equations for all three systems are shown in Equation 3.50 - Equation 3.52, and are shown in Figure 3.28 - Figure 3.30:

$$y = 0.98x + 0.35$$

Equation 3.50 - Propanol/water averaged sensor value vs predicted sensor value (dielectric properties and Qv) fitting equation.

$$y = 0.61x + 5.90$$

Equation 3.51 - Acetone/water averaged sensor value vs predicted sensor value (dielectric properties and Qv) fitting equation.

$$y = 0.82x + 2.31$$

Equation 3.52 - Acetonitrile/water averaged sensor value vs predicted sensor value (dielectric properties and Qv) fitting equation.
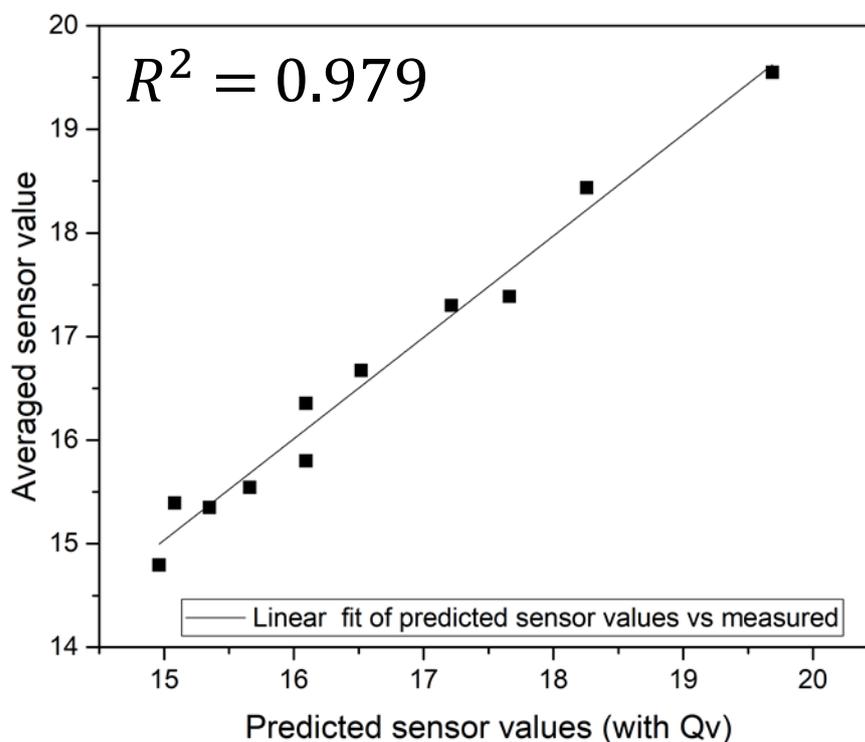
Figure 3.28 - Plot showing propanol/water averaged sensor value vs predicted sensor value (dielectric properties and Qv).
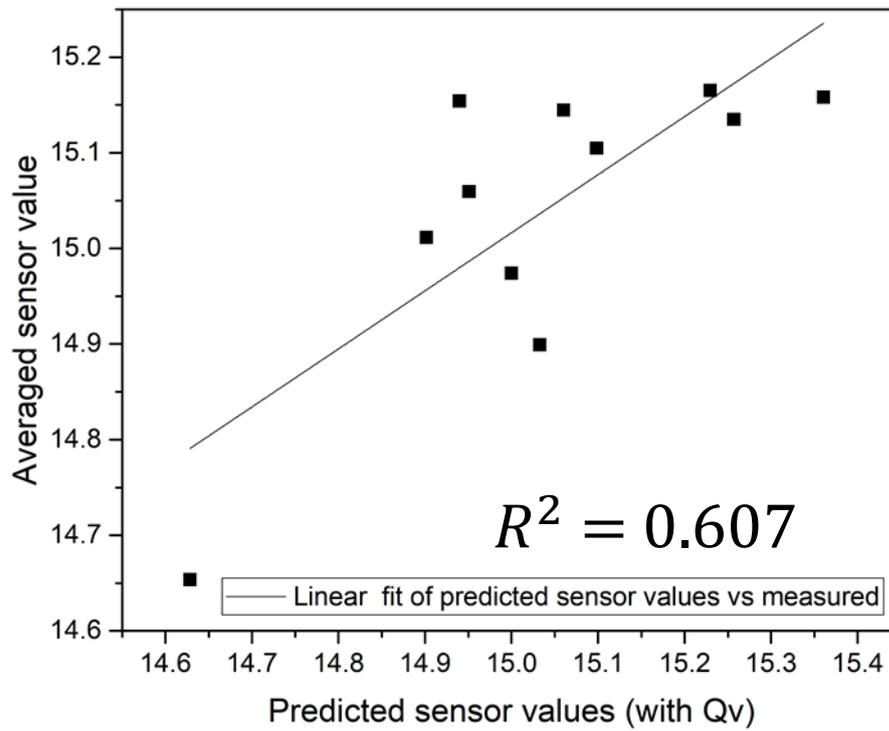
Figure 3.29 - Plot showing acetone/water averaged sensor value vs predicted sensor value (dielectric properties and Qv).
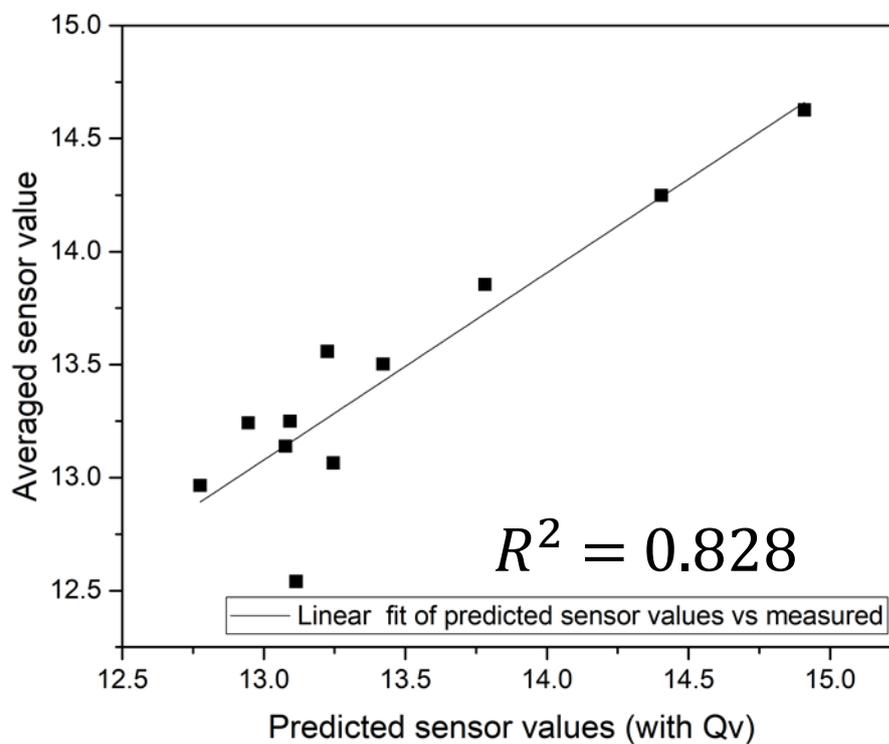

Figure 3.30 - Plot showing acetonitrile/water averaged sensor value vs predicted sensor value (dielectric properties and Qv).

The inclusion of swelling factor in the regression model only improved the predictive capability of the propanol/water system. Addition of swelling values did not improve the predictive capability of the water/acetone system as it was expected to. One of the limiting factors of the regression model is that only the mean sensor value can be used when comparing independent variables. With regards to the water/acetone system, the range of error values from the mean are significant. Furthermore, as the relative acetone content for the system increases, the ranges from the mean for the sensor data increases, shown in Figure 3.31:
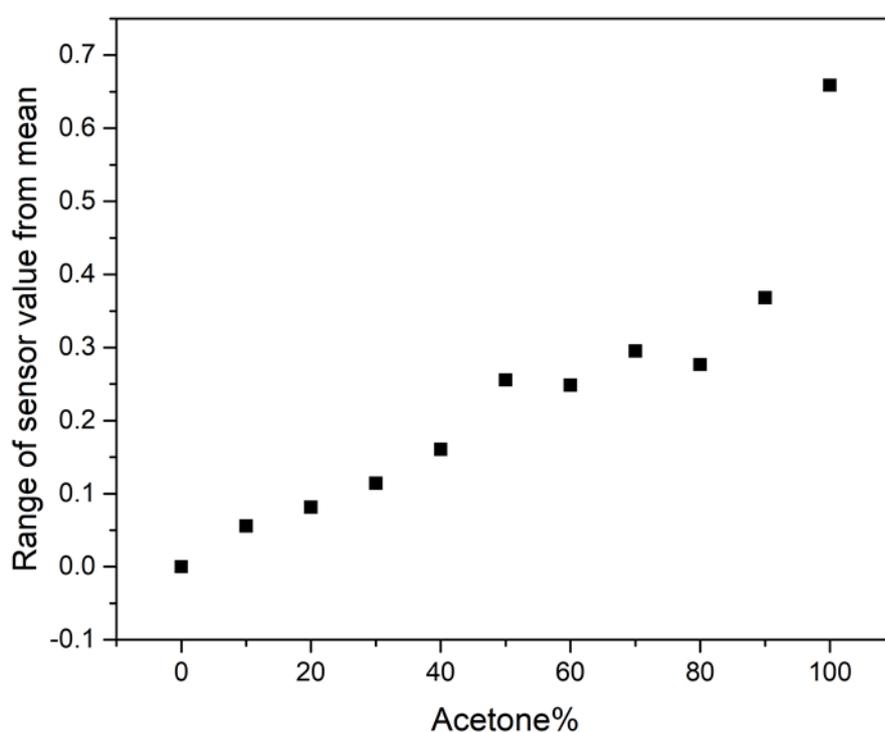

Figure 3.31 – Range of sensor values from the mean for the water/acetone system.

Correlation analysis was performed on this dataset against swelling data, and there was a strong 0.92 correlation between the two datasets. Whilst correlation cannot be used to prove that one variable is causally linked to another, the strong correlation between the two datasets is notable. Including swelling data did not improve the predictive capability of the regression model, meaning that swelling is not a variable that significantly effects the water/acetonitrile system. Moreover, the water/acetonitrile system shows an opposite trend to the alcohols, with sensor

values decreasing as the acetonitrile content increases. This suggests there is at the least an unknown quaternary variable responsible for the change in sensor values for the water/acetonitrile system that is unaccounted for.

3.3.8. Commercial alcohol sensor code studies

Having established that the platform is capable of determining the concentration of alcohols, commercial alcohols were tested with the platform to determine the feasibility of the platform as a commercial alcohol sensor. The 5 off the shelf alcohols were then plotted against the ethanol peaks shown in Section 3.3.2 to observe if the additional additives in commercial alcohols change the observed sensor values significantly compared to the neat ethanol/water mixes. The ethanol content of each commercial alcohol as labelled was used as the ethanol percentage plotted in Figure 3.32:
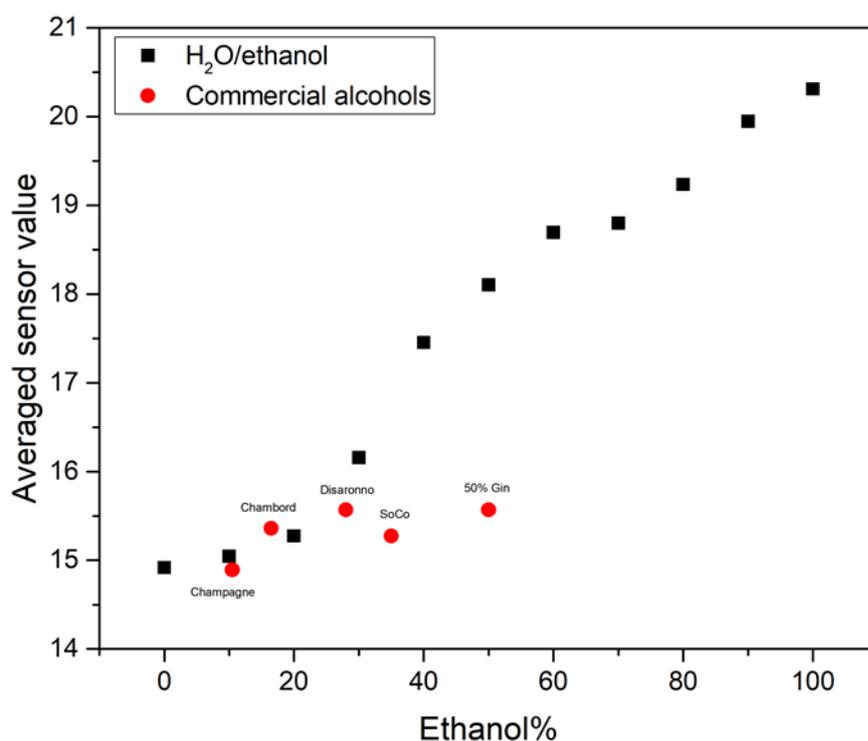

Figure 3.32 – Plot showing the sensor values obtained from commercial alcohols and H₂O/ethanol mixes.

Commercial alcohols with a lower alcohol percentage were observed to have similar sensor values to water/ethanol. Champagne, Chambord and Disaronno follow a relatively linear increase in sensor value as the relative amount of ethanol increases. However, Southern Comfort and Marylebone Gin do not show the same increase with increased ethanol content. Southern Comfort, which has over double the expected ethanol content of Chambord (37.5 % compared to 18 %) has a lower measured sensor value, and Marylebone Gin has a measured sensor value comparable to Disaronno (28 %). Moreover, the 50 % ethanol/water mix had a measured sensor value of approx. 18, whereas Marylebone Gin had a measured value of only 15.5. Despite the composition of the commercial alcohols having increased ethanol content, the other components in the mix affect the overall dielectric properties of the system. Due to this, utilising the system as a commercial alcohol detector was not investigated further.

3.4. Conclusions and future work

Mixtures of water/organic solvents were prepared and had dielectric and conductive properties tested, followed by being tested with a PDMS modified commercially available UHF RFID tag (RFMicron RFM 2100-AER), to see if the system could be effectively implemented for usage as a passive measurement system that could reveal the degree of water contamination if an organic solvent (or vice versa). The water/solvent mixes also had PDMS samples swollen in an excess of them, to determine how the presence of water in different relative quantities affects the swelling of PDMS.

It became clear that the tag is suitable for the monitoring of mixtures of water/alcohol solutions, but the monitoring of other water/organic solvent mixes has showed inconsistent readings, which have yet to be explained fully. The possibility of inconsistent readings as a result of the PDMS substrate being swollen by the water/organic solvent mix was also explored. Whilst it was found that acetone does result in the PDMS substrate being swollen as the organic solvent content increases, acetonitrile's inconsistent results could not be explained as a result of swelling. Moreover, the sensor data showed that water/propanol mixes could be effectively measured, despite the relatively high swelling capability of propanol with regards to PDMS.

After establishing that the system could be utilised for the monitoring of two part water/alcohol mixes, the system was tested to see if it could be implanted for the monitoring of commercial alcohol solutions. relatively low ethanol content alcohol mixtures showed similar sensor data values to that of their water/ethanol counterparts, but high ethanol content commercial alcohol mixtures did not show similar sensor data values to their water ethanol counterparts.

The primary reason for exploring water/organic mixes originally was as a further proof for the explanation as to why the sensor data values decreased with regards to higher concentration NaCl solutions despite the fact that the dielectric constant of the solutions decreased. With the organic solutions, as the relative amount of organic solvent is increased, the dielectric constant of the mix decreases, without the sharp increase in the conductivity (and as a result the tan δ). It was seen for the alcohol solutions that increasing the relative amount of organic solvent increases the sensor data value increased, which was expected with a lowering dielectric constant solution that lacks an increasing conductivity. Whilst this is true as a general trend, it was seen that a predictive model produced for propanol that considered both conductivity and relative permittivity together was more accurate.

Future work for this system would involve testing the system with solvent covering the entire tag, or with the tag fully submerged in the water solvent mix. Alternatively, the system would have to be implemented in such a way that the sensor area is exposed to the analyte whilst the antenna is isolated from the analyte. A proposed use case for the system would be in distillation processes where knowing the relative water content of an organic mix passively and in situ would be advantageous. A secondary use case would be as a simple and inexpensive means of quality control for organic solvent bottles, where being able to quickly determine the degree to which water impurities exist in a bottle passively without having to perform sampling would be of significant use.

3.5. References

1   Y. Marcus, *INTERNATIONAL UNION OF PURE AND APPLIED CHEMISTRY ANALYTICAL CHEMISTRY DIVISION COMMISSION ON ELECTROANALYTICAL CHEMISTRY**

RECOMMENDED METHODS FOR THE PURIFICATION OF SOLVENTS AND TESTS FOR IMPURITIES 1-PROPANOL, 2-PROPANOL, AND 2-METHYL-2-PROPANOL Prepared for publication by, 1986, vol. 58.

2   H. D. Isengard and U. Striffler, *Fresenius. J. Anal. Chem.*, 1992, **342**, 287–291.

3   Karl Fischer titrators for water (moisture) determination | Metrohm, https://www.metrohm.com/en-gb/products-overview/karl-fischer-titration/, (accessed 22 September 2019).

4   Snap 51 Portable Alcohol Meter for Distilled Spirits :: Anton-Paar.com, https://www.anton-paar.com/uk-en/products/details/snap-51-portable-alcohol-meter-for-distilled-spirits/, (accessed 22 September 2019).

5   A. P. Gregory and R. N. Clarke, *IEEE Trans. Dielectr. Electr. Insul.*, 2006, **13**, 727–743.

6   *Broadband Dielectric Spectroscopy*, Springer Berlin Heidelberg, 2003.

7   U. Kaatze, *Radiat. Phys. Chem.*, 1995, **45**, 549–566.

8   G. Smith, A. P. Duffy, J. Shen and C. J. Olliff, *J. Pharm. Sci.*, 1995, **84**, 1029–1044.

9   J. P. Grantts, R. N. Clarke §//, G. T. Symmo and N. M. Spyrout, *Less-Common Met. 49 1-12 Panagopoulos C N 1988 Internal stress in growing Ti02 films J. Less-Common Met*, 1989, vol. 141.

10,   DOI:10.1088/0957-0233/18/5/026.

11   T. Friisø and T. Tjomsland, *Meas. Sci. Technol.*, 1997, **8**, 1295–1305.

12   E. Nyfors, *Subsurf. Sens. Technol. Appl.*, 2000, **1**, 23–43.

13   H. Lobato-Morales, A. Corona-ChaV́ez and J. L. Olvera-Cervantes, in *IEEE MTT-S International Microwave Symposium Digest*, 2013.

14   H. Lobato-Morales, A. Corona-Chavez, J. L. Olvera-Cervantes, R. A. Chavez-Perez and J. L. Medina-Monroy, *IEEE Trans. Microw. Theory Tech.*, 2014, **62**, 2160–2167.

15   A. J. Cole and P. R. Young, *IEEE Sens. J.*, 2018, **18**, 149–156.

16   M. H. Zarifi and M. Daneshmand, *IEEE Microw. Wirel. Components Lett.*, 2017, **27**, 311–313.

17 F. Costa, A. Gentile, S. Genovesi, L. Buoncristiani, A. Lazaro, R. Villarino and D. Girbau, *IEEE Microw. Wirel. Components Lett.*, 2018, **28**, 371–373.

18 V. Makarovaite, A. J. R. Hillier, S. J. Holder, C. W. Gourlay and J. C. Batchelor, *IEEE Sens. J.*, 2019, **19**, 4299–4307.

19 A. A. Abduljabar, A. Porch and D. A. Barrow, in *IEEE MTT-S International Microwave Symposium Digest*, Institute of Electrical and Electronics Engineers Inc., 2014.

20 Tagformance Lite | Voyantic, https://voyantic.com/products/tagformance-lite, (accessed 22 September 2019).

21 K. E. Belsey, A. V. S. Parry, C. V Rumens, M. A. Ziai, S. G. Yeates, J. C. Batchelor and S. J. Holder, *J. Mater. Chem. C*, 2017, **5**, 3167–3175.

22 C. V. Rumens, M. A. Ziai, K. E. Belsey, J. C. Batchelor and S. J. Holder, *J. Mater. Chem. C*, 2015, **3**, 10091–10098.

23 *Proc. R. Soc. London*, 1895, **58**, 240–242.

24 Regression Analysis in Excel - Easy Excel Tutorial, https://www.excel-easy.com/examples/regression.html, (accessed 15 September 2019).

25 X. Hu and W. Yang, , DOI:10.1108/02602281011010772.

26 T. Honda, M. Miyazaki, H. Nakamura and H. Maeda, *Lab Chip*, 2005, **5**, 812–818.

3.6. Appendix

**3.6.2. Multiple regression model including swelling data for methanol/water and ethanol/water systems**

$$R^2 = 0.912$$
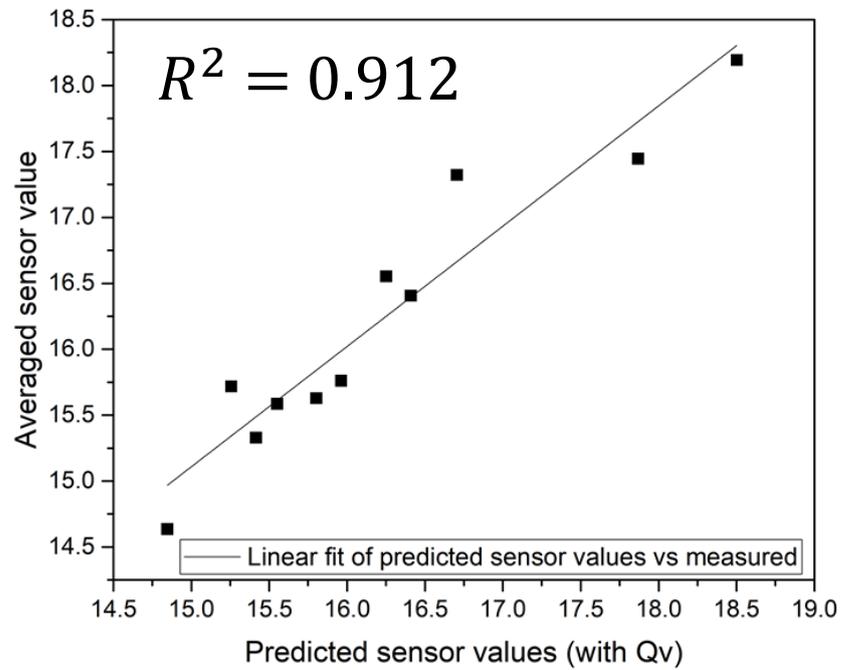
Figure 3.33 - Plot showing methanol/water averaged sensor value vs predicted sensor value (dielectric properties and Qv).

$$R^2 = 0.976$$
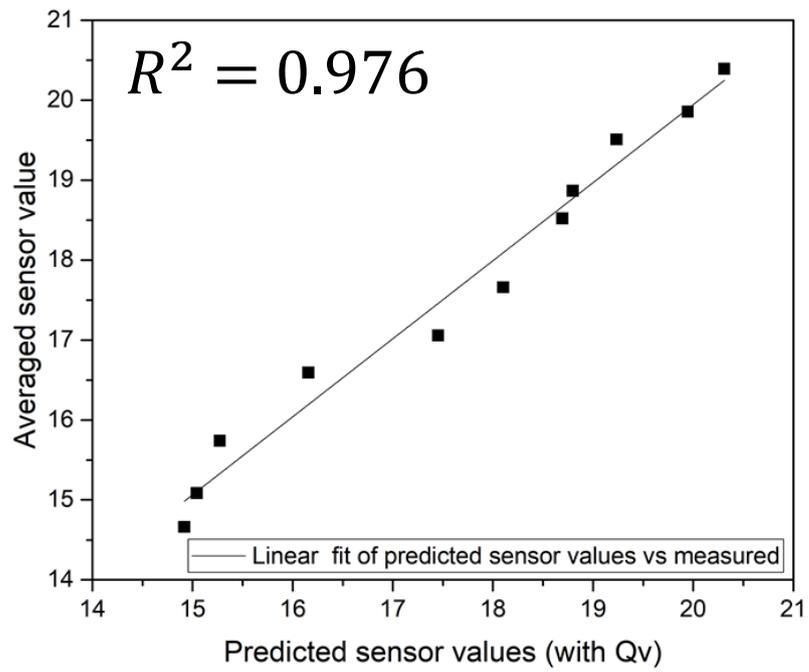
Figure 3.34 - Plot showing ethanol/water averaged sensor value vs predicted sensor value (dielectric properties and Qv).

Chapter 4:   Synthesis and cross-linking of reactive siloxanes for use as pH responsive RFID sensing coatings.

4.1. Introduction

As previously mentioned in Chapter 1, pH is the most commonly studied analyte with regards to wireless chemical sensors[1]. Several passive systems have been developed that allow for the discrimination of a range of pH. Some systems of note and relative to the chapter (i.e capacitive systems and modifying commercial systems) will also be discussed.

A means of sensing pH in a compact form factor without the need for expensive and specific equipment is highly desirable. Utilising RFID is highly attractive, with the idea of a "lab on a chip" being popularised as a term that allows for in situ pH monitoring. Kassal[2] et al developed a passive sensing system that utilised an potentiometer for pH sensing. The system was compared against a pH probe and showed results within an error of ± 0.01. The tag was tested in a practical setting by determining the degree of milk spoilage over time, successfully measuring a pH change of 2.4 over the course of 6 days as lactic acid was produced by milk spoilage, again with good agreement to the results obtained via a pH probe. Gou et al[3] developed a conductometric passive RFID system that allowed for pH sensing by utilising single walled carbon nanotubes (SWCNT's) with a conducting polymer (poly-1amino(anthracene) to be able to detect pH between a range of 2-12. The reason for using SWCNT's instead of the conventional glass electrode used by Kassal was that glass electrodes are probe to breakage and can result in contamination through leakage of electrolytes from the required reference electrode. The system retained sensitivity over the course of a 120 day testing cycle. The sensor was implemented in an RFID tag through a bespoke touch probe and allowed the passive tag to power the system. Whilst the two described systems utilised potentiometric and conductometric transduction mechanisms, a plethora of RFID sensors have been developed that utilise optical transduction mechanisms. These systems usually exploit a change in absorbance or fluorescence or reflectance within a pH sensitive dye to facilitate sensing. Steinberg[4] et al developed a tag that incorporated a pH sensitive dye called bromocresol green that undergoes a colormetric change when exposed to pH between 5.0-8.5. The dye was incorporated into the RFID tag so that the colormetric response could be measured via two LEDs that measured optical

absorption at two discrete wavelengths. Kassal[5] et al developed a system that could be worn as a smart bandage that used to measure pH changes within physiological ranges. The system detected changes in pH by covalently attaching a colormetric pH responsive dye to the cellulose substrate the tag was fabricated on. The tag incorporated a miniaturised optoelectronic probe that was capable of monitoring changes in reflectance as the dye changed colour when exposed to various pH.

Examples of capacitive pH sensing does exist in the literature despite the popularity of ion selective electrode based architectures. Arefin[6] et al developed a capacitive sensing tag that could measure changes in solution pH between 1-4 and 10-12. The system exploited solution permittivity changes that occur when aqueous electrolytes are dissolved in solution. The passive tag operated at 30 MHz and exploited a resonant frequency change associated with antenna detuning when the tag was exposed to solutions of varying pH. Hammarling[7] et al have also developed a capacitive pH sensor that exploited a pH responsive hydrogel that swells and de-swells dependant on solution pH. swelling results in the solution being drawn into the hydrogel, affecting the bulk permittivity of the hydrogel. This then results in an increased capacitive load, detuning the tag. This can then be used to calculate the solution pH.

Potyrallo[8] et al have also developed a system that modified a commercially available Texas instruments RI-I03-112A-03 HF passive RFID tag[9]. The tag was coated in a pH responsive polyaniline polystyrene sulfonate (PANI-PSS) film that allowed for sensing of pH between 2-8, exploiting a performance drop off (at the reader side) from a conductivity change in the film when pH solutions were applied. One inherent issue aside from only exploiting sensing capabilities from the reader side, is that PANI films are notoriously hard to process due to their lack of solubility[10]. Furthermore, electronically conducting polymer films undergo volumetric changes when being doped and de-doped, resulting in swelling (following by shrinkage) that causes cracks in the film to form[11], adversely affected performance and changing the relative surface area that can be exposed to, in turn affecting degree of conductivity.

Here, a cross-linked polymer system consisting of chloromethylphenethyl terminated polydimethylsiloxane and (6-7% aminopropylmethylsiloxane) – dimethylsiloxane co-polymer was tested as a pH responsive coating for the RFMicron RFM 2100-AER. The minimal degree of cross-linking for the polymer network that would produce robust films was determined, with the aim of leaving the highest possible number of free amine groups available to be protonated at the surface of the coated tag. pH testing studies were then performed to determine whether the number of free amine groups available was enough to elicit a conductive change at the surface of the coating through capacitive sensing.

4.2. Experimental

4.2.2. Materials and methods

Hydride terminated polydimethylsiloxane (PDMS) (cSt 100, Mw 4000-5000), (6-7% aminopropylmethylsiloxane) – dimethylsiloxane copolymer (cSt 1,800-2,200 , Mw 50,000), and chloromethylphenethyl terminated polydimethylsiloxane (100-150 cSt, Mw 5,000) were purchased from Gelest inc. 4-Vinylbenzyl chloride (90 %, tert-butylcatechol stabilized) and platinum(0)-1,3-divinyl-1,1,3,3-tetramethyldisiloxane complex solution (~2% in xylene) and aluminium oxide were purchased from Sigma Aldrich. Toluene (analytical grade) and hexane (fraction from petroleum, laboratory grade), activated charcoal, hydrochloric acid and sodium hydroxide were all purchased from Fischer and used as received. FT-IR measurements were performed using Shimadzu IRAffinity-1 spectrometer with a Specac Golden Gate™ ATR sampling accessory, and each sample was subjected to 32 scans, with a resolution of 4 cm^{-1}. ^{1}H, and ^{13}C NMR was acquired on Bruker Avance Neo NMR, running a proton frequency of 400 MHz at room temperature (22 °C). 1H Magic angle spinning (MAS) NMR spectra were acquired on a Bruker Avance Neo NMR at 400 MHz at room temperature (22 °C). The samples were examined using an HR-MAS semi-solids probe, utilizing magic angle (54.736 °) spinning at 5000 Hz. The relaxation delay of the samples was set to 60 seconds. The samples were swollen in deuterated chloroform inside Bruker disposable NMR capsules (poly(triflurorochloroethylene)). These were then placed in a 4mm zirconium spinner with a plastic rotor designed for the 4 mm probe. RFID

measurements were performed on Voyantic® Tagformance equipment with a frequency sweep of 800 – 860 MHz and a power sweep of 8-20 dBm for sensorbench® measurements. Homogenous mixing of the elastomer components was achieved using a DAC 150FV2-K speedmixer and elastomers were then doctor bladed onto an RFMicron RFM-2100 AER using an automatic precision film applicator MTCX4, purchased from mtv-messtechnik (blade width =70 mm, thickness adjustability 0-3000 μm). RFMicron RFM2100-AER tags were purchased from RFMicron. Rheological measurements were performed on an Anton Parr MCR 302 rheometer, with storage and loss modulus of the of Cl-PDMS25 recorded every 1 minute for 1000 minutes at 70 °C.

4.2.3. Synthesis of chloromethylphenethyl terminated polydimethylsiloxane

Synthesis of Chloromethylphenethyl terminated PDMS was based upon a modified procedure from Pinteala[12] For the small-scale reaction, 3 g of hydride terminated PDMS, and 0.5 g of uninhibited 4- vinyl benzyl chloride was dissolved in 25 ml of toluene. After 5 minutes of stirring at 600 rpm, 30 mg of Kartsted's catalyst was added to the reaction mix. The mixed was left stirring for 6 hours at 90 oC. For the large scale reaction, 20 g of hydride terminated PDMS and 3.5 g of uninhibited 4- vinyl benzyl chloride were added to 125 ml of toluene. After 5 minutes of stirring at 600 rpm, 180 mg of Kartsted's catalyst was added to the reaction mix. The reaction mix was left to stir at 600 rpm at 90 °C for 6 hours. The reaction mix was then further dissolved (an additional 25 ml of toluene) and Buchner filtrated through activated charcoal to remove the platinum nanoparticles that formed throughout the reaction. Following this, the reaction mix was then rotary evaporated to remove toluene before being heated overnight at 110 °C. Heating overnight causes the thermal polymerization of the excess 4-vinylbenzyl chloride in the reaction mix, and removes any residual toluene. The mix changes colour from colourless to white. The reaction mix was then re-dissolved in hexane (fraction from petroleum). The insoluble polymerized 4-vinylbenzyl chloride was then Buchner filtered through activated charcoal. (yield: 2.6 g, 86%).

NMR assignments of chloromethylphenethyl terminated PDMS: ^{1}H NMR (Figure 4.2), 400 MHz, CDCl$_3$, room temperature. δ: = -0.5 - +0.5 ppm [**478H** (**CH$_3$**SiO)], 0.82 ppm [**2H** (Si**CH$_2$**CH$_2$PhCH$_2$Cl)], 1.30 ppm [**2H** (Si**CH$_3$**CHPhCH$_2$Cl)], 2.58 ppm [**2H** (SiCH$_3$**CH**PhCH$_2$Cl)], 2.58 ppm [**2H** (SiCH$_2$**CH$_2$**PhCH$_2$Cl)], 4.5 ppm [**4H**(SiCH$_2$CH$_2$Ph**CH$_2$**Cl)], 6.99 ppm [**1.5H** (SiCH$_2$CH$_2$**Ph**CH$_2$Cl), ortho], 7.10 ppm [**2.5H** (SiCH$_3$CH**Ph**CH$_2$Cl), ortho], 7.14 - 7.22 ppm [**4H** (SiCH$_3$CH**Ph**CH$_2$Cl), meta, (SiCH$_2$CH$_2$**Ph**CH$_2$Cl), meta].

^{13}C NMR (Figure 4.3), 400 MHz, CDCl$_3$, room temperature. Found ppm δ: = 0.1, 0.3, 3.7, 13.2, 19.1, 45.2, 126.6, 127.1, 127.3, 127.6.

IR assignments of chloromethylphenethyl terminated PDMS:

C-H stretch (CH3),(2966). Si-CH3 stretch, asym (1438). Si-CH3 stretch, sym (1261). Si-O-Si stretch (1103), (1120). Si-C stretch (786).

4.2.4. Cross-linking of chloromethylphenethyl-terminated polydimethylsiloxane with (6-7%) aminopropylmethylsiloxane dimethylsiloxane co-polymer

For cross-linking studies of the two polymer mixes, 2 g of aminopropylmethylsiloxane-dimethylsiloxane co-polymer was mixed with 2.365 g of chloromethylphenethyl-terminated polydimethylsiloxane. When mixed in these ratios, the relative amount of NH$_2$ groups to Cl groups was 1:1. Crosslinking ratios of 1:0.75, 1:0.65, 1:0.50, 1:0.35, 1:0.25 & 1:0.15 were also used (and from here onward are referred to as a density of Cl groups as a percentage).

4.2.5. Mould casting of cross-linked chloromethylphenethyl-terminated polydimethylsiloxane with (6-7%) aminopropylmethylsiloxane dimethylsiloxane co-polymer

Both components were speed-mixed for 120 seconds at 3500 rpm, and then poured into recessed moulds made of PTFE (Teflon) with dimensions (20 mm x 20 mm x 2 mm) before being transferred to a 65 °C oven. The filled moulds were moved on a glass tile, and a small amount of the remaining mix would be poured onto the tile next to the moulds (as a test sample) then left in an oven overnight. The next day, the moulds would first be taken out of the oven and left to cool to room temperature. During this time, the test sample left on the glass would be prodded with a spatula to see if it had solidified or not. If the test sample was no longer fluid-like then

the moulds were prodded with a spatula. The pads were removed by following along the edges of the mould with a scalpel blade to remove the cross-linked polymer from the edges of the mould. Following this, a long thin spatula was used to pry the polymer out of the mould. Due care was taken to reduce the likelihood of the cross-linked polymer from tearing (although lower cross-linking density polymers were more prone to breakage).

4.2.6. Doctor-blading of cross-linked chloromethylphenethyl terminated polydimethylsiloxane with (6-7%) aminopropylmethylsiloxane dimethylsiloxane co-polymer

The RFMicron RFM 2100-AER was used as the commercial tag for studies with the two-part polymer mix. The two polymers were mixed together with the same method as in section. After mixing, the mix was placed into a 70 ^{O}C oven for 3 hours. Before the polymer mix was removed from the oven, the tag was placed onto a glass tile with the protective acetate layer removed. The tag was then adhered to the tile using scotch tape. Following this, more scotch tape was applied to create a well for the polymer mix to be poured into. The tape was pressed down with the underside of a chattaway spatula. The depth of the well was measured with Vernier callipers. The well height used was 500 μm. Layering the tape resulted in each corner of the tag being double the height of the length and the width of the tape used to make a boundary around the tag. Additional tape was applied over the length and width of the tape to compensate.

Once the well was made, the polymer mix was taken out of the oven and visually examined after tilting the container. If the mix was still fluid (but less so than when it placed in the oven) then it was mixed at 3500 rpm in the speedmixer for a further 120 seconds. The mix was then poured into the scotch tape well, and the doctor blade was then moved over the top of the tag with the polymer in the well, just above the height of the tape boundary. Following this, the glass tile was moved to a 70 ^{O}C oven to be cured. A 2 dimensional spirit level was placed on all 4 corners of the tile to ensure that the substrate was level and to reduce the likelihood of uneven curing due to sloping. The samples would be let to cure overnight, and examined firstly by tilting the tile to observe if the sample flowed. If the sample did not flow, it would be prodded with a micro

chattaway spatula. If the sample was firm to touch, the tag would be removed from the tile by cutting away the excess tape with a scalpel.

4.2.7. Rheology of chloromethylphenethyl terminated polydimethylsiloxane/ (6-7 %) aminopropylmethylsiloxane dimethylsiloxane cross-linked polymer films.

Crosslinking studies were performed using a plate with a disposable measuring probe at relative Cl densities of 100 %, 75%, 65 %, 50 %, 35 %, 25 %, and 15%. 1 g of the two components was speedmixed at 3500 rpm for 2 minutes, and then applied to the rheology plate (heated to 70 ^{o}C). The separation from the plate to the measuring plate was set to 0.200 mm. storage and loss modulus were measured every 60 seconds for 1000 minutes For 15, 25, & 75%, and for 705 minutes for 35, 50, 65 & 100% in all measurements performed.

4.2.8. Relative permittivity measurements of aqueous hydrochloric acid, sodium hydroxide and sodium chloride.

Relative permittivity measurements were performed on aqueous hydrochloric acid, sodium hydroxide and sodium chloride using the same method described in chapter, with a DAK 3.5 probe from Speag, using the open/short/load method described in Chapters 2 & 3.

4.2.9. RFID studies of chloromethylphenethyl terminated polydimethylsiloxane/ (6-7%) aminopropylmethylsiloxane Dimethylsiloxane cross-linked polymer films.

RFID measurements were performed using the same method described in chapter 2, with solution depositions being performed using the same method as described in both chapters 2 and 3, with a 3D printed reservoir with the same dimensions used in chapters 2 and 3 being used. Instead of performing solution depositions of NaCl only, depositions were performed with NaOH, HCl and NaCl. 0.8 ml of liquid was applied using an auto-pipette.

4.3. Results and discussion

4.3.2. Synthesis of the chloromethylphenethyl terminated polydimethylsiloxane

Chloromethylphenethyl terminated PDMS is normally purchasable, but due to material shortage at the time it had to be synthesised. Hydride terminated PDMS was used as the precursor, and was functionalised using a 4 fold excess of 4-vinyl benzyl chloride via hydrosilylation, using a modified procedure from Pinteală[12]. The addition reaction typically reaches completion after 2 hours, by which time the reaction mix changes colour from transparent to a dark brown colour due to the formation of colloidal platinum as the reaction proceeds, shown in Figure 4.1:
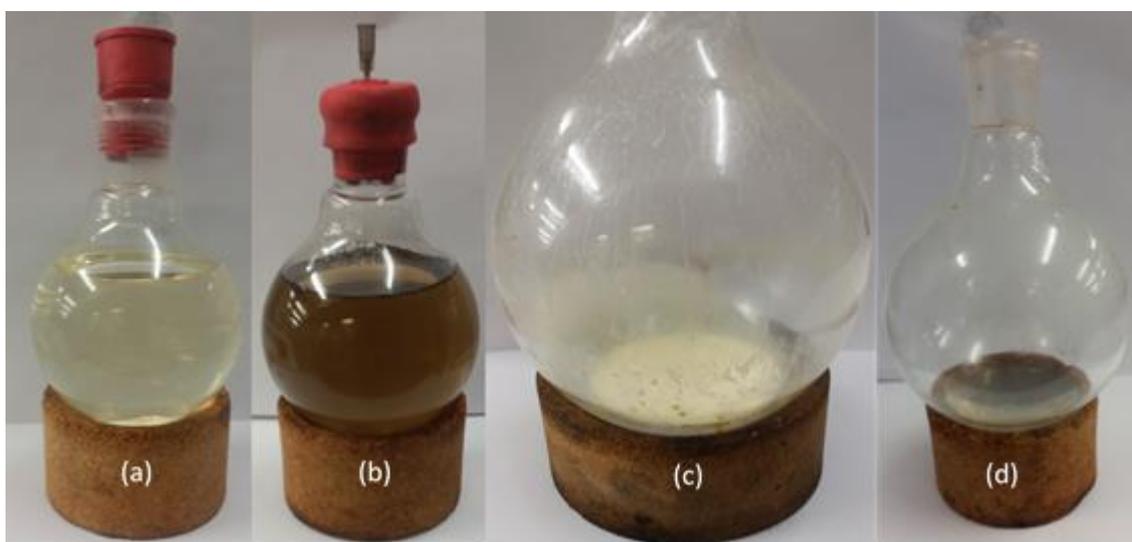
Figure 4.1 - (a) the pre reaction mix, (b) the post-reaction mix, (c) the post reaction mix after excess 4-vinylbenzyl chloride polymerisation, and (d), the purified product after purification.

Following a Buchner filtration with activated charcoal to remove colloidal platinum and vacuum removal of toluene, the mix was heated to thermally polymerise the excess 4-vinyl benzyl chloride. Polymerisation of the excess 4-vinyl benzyl chloride causes the reaction mixture to turn white. The white reaction mix was then re-dissolved in hexane and the insoluble poly (vinyl benzyl chloride) was Buchner filtrated. Following this, the heating process would be repeated after the removal of hexane. If the product did not turn white upon heating, ^{1}H and ^{13}C NMR was performed to confirm the functionalisation was successful, shown in Figure 4.2 & Figure 4.3 (1H & 13C of the hydride terminated PDMS precursor can be found in appendix 4.6:
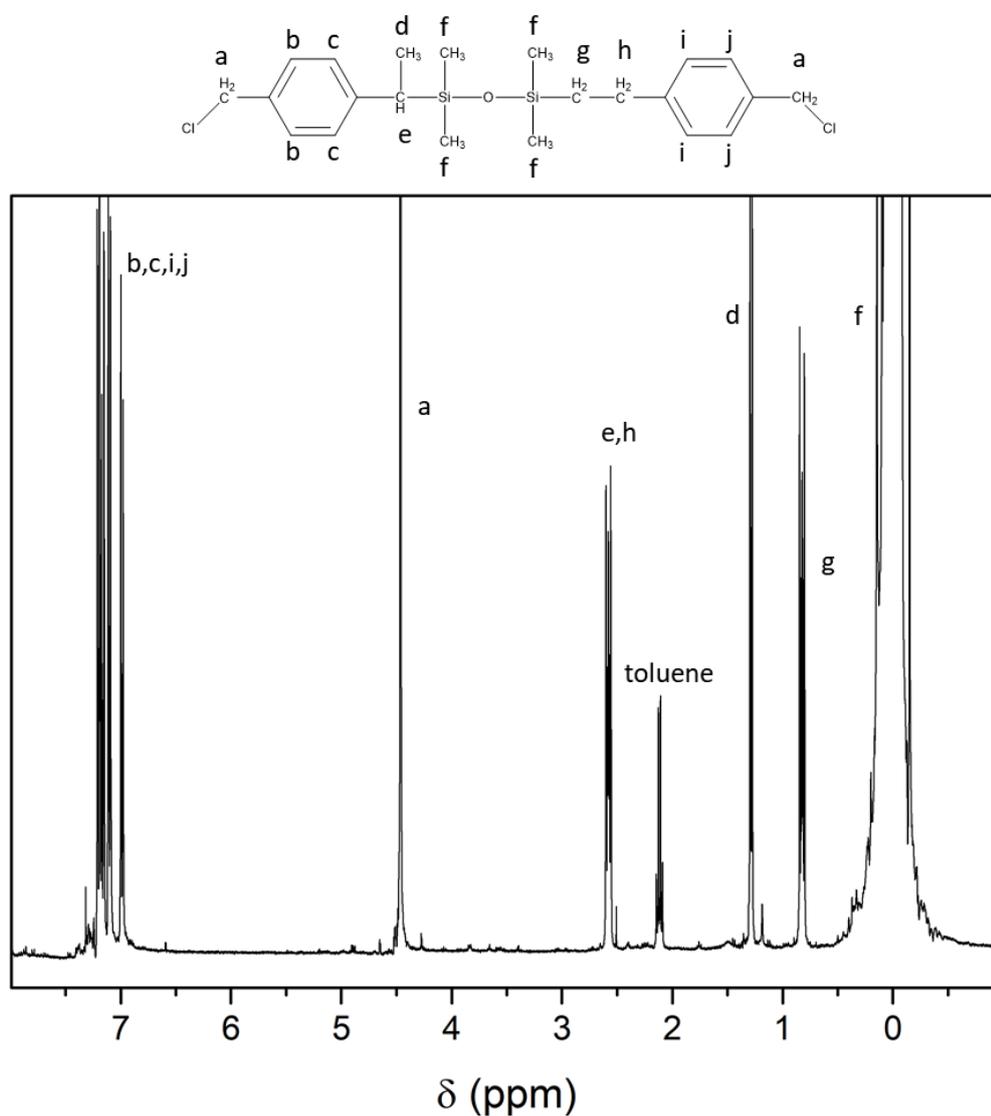
Figure 4.2 - 1H NMR of chloromethylphenethyl terminated PDMS functionalised Chloromethylphenethyl terminated polydimethylsiloxane.
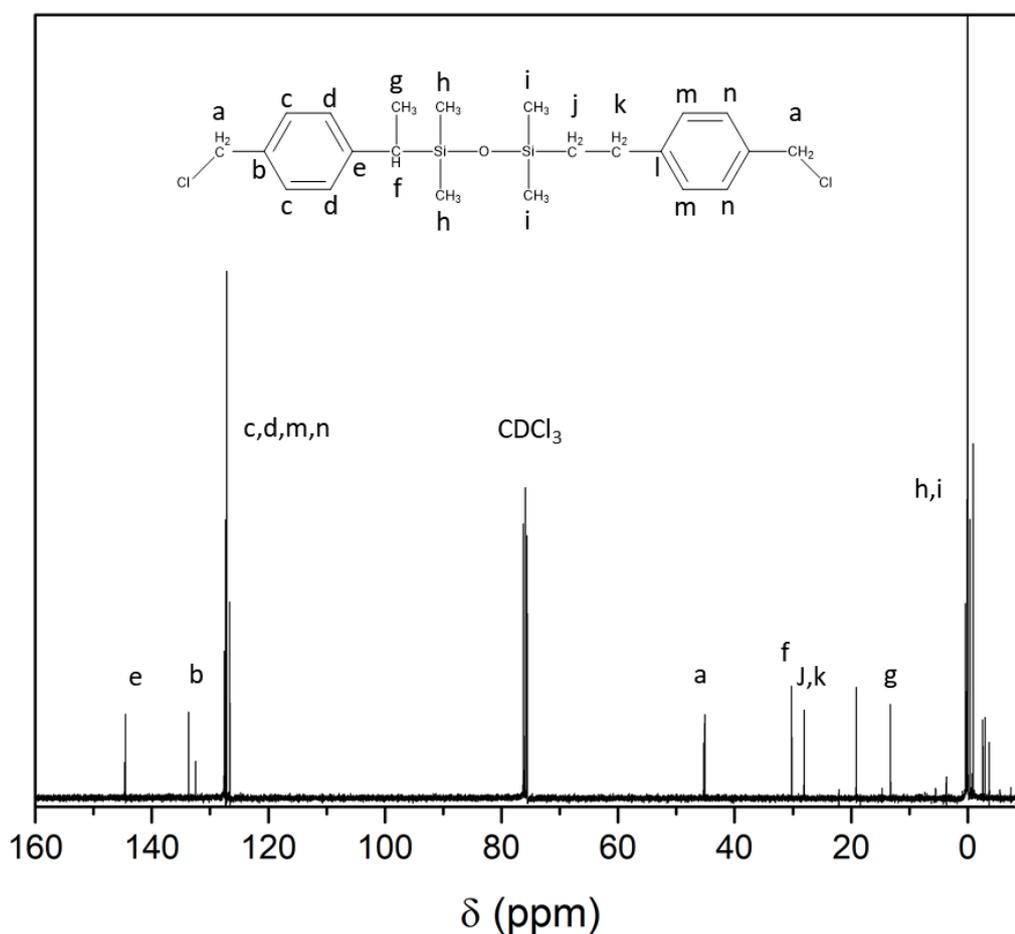
Figure 4.3 - **13C** **NMR of chloromethylphenethyl terminated PDMS functionalised Chloromethylphenethyl terminated polydimethylsiloxane.**

Disappearance of the characteristic Si – H peak at 4.7 ppm[13] indicates successful hydrosilylation of the 4-VBC. Instead, the characteristic peak at 4.5 ppm represents the CH_2-Cl ascribed to the functionalised 4-VBC in Figure 4.2. Peaks d,e,g & h in Figure 4.2 shows that the hydrosilylation occurs at either side of the vinyl bond[14], and showed good agreement with literature. With regards to the 13C NMR (Figure 4.3), the peaks at 45 ppm, the series of peaks at 125-130, 135 & 145 ppm ascribed to the aromatic carbons also showed good agreement with literature[15].

4.3.3. Cross-linking studies of chloromethylphenethyl terminated polydimethylsiloxane/ (6-7 %) aminopropylmethylsiloxane Dimethylsiloxane cross-linked polymer

The amino-chloro system was tested at different crosslinking densities to determine the minimum amount of crosslinking that would produce a rigid film suitable to be used as a coating for the RFMicron RFM 2100-AER. The required ratio of the aminopropyl PDMS that needed to

be mixed with the chloromethylphenethyl terminated PDMS initially was a 1:1 ratio of NH_2:Cl. This was expressed as a percentage of Cl groups relative to NH_2 as a percentage (100% for 1:1, 75% for 1:0.75 for 75% etc.) and through a naming code (shown next to each percentage in Table 4.1). The used were 100%, 75%, 65% 50%, 35%, 25% and 15%. The table below shows the results of the crosslinking studies:

Table 4.1 - Table showing whether various crosslinking densities of amino-chloro solidified after heating.

Relative Cl groups	Solidification
100% (Cl-PDMS100)	☑
75%(Cl-PDMS75)	☑
65%(Cl-PDMS65)	☑
50%(Cl-PDMS50)	☑
35%(Cl-PDMS35)	☑
25%(Cl-PDMS25)	☑
15%(Cl-PDMS15)	☑ (solidified but was incredibly brittle)

The minimum extent of crosslinking that would result in solidification of the film was found to be in **Cl-PDMS25**. **Cl-PDMS15** would result in a partial solidification; however the partially cured mix would tear and split even with gentle pressure applied. **Cl-PDMS25** was chosen for use as the proposed pH sensing film, as it provided the highest amount of free amines that could be protonated, whilst solidifying enough to be used as a coating.

4.3.4. Infrared spectroscopy of the cross-linked amino-chloro PDMS

Infrared spectra were taken of both the individual reactive silicones, as well as a cured tile of the polymers mixed together. The infrared spectra all three is shown in Figure 4.4:
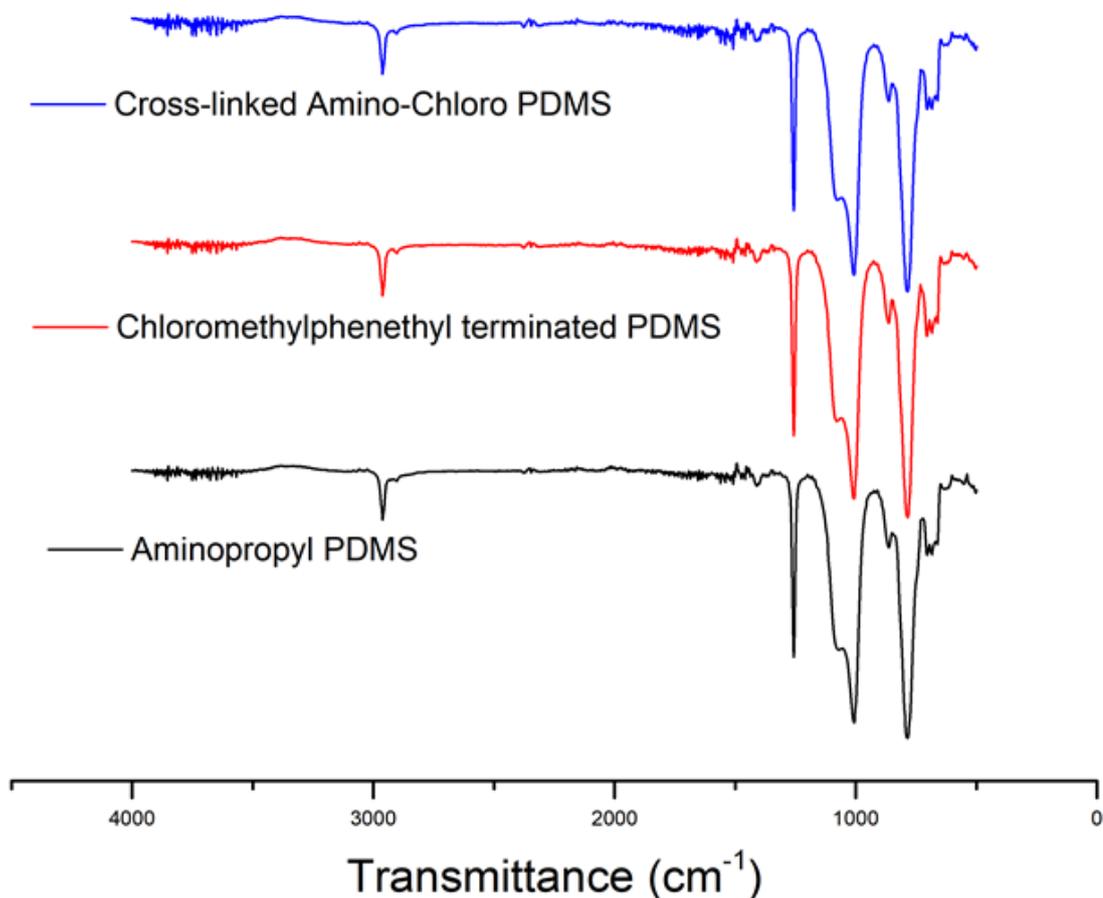
Figure 4.4 - Offset plots of both FT-IR spectra of polymer components and the mixed tile that had been cured with a 100% Cl concentration.

As the predominant species in both polymers is the dimethylsiloxane backbone, the three infrared spectra showed no pronounced change in infrared spectra across all three observed samples. In the aminopropyl dimethylsiloxane co-polymer, a peak at 3500 cm^{-1} for primary amines should be observed[16], and a secondary amine peak[17] in the cross-linked tile should also be seen at 3310 − 3350 cm^{-1}. However, the N − H bonds could not be observed through FT-IR due to the fact the aminopropyl moiety only comprises 6% of the polymer backbone. As in chapter 2, the characteristic peaks of PDMS were observed as reported in literature[18].

In order to observe the crosslinking of the polymer species, a different analytical method would need to be employed.

4.3.5. 1H magic angle spinning (MAS) NMR analysis of amino chloro PDMS mix

Whilst the two mixes can be examined individually and mixed, once cross-linked, solution state NMR broadens the observed peaks[19], to the extent where useful analysis cannot be performed to determine degree of crosslinking[20,21]. Spinning at the magic angle allows for a significant peak sharpening that means peaks can be resolved in the solid state, and has previously been used extensively with silicones[22]. Unfortunately, the solid state NMR was only available towards the latter end of the project, and as such, only a limited amount of samples could be obtained, so only Cl-PDMS100 could be measured. 1H and 13C NMR of the aminopropyl dimethylsiloxane co-polymer are shown in Figure 4.5 & Figure 4.6:
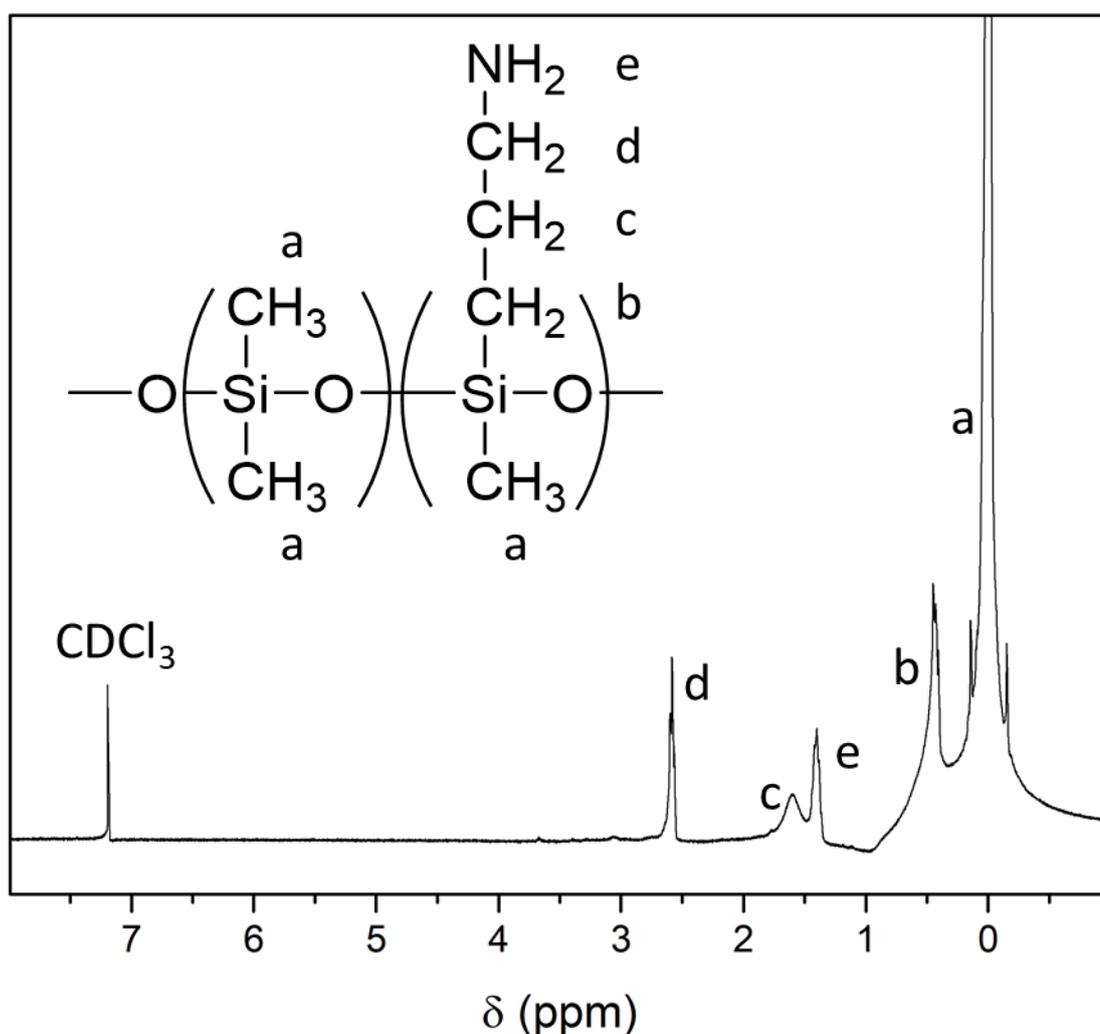
Figure 4.5 - ¹H NMR of aminopropyl dimethylsiloxane co-polymer.
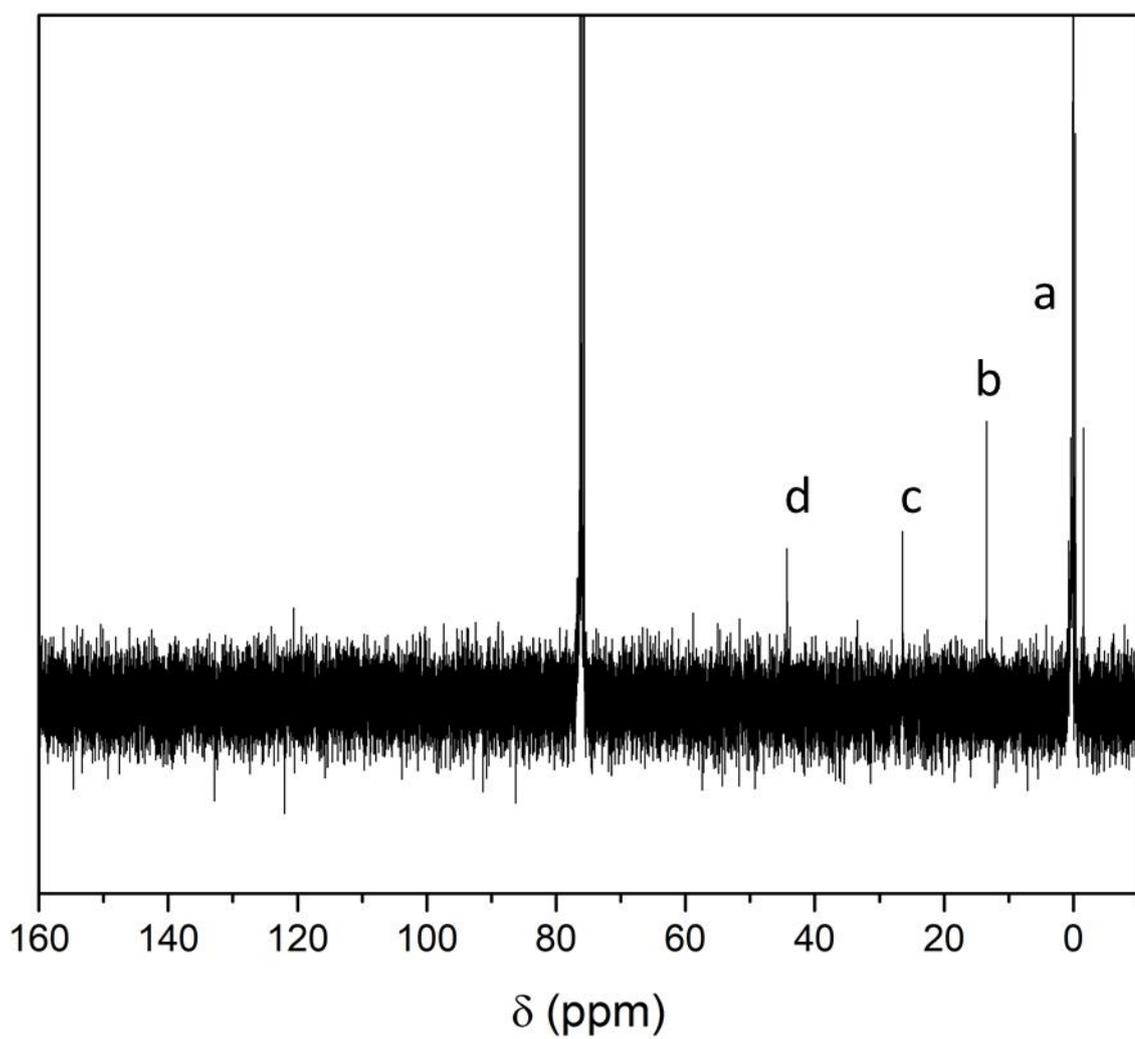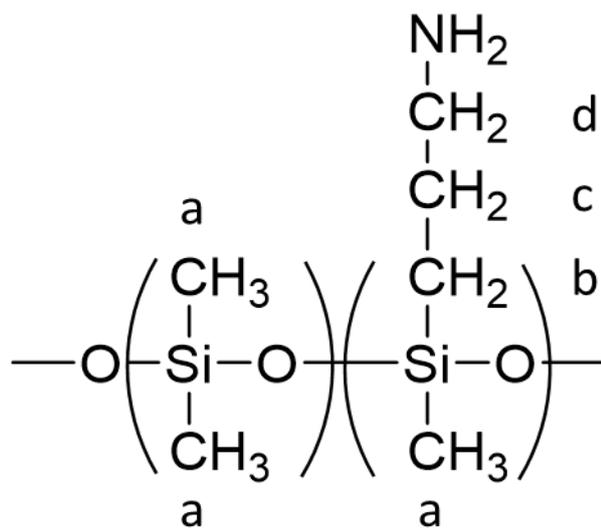
Figure 4.6 – ^{13}C NMR spectrum of aminopropyl dimethylsiloxane co-polymer.
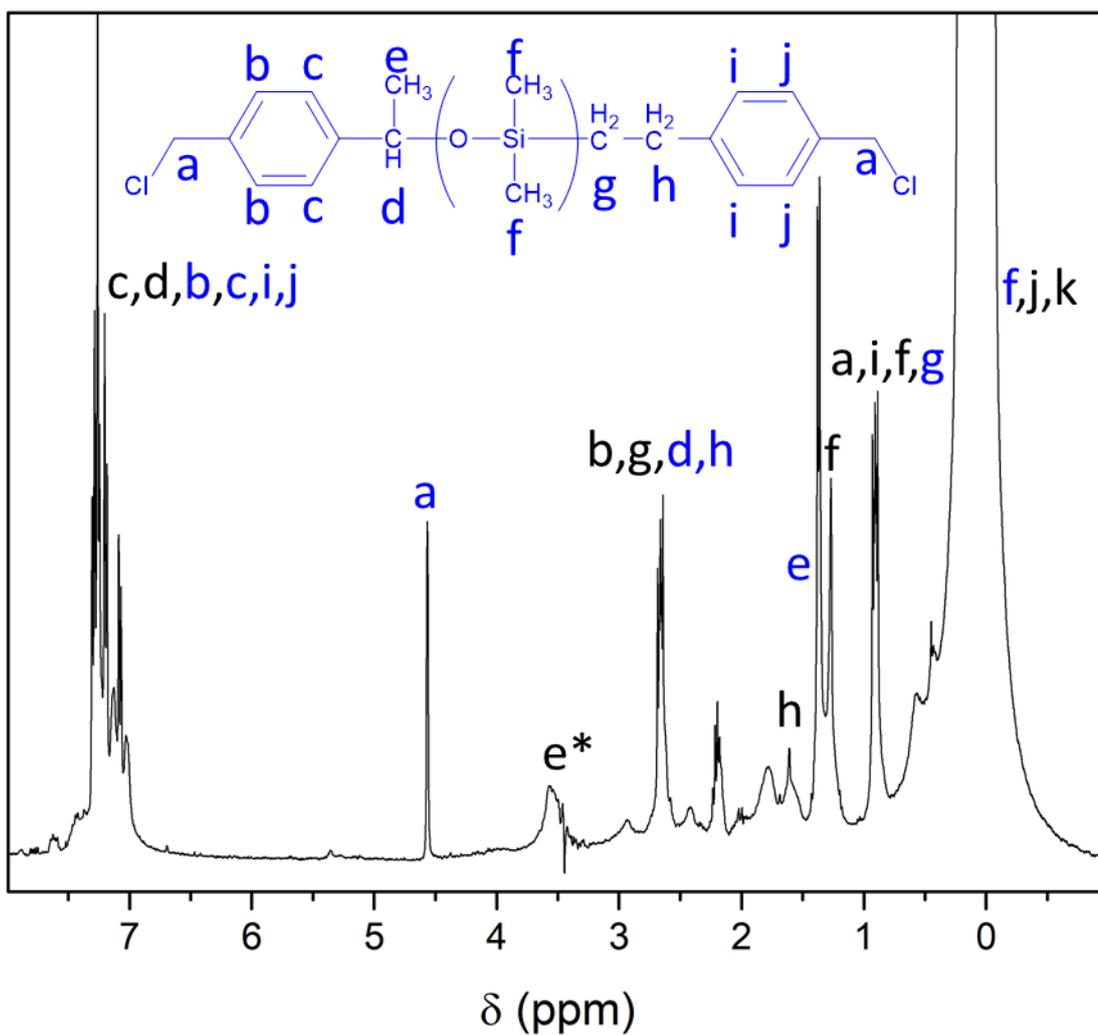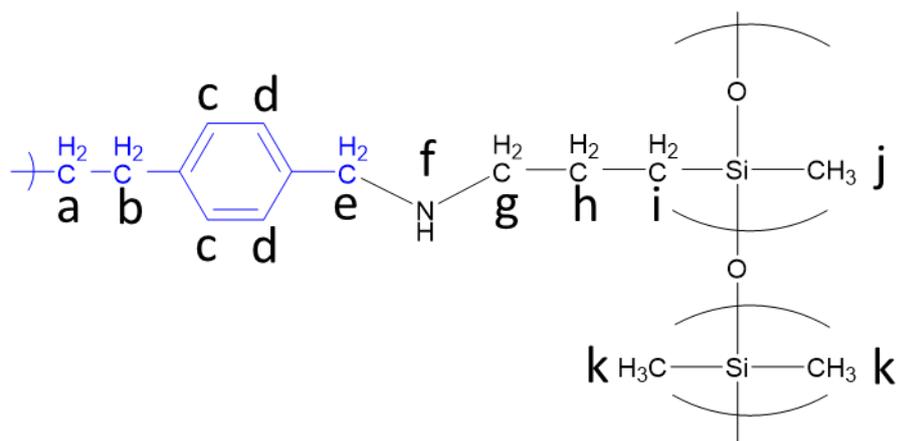
Figure 4.7 - ¹H MAS NMR of the crosslinked CL-PDMS100.

There are two possible peaks that can be used to determine the degree of cross-linking in Cl-PDMS100, peak e (marked with an asterisk) and peak g in the cross-linked structure shown in Figure 4.7. peak g overlaps with peak f in the same structure, so peak e was used. Degree of cross-linking was determined by comparison of the integrals of peak e (3.5 ppm) in the cross-

linked structure with peak a (4.5 ppm) in the unreacted chloromethylphenethyl terminated PDMS. An artefact at 3.5 ppm was always observed that extended underneath the baseline and reduces the integral for the peak observed at 3.5 ppm. This means only a minimum crosslinking density can be quoted by comparison of the integrals of the two peaks. The degree of crosslinking for CL-PDMS100 was found to be 82.7% by comparison of the two integrals (peak a 1: 3.03 peak e, but peak a corresponds to 4 protons compared to 2 in peak e.

4.3.6. Film deposition optimisation studies

The two part mix was initially mixed together for 120 seconds and 3500 rpm and then applied immediately to the tag substrate, before being doctor bladed uniformly over the top of the substrate at the set height. It was found that after being left for 8 hours, the mix had cross-linked and subsequently solidified, however, the mix had dispersed significantly over the glass tile. As a result, the thickness of the mix was always no greater than 80 μm in all cases (performed in triplicate), irrelevant of the doctor blade set height and crosslinking density. As the previous chapters have demonstrated that a 500 μm film thickness was the minimum required for a useful degree of sensing, optimising the film application procedure was required. These initial film deposition studies showed that the methods employed with catalytic cross-linked PDMS could not be used to produce thick enough films for further sensing studies. Two modifications were made to the film application procedure to increase the thickness of the films. Firstly, a curing study to determine if partially crosslinking the polymer mix prior to deposition was viable. Secondly, using an increased thickness tape recess was also employed. Cl-PDMS25 was used for the film optimisation studies. A schematic diagram of both modifications can be seen in Figure 4.9 & Figure 4.8:
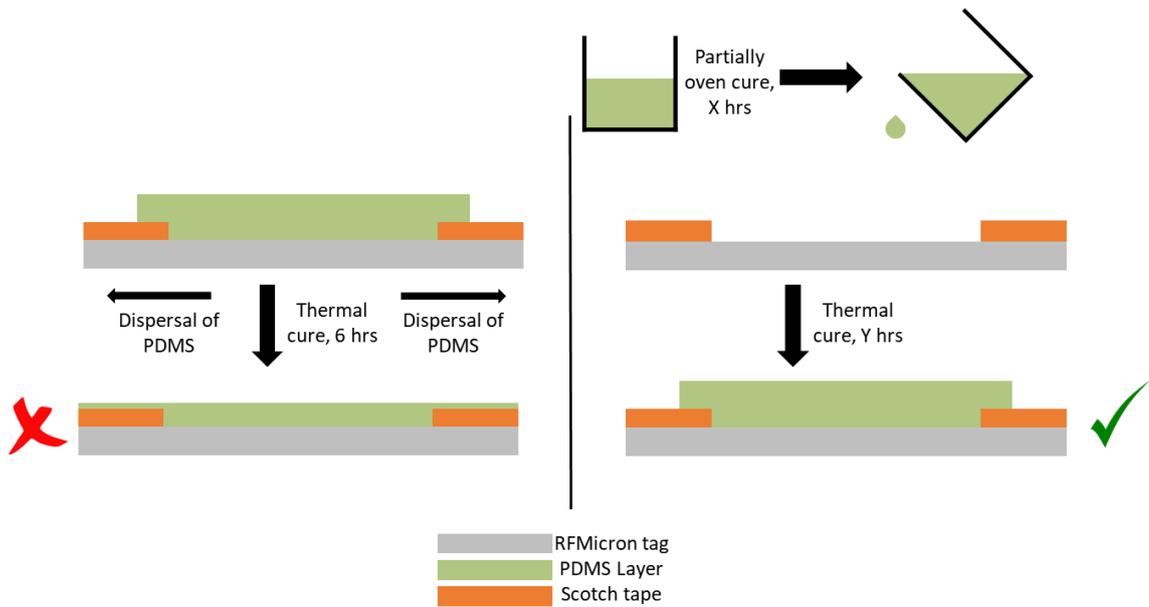
Figure 4.9 – Schematic diagram comparing the previous film application technique (left) and the proposed partial curing technique (right).
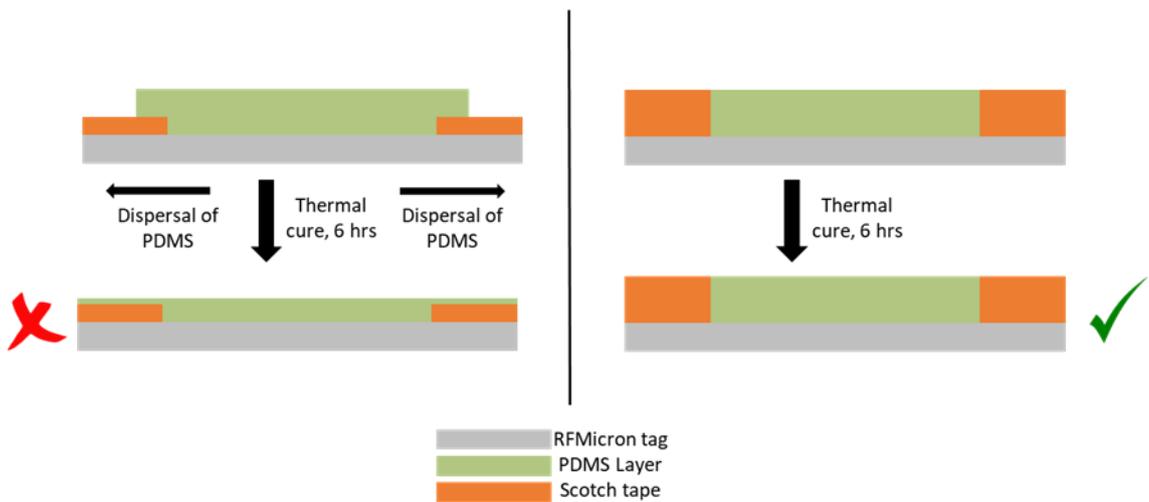

Figure 4.8 – Schematic diagram comparing the previous film application technique (left) and the proposed tape boundary technique (right).

Both modifications were tested separately and compared to triplicate measurements from the unmodified procedure.

4.3.7. Tape recess film deposition study

The initial film deposition study yielded films 80,70 & 80 μm thick respectively. A 500 μm thick scotch tape boundary was used, and yielded films 260, 280 and 290 μm respectively.

4.3.8. Partial crosslinking of Cl-PDMS100 film deposition study

4.3.8.1. Rheological studies of the amino-chloro polymer mix

Rheology was performed in order to determine the gel point of each of the tested crosslinking densities of the amino chloro polymer mix. The crude studies allowed for an approximation at the point where the mix could no longer be poured with differing crosslinking densities, but confirmation of when gel point is reached for the system needed to be determined. By comparing the crude data to the gel points observed through rheological studies, the exact point where the mixes are still pourable can be determined. It was suspected that when any mix of a given crosslinking density begins to have an increase in storage modulus that the mix becomes increasingly difficult to pour. Rheology was performed on Cl-PDMS100, Cl-PDMS75, Cl-PDMS65, Cl-PDMS50, Cl-PDMS35, Cl-PDMS25 & Cl-PDMS15, shown in Figure 4.11:
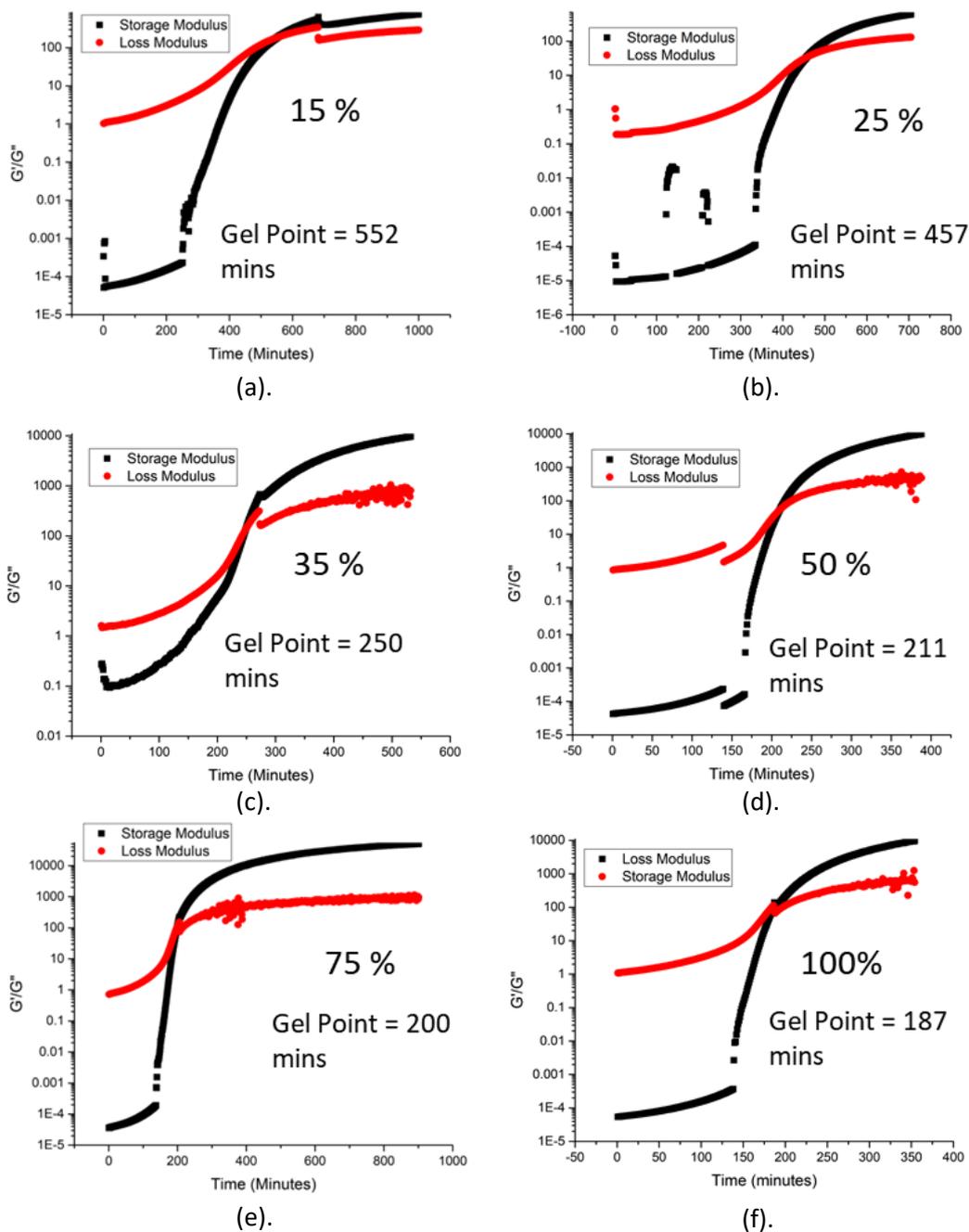
Figure 4.10 – Plot of time taken to reach gel point over time for aminopropyl Dimethylsiloxane co-polymer and chloromethylphenethyl terminated PDMS.

Increasing the ratio of Cl-CH$_2$ groups to NH$_2$ groups from 15% up to 100% led to the gel point being reached faster. As discussed in section 4.3.3 , a 15 % relative Cl ratio is sufficient to cause solidification of the two part mix. However, the time taken to reach gel point is almost triple the amount of time taken to reach gel point in a 100% Cl ratio. The gel points of all crosslinking densities were plotted over time, shown in Figure 4.10:
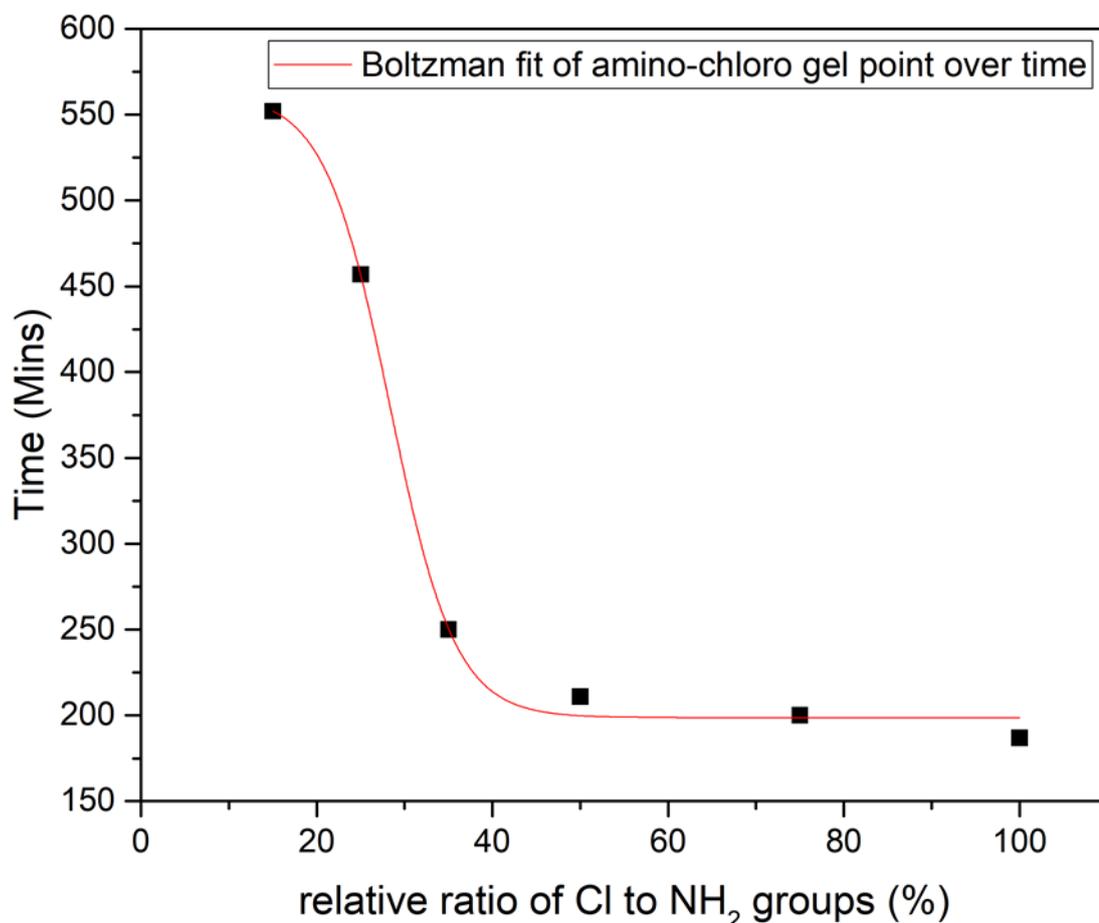
Figure 4.11 - Plots of change in storage and loss modulus over time for (a) 15% (b) 25% (c) 35% (d) 50% (e) 75% and (f) 100%.

Once the gel point of the system reaches below 35 %, the time taken to reach gel point increases significantly. In Section 4.3.3, films with a 25% Cl ratio were shown to solidify and make films rigid enough to use, and will lead to a higher concentration of free amines in the film. It takes Cl-PDMS25 352 minutes start to reach gel point (commonly referred to as T_{gel} or working time[23]). For the film depositions used in the partial curing study, Cl-PDMS25 was partially cured for 300 minutes and then applied to the tag.

Using the partial curing method shown schematically in Figure 4.9, Cl-PDMS25 yielded films 220, 200 & 200 µm thick, respectively.

Both methods employed led to an increased film thickness. The addition of the tape recess was the more effective of the two as it elicited a film thickness that was closer to the target 500 µm thicknesses. However, neither method alone produced films of the target 500 µm thickness.

4.3.9. Film deposition using both tape recess and partial curing of the amino-chloro polymer mix

A study where both methods were employed was next used, with the partially cured mix being poured into the tape recess well. The derived thicknesses for the partially cured mix and the tape recess method were then compared to the combination of both methods, shown in Table 4.2:

Table 4.2 - Table showing the comparison of film thicknesses with the initial film application procedure against the modified film application procedure that used a heating step before application.

Tag number	Film thickness (Tape recess film application procedure)	Film thickness (Pre-heating application procedure)	Film thickness (combinative application procedure)
1	260 µm	220 µm	460 µm
2	280 µm	200 µm	470 µm
3	290 µm	220 µm	450 µm

Using both methods in tandem increased the resultant thickness of the cast films. The measured thickness of the tape well was 500 µm, with the resultant film thickness of the films derived being only 40 µm shorter than the well height. One of the predominant reasons the tape well was less effective as an individual change to the procedure (when compared to using both modifications in tandem) was that the mix would seep into the scotch tape well and away from the . By partially crosslinking the amino-chloro mix, the viscosity of the mix was increased, reducing the degree of dispersal and seepage into the tape well. Furthermore the time with which the mix needed in order to cure was greatly reduced, so the time the mix had to seep was massively reduced. The films deposited as a result of this method with an aim thickness were on

average 40 µm thinner than the required thickness (based on the studies from chapter 2 that used a 500 µm film). The well size was increased to 550 µm, with the partial crosslinking step remaining unchanged. The resultant film thicknesses are shown in Table 4.3 (more than 3 studies were performed in this case as 3 tags of 500 µm were required for RFID studies):

Table 4.3 - Table showing the derived film thickness.

Tag number (target film thickness 500 µm)	Film thickness (combinative application procedure)
1	510 µm
2	500 µm
3	480 µm
4	500 µm
5	480 µm
6	500 µm

6 attempts were required to produce 3 films of the required thickness, with an average film thickness 495 µm ± 11.2 µm.

4.3.10. pH solution testing studies

pH solution studies were performed to determine if the amino-PDMS tags could sense pH changes. Aqueous solutions of sodium hydroxide and hydrochloric acid were tested on a 500 µm amino chloro coated RFMicron RFM 2100-AER, as shown in Figure 4.12:
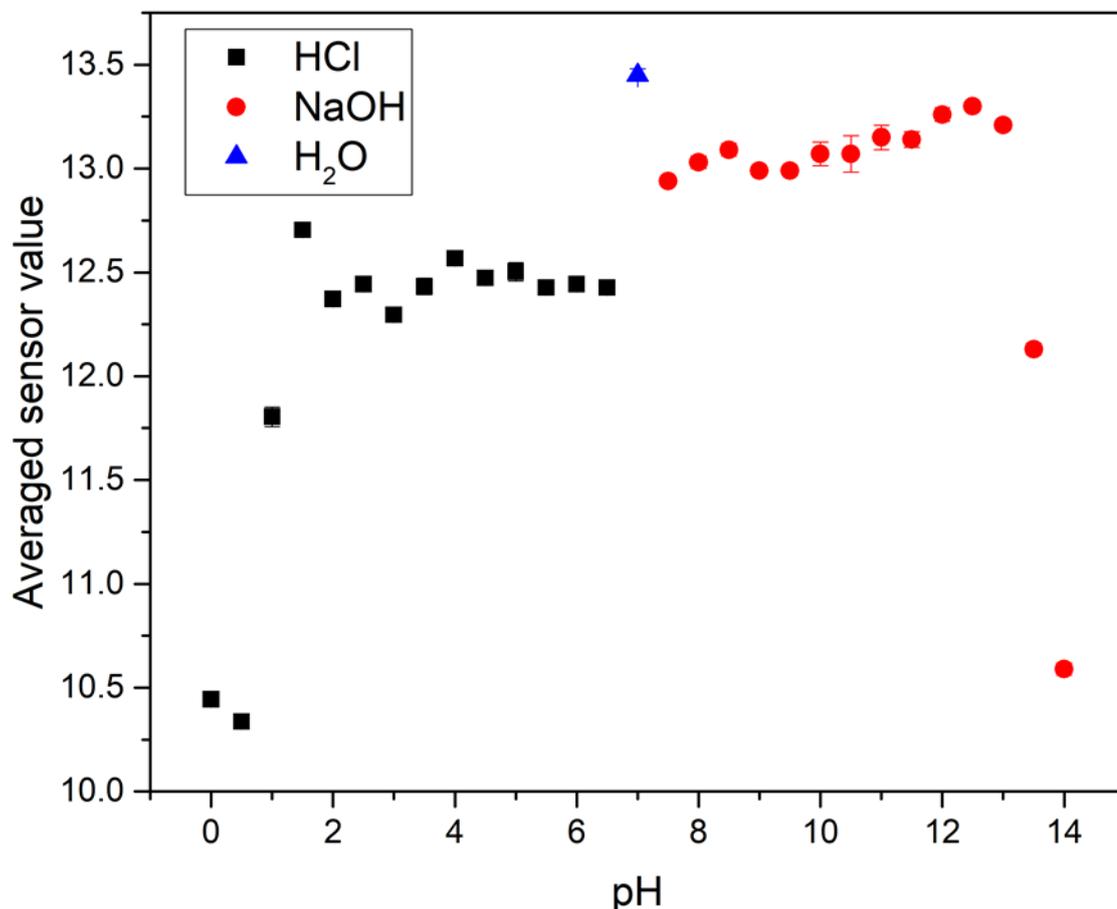
Figure 4.12 - Plots of sensor code values between pH 0 - 14.

The most prominent changes in sensor value were seen at the extremes of the pH scale. With regards to HCl and NaOH, a pH of 0 is equivalent to a concentration of 1 M and shows a significant difference in sensor value to the midrange pH values of HCl, which show a flat line between 2-6.5. With regards to the NaOH solutions, a similar phenomenon was observed. The extreme high pH's of 13.5 and 14 show an observable difference to the remainder of the NaOH readings. However, the lower concentrations of NaOH still show a lack of change in response comparative to the higher concentrations.

To confirm whether the response was as a result of a change in pH at the higher concentrations, a comparison of HCl, NaOH and NaCl was performed against concentration. Chapter 2 showed that increased NaCl concentration reduced sensor values as tan δ increased. was used as a blank in this instance to determine whether the observed change was due to a change in aqueous electrolyte concentration, shown in Figure 4.13:
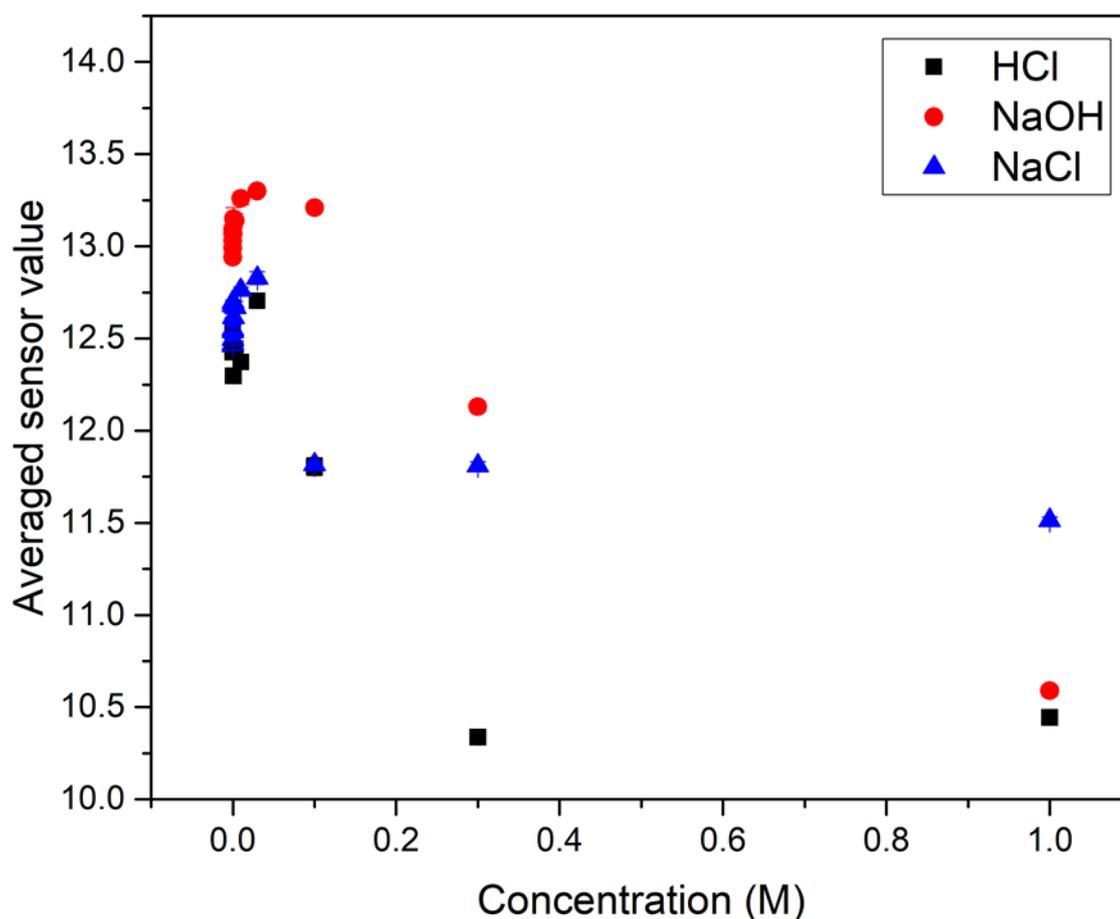

Figure 4.13 – Plots of molarity against averaged intensity for HCl, NaOH and NaCl.

The predominant decrease in sensor values for NaOH and NaCl occur at higher concentrations, as is the case for NaCl. The lower concentrations show an almost flat line, with some outliers present. Nonetheless, only higher concentrations of aqueous electrolyte were distinctly different. To confirm the changes in sensor value were as a result of dielectric properties changing, a silanol terminated PDMS tag was used and compared all three aqueous electrolytes.

4.3.11. Comparison of sensor values for silanol terminated PDMS with aqueous NaCl to Aqueous HCl and Aqueous NaOH.
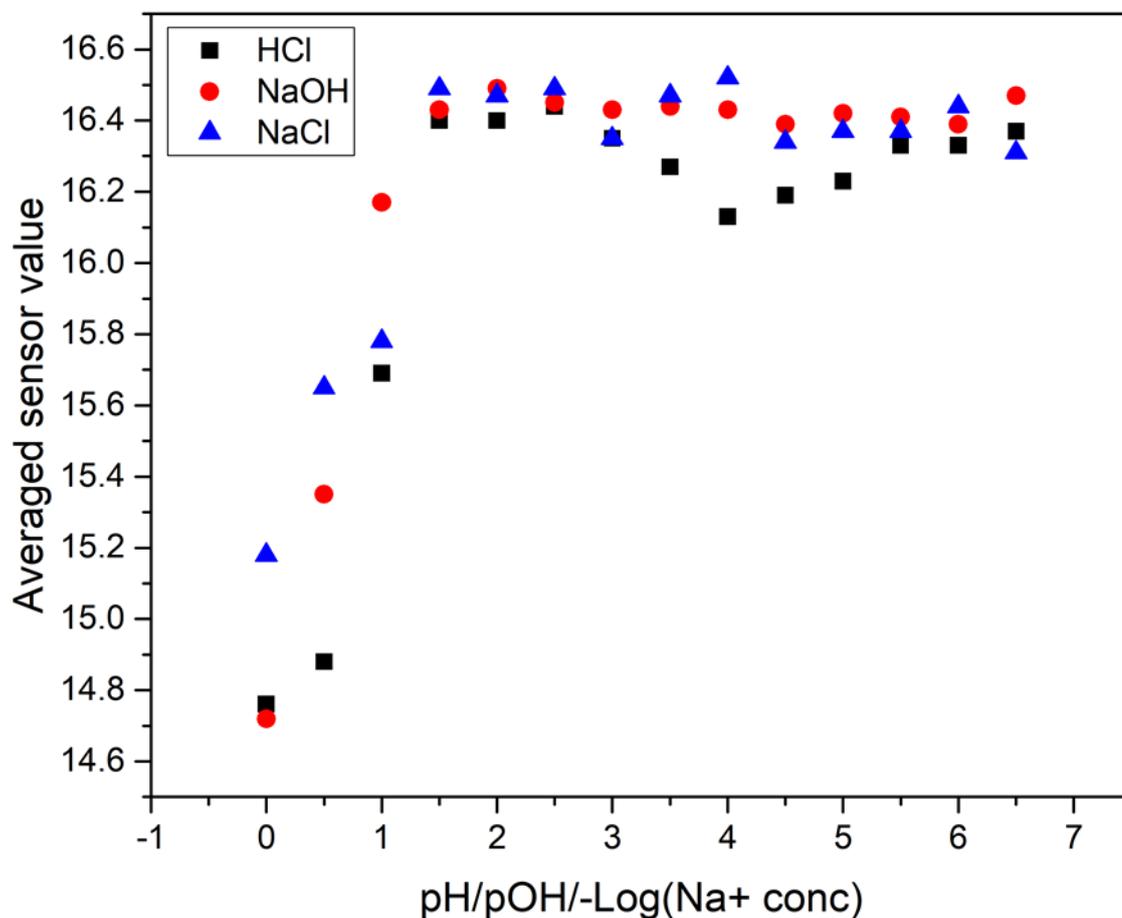

Figure 4.14 – Plots of sensor code values for relative amounts of ions in solution for [H+] [Cl-] vs [Na+] [OH-] vs [Na+] [Cl-] for silanol terminated PDMS.

A similar trend is observed in silanol terminated PDMS to that in the amino-chloro polymer mix (albeit with higher observed sensor values across the entire range of pH). Only the higher concentrations show a significant decrease in sensor values, suggesting that the amino-chloro polymer mix does not elicit a pronounced enough change in its conductivity as a result of protonation of the free amines in the polymer network. Tan δ was acquired for all of the aqueous electrolyte solutions and compared, shown in Figure 4.15:
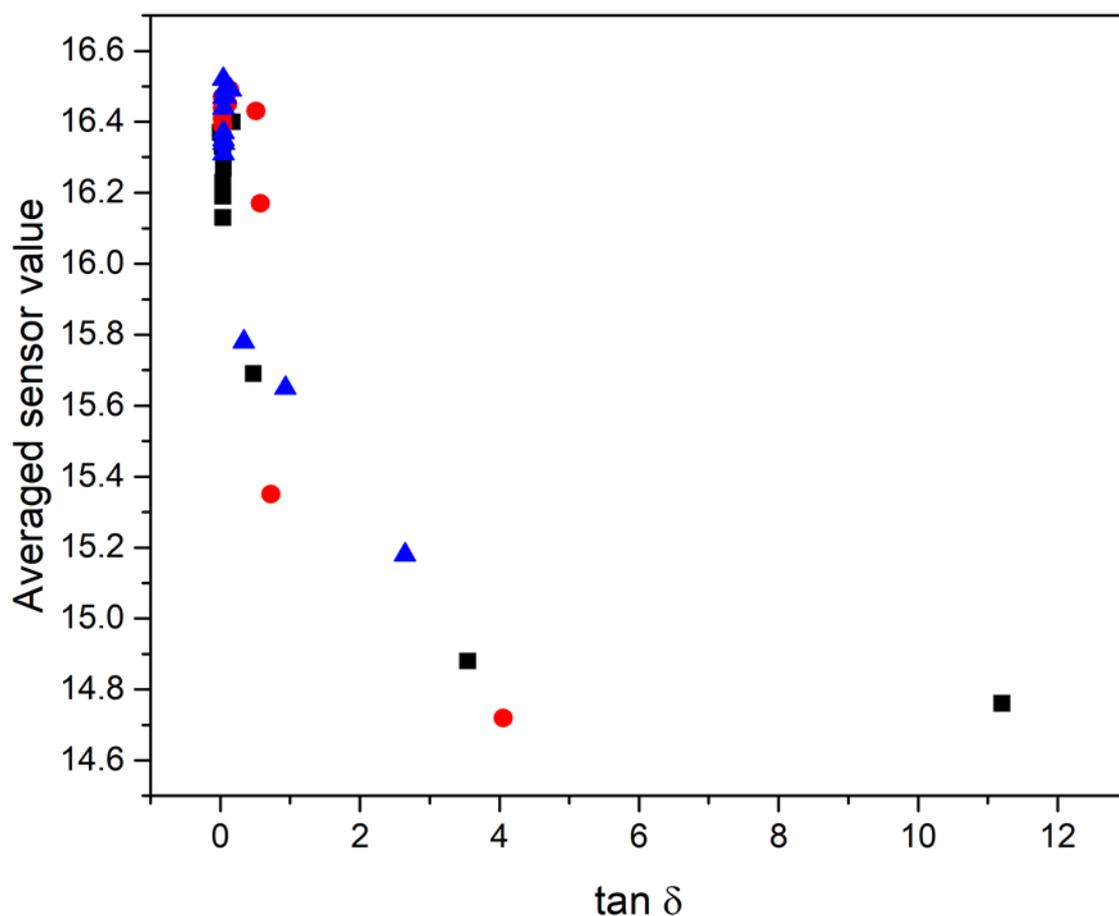
Figure 4.15 - Plots of tan δ against measured sensor value for [H$^+$] [Cl-] vs [Na$^+$] [OH$^-$] vs [Na$^+$] [Cl$^-$] for Silanol terminated PDMS.

Chapter 2 showed that tan δ increasing results in a linear decrease of sensor value (with regards to NaCl). As pH is an exponential scale, if the tag was able to sense pH by conductive change in the amino-chloro polymer mix from protonation of the free amine, this would be observable as a linear change in sensor response as a function of pH. Instead, all three aqueous electrolytes show a similar trend. Only concentration within a similar sensing range to the aqueous electrolyte range show measurable changes in sensor value.

4.4. Conclusions and future work

Chloromethylphenethyl terminated polydimethylsiloxane was successfully synthesised via a one-step functionalisation of hydride terminated polydimethylsiloxane via platinum catalysed hydrosilylation, with 4-vinyl benzyl chloride being the moiety used to functionalise the terminal groups. The product was then cross-linked with a commercially purchased aminopropyl

functionalised polydimethylsiloxane through thermal curing. Test films were applied to a commercially available capacitive sensing tag (RFMicron RFM2100-AER) using a doctor blade, with the components mixed together in a 1:1 ratio, relative to the free amine groups and Cl groups in each respective component. Due to the relatively slow curing time of thermal cure systems, a significantly thinner actual film thickness was observed compared to the set height of the doctor blade used to apply the mix over the substrate. The observed values were also significantly lower than films applied with catalytically cross-linked polymer systems at the same set heights.

 In order to be able to optimise the film application process of the two part mix, modifications to the film application procedure were made; namely, partially curing the polymer mix prior to application, and using a scotch tape layer that surrounded the tag substrate so that the mix had a well to cure in. with regards to partially curing, crude heating studies were first performed to determine whether the polymer mix would solidify. This was then compared to rheological studies. It was found that the gel point was reached for 100 % relative Cl: NH_2 at 187 minutes. With regards to 25 % relative Cl:NH_2, gel point was reached at 452 minutes, but the storage modulus began to increase rapidly at 352 minutes. As a result, partial crosslinking studies were performed with the mix where a 25 % relative Cl:NH_2 polymer mix was oven heated for 300 minutes before being applied to the substrate. Both methods employed increased the thickness of deposited films approximately three fold. A modified procedure where both methods were used in tandem was then used, where the elicited film thickness was increased to very close to the desired 500 μm for RFID studies. Finally, the size of the well was increased to 550 μm, yielding three tags with the desired film thickness after 6 attempts.

Finally, RFID studies were performed on the Amino-Chloro composite. It was found that although the tags did show a significant decrease in sensor values for extremely high and low pH, this was solely a consequence of changes in dielectric properties of the higher concentration aqueous electrolytes (found by comparison to NaCl at an equivalent concentration). In order to be able to measure pH changes with a capacitive sensing system, the applied film would need

to have a linear change in conductivity as a result of protonation/ deprotonation with increased acidity/basicity.

4.5. References

1 P. Kassal, M. D. Steinberg and I. M. Steinberg, *Sensors Actuators B Chem.*, 2018, **266**, 228–245.

2 P. Kassal, I. M. Steinberg and M. D. Steinberg, *Sensors Actuators B Chem.*, 2013, **184**, 254–259.

3 P. Gou, N. D. Kraut, I. M. Feigel, H. Bai, G. J. Morgan, Y. Chen, Y. Tang, K. Bocan, J. Stachel, L. Berger, M. Mickle, E. Sejdić and A. Star, *Sci. Rep.*, 2015, **4**, 4468.

4 M. Caldara, C. Colleoni, E. Guido, V. Re and G. Rosace, *Sensors Actuators B Chem.*, 2016, **222**, 213–220.

5 P. Kassal, M. Zubak, G. Scheipl, G. J. Mohr, M. D. Steinberg and I. Murković Steinberg, *Sensors Actuators B Chem.*, 2017, **246**, 455–460.

6 M. S. Arefin, M. B. Coskun, T. Alan, A. Neild, J. M. Redoute and M. R. Yuce, in *Proceedings of IEEE Sensors*, Institute of Electrical and Electronics Engineers Inc., 2014, vol. 2014-December, pp. 1792–1794.

7 K. Hammarling, M. Engholm, H. Andersson, I. M. Sandberg and H.-E. Nilsson, , DOI:10.3390/chemosensors6030030.

8 R. A. Potyrailo, C. Surman, T. Sivavec and T. Wortley, in *2011 IEEE International Conference on RFID-Technologies and Applications, RFID-TA 2011*, 2011, pp. 533–536.

9 RI-I03-112A-03 from Texas Instruments, https://www.electronicsdatasheets.com/manufacturers/texas-instruments/parts/ri-i03-112a-03, (accessed 25 September 2019).

10 A. V. Quintero, F. Molina-Lopez, E. C. P. Smits, E. Danesh, J. van den Brand, K. Persaud, A. Oprea, N. Barsan, U. Weimar, N. F. de Rooij and D. Briand, *Flex. Print. Electron.*, 2016, **1**, 025003.

11 D. S. Patil, J. S. Shaikh, D. S. Dalavi, S. S. Kalagi and P. S. Patil, *Mater. Chem. Phys.*, 2011,

128, 449–455.

12   M. Pinteală, V. Harabagiu, C. Cotzur and B. C. Simionescu, *Eur. Polym. J.*, 1994, **30**, 309–312.

13   M. R. Ramli, M. B. H. Othman, A. Arifin and Z. Ahmad, *Polym. Degrad. Stab.*, 2011, **96**, 2064–2070.

14   D. A. Brown, G. J. Price, D. A. Brown and G. J. Price, , DOI:10.1016/S0032.

15   L. Lutsen, G. P. G. Cordina, R. G. Jones and F. Schué, *Eur. Polym. J.*, 1998, **34**, 1829–1837.

16   Infrared Spectroscopy Absorption Table - Chemistry LibreTexts, https://chem.libretexts.org/Ancillary_Materials/Reference/Reference_Tables/Spectroscopic_Parameters/Infrared_Spectroscopy_Absorption_Table, (accessed 24 September 2019).

17   S. Wachholz, F. Keidel, U. Just, H. Geissler and K. Käppler, *J. Chromatogr. A*, 1995, **693**, 89–99.

18   E. Llez, J. Rubio, F. Rubio, E. Morales and J. L. Oteo, *Synthesis of inorganic-organic hybrid materials from TEOS, TBT and PDMS*, .

19   K. Schmidt-Rohr and H. W. Spiess, *Multidimensional Solid-State NMR and Polymers*, Elsevier Ltd, 2012.

20   L. J. Mathias, Ed., *Solid State NMR of Polymers*, Springer US, Boston, MA, 1991.

21   F. A. (Frank A. Bovey and P. A. Mirau, *NMR of polymers*, Academic Press, 1996.

22   R. S. Maxwell, J. P. Lewicki, B. P. Mayer, A. Maiti and S. J. Harley, *The Development and Application of NMR Methodologies for the Study of Degradation in Complex Silicones Concise Encyclopedia of High Performance Silicones*, 2013.

23   V. Heinrichs, S. Dieluweit, J. Rg Stellbrink, W. Pyckhout-Hintzen, N. Hersch, D. Richter and R. Merkel, , DOI:10.1371/journal.pone.0195180.

4.6.2. 1H NMR of the hydride terminated PDMS
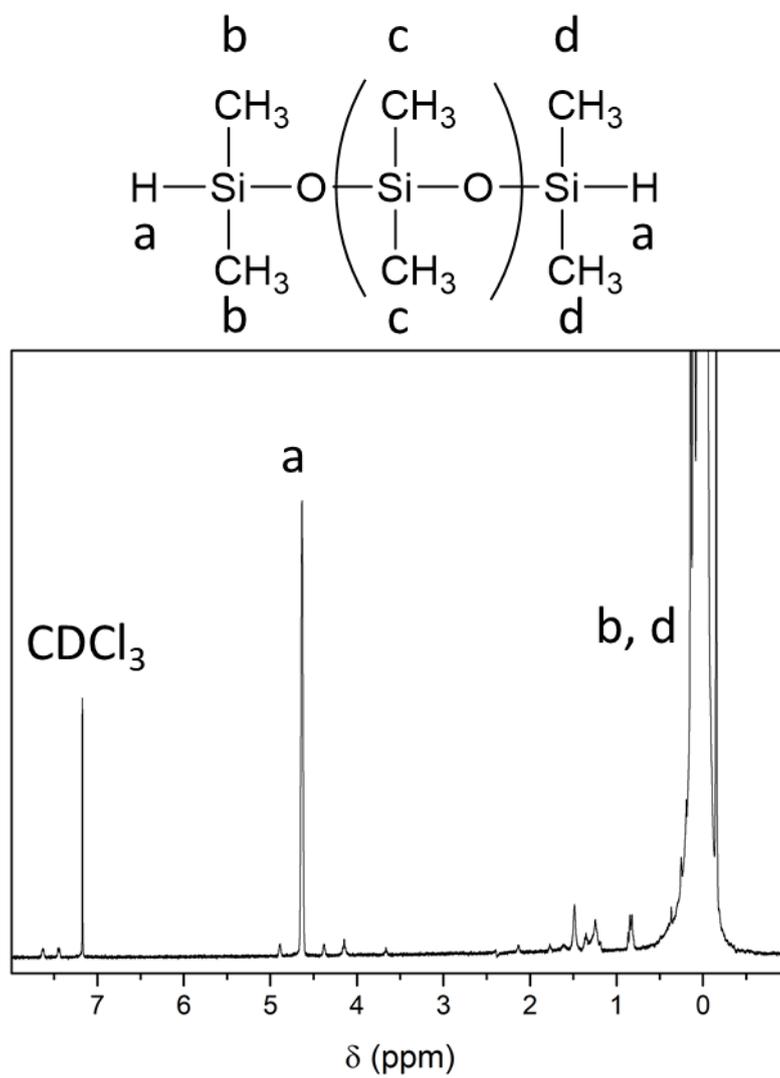
**Figure 4.16 - ^{1}H NMR of hydride terminated PDMS.**

### 4.6.3. 13C NMR of the hydride terminated PDMS
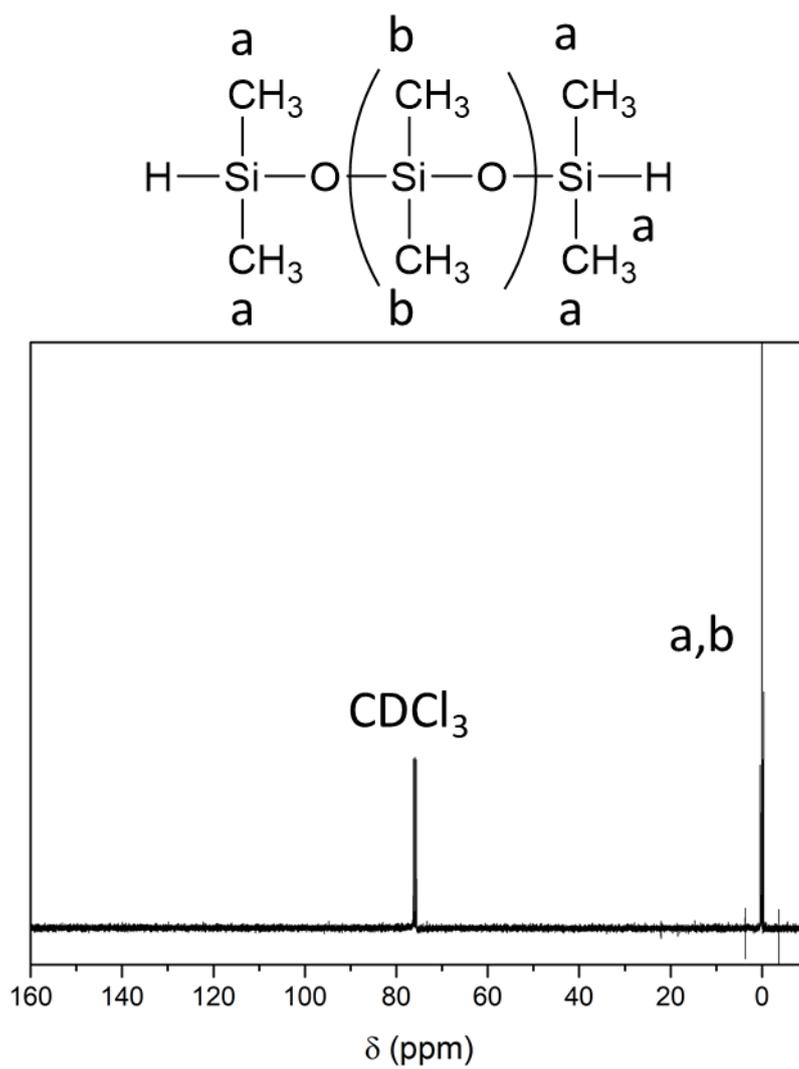
Figure 4.17 – ^{13}C NMR of hydride terminated PDMS.

Chapter 5: Polydimethylsiloxane (PDMS)/polyaniline(PANI) composites as pH responsive RFID sensor components.

5.1. Introduction

Polyaniline (PANI) was first discovered in 1862 by Letheby[1], but was largely underutilised until the 1980's due to the inability to effectively characterise it[2]. Since then, there have been a number of publications utilising polyaniline, with a predominant research focus on batteries[3], fuel cells[4] and supercapacitors[5]. PANI has also been utilised for a number of sensing applications, including ammonia detection[6], pH sensing[7] and gas sensing[8]. A series of wireless sensors have also incorporated polyaniline. Quintero[9] et al developed a HF passive RFID system that could sense multiple variables, but incorporated PANI/carbon composites into a sensing layer that allowed for sensing of ammonia concentration between 0-25 ppm. Kim et al[10] developed an NO_2 gas sensor that utilised a nanocomposite paste comprised of Fe_2O_3 nanoparticles loaded into polystyrene sulfonic acid doped polyaniline (PANI:PSS). The paste as both the RFID antenna and the transduction mechanism in this system, and allows for NO_2 sensing with a detection limit as low as 0.5 ppm. Shen et al[11] have also developed a wireless gas sensor that utilised a polyaniline/carbon nanotube (PANI/CNT) composites into a passive RFID system that allowed for gas sensing. The system allowed for ammonia detection with 0.04 MHz/ppm sensitivity in an atmosphere with a 300 ppm ammonia concentration.
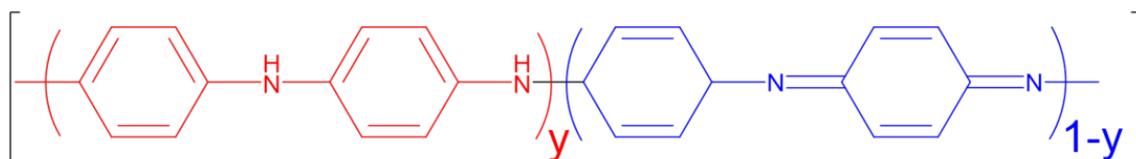

Figure 5.1 - The different forms of polyaniline.

Polyaniline has had widespread research interest for numerous applications due to its electrical properties. Furthermore, it has a simple elemental composition (comprised of C, H and N). There are two monomer units in PANI, shown in Figure 5.1. Either the reduced form (denoted as y) or the oxidised form (denoted as 1-y) make up PANI, and the relative ratio of one monomer unit to the other varies the bulk oxidation state. PANI can exist in three oxidation states accordingly, either the fully reduced leucoemeraldine (where y = 1 in Figure 5.1), the half oxidised emeraldine

base (where y = 0.5, meaning there is an equivalent ratio of either monomer unit in Figure 5.1) or the fully oxidised pernigraniline (where y = 0). Whilst the emeraldine base form is the most favoured form for energy storage applications, polyaniline based sensors typically exploit conductometric changes as a result of changing oxidation state, or by addition of dopants, which alters the conductivity of PANI by several orders of magnitude[12]. In the instance of the most stable of the six states of polyaniline (six being due to the fact that the emeraldine, leucoemeraldine or pernigraniline forms can all be doped or undoped[13]) is the emeraldine base, illustrated in Figure 5.2:
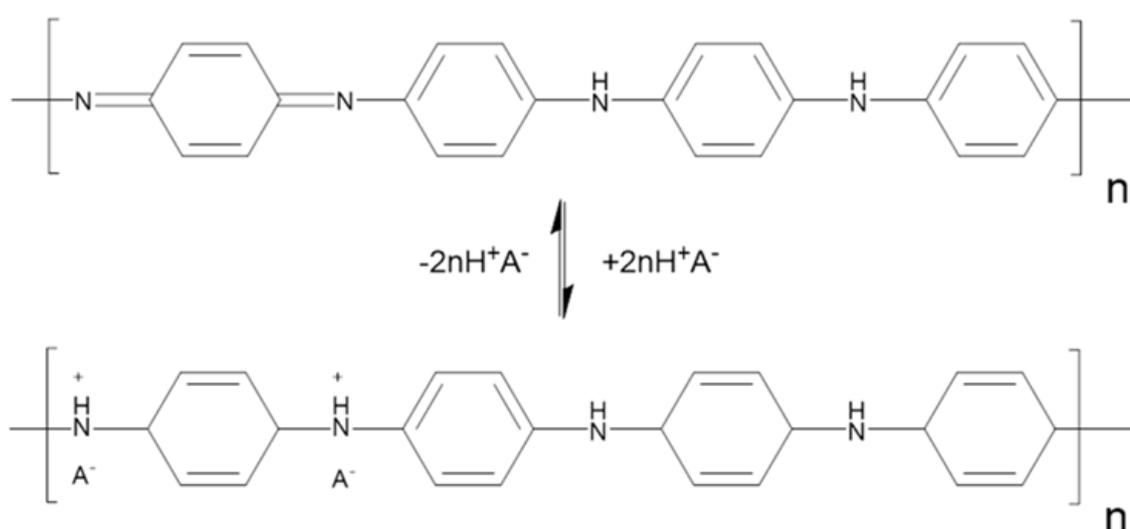
Figure 5.2 - Protonation and deprotonation of emeraldine base (top) to emeraldine salt (bottom).

Basifying the emeraldine results in converting the salt to a non-conductive emeraldine base, and vice versa for the protonation of the emeraldine salt. As previously mentioned, the degree of doping effects the conductivity of the PANI, in a very wide range (between approx. 10^{-12} to 10^5 S cm^{-1})[12]. This large degree of conductivity change with protonation has allowed for polyaniline based sensors to be exploited to be able to sense a multitude of variables, for example the protonation or basifying of the emeraldine species has been exploited to sense pH changes between 2-8 by Potyrailo[14] using PANI films doped with poly(styrene sulfonate) (PSS).

One of the largest obstacles with utilising polyaniline in a wider capacity is its notorious unprocessability[15,16]. Of all of the oxidation states, only the emeraldine base is soluble in any

solvent, and only in select polar solvents such as NMP and DMSO[17]. This is due to several factors. Firstly, the delocalised π electron structure of conducting polymers lead to a high electronic polarizability, favouring aggregation of a polymer system over solvation. Moreover, the backbone has two vastly different solubility's with regard to the organic and ionic components, meaning that finding a solvent suitable for both of these portions is remarkably difficult[18]. Polyaniline films can be produced, but comparative to elastomeric materials such as siloxanes film deposition is not trivial. Furthermore, polyaniline films tend to be in the order of 0.04 mm[19]. It was already established from Chapters 2,3 & 4 that a film thickness of 500 μm was required for bulk liquid studies with the RFMicron RFM-2100 AER. The lack of response change to pH solutions in Chapter 4 also showed that a material would need a more pronounced conductive change in order to elicit a response to higher pH's. Here, polyaniline was used as the responsive material to test viability for use with a commercially available capacitive sensing tag. To produce a film thick enough for usage as a pH sensor, a PDMS/PANI composite was used and tested for viability with a range of HCl solutions from 0-7, with an aim to benefit from the good mechanical properties and processability of PDMS whilst retaining the sensing characteristics of the PANI.

5.2. Materials and apparatus

Aniline (99.8%, pure) was purchased from Sigma Aldrich. Ammonium persulfate (98%) was purchased from Acros organics. Hydrochloric acid solution (32%), ammonium hydroxide (ACS reagent, 28-30% solution in water) and sodium hydroxide pellets were purchased from Fisher. Homogenous mixing of the elastomer components was performed using a DAC FV2-K speedmixer, and the composites were doctor bladed onto an RFMicron RFM-2100 AER using an automatic precision film MTCX4 from Mtv-Messtechnik (blade width = 70 mm, thickness adjustability 0 – 3000 μm). RFID measurements were performed on a Voyantic® Tagformance pro from 800 – 870 MHz. Relative permittivity measurements were performed using a Speag DAK 3.5 dielectric probe attached to a Rohde & Schwarz ZXX vector network analyser. FT-IR measurements were performed using a Shimadzu IRAffinity-1 spectrometer with a Specac Golden Gate™ ATR sampling accessory, and each sample was subjected to 64 scans, with a

resolution of 4 cm^{-1} (between 500 - 4500 cm^{-1}). Electron micrographs were obtained using a Hitachi S-3400 scanning electron microscope. Particle sizes were measured using ImageJ image processing software.

5.2.2. Synthesis of polyaniline, emeraldine salt and emeraldine base.

The synthesis of polyaniline emeraldine salt followed a modified procedure reported by Stejskal[12]. Aniline (2.59 g, 0.2 M) was dissolved in a aqueous hydrochloric acid (50 ml , 0.2 M) in a 250 ml conical flask. In a separate beaker, ammonium persulfate (5.71 g, 0.2 M) was dissolved in 50 ml of water. Both solutions were stirred manually using a stirrer bar for 3-5 minutes and left to dissolve at ambient temperature (22 °C) for 1 hour. The ammonium persulfate solution was then added to the aniline hydrochloride solution, and the mix was stirred manually for 5 minutes until the solution began to turn a dark orange colour. Following this, 10 ml of 0.2 M hydrochloric acid was added to the mix, briefly stirred manually and then left for 24 hours to polymerise. After 24 hours, the PANI precipitate was Buchner filtrated, and then washed with three 100 ml portions of 0.2 M HCl, and three 100 ml portions of methanol. The PANI filtrate (emeraldine salt) was then dried in air for 2 hours, before being dried under vacuum for 18 hours at 60 °C.

For the preparation of the PANI base, the dried emeraldine salt (0.5 grams) was stirred in 50 ml of ammonium hydroxide (0.2 M) for 24 hours, before being Buchner filtrated, and then washed with three portions (100 ml) of 0.2 M ammonium hydroxide and one portion of methanol (100 ml). The PANI base filtrate was then air-dried for 2 hours before being dried under vacuum at 60 °C.

IR assignments of polyaniline emeraldine salt:

C – C Bond (Ar) (569), C – H bond (Ar) (684), C – H bend (Ar) (800), C – H bend (Ar) (1145), C – N stretch (1298), C = C stretch (benzenoid ring) (1489), C = C stretch (quinoid ring) (1556).

IR assignments of polyaniline emeraldine base:

C – C Bond (Ar) (569), C – H bond (Ar) (684), C – H bend (Ar) (800), C – H bend (Ar) (1145), C – N stretch (1298), C = C stretch (benzenoid ring) (1489), C = C stretch (quinoid ring) (1556), N – H stretch (NH) (3263).

5.2.3. Mechanical grinding and ball milling of PANI

PANI emeraldine base (0.5 grams) was ground manually using a pestle and mortar for 30 minutes, and also was balled milled separately using a Fritsch pulverisette 7 planetary ball mill at 600 rpm for 30 minutes.

5.2.4. Preperation and cross-linking of PDMS/PANI composites

For the PDMS/PANI 5 wt.% composite, 4 g of silanol terminated PDMS were mixed with 0.2 g of PANI, for both the emeraldine salt and the PANI base followed by TEOS (0.07 g, $3.36e^{-4}$ M). The composites were then speedmixed for 60 seconds at 3500 rpm. Following this, 0.8 ml of tin (II) ethyl hexanoate was added to the mix. This was followed a further 60 seconds of speed mixing at 3500 rpm.

For the 10 % wt. weight PANI relative to PDMS the above procedure was followed using 0.4 g of polyaniline, 4g of PDMS, 0.09 g TEOS ($4.32e^{-4}$).

For the 20 % wt. weight PANI relative to PDMS the above procedure was followed using 0.8 g of polyaniline, 4g of PDMS, 0.09 g TEOS ($3.84e^{-4}$).

5.2.5. Film application and curing of PDMS/PANI composites

Following the speed mixing process, the PDMS/PANI composites were doctor bladed onto the RFMicron RFM-2100 AER. For all films, a blade set height of 900 μm was used, producing ~500 μm films. after being allowed to cure in place for 2 hours, the mix was then moved to a 60 °C oven for 18 hours before being cut from the glass substrate using a scalpel.

5.2.6. DAK measurements of PDMS/PANI composites

The dielectric properties for all of the PANI base/PDMS composite films were all measured after pH solutions were dried from the composite surface (the deposition study is outlined in 5.2.7)

All measurements performed were with a frequency sweep of 700 – 5995 MHz at ambient temperature (22 °C), with a temperature of 22.7±0.2 °C (checked periodically using a laser thermometer), but only 800 – 860 MHz was used to determine dielectric properties of the surface.

5.2.7. RFID studies of PDMS/PANI composite sensing tags

RFID measurements were performed on PDMS/PANI composites for both the emeraldine salt and the emeraldine base with 5, 10 & 20% wt. loading. Measurements were performed in read mode with an initial frequency sweep of 800 – 870 MHz and a step of 1 MHz. averaged sensor values were calculated using 800 – 860 MHz.

pH solutions between pH 0-7 were used on the 5,10, & 20% PDMS/PANI composites for the pH study, with a pH step of 1. 0.8 ml of each liquid was applied to the tag, and then had the RFID frequency sweep performed. Following this, the tag was dried with tissue paper and washed with RO water, then the RFID frequency sweep was performed again. Following this, the tag was tested on the DAK using the method outlined in Section 5.2.6 NaOH was also used with a pH of 14 for the PDMS/PANI 20% wt. composite for a deprotonation test.

5.3. Results and discussion

5.3.2. Flow diagram of PDMS/PANI composite pH sensor development

A flow diagram outlining the general procedure for the composite development is shown in Figure 5.3:

Following the synthesis and characterisation of the polyaniline emeraldine salt and emeraldine
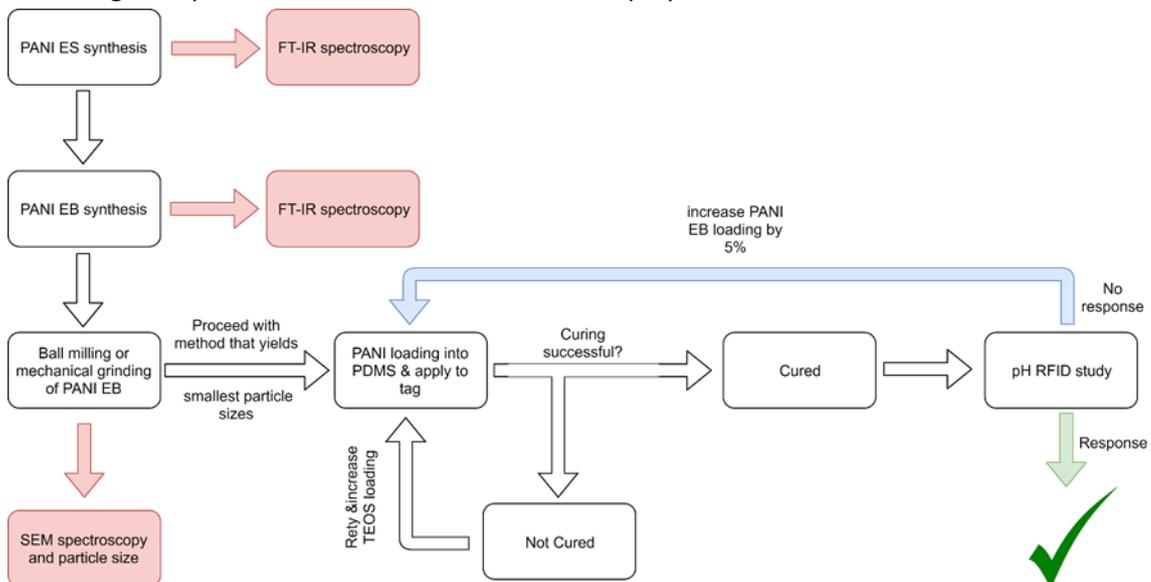
Figure 5.3 – Flow diagram of PDMS/PANI composite pH sensor development.

base, processing techniques were assessed and characterised. Following this, composite curing studies were performed to determine if the composite would form a film when applied to the RFID tag. following this, the composites were tested with a series of pH solutions to determine their sensitivity to pH.

This general scheme describes the route to synthesis of the pH responsive composites after the initial testing of composites in Section 5.3.4.

5.3.3. IR spectroscopy of polyaniline emeraldine salt & emeraldine base

PANI emeraldine salt was synthesised following a modified procedure reported by Stejskal[12]. Following synthesis of PANI, FT-IR spectroscopy was performed to determine successful synthesis, shown in Figure 5.4 :
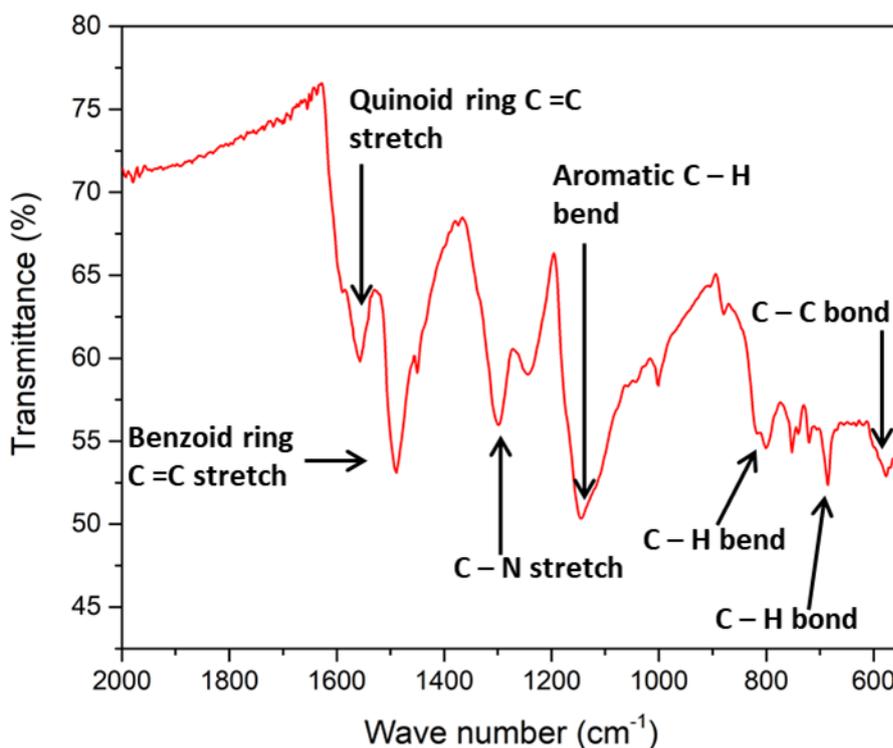
Figure 5.4 – FT-IR spectrum of PANI emeraldine salt.

Characteristic absorption peaks for PANI are seen, notably with peaks at 592 cm^{-1} and 696 cm^{-1}, relating to the C – C bonds and C – H bonds of the aromatic ring[20], the C –H that corresponds to the out of plane C – H bends of the benzene ring[21]. The broad region that overlaps the aromatic C – H bend at 1100 cm^{-1} is indicative of the PANI emeraldine salt, and the two labelled peaks at 1450 – 1600 cm^{-1} are related to the benzenoid and quinoid rings respectively.

Following this, the emeraldine salt was then functionalised into the emeraldine base via stirring in ammonium hydroxide, as described in Section 5.2.2. Functionalisation of the emeraldine base

to the emeraldine salt results in a colour change from a dark green to a dark purple powder, shown in Figure 5.5:
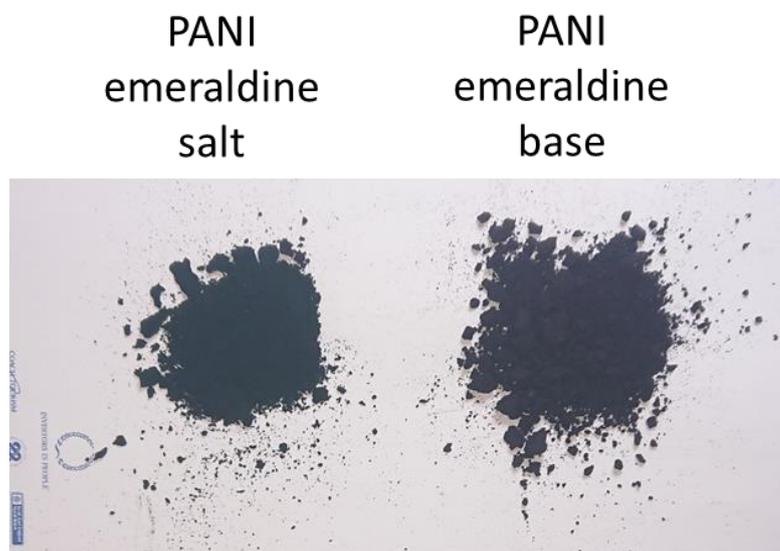
Figure 5.5 – Photographs of the PANI emeraldine salt (left) and the PANI emeraldine base (right).

Although difficult to observe in a photograph due to the darkness of the samples photograph, the PANI emeraldine base has a distinct dark green colour and the PANI emeraldine base has a distinct dark purple colour, To confirm, IR spectroscopy was performed and compared to the emeraldine base, shown in Figure 5.6:
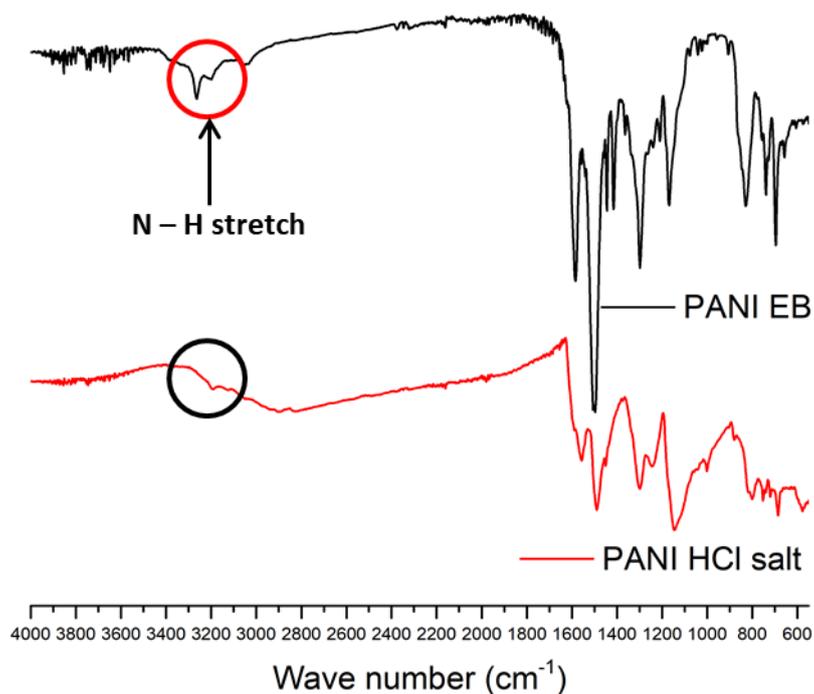
Figure 5.6 – FT-IR comparison of PANI HCl emeraldine salt and PANI emeraldine base (EB).

PANI emeraldine base FT-IR was compared to findings from Macdiarmid[22] and Harada[23]. Acid treatment of the emeraldine salt results in a disappearance of the N – H stretches circled in Figure 5.6 between 3200 – 3400 cm^{-1}. In this instance, the reciprocal deprotonation of the emeraldine salt results in the emergence of the peak. Furthermore, the characteristic broad peak at 1100 cm^{-1} also sharpens for the emeraldine base upon deprotonation.

5.3.4. Initial film application studies on loose PANI salt

Initially, film application studies were performed on PANI that had been isolated, but no processing post drying had been performed. This meant that the PANI being added to the PDMS solution had large aggregates in the mix. The result of this was inconsistent film depositions, with large clumps of PANI in the deposited films, as shown in Figure 5.7:

Figure 5.7 - Initial film application studies on unprocessed PANI salt.

To reduce particle sizes, PANI was ground for a longer step using a pestle and mortar. Ball milling was also used with the same duration using a planetary ball mill. After an equivalent duration (30 mins) of mechanical grinding and ball milling, the resultant particles were examined by scanning electron microscopy. ImageJ was used to measure particle size with n = 104 measurements performed for both sample types, and then particle distributions were compared for both samples. Images of the SEM micrographs are shown on the following page in Figure 5.8 and particle size distributions are plotted in Figure 5.9:
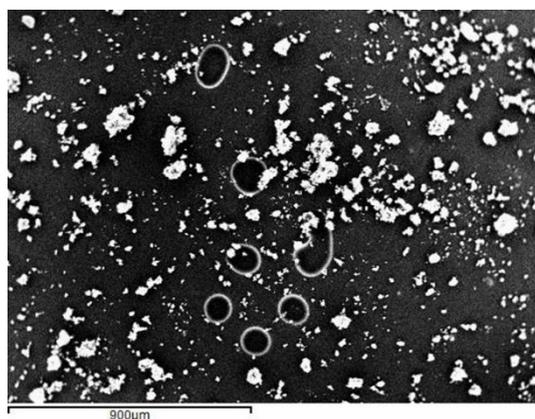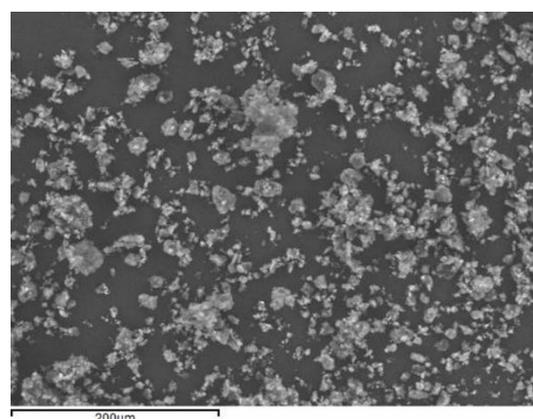
(a).   (b).

Figure 5.8 – SEM micrograph of (a) mechanically ground PANI emeraldine base and (b) ball milled PANI emeraldine base.
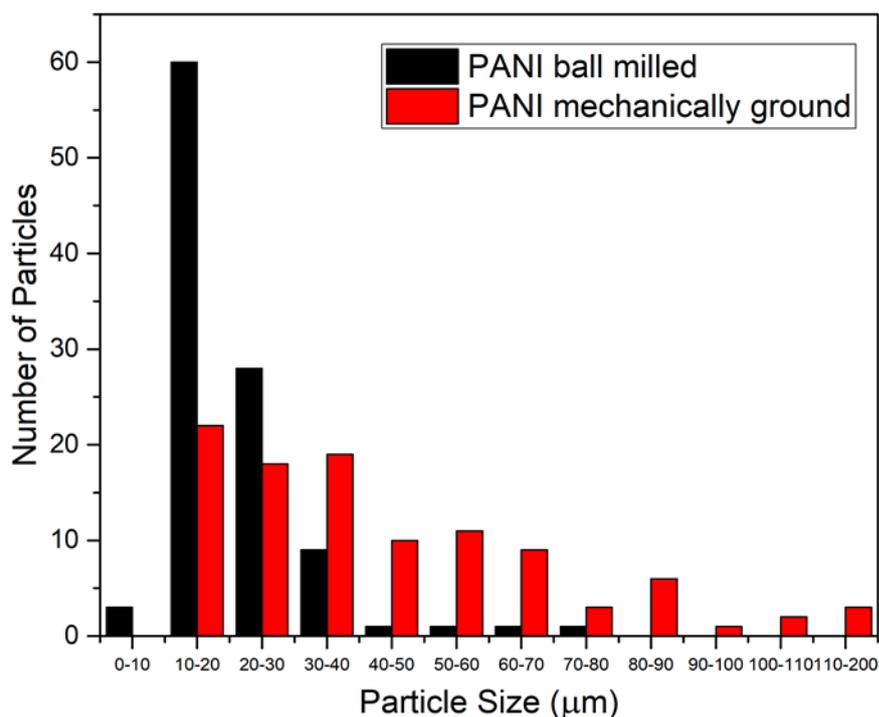
Figure 5.9 - Comparison of PANI emeraldine base particle sizes for the emeraldine base after mechanical grinding and ball milling.

Size distribution of particles were far less disperse for ball milled samples than for the mechanically ground PANI, with no particles observed under SEM being larger than 80 μm in size. The majority of particle sizes (57%) of ball milled PANI are in the 10-20 μm range. Smaller particle sizes should help to disperse PANI in the polymer matrix, and reduce the likelihood of larger particles causing uneven film depositions (seen in Figure 5.7). Ball milling was chosen over mechanical grinding for dispersal of PANI in the PDMS/PANI composite.

5.3.5. Film application studies of PDMS/PANI composites (5, 10 & 20 wt. %).

Considering the 5% wt. composite; the resultant film in Figure 5.10 (b) visually had far less variation in surface topology than the first iteration attempted in Figure 5.10 (a). Furthermore, as a result of having smaller PANI particles in the network, no large aggregates resulted in disruption of the film onto the RFID tag substrate, which caused the streaks seen in Figure 5.10 (a):
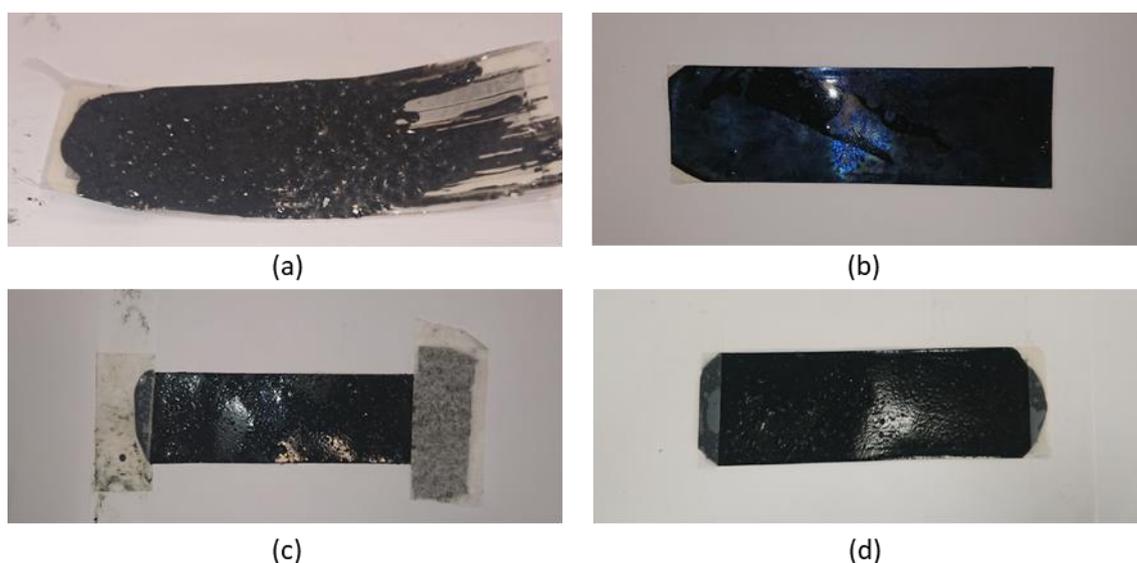
Figure 5.10 - Photographs of the PDMS-PANI composite with variable PANI loading. (a) initial application attempt before ball milling (b) 5% wt. (c) 10% wt. & (d) 20% wt.

Initial crosslinking studies of the PDMS/PANI composites showed inconsistent results for both the PANI salt and the PANI base. Whilst the 5 % wt. loading composites would solidify with no change to the required cross-linker ratio or catalyst loading. The 10 % wt. loading composites didn't solidify in initial curing studies. The suspected reasoning for this was due to the increased surface area of the 10 % wt. weight loading PANI inhibiting the crosslinking reaction, although hasn't been validated. The resolution taken was to increase the relative loading of TEOS in the mix, and the catalyst volume such that the amount of PANI used in the crosslinking was treated as PDMS when calculating the amount of TEOS and tin (II) ethyl hexanoate to add to the composite mix (e.g for 4 grams of PDMS and 0.4 grams of PANI, stoichiometric amounts of TEOS and tin (II) ethyl hexanoate would be added as if adding to 4.4 grams of PDMS). Whilst curing times were increased, PDMS/PANI films solidified with a 10% wt. & 20% wt. weight loading following the modified procedure. Even when using ball milled PANI, the increase in loading resulted in marginally uneven surface topology for the 10 & 20% wt. composites. Nonetheless, the reduced particle size compared to the previous film application attempt meant that the composite could be applied without the particles inhibiting the flow of the composite across the substrate. Following this, all three composites were tested for viability as pH sensing composites.

5.3.6. pH testing of PDMS/PANI composites

A diagram to show both the measurement setup and the testing protocol for the PDMS/PANI

composite is shown in Figure 5.11:
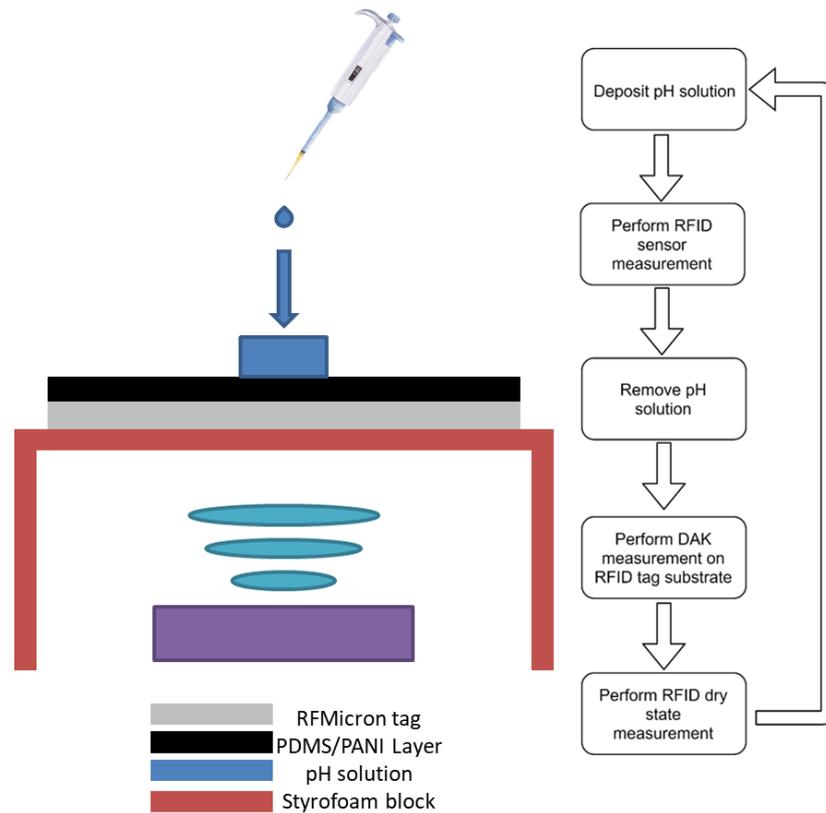
Figure 5.11 – Schematic diagram showing the measurement setup (left) and a flow diagram

showing the pH testing protocol.

The 5, 10 & 20 % composites were all tested with pH solutions prepared by serial dilution of 1M

HCl, making a range of 0-7, shown in Figure 5.12, Figure 5.13 & Figure 5.14:
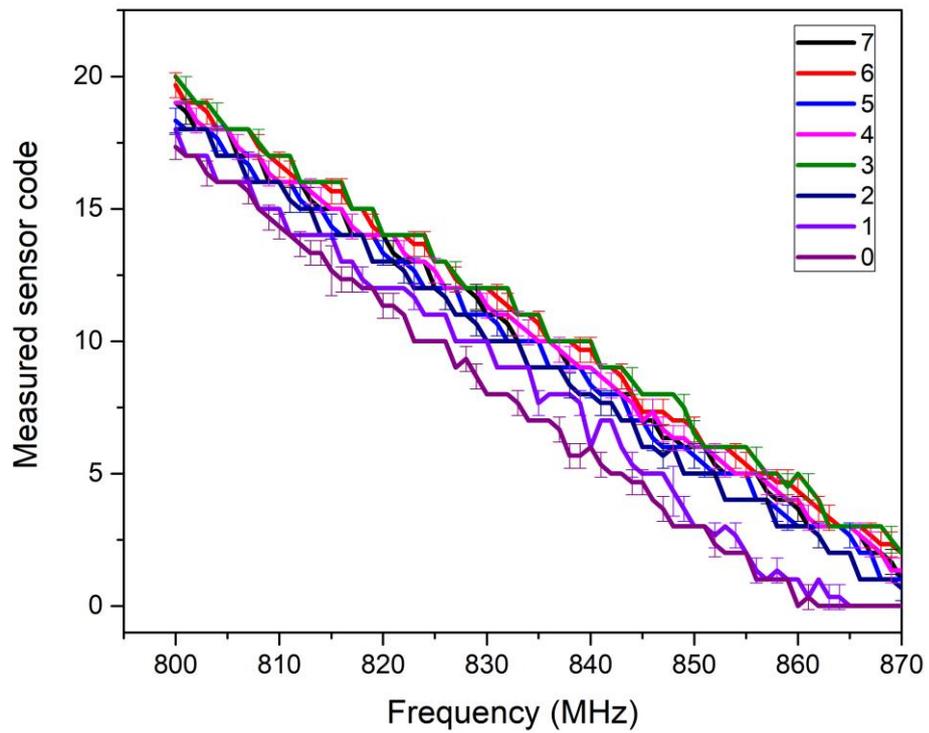
Figure 5.12 - Plot of sensor values of the PDMS-PANI 5% wt. emeraldine base composite upon exposure to pH solutions from 0 - 7.
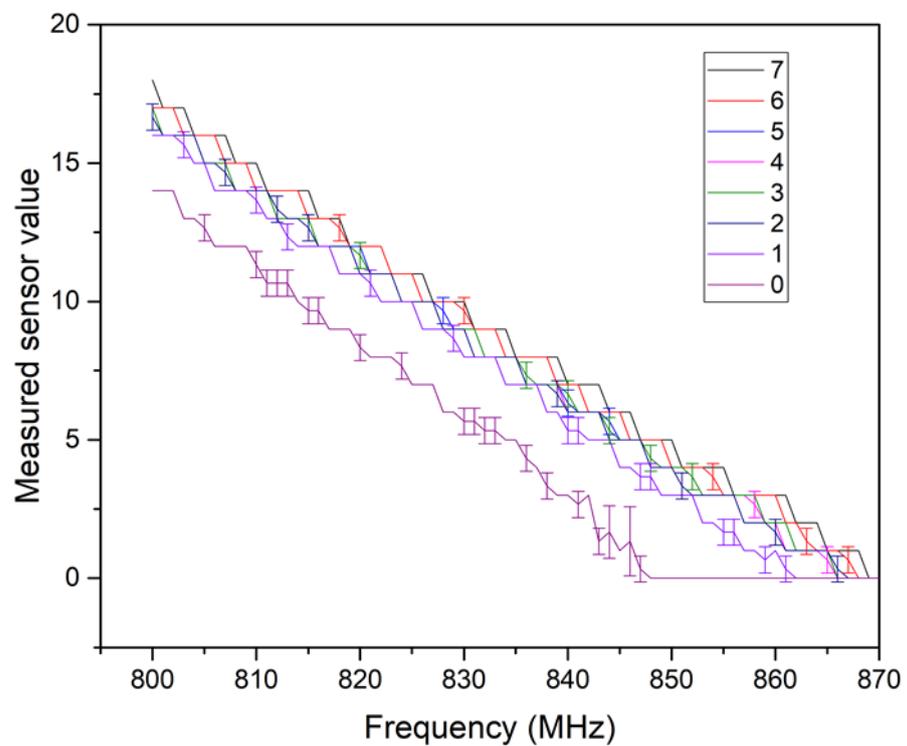
Figure 5.13 - Plot of sensor values of the PDMS-PANI 10% wt. emeraldine base composite upon exposure to pH solutions from 0 - 7.
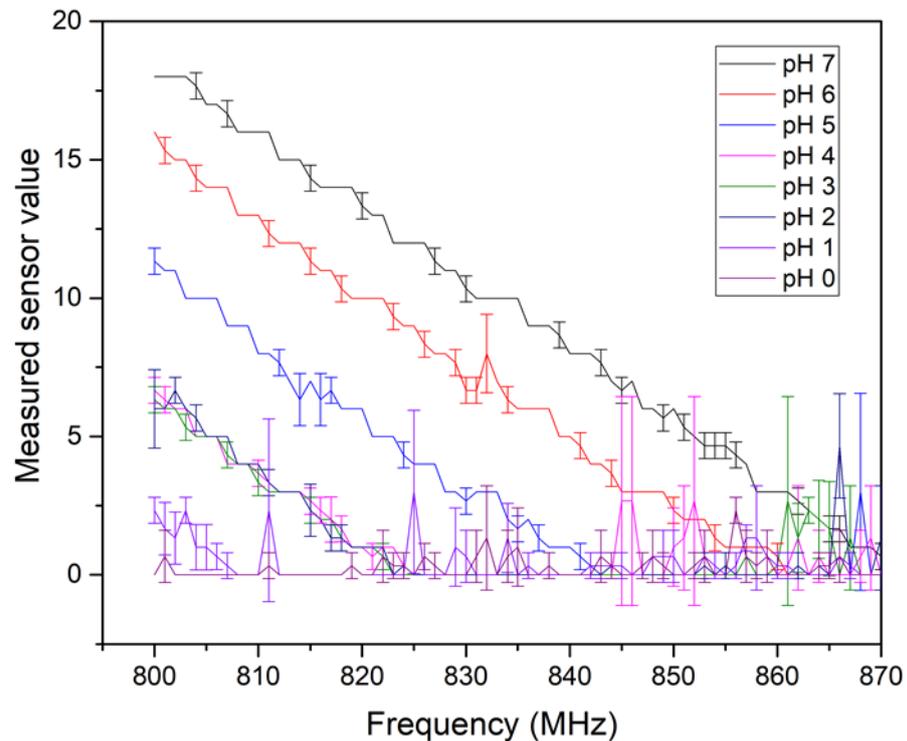
Figure 5.14 - Plot of sensor values of the PDMS-PANI 20% wt. emeraldine base composite upon exposure to pH solutions from 0 - 7.

It was immediately clear that the 20% composite showed a distinct response to pH, with sensor values across the frequency range lowering with decreasing pH. The degree of difference between the sensitivity of the 10% composite to the 20% composite is incredibly large, especially when considering the differences between the 5 & 10 % composites are not as prounounced as the differences between 10 & 20%.

In all composites, pH 0 & 1 showed distinctly lower sensor values than the remainder of solutions tested across the entire frequency range. This was expected given that in Chapter 4 it was observed that even in non-responsive silanol terminated PDMS pH 0 & 1 have distinctly lowered sensor code values compared to the rest of the pH range.

The measured sensor values for all three composites were averaged between 800 – 860 MHz to see if any trend could be observed for the 5 & 10 % composites, Shown in Figure 5.15 and Figure 5.16. Values were also averaged for the 20% composite, shown in Figure 5.17:
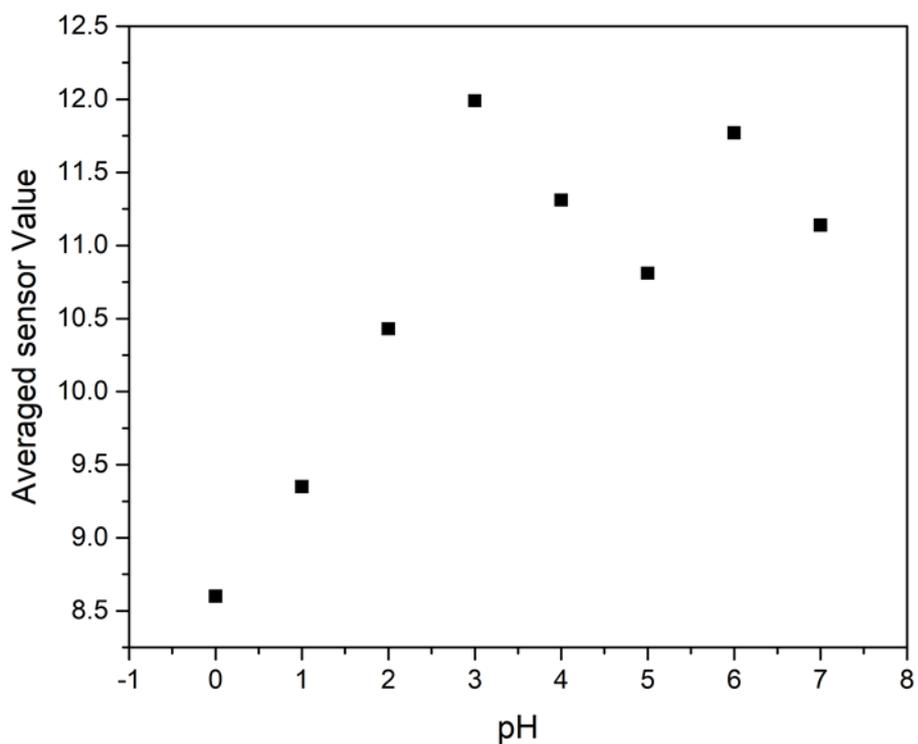
Figure 5.15 - Plot of averaged sensor values of the PDMS-PANI 5% wt. emeraldine base composite upon exposure to pH solutions from 0-7.
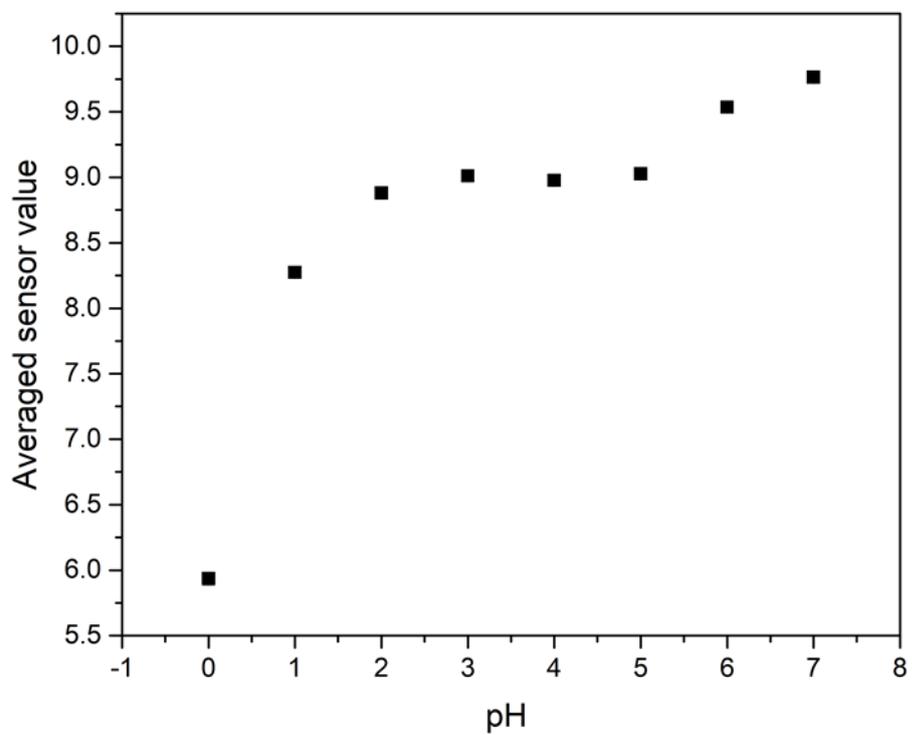

Figure 5.16 - Plot of averaged sensor values of the PDMS-PANI 10% wt. emeraldine base composite upon exposure to pH solutions from 0 - 7.
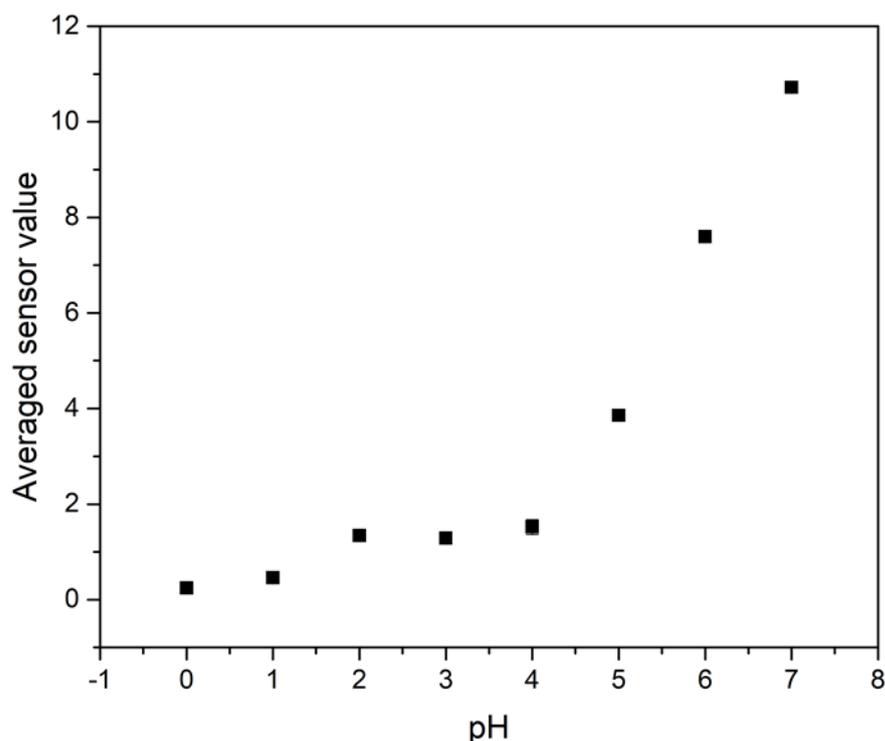
Figure 5.17 - Plot of averaged sensor values of the PDMS-PANI 20% wt. emeraldine base composite upon exposure to pH solutions from 0 - 7.

The 5% composite plotted in showed no trend in sensor value change with decreasing pH between 7-2 when averaging the values obtained across the frequency range. The values of 1 & 0 are distinctly lower than the remainder of the pH scale, but as previously mentioned, this is mostly (if not wholly) due to the change in tan δ of higher concentration aqueous electrolyte solutions[24].

The 10% composite plotted in Figure 5.16 did have a decrease in averaged sensor values with decreasing pH, however, pH's 2,3,4 & 5 all showed similar sensor values, to the point where they cannot be discerned from one another. Only either extreme of the pH scale could be effectively measured in the 10% composite. Again, pH 0 & 1 are measureable in an inert PDMS substrate with the RFMicron RFM2100-AER so this was expected.

The 20% loading composite shows distinctly different averaged sensor values for pH 7, 6 & 5, with a sharp decrease in sensor values as pH decreases. pH 2,3 & 4 all showed similar sensor values, with pH 0 & 1 showing lower values than the midrange pH solutions, but similar values to one another. The extent of detuning from pH 0 & 1 in the 20 % composite is so great that the

majority of the frequency sweep shows values of 0. As a result, pH 0 & 1 (which can normally be distinguished from one another based purely on their dielectric properties) cannot be distinguished in the 20% composite based on averaged sensor code values.

To summarise, in the 5% composite, only pH 0 & 1 could be reliably distinguished from the remainder of the pH solutions tested by averaging sensor values. The remainder of solutions (between 2-7) shows erratic changes in sensor values suggesting that the 5% composite is not suitable for pH sensing. The 10% composite showed distinct averaged sensor values at pH 7 & 6, as well as distinct sensor values for pH 0 & 1, with the midrange values of 2-5 being similar to one another but distinct from the rest of the pH range tested, meaning 5 distinct pH regions could be sensed in the 10% composite. Finally, the 20% composite showed massively different measured sensor values as solution pH decreased. Considering the averaged sensor values, 5 distinct sensing regions were also observed, being pH 7, 6, 5, between 4-2 and between 0-1.

5.3.7. Dry state RFID studies of the PDMS-PANI composites

For each composite array, after pH solution measurements were performed, the tag was read after being dried to see if there was an observable decrease in sensor values due to pH solution exposure. RFID measurements were performed, and are presented as averaged values for 5,10 & 20% respectively, shown in Figure 5.18, Figure 5.19 & Figure 5.20:
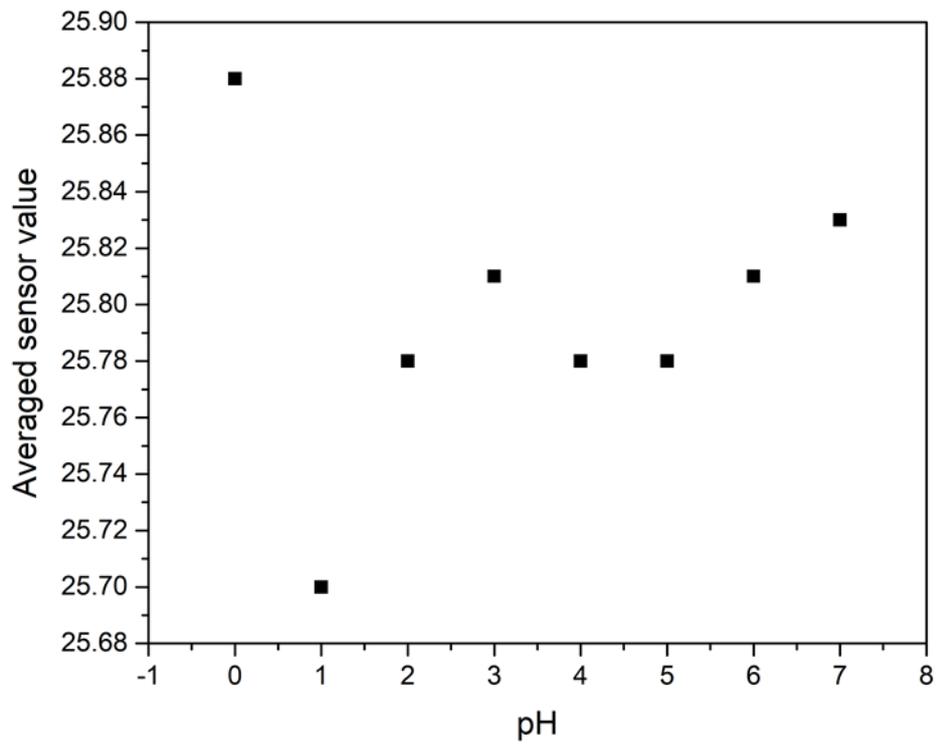
Figure 5.18 - Plot of dry state averaged sensor values of the PDMS-PANI 5% wt. emeraldine base composite after exposure to pH solutions from 0 - 7.
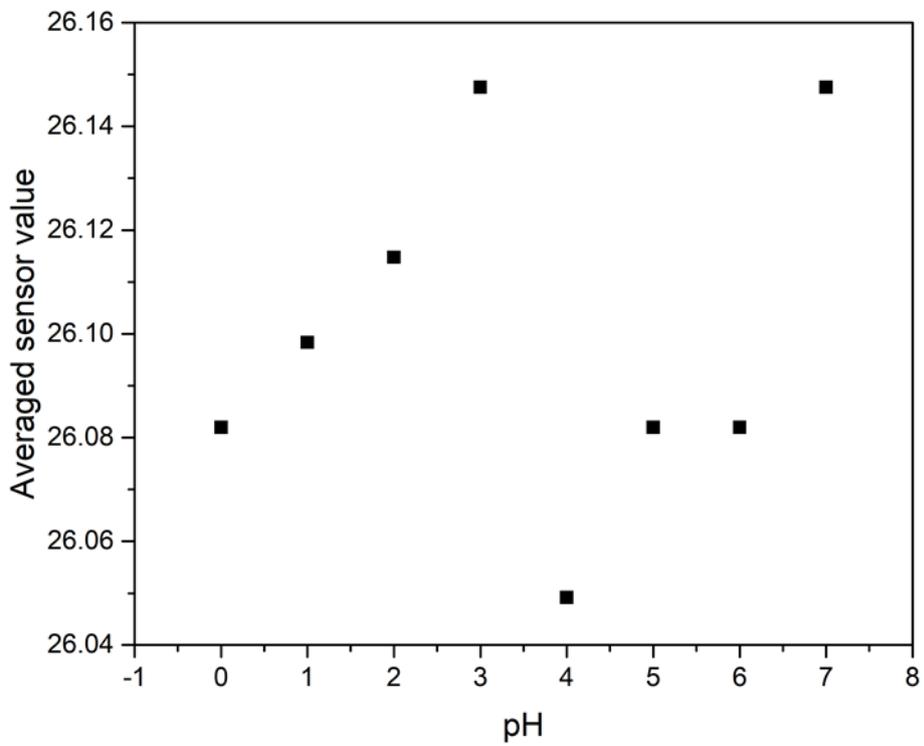

Figure 5.19 - Plot of dry state averaged sensor values of the PDMS-PANI 10% wt. emeraldine base composite after exposure to pH solutions from 0 - 7.
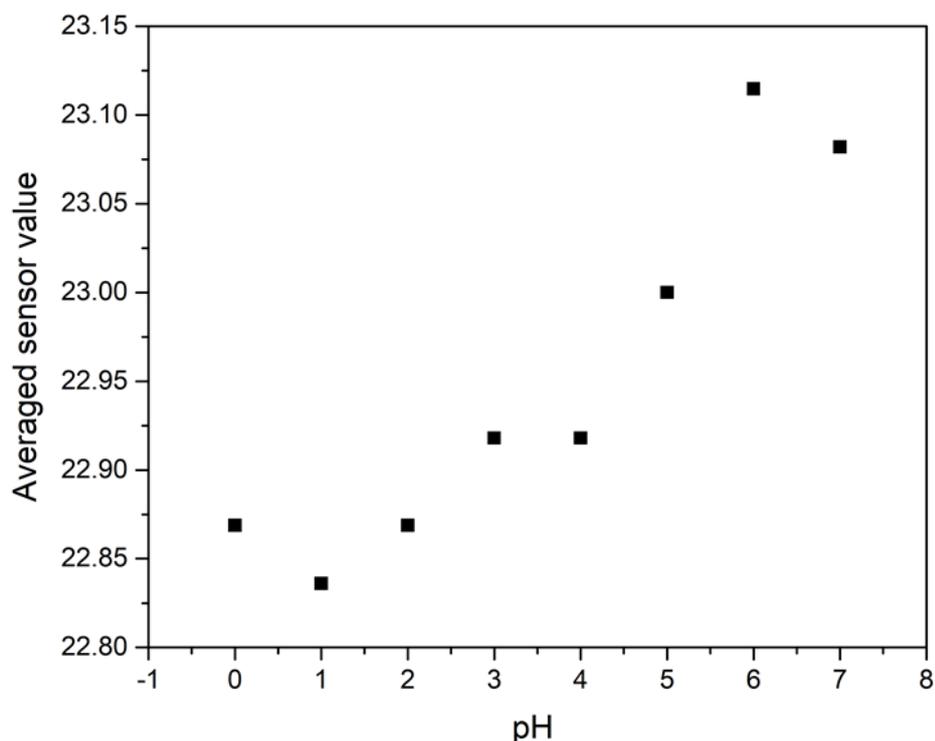
Figure 5.20 - Plot of dry state averaged sensor values of the PDMS-PANI 20% wt. emeraldine base composite after exposure to pH solutions from 0 - 7.

The 5 & 10% wt. composites showed no observable trend in averaged sensor values with decreasing pH they were exposed to. Contrastingly, the 20% composite did show a decrease in sensor values with decreasing pH exposed to. It was suspected that when dried, the protonation from HCl would result in slightly reduced sensor values as the concentration of HCl was increased. However, any consistent change in the dry state values could have been contributing to the gradual reduction in the observed sensor values in Figure 5.16. However that was not the case for the 5 or 10% composites This may still be the case, but it was inconclusive from the dry state study, suggesting that if there was any surface conductivity change, it wasn't sufficient to cause a change in observed sensor values. With regards to the 20 % composite, the gradual change in dry state sensor values could be contributing to the measured sensor values observed in Figure 5.14.

5.3.8. Conductivity change of the PDMS/PANI composites

DAK measurements were performed on the composites after each pH solution measurement (once the solution had been dried from the tag). It was expected that the surface of the composite was being protonated as it was being exposed to lower pH solutions. DAK measurements were performed to confirm. One limitation is that the DAK measurements actually provide the composite surface conductivity but the entire composite conductivity, as a result, the differences for all three composites were expected to be minimal as the vast majority of the composite was not being affected by the pH depositions. Composite conductivity was plotted for the 5, 10 & 20% PDMS/PANI composites, shown in Figure 5.21, Figure 5.22 & Figure 5.23:
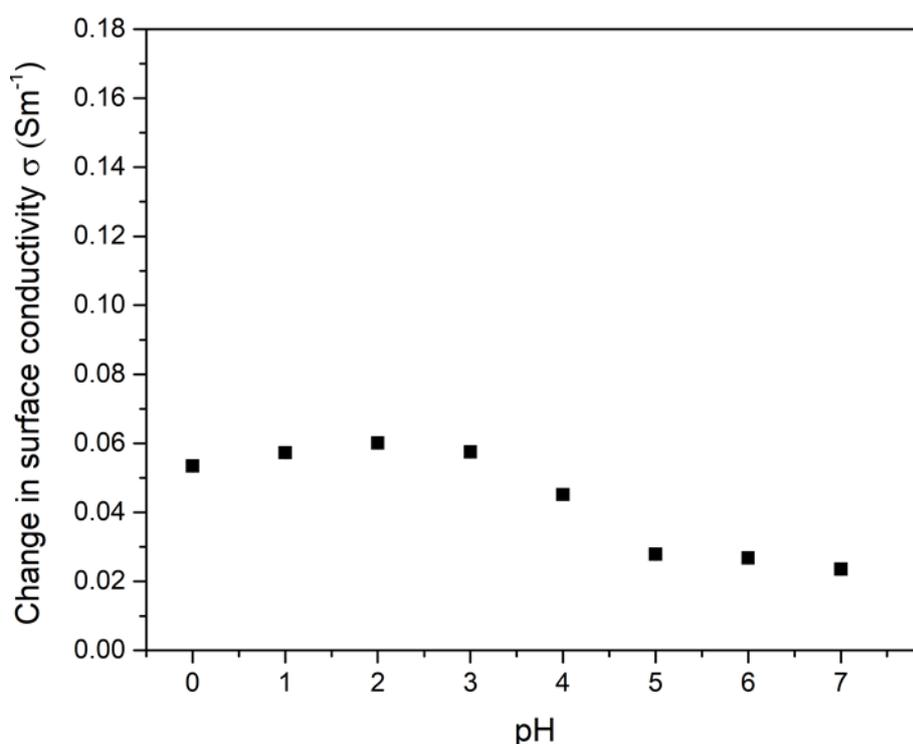

Figure 5.21 - Plot of conductivity of the PDMS-PANI 5% wt. emeraldine base composite after exposure to pH solutions from 0 - 7.
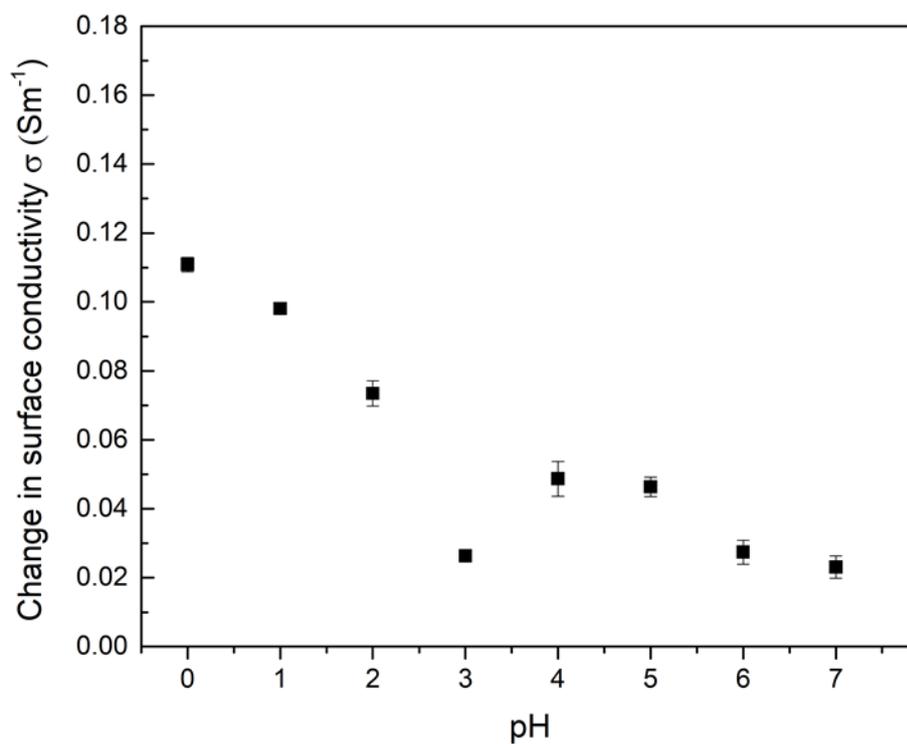
Figure 5.22 - Plot of conductivity of the PDMS-PANI 10% wt. emeraldine base composite after exposure to pH solutions from 0 - 7.
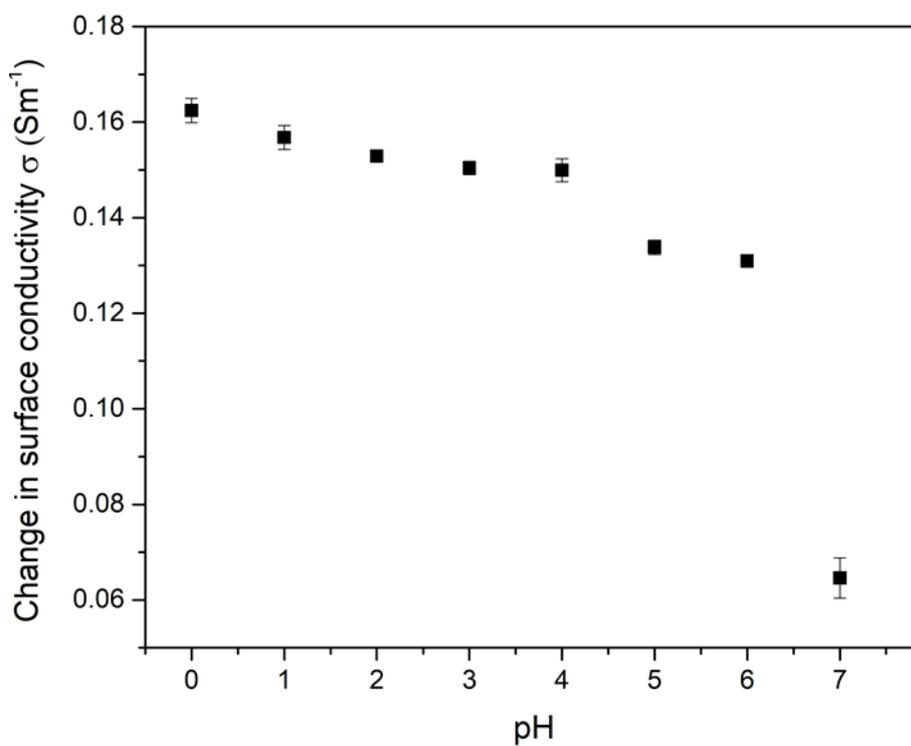

Figure 5.23 - Plot of conductivity of the PDMS-PANI 20% wt. emeraldine base composite after exposure to pH solutions from 0 - 7.

Conductivity changes in the 5% composite were minimal, but did increase following exposure to pH solutions from 2-5. The 10% composite showed an increase in conductivity following exposure to decreased pH solutions as a trend, aside from a decreased value at pH 3. The 20% composite showed a pronounced change in conductivity from pH 7-6, followed by a less pronounced but steady increase in conductivity across the pH range. Comparing the conductivities between the composites, the conductivity of PDMS/PANI composites increases following exposure to pH solutions, and the higher the PANI loading in the composite, the higher the surface conductivity after exposure. Using the DAK as a means of assessing conductivity change is limited. Ideally, a surface analysis technique such as X-ray photoelectron spectroscopy (XPS) would be beneficial in understanding the degree of surface conductivity change.

5.3.9. Scrutiny of the PDMS/PANI 20% wt. composite

As previously mentioned, the PDMS/PANI 20% wt. loading composite showed an unexpectedly large response change comparative to the lower loading composites. Whilst the comparison of the sensor values performed in Section 5.3.6 focused on the averaged values between the composites, the values plotted in Figure 5.14 were so distinct that it was checked to see if a single frequency (815 MHz) could be used to determine solution pH, shown in Figure 5.24:
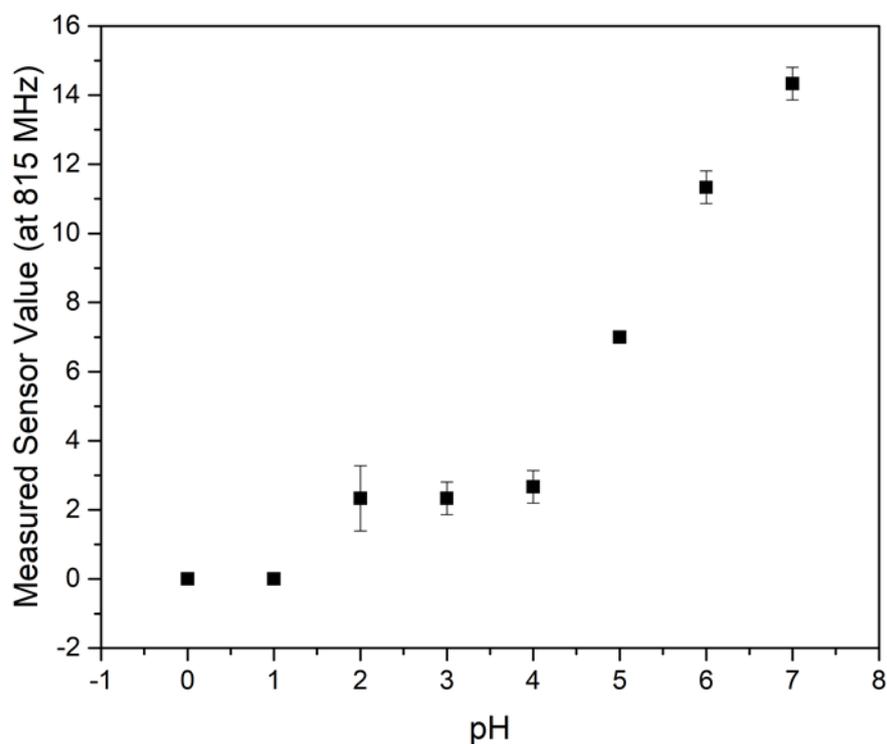

Figure 5.24 - Plot of sensor values of the PDMS-PANI 20% wt. emeraldine base composite at 815 MHz upon exposure to pH solutions from 0 - 7.

Distinct values for pH 7, 6 & were observed at 815 MHz. pH 2-4 all show very similar sensor values, to the point where defining a pH of 2-4 is not possible. The same can be said of pH 0 & 1. The reason for why the midrange pH scale shows similar sensor values is still unknown. Addition of pH 0 &1 solutions resulted in such a high degree of detuning of the tag that both solutions show a zero value at 815 MHz. This same trend is observed when considering the averaged sensor values in Figure 5.17, but in the case of the 20% composite (unlike the other

composites); only a single frequency is needed to determine solution pH. That being said, 815 MHz is significantly detuned considering that the tag normally is meant to be used at 868 MHz

One alteration to the tag-composite to facilitate sensing the lower pH extremes would be to increase the composite thickness to larger than 500 µm, however this may lower the sensitivity of the tag with regards to the higher end of the pH scale. Furthermore, increasing the composite thickness should decrease the extent of detuning (as seen in the variable thickness study in Chapter 2) meaning a frequency closer to 868 MHz may be able to be used to determine solution pH.

5.3.10. Secondary pH exposure study

Following the initial pH exposure study, the PDMS/PANI 20% wt. composite was exposed to pH solutions a second time to see if the tag was reusable upon exposure to the full pH range, shown in Figure 5.25:
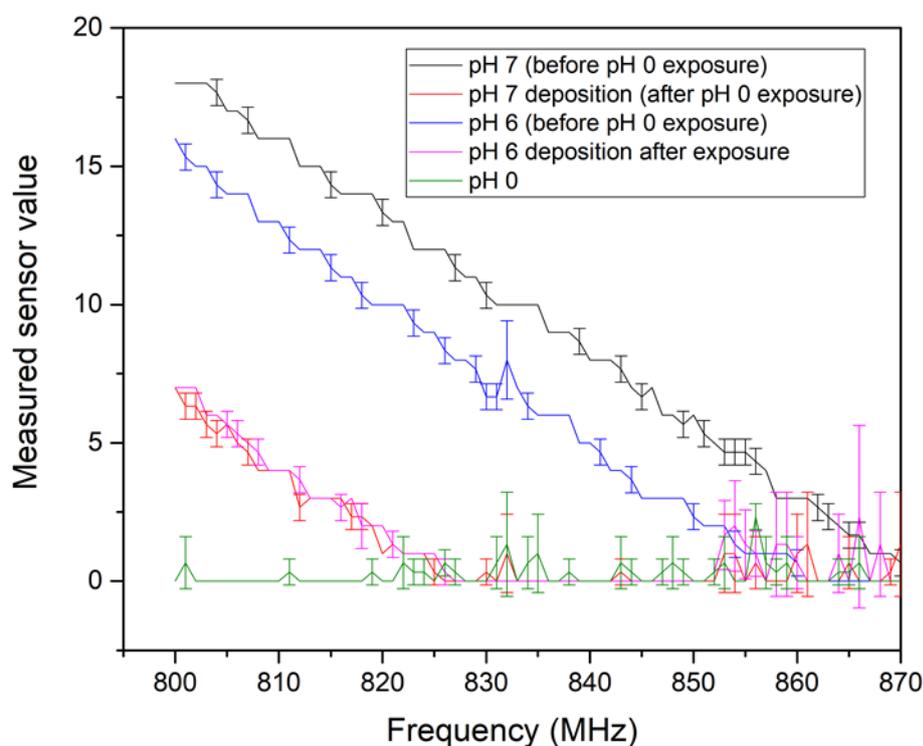

Figure 5.25 - Comparison of PDMS-PANI emeraldine base 20% wt. initial deposition study followed by a second deposition study with pH solutions of 6 & 7.

Unexpectedly, the sensor values for pH 6 & 7 were markedly different in the second run compared to that of the first run. It was expected that exposure to a higher pH solution would result in an equilibrium shift in the degree of surface protonation in the PANI, resulting in the sensor values being constant for each given pH solution exposed to. This was not the case with the PDMS-PANI composite based on the second deposition study. The measured sensor values were compared with the initial sensor values from the first deposition study, shown in Figure 5.26:
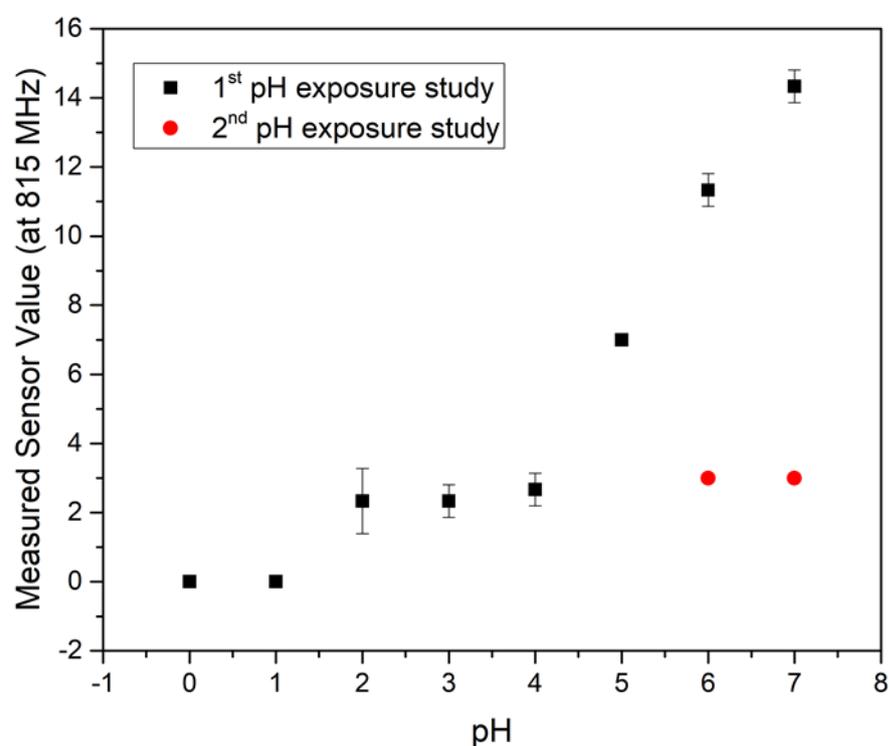

Figure 5.26 - Comparison of PDMS-PANI emeraldine base 20% wt. initial deposition study followed by a second deposition study with pH solutions of 6 & 7 (at 815 MHz).

Depositions for pH 6 & 7 were similar to that of the pH values seen for solutions 2-4. The reason for this is still unknown and would require further testing of the composite to determine the cause of the change in sensor values with second exposure. Nonetheless, the observed difference in pH for the 1st run means that the sensor could be used as a tamper tag.

5.4. Conclusions and future work

Here, a hybrid composite of PDMS and polyaniline (PANI) was developed for use as a pH responsive composite for sensing purposes. PANI emeraldine salt and base were successfully synthesised, and the emeraldine base was incorporated into a cross-linked PDMS matrix. Different preparation techniques for PANI were also tested as a necessity following an unsuccessful PANI loading attempt due to the large particle sizes of PANI post synthesis. Ball milling was determined to be a more effective method of processing routine PANI particles (compared to mechanical grinding) through scanning electron microscope (SEM). Ball milled PANI allowed for routine distribution of the composite material, with a loading of 5, 10 & 20% wt. PANI achieved. The composites were then exposed to pH solutions after being applied to the RFMicron RFM2100-AER and tested as pH sensitive composites. It was found that the 20% PDMS-PANI showed sensitivity to pH solutions (predominantly in the higher pH range of 7-5) at that could be shown at a single frequency (815 MHz). The same composite was tested on a second occasion to see if the tag was reusable, but showed what appears to be a loss of sensitivity after the initial exposure to the low pH range. The reason for this has still not been determined.

Future work should look to characterise what causes the loss of performance of the composite after the initial exposure. This work was attempted late into the project, so the film thicknesses could not be optimised to see if the pH range the tag could be modified with variable thickness. Furthermore, if the substrate surface changes conductivity, using a much thinner film might facilitate using the tag as a tamper tag that could be used for determining the pH exposure the tag was subjected to after being dried. This study may also be useful as the dry state sensor readings performed on the composites showed that with pH exposure the 20% wt. composite values reduced as a trend.

5.5. References

1   *61 XXIX-On the Production of a Blue Substance by the Electrolpsis of Sulyhate of Aniline*, .

2   A. G. Macdiarmid and A. J. Epstein, *Polyanilines: A Novel Class of Conducting Polymers*, .

3   H. Wang, J. Lin and Z. X. Shen, *J. Sci. Adv. Mater. Devices*, 2016, **1**, 225–255.

4   S. K. Simotwo and V. Kalra, *Electrochim. Acta*, 2016, **198**, 156–164.

5   K. Wang, J. Huang and Z. Wei, *J. Phys. Chem. C*, 2010, **114**, 8062–8067.

6   S. K. Dhawan, D. Kumar, M. K. Ram, S. Chandra and D. C. Trivedi, *Sensors Actuators B Chem.*, 1997, **40**, 99–103.

7   Z. Jin, Y. Su and Y. Duan, *Sensors Actuators B Chem.*, 2000, **71**, 118–122.

8   †,‡ Shabnam Virji, ‡ Jiaxing Huang, *,‡ and Richard B. Kaner and † Bruce H. Weiller*, , DOI:10.1021/NL035122E.

9   A. V. Quintero, F. Molina-Lopez, E. C. P. Smits, E. Danesh, J. van den Brand, K. Persaud, A. Oprea, N. Barsan, U. Weimar, N. F. de Rooij and D. Briand, *Flex. Print. Electron.*, 2016, **1**, 025003.

10   S. G. Kim, J. Jun, J. S. Lee and J. Jang, , DOI:10.1039/c9ta00198k.

11   S. Shen, Z. Fan, J. Deng, X. Guo, L. Zhang, G. Liu, Q. Tan and J. Xiong, *Sensors (Basel).*, , DOI:10.3390/s18093022.

12   R. G. Gilbert, *POLYANILINE. PREPARATION OF A CONDUCTING POLYMER (IUPAC Technical Report)*, 2002, vol. 74.

13   B. Malhotra, C. Dhand, R. Lakshminarayanan, N. Dwivedi, S. Mishra, P. Solanki, M. Venkatesh, R. W. Beuerman and S. Ramakrishna, *Nanobiosensors Dis. Diagnosis*, 2015, 25.

14   R. A. Potyrailo and T. Wortley, in *2011 IEEE International Conference on RFID-Technologies and Applications*, IEEE, 2011, pp. 533–536.

15   H. S. Nalwa, *Handbook of organic conductive molecules and polymers*, Wiley, 1997.

16   B. Wessling, *Polymers (Basel).*, 2010, **2**, 786–798.

17   *Synth. Met.*, 1993, **53**, 365–377.

18   Y. Cao, P. Smith and A. J. Heeger, *Synth. Met.*, 1992, **48**, 91–97.

19   M. Angelopoulos, G. E. Asturias, S. P. Ermer, A. Ray, E. M. Scherr, A. G. Macdiarmid, M. Akhtar, Z. Kiss and A. J. Epstein, *Mol. Cryst. Liq. Cryst. Inc. Nonlinear Opt.*, 1988, **160**, 151–

163.

20   A. Mostafaei and A. Zolriasatein, *Prog. Nat. Sci. Mater. Int.*, 2012, **22**, 273–280.

21   Y. Sun, S. Wang, H. Cheng, Y. Dai, J. Yu and J. Wu, *Electrochim. Acta*, 2015, **158**, 143–151.

22   Quillard, Louarn, Lefrant and Macdiarmid, *Phys. Rev. B. Condens. Matter*, 1994, **50**, 12496–12508.

23   I. Harada, Y. Furukawa and F. Ueda, *Synth. Met.*, 1989, **29**, 303–312.

24,   DOI:10.1209/0295-5075/109/26002.

5.6. Appendix

5.6.2. 5% wt. PDMS/PANI composite dielectric properties

5.6.2.1. Permittivity change of PDMS/PANI 5% wt. composite after pH exposure
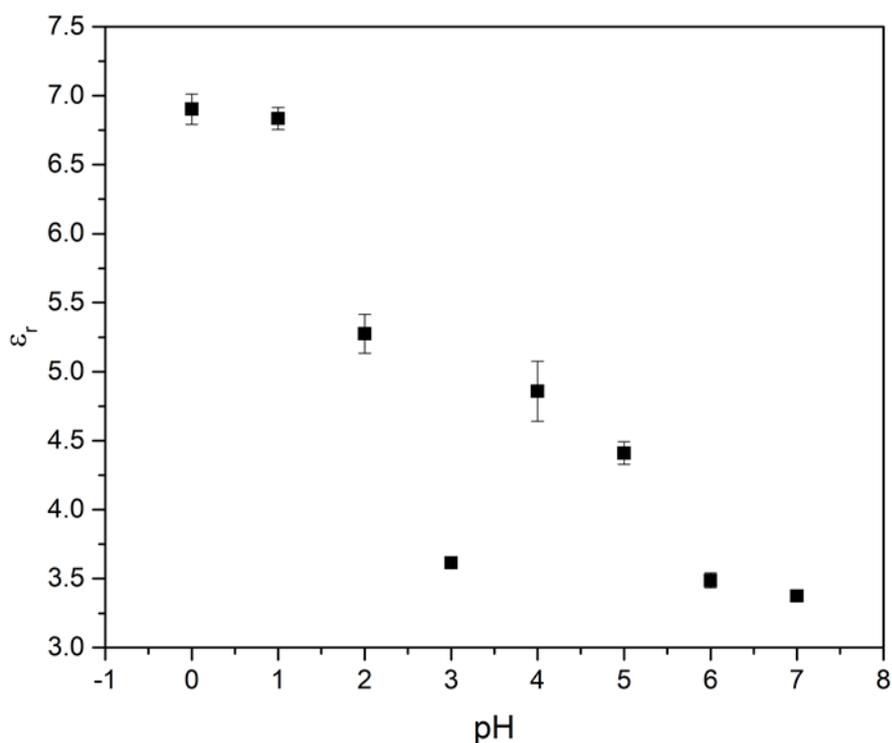

Figure 5.27 – Surface permittivity change of the PDMS/PANI 5% wt. composite.
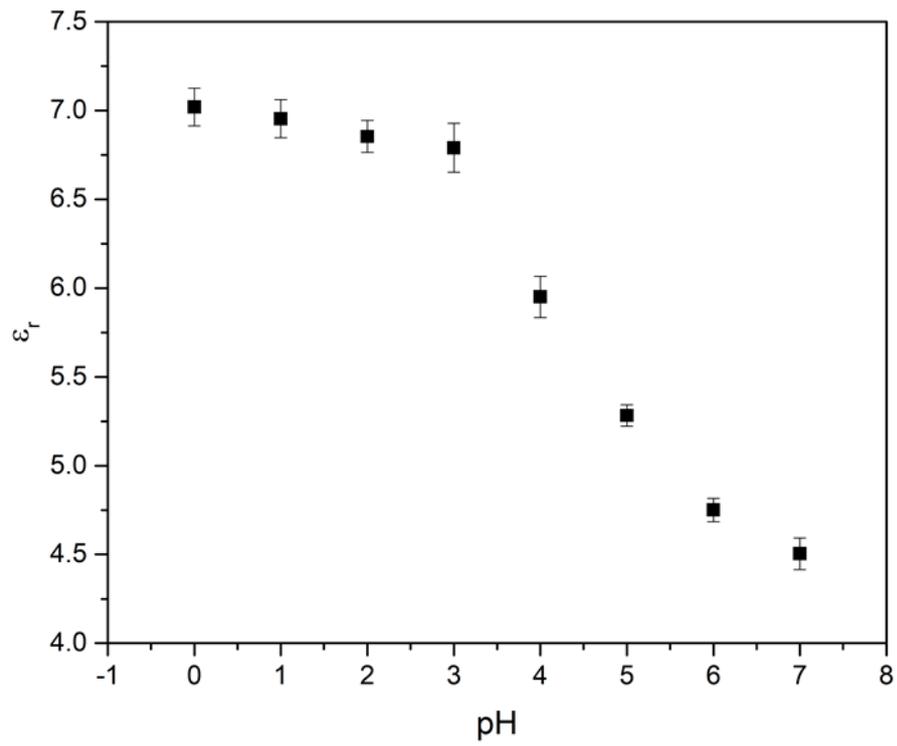
**Figure 5.28 - Surface permittivity change of the PDMS/PANI 10% wt. composite.**
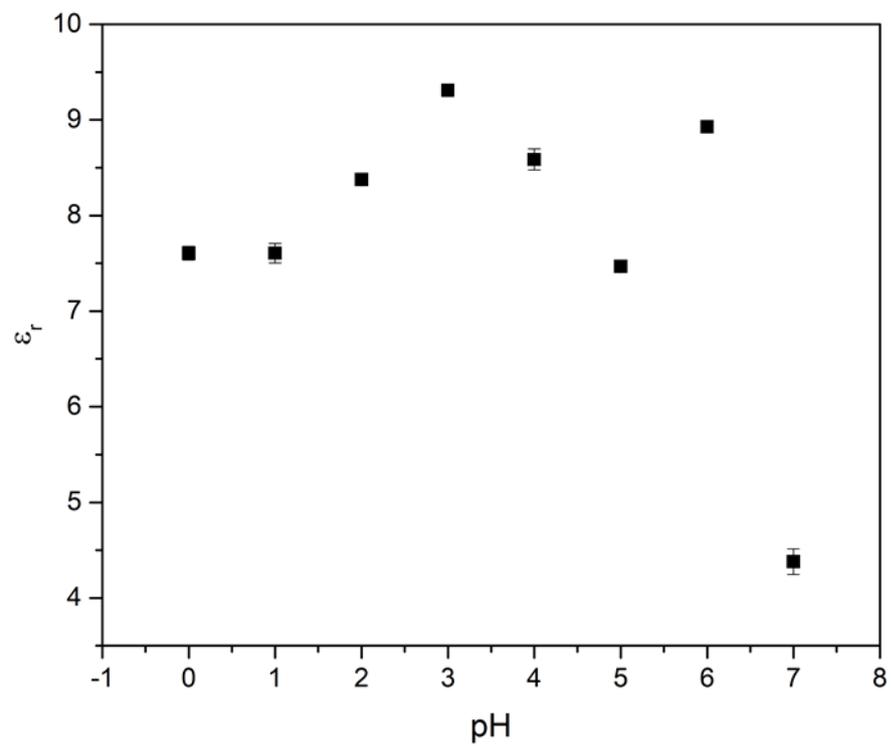
Figure 5.29 - Surface permittivity change of the PDMS/PANI 20% wt. composite.
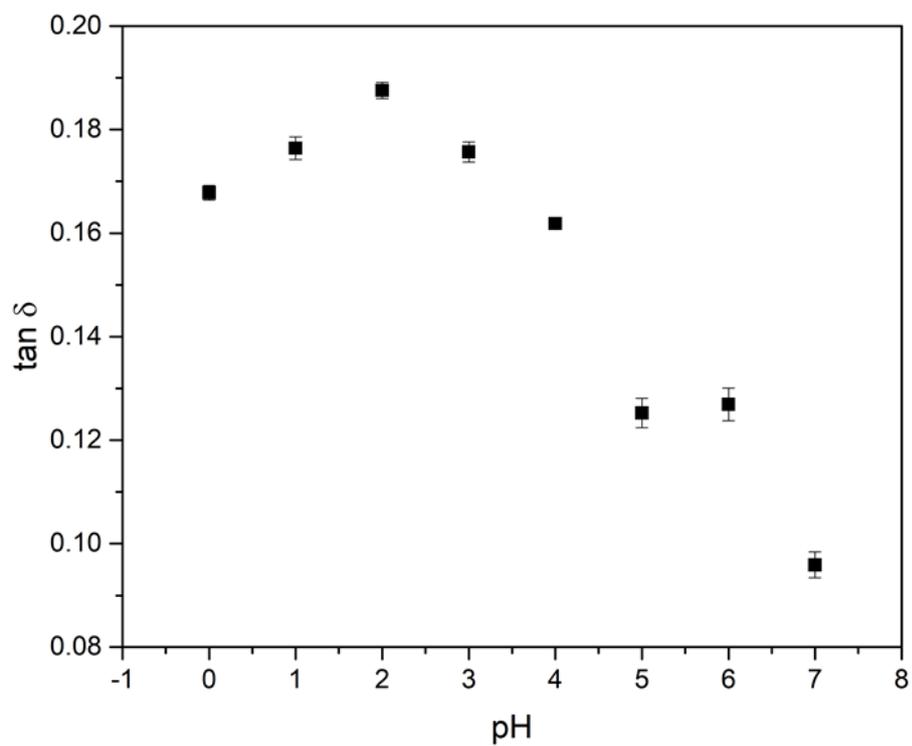
**Figure 5.30 – Tan δ change of the PDMS/PANI 5% wt. composite.**
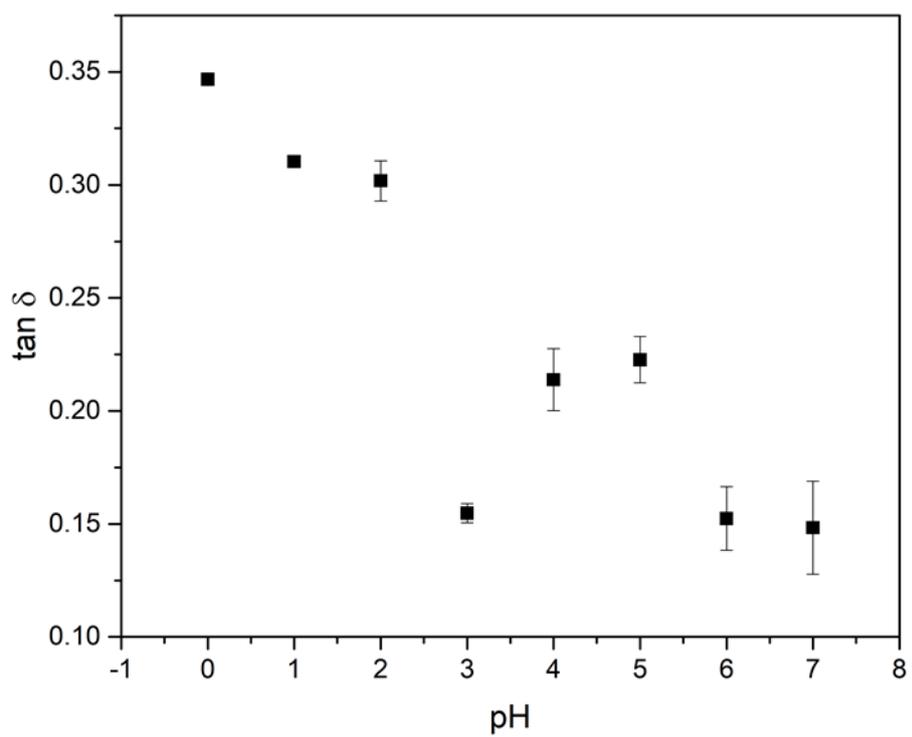
**Figure 5.31 - Tan δ change of the PDMS/PANI 10% wt. composite.**
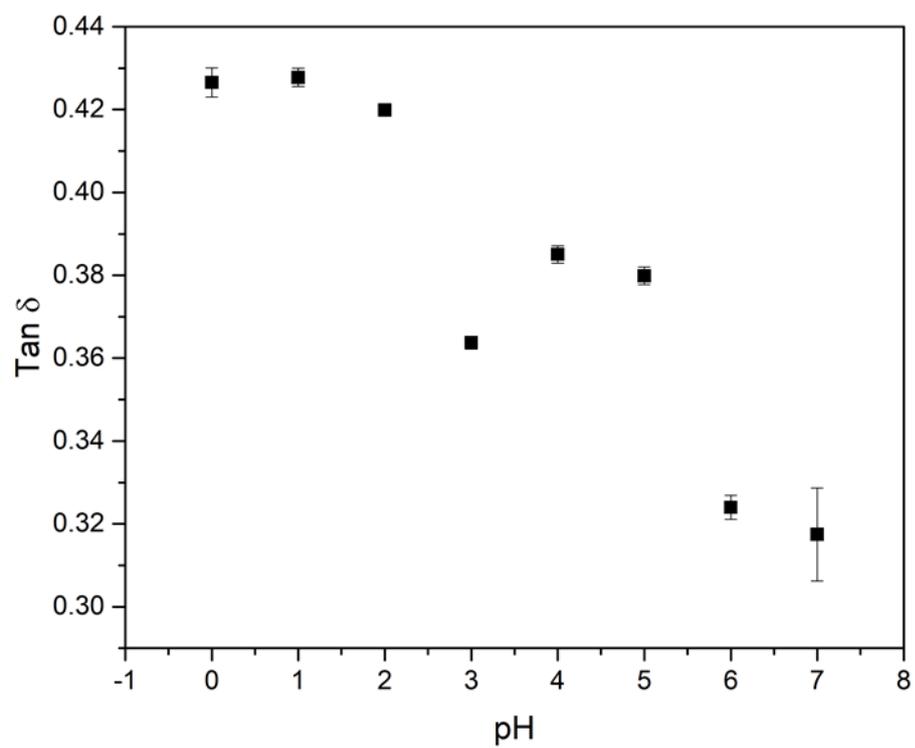
Figure 5.32 - Tan δ change of the PDMS/PANI 20% wt. composite.

Chapter 6:   Final conclusions

6.1. Thesis conclusion

The primary aim of this work was to modify commercially available RFID tags in order to repurpose their function.

Chapter 1 of this focused on the development of radio frequency identification (RFID) and RFID sensing platforms, as well as the most utilised polymer system in this research, polydimethylsiloxane (PDMS). Chapter 2 showed that a commercially available humidity sensing tag (RFMicron RFM-2100 AER) could be modified using a cross-linked silanol terminated PDMS layer, and exploited to detect aqueous electrolyte content from 0-2 M. It also served as a good reference to the film thicknesses required to tune the sensitivity of the tag for bulk liquid sensing for the subsequent chapters.

Chapter 3 showed that the PDMS coated RFMicron RFM-2100 AER could also be used sense variable ratios of water/alcohol mixes. It also served to show that when solution conductivity is negligible, lowering the relative permittivity of the liquid atop the sensor decreases the capacitive loading the tag experiences. This is expressed by an increase in an arbitrary sensor value sent from the RFID tag to a nearby reader and allows for sensing in a two-way fashion from both the tag and the reader. The chapter also showed that the system was not suitable for use with water/acetone and water/acetonitrile mixes. Swelling of the PDMS layer was explored as a potential reason for this unexpected result, but could not explain the aberrant sensor values that were measured.

Chapter 4 attempted to use free primary amines within a partially cross-linked PDMS network comprised of (6-7 %) aminopropylmethylsiloxane dimethylsiloxane co-polymer & chloromethylphenethyl terminated polydimethylsiloxane. The two-polymer fluid mix was applied to the RFMicron RFM-2100 AER with a 25% relative ratio of Cl groups in the chloromethylphenethyl terminated polydimethylsiloxane relative to the NH_2 groups in the (6-7 %) aminopropylmethylsiloxane dimethylsiloxane co-polymer, with the intention of surface protonation of these groups leading to an increased capacitance, allowing for pH to be sensed. After an optimisation process to produce films of the required 500 μm thickness, the tag was

tested with a range of pH solutions from 0-14. It was found that although the tag could sense either extreme of the pH scale (0, 1, 13 & 14) this was due to the dielectric properties of the higher concentration solutions.

Having established from chapter 4 that an increased conductivity change in the coating would be required to sense changes in pH, Chapter 5 introduced some preliminary work that used a composite comprised of PDMS and polyaniline (PANI). The composite was used over PANI alone to exploit the relatively easy processability and control of film thickness of PDMS. PANI was used as it is an intrinsically conductive polymer that has variable conductivity with variable pH. Three different weight loadings of PANI were tested, 5, 10 & 20 % respectively. It was found that as the PANI content in the composite was increased, the bulk conductivity of the composite would increase with decreasing pH solution applied to the tag. In the case of 20% PANI loading, the composite was able to sense pH at five distinct pH levels (7, 6, 5, 4-2, 1 & 0 respectively) at a single frequency (815 MHz). However, after being exposed to lower pH solutions, the composites did not show reproducible sensor values after being tested with pH solutions in a second exposure study.

Overall, the aims of the thesis were well met. Commercial tags were successfully modified with the intention of repurposing them using PDMS oriented coatings, and allowed for sensing of different liquids with variable dielectric properties. Being able to adjust the tag sensitivity using a one step functionalisation in particular is an attractive feature with regards to versatility for future applications. Furthermore, a composite was developed that has shown promise as a pH responsive composite that could be utilised to repurpose commercially available sensing architectures.

6.2. Future work

Future work is currently being performed within the research group, with a focus on developing the work in chapters 2 & 3 for a specific research application in collaboration with DSTL. Potential alterations to the systems researched here include incorporation of microfluidic channels within the PDMS matrix to allow for higher sensitivity of the system, whilst controlling the volume of

solution allowed to flow towards the interdigitated capacitor(IDC). The main issue with reducing the film thicknesses in chapters 2 & 3 was that exposure to bulk liquid to close to the IDC would result in a gross detuning of the tag. By incorporating microfluidic channels, this can be circumvented, as the majority of the liquid atop the tag would be kept at the required 500 µm distance to prevent gross detuning, whilst allowing a controlled volume to be brought closer to the fringing fields.